

LUND UNIVERSITY

Galactoglucomannan recovery from softwood spent sulfite liquor: Challenges, process design and techno-economic evaluations

Al-Rudainy, Basel

2020

Document Version:
Publisher's PDF, also known as Version of record

Link to publication

Citation for published version (APA):
Al-Rudainy, B. (2020). *Galactoglucomannan recovery from softwood spent sulfite liquor: Challenges, process design and techno-economic evaluations*. [Doctoral Thesis (compilation), Division of Chemical Engineering]. Chemical Engineering, Lund University.

Total number of authors:
1

General rights
Unless other specific re-use rights are stated the following general rights apply:
Copyright and moral rights for the publications made accessible in the public portal are retained by the authors and/or other copyright owners and it is a condition of accessing publications that users recognise and abide by the legal requirements associated with these rights.
• Users may download and print one copy of any publication from the public portal for the purpose of private study or research.
• You may not further distribute the material or use it for any profit-making activity or commercial gain
• You may freely distribute the URL identifying the publication in the public portal

Read more about Creative commons licenses: https://creativecommons.org/licenses/

Take down policy
If you believe that this document breaches copyright please contact us providing details, and we will remove access to the work immediately and investigate your claim.

LUND UNIVERSITY

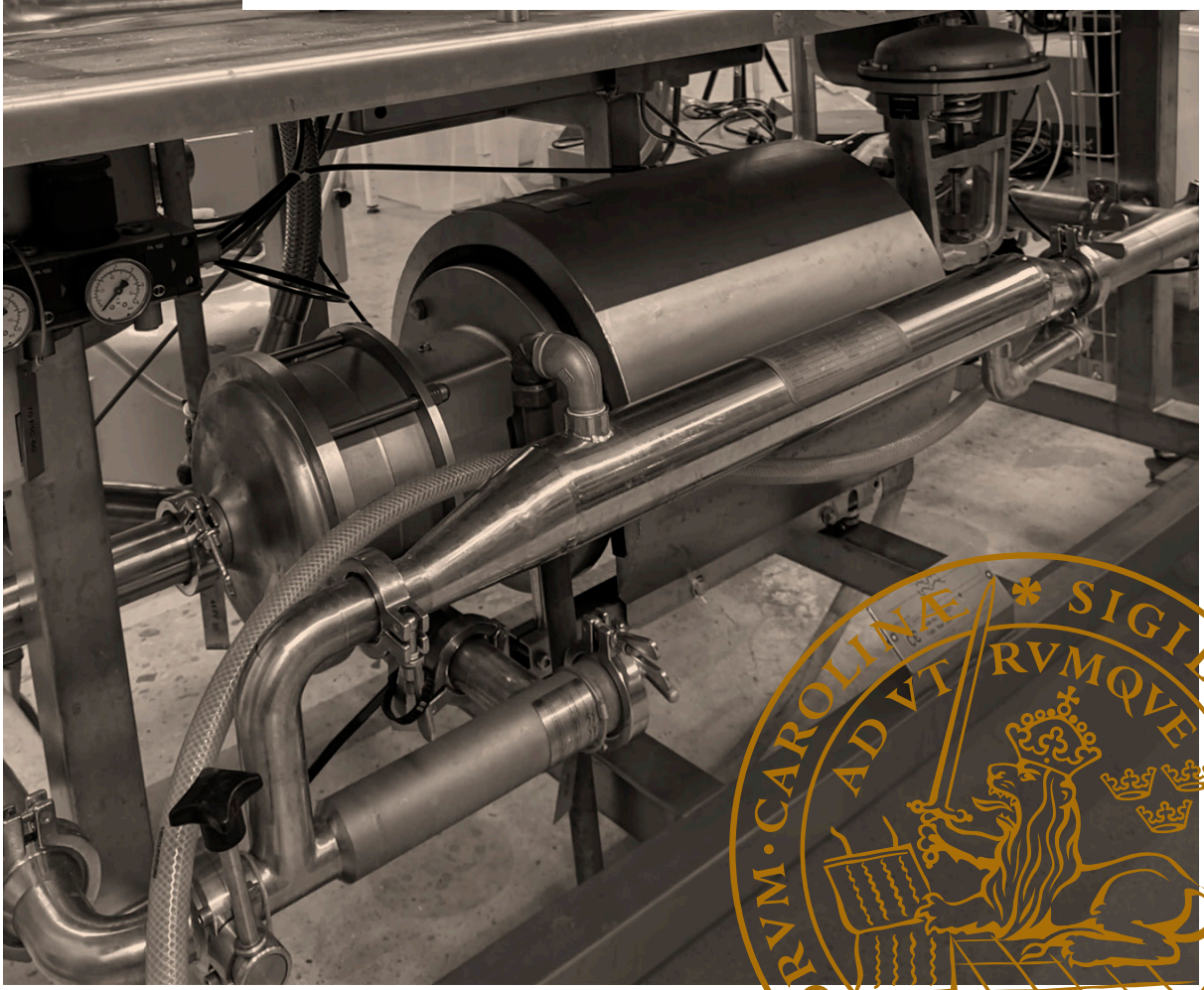
PO Box 117
221 00 Lund
+46 46-222 00 00



Galactoglucomannan recovery from softwood spent sulfite liquor

Challenges, process design and techno-economic evaluations

BASEL AL-RUDAINY | CHEMICAL ENGINEERING | LUND UNIVERSITY



Galactoglucomannan recovery from softwood spent sulfite liquor

Challenges, process design, and techno-economic evaluations

Basel Al-Rudainy

Department of Chemical Engineering

Lund University, Sweden

2020

DOCTORAL THESIS

by due permission of the Faculty of Engineering, Lund University, Sweden, will be publicly defended on the 18th of September at 09:15 in lecture hall KC:B at the Center for Chemistry and Chemical Engineering, Naturvetarvägen 14, Lund, Sweden.

The faculty opponent will be Professor Mika Mänttäri, Lappeenranta University of Technology, Finland



LUND UNIVERSITY

Organization LUND UNIVERSITY Department of Chemical Engineering	**Document name** DOCTORAL DISSERTATION
Author(s) Basel Al-Rudainy	**Date of issue** 25th of August 2020
	Sponsoring organization Swedish Foundation for Strategic Research (SSF)

Title and *subtitle*

Galactoglucomannan recovery from softwood spent sulfite liquor

Challenges, process design, and techno-economic evaluations

Abstract

In the production of pulp and paper, water-soluble components, such as hemicellulose, monosaccharides, and lignin, are released and accumulate in the process water. The process water is usually concentrated and incinerated for heat generation and the recovery of pulping chemicals, such as in the Kraft and sulfite processes. The growing trend toward a more sustainable forest industry has increased the interest in the biorefinery concept. The utilization of wasted wood components, such as hemicelluloses and lignin, as raw materials for the development of specialty chemicals and biofuels is essential for continued growth of the forest industry.

The aim of the work that is described in this thesis was to separate and purify hemicellulose (galactoglucomannan (GGM)) from softwood-based spent sulfite liquor (SSL). To this end, various separation techniques were investigated, of which membrane filtration, antisolvent precipitation, and adsorption were primarily used. The SSL in these studies was diluted and therefore needed to be concentrated before any further treatment. The concentration was performed using ultrafiltration (UF), and the purity was increased using diafiltration (DF). In the first UF study, 3 hydrophobic polysulfone (PS) membranes were used to achieve this goal. The 50-kDa UF membrane performed best in terms of low fouling, high flux, and retention of the products. Although the membrane fouling was among the lowest for the 50-kDa UF membrane, the fouling remained high. To reduce the fouling, two prefiltration methods were investigated—microfiltration (MF) and dead-end filtration (DEF)—of which DEF was the most appropriate method, given the low loss of products, which was negligible. DEF required the use of diatomaceous earth as a filter aid, which could have a negative influence on the pulp-mill, in case of membrane failure. For this reason, the membrane material was changed from PS to regenerated cellulose (RC), which is hydrophilic, at the UF stage. The results showed that the RC membranes were far superior to the PS membranes, with higher fluxes and less fouling. Also, the retention of lignin was lower using the RC membranes, which led to higher separation between the GGM and lignin. The best-performing RC membrane (RC70PP) was incorporated into on-site pilot equipment, in which the operating conditions from the lab-scale equipment were scaled up. The pilot had worse performance than the lab-scale setup, perhaps due to the higher Reynolds number and shear rates in the latter, as revealed by computational fluid dynamics. The pilot studies also showed that a 1-hour alkaline cleaning step was sufficient to remove foulants and maintain a stable flux. The separation of GGM and lignin using membrane filtration was not possible, likely due to the narrow difference in molecular weights between them and the formation of a gel layer or cake on the membrane surface that made the separation difficult. The separation was instead achieved with antisolvent precipitation and adsorption. For the antisolvent precipitation, this step was performed after the UF step to reduce the required amount of antisolvents, whereas for the adsorption, it was included as a pretreatment step prior to the UF to determine the influence of the lignin content on the UF step. Separation was possible using both methods, with antisolvent precipitation giving a separation degree of 76% using acetone as the antisolvent, versus 60% for adsorption, which corresponded to an 85% removal rate of the lignin. Finally, a techno-economic evaluation was conducted on various predetermined process configurations, showing that the combination of UF and adsorption (as the post-treatment step) was the most cost-efficient process that also fulfilled the design criteria.

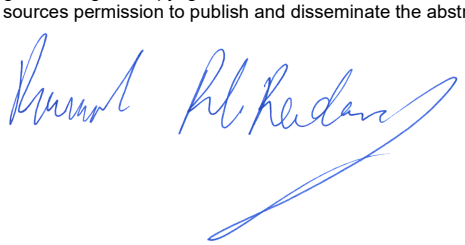
Keywords

Galactoglucomannan, Lignin, Lignosulfonates, Lignin-carbohydrate-complexes, Membrane filtration, Dead-end filtration, Precipitation, Adsorption

Classification system and/or index terms (if any)

Supplementary bibliographical information	**Language** English
ISBN (print) 978-91-7422-748-2	**ISBN (pdf)** 978-91-7422-749-9
Recipient's notes	**Number of pages** 244 / Price
	Security classification

I, the undersigned, being the copyright owner of the abstract of the above-mentioned dissertation, hereby grant to all reference sources permission to publish and disseminate the abstract of the above-mentioned dissertation.

Signature  Date 2020-08-10

Galactoglucomannan recovery from softwood spent sulfite liquor

Challenges, process design, and techno-economic evaluations

Basel Al-Rudainy
Department of Chemical Engineering
Lund University, Sweden
2020



LUND
UNIVERSITY

Cover photo by Basel Al-Rudainy

© Basel Al-Rudainy 2020

Faculty of Engineering
Department of Chemical Engineering

ISBN (print) 978-91-7422-748-2
ISBN (pdf) 978-91-7422-749-9

Printed in Sweden by Media-Tryck, Lund University
Lund 2020



Media-Tryck is a Nordic Swan Ecolabel
certified provider of printed material.
Read more about our environmental
work at www.mediatryck.lu.se

MADE IN SWEDEN

Science never solves a problem without creating ten more

- George Bernard Shaw

Abstract

In the production of pulp and paper, water-soluble components, such as hemicellulose, monosaccharides, and lignin, are released and accumulate in the process water. The process water is usually concentrated and incinerated for heat generation and the recovery of pulping chemicals, such as in the Kraft and sulfite processes. The growing trend toward a more sustainable forest industry has increased the interest in the biorefinery concept. The utilization of wasted wood components, such as hemicelluloses and lignin, as raw materials for the development of specialty chemicals and biofuels is essential for continued growth of the forest industry.

The aim of the work that is described in this thesis was to separate and purify hemicellulose (galactoglucomannan (GGM)) from softwood-based spent sulfite liquor (SSL). To this end, various separation techniques were investigated, of which membrane filtration, antisolvent precipitation, and adsorption were primarily used. The SSL in these studies was diluted and therefore needed to be concentrated before any further treatment. The concentration was performed using ultrafiltration (UF), and the purity was increased using diafiltration (DF). In the first UF study, 3 hydrophobic polysulfone (PS) membranes were used to achieve this goal. The 50-kDa UF membrane performed best in terms of low fouling, high flux, and retention of the products. Although the membrane fouling was among the lowest for the 50-kDa UF membrane, the fouling remained high.

To reduce the fouling, two prefiltration methods were investigated—microfiltration (MF) and dead-end filtration (DEF)—of which DEF was the most appropriate method, given the low loss of products, which was negligible. DEF required the use of diatomaceous earth as a filter aid, which could have a negative influence on the pulp mill, in case of membrane failure. For this reason, the membrane material was changed from PS to regenerated cellulose (RC), which is hydrophilic, at the UF stage. The results showed that the RC membranes were far superior to the PS membranes, with higher fluxes and less fouling. Also, the retention of lignin was lower using the RC membranes, which led to higher separation between the GGM and lignin.

The best-performing RC membrane (RC70PP) was incorporated into on-site pilot equipment, in which the operating conditions from the lab-scale equipment were scaled up. The pilot system performed worse than the lab-scale setup, perhaps due to the higher Reynolds number and shear rates in the latter, as revealed by computational fluid dynamics. The pilot studies also showed that a 1-hour alkaline cleaning step was sufficient to remove foulants and maintain a stable flux. The separation of GGM and lignin using membrane filtration was not possible, likely due to the narrow difference in molecular weight between them and the formation of a gel layer or cake on the membrane surface that made the

separation difficult. The separation was instead achieved with antisolvent precipitation and adsorption.

For the antisolvent precipitation, this step was performed after the UF step to reduce the required amount of antisolvents, whereas for the adsorption, it was included as a pretreatment step prior to the UF to determine the influence of lignin content on the UF step. The separation was possible using both methods, with antisolvent precipitation giving a separation degree of 76% using acetone as the antisolvent, versus 60% for adsorption, corresponding to an 85% removal rate of lignin.

Finally, a techno-economic evaluation was performed on various predetermined process configurations, showing that the combination of UF and adsorption (as the post-treatment step) was the most cost-efficient process that also fulfilled the design criteria.

Populärvetenskaplig sammanfattning

Fossila bränslen som naturgas, kol och råolja används som en energikälla och råmaterial i många olika sektorer. De används för att generera el och fjärrvärme, producera olika konsumentprodukter och inom transportsektorn som bränsle till olika fordon. Användningen av fossila bränslen stödjer med andra ord vårt samhälle och vi är beroende av dem i vår vardag. Fossila bränslen är dock en ändlig och icke-hållbar källa där förbränningen av dessa släpper miljöfarliga gaser som i sin tur ansamlas i atmosfären samt bidrar till den ökande globala uppvärmningen. Det är därför viktigt att hitta alternativ till fossila bränslen som är hållbara och förnybara.

Den mest tillgängliga, förnybara och hållbara bioresursen är lignocellulosa som är en grundläggande beståndsdel av olika växter. Biomassa är huvudsakligen uppbyggt av tre komponenter, cellulosa, hemicellulosa och lignin. Cellulosan används idag för att producera papper, biobränslen, textilier och plaster. Men fram tills idag, har den fulla potentialen för biomassa inte realiserats eftersom cellulosa står för 45% av den totala biomassan. De återstående komponenterna (hemicellulosa och lignin) utnyttjas inte fullt ut, särskilt hemicellulosan som inte utvinns och inte används kommersiellt. Även om hemicellulosa inte produceras kommersiellt har forskning visat på många tillämpningar för råvaran. Bland dessa är produktion av hydrogeler för jordbruks- eller medicinska tillämpningar, som tillsatser i pappersframställningsprocessen, som gasbarriärer, lacker och som stabiliserings- och geleringsmedel inom livsmedelsindustrin. Lignin har också visat sig att ha många lovande tillämpningar som tillverkning av biobränslen, kemikalier eller olika kompositmaterial.

De tre komponenterna (cellulosa, hemicellulosa och lignin) är bundna till varandra i ett stabilt närverk som måste brytas för att vi ska kunna använda dem individuellt i olika tillämpningar. Inom industrin görs detta genom olika kemiska behandlingar kopplat med någon form av termisk och/eller mekanisk behandling för att separera cellulosan och hemicellulosan från ligninet. Dessa processer slutar vanligtvis med en massa som innehåller mestadels cellulosa. Men man får även mycket utspädda avfallsströmmar som innehåller resten av biomassakomponenterna (såsom hemicellulosa och lignin) men också en del föroreningar. Inom t.ex. massa- och pappersindustrin koncentreras dessa avfallsströmmar och biomassakomponenterna förbränns för att generera värme och el. Borttagningen av dessa komponenter från avfallsströmmarna kan vara fördelaktigt genom att det skulle minska belastningen på återvinningsprocessen och samtidigt utvidga fabrikens produktportfölj eftersom lignin och hemicellulosa då kommer finnas tillgängliga som råvaror. En förutsättning för detta är att biomassakomponenterna är separerbara från varandra och från de andra föroreningarna. Målet med mitt projekt var att separera och rena upp

hemicellulosa från en industriell avfallsström som förutom hemicellulosa även innehöll lignin och andra mindre föroreningar på ett kostnadseffektivt sätt.

Jag har i mitt arbete använt och undersökt olika separationstekniker för att uppfylla målet med projektet. Avfallsströmmen som användes i arbetet var väldigt utspädd. För att koncentrera lösningen användes en teknik som kallas för membranfiltrering. I denna separationsteknik användes ett filter (membran) med väldigt små porer (syns inte med blotta ögat) för att filtrera bort vatten och föroreningar samt hålla tillbaka hemicellulosan och ligninet. För att utföra membranfiltreringen på ett kostnadseffektivt sätt är det viktigt att förlusterna av hemicellulosa minimeras samtidigt som man filtrerar en stor del av avfallsströmmen med en liten membranyta och på kort tid. Detta är emellertid inte enkelt och beror på många olika parametrar som tryck, temperatur, hastighet av avfallsströmmen ovanför membranet, membranmaterialet, porstorleken på membranet och antalet membranfiltreringssteg i serie. En kombination av olika driftsparametrar och filtreringssteg har studerats i detta arbete för att maximera hemicellulosa produktionen och reducera kostnaden för filtreringen. Membranfiltreringen fungerade bra för uppkoncentreringen av avfallsströmmen och reduceringen av föroreningar men mindre bra för separationen av hemicellulosan och ligninet. Anledningen var att hemicellulosan och ligninet har en storlek som är ungefär lika och som hålls tillbaka av membranet i lika hög grad.

För att separera dem har andra separationstekniker undersökts, såsom fällning och adsorption. Med fällning blandas den nu koncentrerade avfallsströmmen med aceton eller alkoholer vilket leder till att hemicellulosan faller ut i fast form och ligninet stannar i lösning. Hemicellulosan kan då separeras från lösningen genom vanlig filtrering (med ett enkelt filter) eller genom centrifugering (utnyttjar centrifugala krafter som gör att hemicellulosan lägger sig på botten av behållaren). Med adsorption, används istället en så kallad adsorbent som har formen av millimeter stora glaspärlor för att ta bort ligninet från avfallsströmmen. Adsorbenten har speciella egenskaper som binder lignin till sig och lämnar hemicellulosan i lösning. Ligninet tas då bort genom att filtrera av adsorbentpärlorna genom ett enkelt filter. För att separationen skall kunna utföras på ett kostnadseffektivt sätt måste man minska andelen aceton/alkoholer eller mängden adsorbent som används eller försöka återvinna dessa. Detta har närmare undersökts i detta arbete genom både experiment och olika typer av datorsimuleringar. Slutligen så har olika separationstekniker kombinerats för att komma fram till den mest lönsamma processlösningen för att koncentrera och rena upp hemicellulosa.

List of Publications

This thesis is based on the publications listed below, which will be referred to by their Roman numerals throughout the thesis.

I. **Al-Rudainy, B.**, Galbe, M., & Wallberg, O. Influence of prefiltration on membrane performance during isolation of lignin-carbohydrate complexes from spent sulfite liquor. *Separation and Purification Technology*, 2017, 187, 380-388.

II. **Al-Rudainy, B.**, Galbe, M., Schagerlöf, H., & Wallberg, O. Antisolvent precipitation of hemicelluloses, lignosulfonates and their complexes from ultrafiltrated spent sulfite liquor (SSL). *Holzforschung*, 2018, 72(10), 839-850.

III. **Al-Rudainy, B.**, Galbe, M., Arcos Hernandez, M., Jannasch, P., & Wallberg, O. Impact of lignin content on the properties of hemicellulose hydrogels. *Polymers*, 2019, 11(1), 35.

IV. **Al-Rudainy, B.**, Galbe, M., Lipnizki, F., & Wallberg, O. Galactoglucomannan recovery with hydrophilic and hydrophobic membranes: process performance and cost estimations. *Membranes*, 2019, 9(8), 99.

V. **Al-Rudainy, B.**, Galbe, M., & Wallberg, O. From lab-scale to on-site pilot trials for the recovery of hemicellulose by ultrafiltration: Experimental and theoretical evaluations. *Separation and Purification Technology*, 2020, 250, 117187.

VI. **Al-Rudainy, B.**, Galbe, M., & Wallberg, O. Hemicellulose recovery from spent sulfite liquor: Lignin removal by adsorption to resins for improvement of the ultrafiltration process. *Molecules*, 2020, 25(15), 3435

My Contributions to the Studies

I. I planned and performed the experiments. The results were evaluated with Ola Wallberg, and the paper was written with the coauthors. The spent sulfite liquor that was used in the study was provided by Domsjö Fabriker.

II. I planned and performed the experiments. The NMR analysis was performed with the aid of Göran Carlström, and I evaluated the results. The paper was written by me and the other coauthors. The spent sulfite liquor that was used in the study was provided by Domsjö Fabriker.

III. I planned and performed the experiments. The LC-MS analysis was conducted with the help of Herje Schagerlöf. The results were evaluated with Patric Jannasch, and the paper was written by me and the other authors. The spent sulfite liquor that was used in the study was provided by Domsjö Fabriker.

IV. I planned and performed the experiments. The results were evaluated with Ola Wallberg, and the NMR analysis was performed with Monica V. Arcos-Hernandez. The paper was written by all of the coauthors. The spent sulfite liquor that was in the study was provided by Domsjö Fabriker.

V. I planned and performed all of the experiments and simulations. The results were evaluated by me, and the paper was written by all of the authors. The spent sulfite liquor that was used in the study was provided on site by Domsjö Fabriker.

VI. I planned and performed all of the experiments. The results were evaluated by me, and the paper was written with the other authors. The spent sulfite liquor that was used in these studies was provided by Domsjö Fabriker.

Other related publications

I. Li, K., **Al-Rudainy, B.**, Sun, M., Wallberg, O., Hulteberg, C., & Tunå, P. Membrane Separation of the Base-Catalyzed Depolymerization of Black Liquor Retentate for Low-Molecular-Mass Compound Production. *Membranes*, 2019, 9(8), 102.

II. Virtanen T., Rudolph G., Lopatina A., **Al-Rudainy B.**, Schagerlöf H., Puro L., Kallioinen M., & Lipnizki F. Analysis of membrane fouling by Brunauer-Emmet-Teller nitrogen adsorption/desorption technique. *Scientific Reports*, 2020, 10, 3427

III. Rudolph G., **Al-Rudainy B.**, Thuvander J., & Jönsson A-S. Identification of foulants in an ultrafiltration membrane used to treat bleach plant effluent in a sulphite pulp mill. *Manuscript*, 2020

IV. S. J. Butler, **B. Al-Rudainy**, A. Bhattacharya, O. Wallberg & H. Stålbrand. Evaluating the efficacy of enzymatic saccharification of GGM from SSL and the impact of downstream purification of the SSL waste stream. *Manuscript in preparation*, 2020

Acknowledgments

I would like to start by thanking my main supervisor, Professor Ola Wallberg, for his support and encouragement and for always believing in me, especially when I was facing problems—you would always say something along the lines of, "Ahh, du fixar det." Thank you for always taking the time to discuss "the membrane toolbox", guiding me when I felt that I needed it and giving me the freedom of experimentally trying out different thoughts and ideas.

I would also like to thank my co-supervisor, Professor Mats Galbe, for his support and fruitful discussions and for always pushing me to do better. Thank you for always being there and showing interest in my ideas and results. Without you, Mats, this work would not have been possible**.** I just hope that someday you will realize how much better Google is compared with Apple and Microsoft so we can stop fighting about it.

I would like to thank my co-supervisor, Professor Frank Lipnizki, for sharing his industrial knowledge with me and for saving me during the pilot trials, when I was in need of a set of new membranes. Thank you for showing and convincing me that membranes could be used in any thinkable application. It is truly inspiring to listen to you talk about applications, ideas, and membranes in general.

I would like to thank the best and coolest analytical chemist that I know, Dr. Herje Schagerlöf, for his help with the LC-MS, for helping me find analytical equipment that no one has ever used or heard of in my field of research, and for discussing research and chemistry in general. Thank you for supporting me and pushing me toward my goals of learning and using all of our analytical equipment. It was both a fun and instructive journey.

Special thanks go to Professor Ann-Sofi Jönsson, who is the reason for my being where I am today. If it were not for your membrane course that I took at the end of 2011, I would probably have become an analytical chemist (yes, it was that close, Herje). It was in that course that I met Dr. Anders Arkell, who supervised me during the course and during my master's thesis, for which I am grateful. Thank you, Anders, for teaching me all of your membrane tricks, believing and trusting in my knowledge and abilities, and dragging me with you through all of the black liquor projects. It was both fun and challenging, and it truly taught me a lot of what I know about membranes today.

Big thanks to my colleagues, Dr. Johan Thuvander, Gregor Rudolph, Miguel Sanchis-Sebastiá, and Dr. Borbála Erdei, for being there to discuss research (both with regard to membranes and cellulose I/II) and for their company in the lab and at conferences. I would like to express extra thanks to Johan, who simply made everything in the membrane lab and analysis lab work. I know that I can be messy sometimes, and I did not realize this until you left the department.

Thank you to my officemates, Dr. Pia-Maria Bondesson and Simon Gidstedt. Special thanks go to Pia-Maria, who helped me in “Energitekniken” and also for supporting and guiding me during the frustrating times of writing.

I would like to thank my friend and former colleague, Filip Vrgoc, for being the best companion during our 5 years of studying, in the lab and at “fika.”

I would like to thank Kena Li and Tiina Virtanen (LUT University) for their expertise and collaboration on our joint papers and for the interesting discussions in the department and at conferences.

Much of my work would not have been possible without the help and contribution of Leif Stanley, for which I am very grateful.

Many thanks to our administrative staff, Lena Nilsson, Maria Messer, and Gity Yahoo, who made my life in the department easier. Special thanks to Lena for being so kind and patient with me—you are dearly missed.

A very big thanks to Dr. Monica V. Arcos-Hernandez and Professor Patric Jannasch, who showed and taught me that working across departments is both possible and fun. Special thanks to Monica, who always helped when asked. I owe you big time!

I would like to thank the personnel at Domsjö Fabriker, who welcomed me with such kindness. Special gratitude goes to Ole Norberg, Magnus Hörnsten, and Kristina Elg Christoffersson for their help, support, and feedback during the pilot study done on-site. I would also like to thank Dr. Hans Grundberg for his input and feedback during his time at Domsjö Fabriker.

I would also like to thank Professor Henrik Stålbrand and his group for interesting meetings and discussions.

This work was funded by the Swedish Foundation for Strategic Research (SSF), which is gratefully acknowledged.

Last, but not least, I would like to thank my loving wife, Karez (qurbane äbum!), my family (incl. Simba), and my friends for their love and support. To my parents, I would also like to add the following:

شكرا لكم على كل شي لولا دعم امي وابي لي لما وصلت الى هدفي، بحبكم كتير

Abbreviations and Symbols

Abbreviations

AGX	Arabinoglucuronoxylan
BET	Brunauer-Emmett-Teller
CFV	Cross-flow velocity (m/s)
DF	Diafiltration
DP	Degree of polymerization
DMSO	Dimethyl sulfoxide
FTIR	Fourier-transform infrared spectroscopy
GGM	(O-acetyl) galactoglucomannan
HPLC	High-performance liquid chromatography
LCC	Lignin-carbohydrate-complexes
LS	Lignosulfonates
MF	Microfiltration
MW	Molecular-weight
MWCO	Molecular-weight cut-off
NF	Nanofiltration
NMR	Nuclear magnetic resonance spectroscopy
PWF	Pure water flux (L/m^2h)
RI	Refractive index
SEC	Size-exclusion chromatography
SSL	Spent sulfite liquor
TMP	Trans-membrane pressure (bar)
UF	Ultrafiltration
UV	Ultraviolet
VR	Volume reduction (g/g or %)

Symbols

c_b	Concentration of solute in the bulk/feed solution (g/L)
c_p	Concentration of solute in the permeate (g/L)
c_m	Concentration of solute at the membrane surface (g/L)
D	Mass diffusivity (m^2/s)
J	Permeate flux (L/m^2h)
k	Mass transfer coefficient (m/s)
P_{feed}	Pressure at the feed/inlet (bar)
P_{ret}	Pressure at the retentate/outlet (bar)
P_{perm}	Permeate pressure (bar)
A_m	Membrane area (m^2)
R_c	Resistance due to cake formation (m^{-1})
R_{cp}	Resistance due to concentration polarization (m^{-1})
R_m	Hydraulic resistance of the membrane (m^{-1})
R_{obs}	Observed retention (g/g or %)
R_{true}	True retention (g/g or %)
μ	Dynamic viscosity (Pa s)
t	Time (min)
q_e	Adsorption capacity at equilibrium (mg/g)
q_t	Adsorption capacity at time, t (mg/g)
C_0	Concentration of solute at the beginning (g/L)
C_e	Concentration of solute at equilibrium (g/L)
C_t	Concentration of solute at time, t (g/L)
Q_x	Maximum adsorption capacity (mg/g), where x denotes the model (B = BET, S = Sips, L = Langmuir)
K_x	Isotherm constant (mL/mg), where x denotes the model (L = Langmuir, F = Freundlich, S = Sips, B = BET)
n_x	Intensity of adsorption (-), where x denotes the model (F = Freundlich, S = Sips)

C_s	Saturation concentration (g/L)
k_x	Adsorption rate constant [mg/(g min)], where x denotes the model (0 = pseudo zero-order, 1 = pseudo first-order, 2 = pseudo second-order, p = intra-particle diffusion)
α	Initial adsorption rate [mg/(g min)]
β	Desorption constant (g/mg)

Contents

1. Introduction 1
1.1 Background 1
1.2 Aims and outline of this thesis 2
2. Softwood biomass 4
2.1 Cellulose 5
2.2 Hemicellulose 5
2.2.1 (O-acetyl) galactoglucomannan 5
2.2.2 Arabinoglucuronoxylan 6
2.2.3 Other polysaccharides 7
2.3 Lignin 7
2.3.1 Lignin-carbohydrate-complexes 8
2.4 Residual components 9
3. Dissolution of lignocellulosic components in pulping processes 10
3.1 Mechanical pulping 10
3.2 Kraft pulping 11
3.3 Sulfite pulping 11
3.4 Other pulping processes 14
4. Separation of biomass components 15
4.1 Dead-end filtration 15
4.2 Membrane filtration 16
4.2.1 Fundamentals of cross-flow membrane filtration 17
4.2.2 Operating conditions 19
4.2.3 Fouling and cleaning 22
4.2.4 Separation of hemicellulose 25
4.3 Precipitation 26
4.4 Adsorption 29
4.4.1 Fundamentals 29
4.4.2 Separation of biomass components 33
4.5 Other methods 33

5. Materials and methods 35
5.1 Experimental equipment 35
5.1.1 Membranes 35
5.1.2 Lab-scale membrane filtration 36
5.1.3 Pilot-scale membrane filtration 37
5.1.4 Batch antisolvent precipitation 37
5.1.5 Batch adsorption of lignin 38
5.2 Analytical methods 38
5.2.1 Raw material 38
5.2.2 Total dry substance and ash content 39
5.2.3 Lignin content 39
5.2.4 Hemicellulose, monosugars, sugar acids, and acid-insoluble solids 39
5.2.5 Acetic acid and glycerol content 39
5.2.6 Size-exclusion chromatography 40
5.2.7 Sulfonate, carboxylic and phenoxyl group content 40
5.2.8 Fourier transform infrared spectroscopy 41
5.2.9 HSQC 2D-NMR 41
5.2.10 Thermogravimetric analysis 41
5.2.11 Swelling capacity 41
5.2.12 Compression stress and strain 42
5.2.13 Bromothymol blue diffusion from hydrogels 42
5.2.14 Liquid chromatography–mass spectrometry (LC-MS) 42

6. Raw material composition 43

7. Membrane filtration of the SSL 48
7.1 Hydrophobic membranes (Paper I) 49
7.1.1 Parameter study 50
7.1.2 Membrane fouling 51
7.1.3 Concentration and diafiltration study 52
7.1.4 Prefiltration with MF and DEF 53
7.2 Hydrophilic membranes (Paper IV) 55
7.2.1 Concentration study 56
7.2.2 SEC of retentates 58
7.3 On-site pilot study (Paper V) 60
7.3.1 Concentration study under lab-scale operating conditions 60
7.3.2 Increasing the flux 61
7.3.3 CFD of the membrane modules 63
7.3.4 Fouling and cleaning 66

8. Separation of GGM and lignin 69
8.1 Antisolvent precipitation (Paper II) 69

8.1.1 Precipitation of the retentate 71
8.1.2 Characterization of the fractions 74
8.1.3 Effect of concentration on precipitation 75
8.1.4 Effect of pH and temperature on precipitation 76
8.2 Adsorption (Paper VI) 78
8.2.1 Adsorbent screening 78
8.2.2 Equilibrium experiments 79
8.2.3 Adsorption kinetics 81
8.2.4 Adsorbent regeneration 82
8.2.5 Ultrafiltration of adsorption permeate 83
9. Techno-economic analysis 84
9.1 Case study I – Ultrafiltration of SSL 84
9.2 Case study II – Adsorption and ultrafiltration of SSL 87
9.2.1 Batch adsorption – Calibration of the kinetics 87
9.2.2 Adsorption column 90
9.2.3 Techno-economic evaluation 100
9.3 Case study III – Ultrafiltration and precipitation of GGM from SSL 103
10. Conclusions and future work 108
References 113

1. Introduction

1.1 Background

The most widely available, renewable, and sustainable bioresource is lignocellulose, a fundamental constituent of plant biomass that is generated through photosynthesis. Replacing existing fossil-based products with lignocellulosic could significantly reduce ambient greenhouse gas emissions and alleviate global warming [1]. This prospect is possible because lignocellulosic biomass is CO_2-neutral and has zero carbon emissions. Another advantage of lignocellulosic biomass is that it does not impact the food chain like other types of biomass. Many products have been produced from the cellulose portion of lignocellulosic biomass, such as paper with varying properties, biofuels, textiles, and plastics [2].

However, the full potential of lignocellulosic biomass has not been realized, given that cellulose accounts for 40% to 45% of the total biomass content [3]. The remaining primary components, hemicellulose and lignin, have not been utilized fully, especially lignocellulosic hemicellulose, which is not produced or used commercially [4]. With regard to the future of lignocellulosic biorefineries, better utilization of biomass could lead to an overall more sustainable and cost-effective process, given the plentiful and renewable waste streams.

Hemicellulose is the second-most abundant lignocellulosic polysaccharide in nature, with amounts exceeding 20% of plant biomass [5] (Paper III). Hemicelluloses are polymers with a heterogeneous structure, containing mainly pentoses, hexoses, and sugar acids. The composition of hemicellulose is diverse and depends on the plant species and extraction method [6,7]. Although lignocellulosic hemicelluloses are not produced commercially, research has revealed many promising applications for this polysaccharide. Among them are the production of hydrogels for agricultural or medical applications [8,9] (Paper III), as additives in the paper-making process [10], gas-barrier films [11,12], coatings [13], and as stabilizers and gelling agents in the food industry [14].

However, to exploit the various biomass components fully, an extraction method is needed. Industrially, various chemical treatments and heat have been used to separate the cellulose and hemicellulose from lignin [15]. These processes usually result in pulp that contains primarily cellulose but also very diluted waste streams that harbor the remaining biomass components (such as hemicellulose and lignin).

In such cases as in the Kraft process and certain sulfite pulping processes, the waste stream is concentrated using evaporators, and the pulping chemicals are recovered using a recovery boiler, resulting in the incineration of valuable biomass components and the generation of heat. The recovery of these components from waste streams before the evaporation step could be beneficial, in that it would reduce the load on the recovery boiler (increasing the productivity) and simultaneously expand the product portfolio of the pulping plant, thus implementing a biorefinery concept. The separation process accounts for 60% to 80% of the total cost of chemical processes and between 20% to 50% for biorefineries [16,17]. It is therefore important economically to establish a separation process that is both efficient and selective.

Membrane filtration is a promising separation process that is expected to play an important role in the future of biorefineries [18]. This technique separates components, based on size, without the addition of any chemicals; requires little energy input; and is thus cost-efficient. However, in cases in which the molecular-weights (MWs) of the various solutes are on the same order of magnitude or in which fouling layers form on the membrane surface, the separation has proven to be difficult (Papers I, II, IV, and V). In such cases, antisolvent precipitation or adsorption on resins could be used for the separation (Papers II and VI). Antisolvent precipitation uses the difference in solubility between compounds and can thus separate solutes with a narrow difference in MW. Separation by adsorption onto resins depends mainly on the properties of the adsorbent and adsorbates (the adsorbing compounds) and can be achieved by physisorption or chemisorption. In either separation process, membrane filtration remains important, for which it can be used to concentrate the raw material, recover the cooking chemicals, and in turn reduce the cost of the separation and pulping processes.

1.2 Aims and outline of this thesis

The aim of this thesis was to separate and purify hemicellulose from an industrial waste stream (SSL) that, in addition to hemicellulose, contained lignin, pulping chemicals, and other minor contaminants. To achieve this goal, various separation techniques were used. For instance, the amount of pulping chemicals was reduced and the concentration of hemicelluloses was increased using membrane filtration. The hemicelluloses were separated from the lignin using anti-solvent precipitation or adsorption using polymeric resins. Finally, a techno-economic evaluation was performed on several process configurations to identify the most cost-efficient solution.

In the two upcoming chapters (**2** and **3**), a brief description of the softwood biomass composition and the dissolution of these components using various pulping processes is presented. Chapter **4** discusses the fundamentals of several separation techniques, focusing on the methods that are primarily used in this thesis: membrane filtration, precipitation, and adsorption. A short description of the equipment and experimental and analytical methods used is presented in Chapter **5,** followed by the SSL composition, which is described in Chapter **6**. Chapter **7** contains the membrane filtration trials, which included the lab-scale and pilot-scale experiments in Papers I, IV, and V. The results from the separation of hemicellulose and lignin using antisolvent precipitation and adsorption are presented in Chapter **8**. Chapter **9** introduces three process alternatives and their economic evaluation. The data in these calculations were based on experimental data and simulations.

The final chapter draws conclusions, based on the previous results, and suggestions for future work are presented.

2. Softwood biomass

Lignocellulose is the most abundant renewable source of biomass, constituting an alternative raw material for the production of fuels, chemicals, and materials. Biomass is composed primarily of two carbohydrate polymers (cellulose and hemicellulose) and one phenolic polymer (lignin), all of which are found in different parts of the plant cell wall. Other minor compounds include extractives, proteins, pectins, and inorganics. Cellulose microfibrils form the main structure of the plant, with 3 to 4 layers of microfibrils in the primary wall and hundreds of layers in the secondary wall [19]. Hemicelluloses are embedded in the cell wall, forming a matrix with cellulose microfibrils, to bind microfibrils and strengthen the cell wall [20]. The plant's rigidity and strength increase further by impregnating and coating the polysaccharide network with lignin [21].

The biorefinery process water that is used in Papers I-VI was generated using softwood, mainly spruce (*Picea abies*) and pine (*Pinus sylvestris*). The typical composition of the main components in softwood is presented in Table 2.1.

Table 2.1: Composition of the major components of softwood.

Source	Content (%)			Reference
	Cellulose	Hemicellulose	Lignin	
Spruce	44.1	25.7	27.7	[22]
Spruce	46.5	25.1	30.9	[23]
Pine	41.1	25.7	25.9	[24]
Pine	47.4	24.4	24.6	[25]

2.1 Cellulose

The major component in lignocellulosic biomass is cellulose. Cellulose is a linear polymeric chain that is composed solely of D-glucopyranose units that are linked by β-(1→4)-glycosidic bonds (Figure 2.1) that in turn form chains of up to 8000 (primary wall) and 15,000 units (secondary wall) [26]. The polymers bind to each other using hydrogen bonds or van der Waals forces, forming a nanostructure (microfibrils), with high- (crystalline) and lower-ordered regions (amorphous). At a degree of polymerization (DP) of 8 and higher, the glucan chains have a greater affinity for each other than water, and thus, native cellulose is insoluble in most solvents. The combination of the strong hydrogen bonds between the cellulose chains and the connection with hemicellulose and lignin renders chemical and microbial degradation of cellulose chains difficult. However, it is possible to degrade and solubilize cellulose through various types of pretreatment [27].

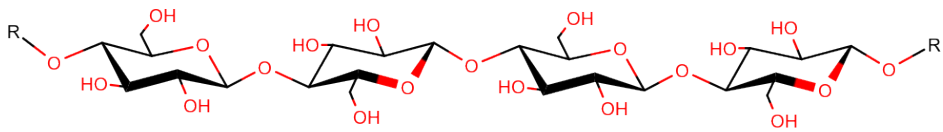


Figure 2.1: The chemical structure of cellulose.

2.2 Hemicellulose

Hemicellulose is the second-most abundant polysaccharide in lignocellulosic biomass. These polysaccharides have a lower DP than cellulose and can be linear and branched. The most common softwood hemicelluloses are (O-acetyl) galactoglucomannan, glucomannan, and arabinoglucuronoxylan. Other minor polysaccharides in softwood are arabinogalactan, xyloglucan, glucans, and pectins [28].

2.2.1 (O-acetyl) galactoglucomannan

The main hemicellulose in softwood is O-acetyl galactoglucomannan (GGM) (Figure 2.2). The backbone of GGM comprises a linear chain of D-mannopyranose and D-glucopyranose, connected by β-(1→4) glycosidic linkages. The GGM chain is also branched by single-unit D-galactopyranose residues that are linked by α-(1→6) bonds and is partially O-acetyl-substituted at the C2 and C3 positions (1

acetyl per 3-4 hexose units) [29]. GGM has a DP of 100 to 150, which corresponds to an MW of 16 to 24 kDa, and is found primarily in the secondary cell wall of softwoods [30]. According to several studies [28-30], 2 main types of GGM exist in softwood: one that is high in galactose, with a galactose:glucose:mannose ratio of 1:1:3, and one that is galactose-low, with ratios of 0.1-0.2:1:3-4, which is sometimes referred to as glucomannan. The two GGMs differ in such properties as solubility, which is lower for glucomannan, given its lower degree of substitution [21,31].

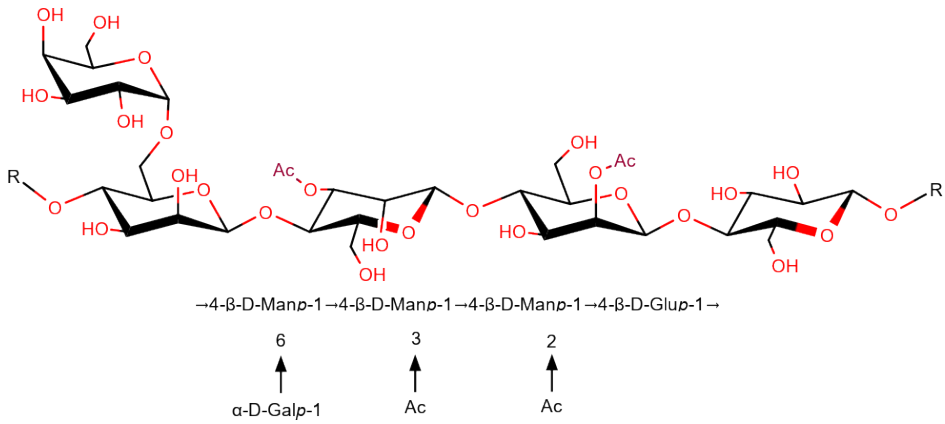


Figure 2.2: The structure of (O-acetyl) galactoglucomannan

2.2.2 Arabinoglucuronoxylan

Arabinoglucuronoxylan (xylan) is the second-most common hemicellulose in softwood. It has a backbone of D-xylopyranose units that are linked by β-(1→4) glycosidic bonds and has 1 unit of 4-OMe-D-glucuronic acid for each 5 to 6 xylose units, linked with α-(1→2) bonds, and 1 L-arabinofuranose unit per 8 to 9 xylose units, attached by α-(1→3) linkages (Figure 2.3) [32]. Xylans have an average DP of 90 to 120, and unlike hardwood xylans, softwood xylans are not acetylated, and their distribution of side groups is regular. Softwood xylans are also more acidic compared with hardwood xylans, due to the high concentration of 4-OMe-D-glucuronic acid substitutions.

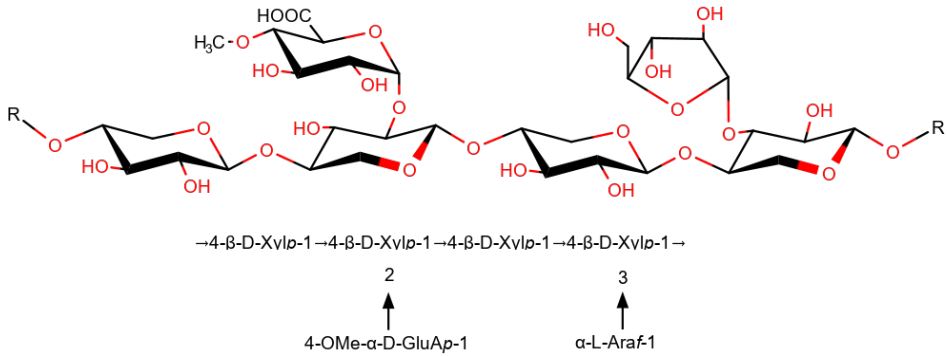


Figure 2.3: The structure of arabinoglucuronoxylan

2.2.3 Other polysaccharides

GGM and xylans are the major hemicelluloses in softwood. However, a potentially important minor polysaccharide is galactan. Galactans are constituents of pectic compounds in the middle lamella and primary cell walls of plants [32]. Arabinogalactans are water-soluble polysaccharides with a β-(1→3)-D-galactopyranose backbone and are branched at the C6 carbon with D-galactose, L-arabinose, or glucuronic acid units. Although arabinogalactan exists in small amounts in softwoods (less than 1%), its high MW (between 11 and 70 kDa) renders it important with regard to separation processes. Another water-soluble galactan is "pectic" galactan, which has a backbone of β-(1→4) galactopyranose units and is substituted at C6 with galacturonic acid (1 of 20 galactose residues).

Other minor polysaccharides in softwoods include:

- Arabinan – Has a backbone of α-(1→5) arabinose units and is branched with arabinose, linked by α-(1→3) bonds.
- Xyloglucan – Has a backbone of β-(1→4) glucose units, branched with xylose and arabinose, galactose, and fucose that are linked to the xylose.

2.3 Lignin

Lignin is one of the most abundant natural polymers on earth, exceeded only by cellulose. It binds to the hemicellulose in plants and adds strength and rigidity to the entire structure. The composition of lignin varies between plant species, and it lacks a defined structure due to its high heterogeneity [33]. However, the biosynthesis of lignin proceeds using 3 known monolignols (monomers)—para-coumaryl alcohol,

coniferyl alcohol, and sinapyl alcohol (Figure 2.4)—of which coniferyl alcohol is the most common precursor in softwoods.

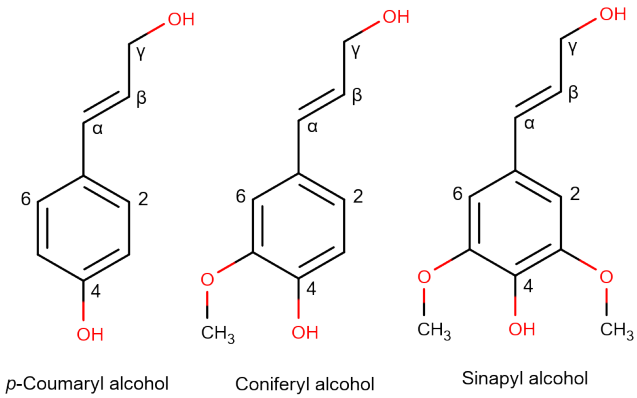


Figure 2.4: Monolignols used in the biosynthesis of lignin.

The common types of bonds between monolignols are ether ([β-O-4], [α-O-4], and [4-O-5]) and carbon-carbon bonds ([β-1], [β-5], [β-β], and [5-5]). The structure of lignin differs between plant species and extraction methods [34]. Thus, lignin has been defined and characterized, based on the frequency of various bonds (for example, per 100 aromatic rings) and the concentration of functional groups, such as methoxyl and phenoxyl groups [35].

2.3.1 Lignin-carbohydrate-complexes

Lignin that is bound covalently to hemicelluloses or lignin-carbohydrate-complexes (LCCs) are generated during the biosynthesis of lignin and is found in the pulp and waste streams that arise from the pulping process [36]. There are up to 8 types of bonds in LCCs, and the most common linkages are benzyl ether, benzyl ester, and phenyl glycosidic [37], illustrated in Figure 2.5. Benzyl ether bonds are alkali-labile in the presence of phenolic hydroxyl groups; otherwise, they are proposed to be alkali-stable [38,39]. Benzyl ester linkages are the most labile and easiest to cleave in alkaline medium. Phenyl glycosidic bonds are the most stable under alkaline conditions and have high lability under acidic conditions. All of these bonds are hydrolyzed easily under acidic conditions.

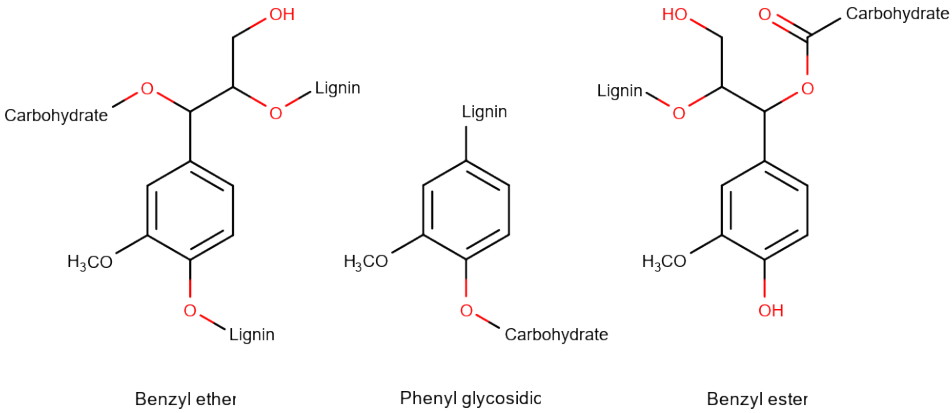


Figure 2.5: The most common bonds in lignin-carbohydrate-complexes.

2.4 Residual components

As seen in Table 2.1, cellulose, hemicellulose, and lignin account for approximately 97% of the dry matter; the remaining 3% can be attributed to other components. Extractives, pectin, protein, and inorganics are examples of such components in softwood [40]. Extractives form a group of monomers, oligomers, and polymers that consist of fats (fatty acids and alcohols), phenols (such as lignans), terpenes, steroids, resin acids, rosin, and waxes. Pectins are polysaccharides that comprise D-galacturonic acid with various sugar residues.

3. Dissolution of lignocellulosic components in pulping processes

The previous chapter presented the components in lignocellulosic biomass. The major components of lignocellulosic biomass or wood comprise 60% to 70% polysaccharides, and the remainder consists of lignin with minor components that are covalently or non-covalently bound. The main goal of pulping processes is to free and separate fibers from the lignin and suspend them in water for further processing. However, all of the pulping processes share the preparation of the raw material: the wood. The raw material is received as chips that can be used directly or as logs that are debarked using rotating drums, chipped, and stored in large piles before the pulping.

3.1 Mechanical pulping

Mechanical pulping is the oldest type of pulping and has largely been replaced by chemical pulping processes but remains in use for low-grade paper, such as newsprint. The pulping process has high yields (90% to 98%) and is responsible for 20% of the total production of pulp worldwide [41,42]. This process uses mechanical action to separate fibers from the wood using 1 of 4 primary techniques: stone groundwood pulping, refiner pulping, thermomechanical pulping, and chemithermomechanical pulping.

Stone groundwood pulping is the least energy-intensive mechanical pulping process. It takes logs instead of wood chips and grinds them down using water-cooled, artificial bonded stones that are made from silicon carbide or aluminum oxide. The advantage of this method is its high pulp yield. However, short fibers are produced, which in turn require expensive strengtheners when used in paper production.

Refiner pulping was developed to use wood chips instead of logs. Pulping is achieved by grinding the wood chips between 2 grooved discs. One main advantage of this technique is that the paper that is produced from the fibers allows for greater surface area per weight of pulp.

Thermomechanical pulping is the most commonly used mechanical pulping process. This process uses steam at a temperature of 115°C to 155°C prior to the refiner pulping to soften the material that would otherwise alter the fracture mechanisms in the wood during the refining process [41]. The resulting pulp is of high-grade compared with the other mechanical processes above. However, this process is energy-intensive and produces darker pulps that require expensive bleaching steps.

Chemithermomechanical pulping involves the use of lignin-softening chemicals, such as sodium sulfite, to impregnate the wood chips before the steam treatment and refining. The use of chemicals allows for less intensive mechanical processing, resulting in longer, stronger, and more flexible fibers. The technique has the same disadvantages as thermomechanical pulping, of which its energy demand is a major drawback.

3.2 Kraft pulping

Kraft pulping is the dominating process for manufacturing pulp and paper products [42]. This process has replaced many sulfite pulping processes worldwide for such reasons as the late development of a recovery process for sulfite pulping chemicals and its yield of stronger fibers. The process starts by pre-steaming and impregnating the wood chips with a mixture of white (NaOH and Na_2S) and black liquor (spent white liquor). The wood chips are then "cooked" for several hours in a digester at temperatures that range from 140°C to 180°C [43], during which the lignin and hemicelluloses degrade and dissolve in the strongly basic cooking liquor, which is then termed black liquor. The pulp (called brown stock) is washed and bleached, whereas the black liquor is concentrated in evaporators and incinerated in the recovery boiler to produce power and heat. The pulping chemicals are also recovered in the recovery boiler and reused in the process [44].

3.3 Sulfite pulping

The use of sulfite processes has decreased drastically in recent years. This is due to the disadvantages of the process and the development of a chemical recovery and better bleaching method for the Kraft process. However, the trend has turned in recent years through a developed pulping method and chemical recovery for sodium- and magnesium-based sulfite processes.

The sulfite liquor that is used in the pulping process contains a mixture of sulfurous acid and bisulfite ion. The chemical is made by the combustion of sulfur in an

exothermic reaction at temperatures that exceed 700°C. The cooled gas (SO_2) is passed in a column that contains an alkaline solution with 1 of the following anions: sodium, magnesium, ammonia, or calcium [42]. By changing the ratio of gas and solution, it is possible to make different sulfite liquors and thus alter the conditions of the subsequent pulping reactions. The wood chips are "cooked" at a pH of 1.5 to 9 in a batch or continuous digester at temperatures of between 130°C and 175°C for 4 to 8 hours [45,46]. The conditions depend on the raw material, anion, and the properties of the resulting end product.

Delignification proceeds with sulfonation of the lignin, which successively increases the water solubility of the compound and its removal with the spent sulfite liquor (SSL). The delignification reactions in the sulfite pulping process depend on the process conditions. Under acidic conditions, the dominating reactions are protonation of the benzylic hydroxyl or ether (α-O-4 bonds) at the α-carbon, elimination of water or the R-OH group, and addition of the bisulfite ion, yielding lignosulfonates (see Figure 3.1) [47].

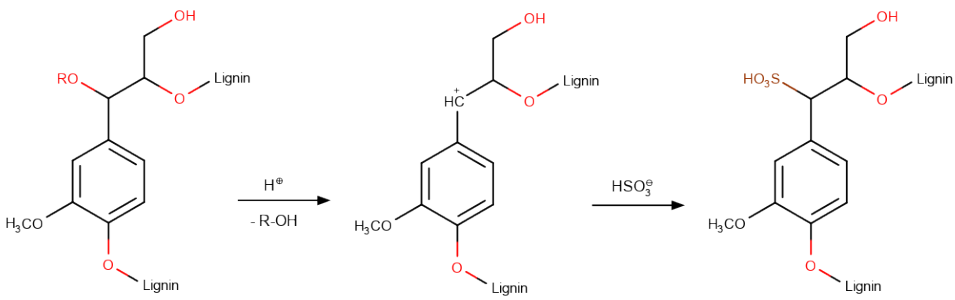


Figure 3.1: Formation of lignosulfonates during acidic sulfite pulping

Under neutral or slightly alkaline conditions, the reactions are analogous to those in the Kraft process, and thus, the cleavage of β-O-4 linkages is expected [47], with the products having several sulfonic acid groups that are attached to the aliphatic chain. Neutral or slightly alkaline conditions are not always possible, especially when using calcium as a base (low solubility at high pH). The high abundance of β-O-4 linkages in lignin will generate lignosulfonates with a high MW, given the stable nature of β-O-4 linkages in acidic media [48].

In single-stage acidic sulfite pulping, the hemicellulose is usually hydrolyzed, whereas the cellulose remains intact, due to the amorphous structure of the hemicellulose, which renders it available and labile to acid hydrolysis. The crystalline structure of cellulose protects it from degradation under normal pulping conditions. However, for the production of dissolving pulp, harsher conditions are used that degrade the cellulose to a certain extent [49]. The hemicelluloses in softwood sulfite pulp are usually glucomannans and glucuronoxylans with a low uronic acid content—these compounds are the products that remain after hydrolysis

of the galactose units, partial removal of the acetyl groups on the GGM chain, and the removal of the labile arabinofuranose units on the xylan chain. The hemicellulose fragments in the SSL continue to degrade, due to the harsh conditions, ultimately into monosaccharides or other degradation products, such as acids.

Single-stage acidic sulfite pulping is an appropriate method for wood with a low extractives content (such as spruce). However, in the case of pine wood, another technique is needed, because under acidic conditions, phenolic extractives (such as pinosylvin and taxifolin) can react with lignin (through condensation reactions) and block the sulfonation, generating darker pulps that are more difficult to bleach. This problem is mitigated by conducting the sulfite pulping in several stages. The first stage is more alkaline, during which the lignin is subjected to partial sulfonation but is still retained in the pulp. In the second stage, normal acidic conditions are applied, under which delignification is achieved—applying partial sulfonation in the first stage protects the lignin from condensation reactions with the extractives during the "main" acidic cooking stage. A 2-stage pulping process also has higher yields, attributed to the deacetylation of GGM in the first stage and, consequently, the retention of the remaining glucomannan in the pulp [49].

In Papers I-VI, hemicelluloses from sodium-based SSL were recovered and used. The SSL was taken from the sodium-based pulping process at Domsjö Fabriker (Örnsköldsvik, Sweden). An overview of the entire process is presented in Figure 3.2. The raw material that is used on site is a mixture of 60% spruce (*Picea abies*) and 40% pine (*Pinus sylvestris*), and the pulping is conducted at a pH of 4.5 in the first stage and approximately 1.0 in the second stage at a temperature of roughly 150°C. The SSL in this work was taken from the first stage, in which the pH was higher than 3, with the hemicelluloses still intact and in their polymeric form.

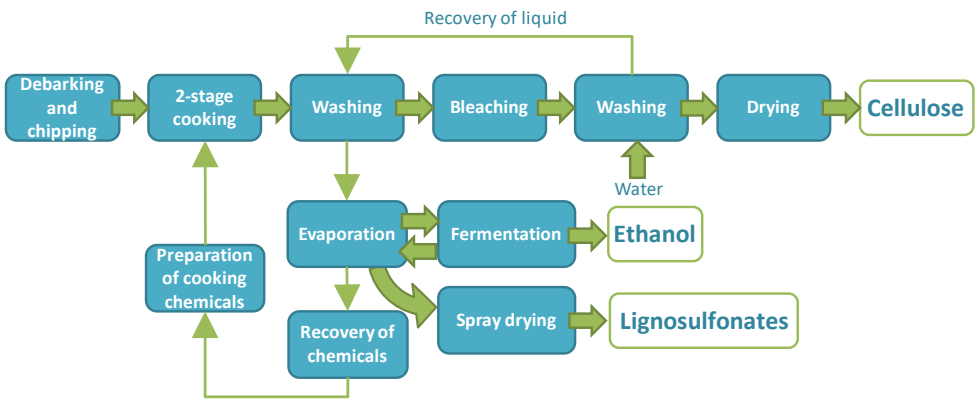


Figure 3.2: Schematic of the pulping process from which the SSL in Papers I-VI was derived.

3.4 Other pulping processes

Semichemical pulping combines chemical and mechanical pulping. This method is similar to chemithermomechanical pulping, in that it uses chemicals initially with steam to soften the wood chips and then mechanical means for the digestion. The chemicals that are used today for these pulp mills are nonsulfurous or neutral sulfite—the former is sodium carbonate, alone or mixed with sodium hydroxide, and the latter is a sodium-based sulfite liquor [50].

Organosolv pulping is a technology that was developed in the 1990s and advanced as far as pilot-scale trials. This process failed to achieve economical sustainability on a large scale and was thus discontinued, despite the high quality and bleachability of the resulting pulp. However, the process regained popularity due to the increasing interest in the development of biorefineries in recent years.

The oraganosolv process uses water with organic solvents (such as ethanol, methanol, and acetone) and a catalyst at temperatures below 200°C to delignify the biomass [51,52]. The catalyst in this process is usually an organic or inorganic acid, which can also be omitted, given that certain biomasses release acetic acid, which in turn acidifies the liquor. The reactions are similar to what is observed in the sulfite process, in which the major bonds that are cleaved are the α-O-4 bonds, with a high likelihood of β-O-4 cleavage under harsher conditions. However, because no sulfur is used in this process, the lignin that is produced is also sulfur-free, an attractive property for certain applications.

4. Separation of biomass components

In the previous chapter, several processes for the dissolution of lignocellulosic biomass components were presented. In Papers I-VI, SSL that contained mainly hemicelluloses, lignin, and pulping chemicals was treated using various techniques to concentrate the solution, separate the biomass components, and recover the pulping chemicals. In this chapter, these techniques are discussed, focusing on the most frequently used method: membrane filtration, precipitation, and adsorption.

4.1 Dead-end filtration

Dead-end filtration is normally used to filter liquids that contain suspended material, precipitates, or other nondissolved particulates using filters or filter cloths with mesh sizes larger than 10 µm [53]. Dead-end filtration has been used to separate fruit juices from pulp [54] and treat waste water, but it is also applied in the pulping industry, in which pulp is separated from liquors. Another application is the separation of acid-precipitated Kraft lignin from black liquor [55]. This technique was used in Paper I as a pretreatment before membrane filtration. Dead-end filtration is a filtration mode in which the feed is directed vertically to the filter without any circulation (see Figure 4.1).

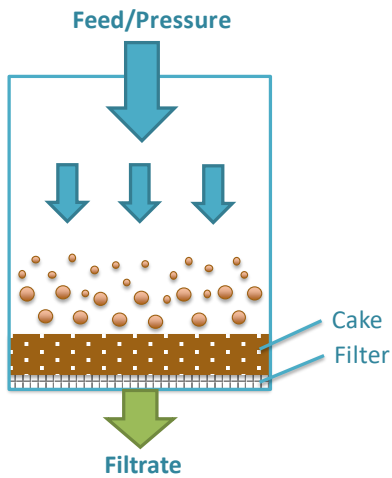


Figure 4.1: Basic principles of dead-end filtration

Nondissolved components are retained on the filter and begin to form a cake, while the solution, with the solutes, passes through (termed the filtrate). As the amount of feed increases, so, too, does the thickness of the filter cake and, consequently, the cake resistance and, with it, the filtrate flow and purity. For solutions that are difficult to filter (high filter cake resistance and low filtrate flow), a filter aid, such as diatomaceous earth, can be mixed with the solution prior to filtration. The

resulting cake will have lower compressibility and thus less resistance to the flow of filtrate. Diatomaceous earth can also aid in the removal of particulates that are smaller than the filter pore size and gel-forming substances that could cause problems in the membrane filtration [56]. Diatomaceous earth (kieselguhr) was used as a filter aid during the dead-end filtration of SSL in Paper I to study the influence of nondissolved substances in the liquor on the impending ultrafiltration process.

4.2 Membrane filtration

Membrane filtration is closely related to conventional filtration, which was discussed in Section 4.1. The largest difference between them concerns the filter medium, which, for the former, is made from a semipermeable membrane of various materials that can mechanically and chemically sieve solutes and nondissolved substances [57]. A membrane is usually classified as a microfiltration (MF), ultrafiltration (UF), nanofiltration (NF), or reverse osmosis (RO) unit, the difference being the size or cutoff at which the membrane can reject particles and solutes. The boundaries between these processes are not fixed, and they often overlap, as seen in Figure 4.2.

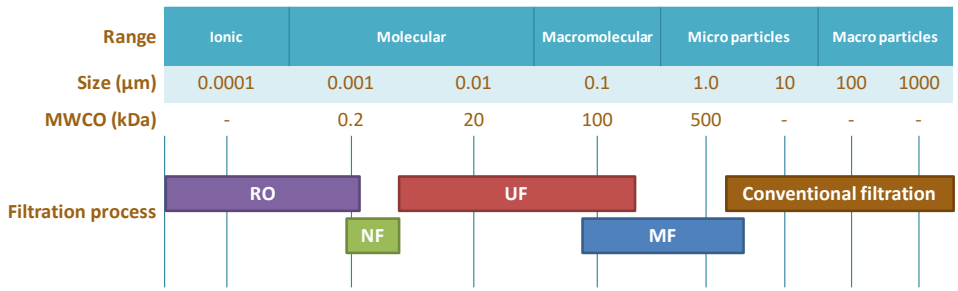


Figure 4.2: Classification of filtration processes. Adapted from Graff [58].

Typical applications for these pressure-driven membrane processes are the removal of cells and other microorganisms (MF), the recovery of proteins and polysaccharides (UF), the removal of monosaccharides and multivalent ions (NF), and desalination (RO) [58]. However, these processes have also gained popularity in the biorefinery industry for their highly selective separation capabilities, lack of chemicals, and low energy requirements.

4.2.1 Fundamentals of cross-flow membrane filtration

Pressure-driven membrane filtration can be performed using dead-end or cross-flow filtration, the former of which was discussed in Section 4.1 and the latter of which is the most commonly used mode of operation. Cross-flow filtration employs a feed flow that is tangential to the membrane surface and thus averts the immediate build-up of a cake (see Figure 4.3).

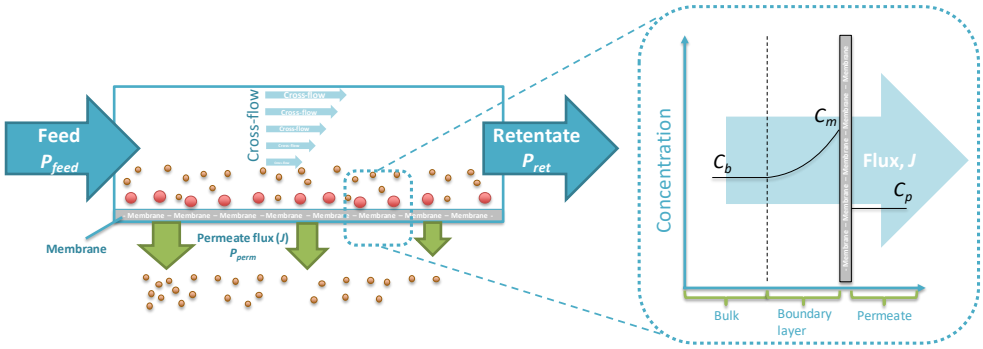


Figure 4.3: Illustration of the basic principles of cross-flow membrane filtration. The close-up at the membrane surface depicts the retention capabilities capacity of the membrane. c_b is the concentration in the bulk solution, c_m is the concentration at the membrane surface, and c_p is the concentration in the permeate.

The filtrate is called the permeate, and the outgoing feed flow (concentrate) is referred to as the retentate. The driving force in this type of setup is the difference in pressure across the membrane (transmembrane pressure, TMP). Due to the drop in pressure in the feed channel, the average of the feed and retentate pressures is used to calculate the transmembrane pressure, per Equation 4.1.

$$TMP = \left(\frac{P_{feed} - P_{ret}}{2}\right) - P_{perm} \tag{4.1}$$

One of the most important parameters in membrane filtration processes is permeate flow (flux). This flux is defined as the volumetric flow of permeate per unit area of the membrane (L/m^2h), and for a pure solvent system, it correlates linearly with the transmembrane pressure, as seen in Equation 4.2.

$$J = \frac{TMP}{\mu R_m} \tag{4.2}$$

When the solvent is water, the flux is called the pure water flux (PWF) and is often used to characterize the membrane and monitor membrane fouling [59], by

calculating the membrane resistance (R_m) before and after filtration, wherein an increase indicates a rise in membrane fouling. If the solvent system contains 1 or more solutes that are retained by the membrane, the concentration of the solutes will be higher in the boundary layer and at the membrane surface (c_m) compared with the bulk solution (c_b). This phenomenon is called concentration polarization and is driven by the convective transport of solutes to the membrane surface and counterbalanced by the diffusion of solutes back to the bulk (see Figure 4.3). Concentration polarization has a major impact on the extent of permeate flux and can be described mathematically by the film model [60], as shown in Equation 4.3:

$$J = k \ln\left(\frac{c_m - c_p}{c_b - c_p}\right) \tag{4.3}$$

where k is the mass transfer coefficient that describes the diffusion of solutes from the membrane surface to bulk solution. The mass transfer coefficient is dependent on the operating conditions of the filtration and changes in parameters, such as temperature, cross-flow velocity (CFV), density, and viscosity of the solution.

Concentration polarization is one of the major flux-reducing effects that are experienced in membrane filtration. Other flux-reducing effects that have been observed are osmotic pressure, cake/gel formation, and adsorption to the membrane surface and in the pores [59]. The osmotic pressure ($\Delta\pi$) acts on the system by decreasing the effective driving force (transmembrane pressure), as seen in Equation 4.4.

$$J = \frac{TMP - \Delta\pi}{\mu(R_m + R_{cp} + R_c + R_a)} \tag{4.4}$$

This effect is common for systems that use NF and RO membranes and less frequent for MF and UF membranes. Equation 4.4 is called the resistance-in-series model and collectively describes the various types of resistance that occur during filtration. The flux-reducing phenomenon is added to the hydraulic membrane resistance (R_m) to account for the decline in flux. The same model can be used to describe reversible and irreversible fouling, which is presented in Section 4.2.3.

The other important membrane filtration parameter is the retention. High retention is often desired if the product is in the retentate but unwanted when it is in the permeate. The retention, or true retention (R_{true}), is defined per Equation 4.5.

$$R_{true} = 1 - \frac{c_p}{c_m} \quad (4.5)$$

R_{true} relates the concentration in the permeate to that on the membrane surface. True retention is considered a membrane/solute property and is usually constant at low permeate flux [61]. However, measuring the concentration at the membrane surface is not trivial, and true retention is therefore replaced by observed retention (R_{obs}), which uses bulk concentration instead (Equation 4.6):

$$R_{obs} = 1 - \frac{c_p}{c_b} \quad (4.6)$$

4.2.2 Operating conditions

4.2.2.1 Parameter study

The operating conditions of a filtration system are usually determined with a parameter study. The study can be performed using several methods [62]; however, in this thesis and Papers I-VI, the following method was used:

The highest cross-flow velocity is set, followed by the lowest transmembrane pressure, to minimize the risk of fouling. The transmembrane pressure is gradually increased, and the flux-versus-TMP graph is drawn, as seen in Figure 4.4. The flux increases linearly at low TMP, because the flux-reducing effects are not as pronounced (per Equation 4.4), but begins deviating at a point, called the critical flux. After the critical flux, the rate at which the flux rises decreases, eventually leveling off and becoming independent of the TMP. This point is called the limiting flux and is caused by the formation of a cake or gel on the membrane surface as a result of saturation of the solutes due to convective transport to the membrane surface.

The critical and limiting fluxes are dependent on the CFV of the system, as seen in Figure 4.4. An increasing CFV will shift the fluxes to higher values as a result of rising shear forces, in turn limiting the formation of a cake or gel but also decreasing the boundary layer thickness, which will increase the mass transfer coefficient and consequently the flux (per Equation 4.3). These fluxes are seen primarily in MF and UF applications and rarely in NF and RO systems, because the flux-reducing effects mostly pronounced in the latter systems are attributed to the increases in osmotic pressure [63].

For economic reasons, a high flux is always desired in membrane processes. However, running the process at the highest possible flux (the limiting flux) could

increase fouling. Thus, processes are more commonly run at or near the critical flux [64], as done in Papers I, IV, V, and VI. In certain applications, it could be beneficial to use the concept of threshold flux—the flux that lies between the critical flux and the sustainable flux (the flux at which minimal fouling occurs), dividing the low- and high-fouling regions. However, determining the threshold flux and sustainable flux is time-consuming, although it could be important economically.

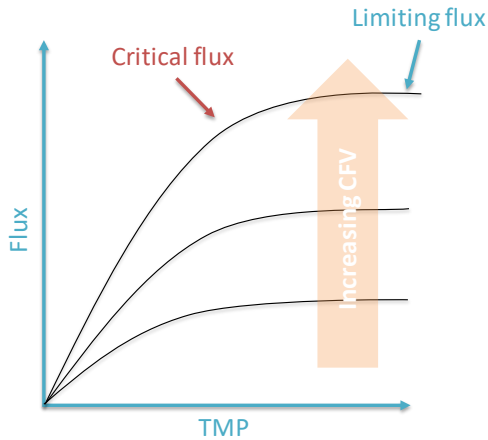


Figure 4.4: Illustration of the relationship between flux, transmembrane pressure, and cross-flow velocity. Shown is a typical set of curves obtained during a parameter study.

4.2.2.2 Concentration study

When determining the optimal operating conditions, the retentate and permeate are circulated back to the feed tank to keep the concentration constant in the system. However, the goal of membrane systems is usually to concentrate a solution that contains the product solute but also other impurities. A membrane is chosen to minimize fouling and to realize high selectivity toward the separation of the product from impurities. This can be achieved in a batch system, in which the feed and retentate are circulated back while the permeate is bled, as seen in Figure 4.5. This setup is a common configuration with a feed pump and circulation pump. The feed pump compensates for the bled permeate—the retentate—and sets the pressure in the system. The circulation pump compensates for the loss of pressure over the membrane module and sets the CFV in the system. Assuming that the observed retention (henceforth termed retention) is constant, for a batch system, the concentration of solutes in the retentate changes, per Equation 4.7 [65]:

$$C_R = C_0 \left(\frac{1}{1-VR}\right)^R \tag{4.7}$$

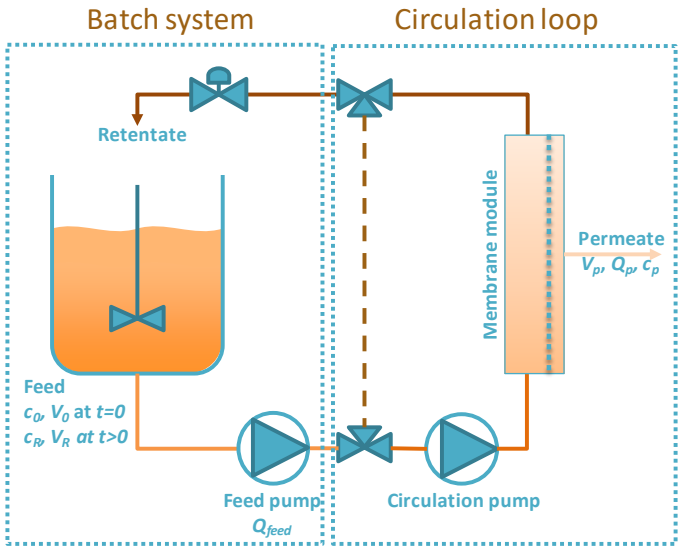


Figure 4.5: Illustration of common membrane filtration setups.

where C_0 is the initial concentration, C_R is the concentration in the retentate, and R is the retention of the solute. VR is the volume reduction and is defined per Equation 4.8.

$$VR = \frac{V_p}{V_0} \tag{4.8}$$

Volume reduction is a measure of the accumulative amount of permeate that is removed in relation to the start volume of the feed and is used to monitor the progress of batch filtration. In such cases as continuous filtration and when the feed pump flow is on the same order of magnitude as the permeate flow, loop volume reduction (VR_{loop}) could be an important parameter to track the progress of filtration. Loop VR is the VR of each circulation loop (in a continuous system) or a single circulation loop (Figure 4.5) and is defined by Equation 4.9.

$$VR_{loop} = \frac{Q_p}{Q_{feed}} \tag{4.9}$$

Equation 4.9 shows that if the feed pump flow (Q_{feed}) is low compared with the permeate flow (Q_p), the VR of the loop could be higher than the VR of the system (Equation 4.8), which would lead to a flux that is lower than expected for a batch process. This phenomenon was observed in Paper V and is explained further in Chapter 7.

4.2.3 Fouling and cleaning

4.2.3.1 Flux reduction

Flux reduction can be described using two phenomena. The first is concentration polarization, which is a natural consequence of the selectivity of membranes toward solutes [59]. The other is fouling and can be divided into several forms, as shown in the following list:

- **Adsorption:** Adsorption occurs when there is a chemical or physical interaction between the solutes and membrane. The solutes can adsorb to the membrane surface or to the pores if they are smaller than the pore size. This action will decrease the pore size, in turn lowering the flux as a consequence of the increasing resistance of adsorption (R_a), as seen in Equation 4.4.
- **Pore plugging:** When the particles in solution are slightly larger than or equal to the pore size of the membrane, pore plugging, or partial blocking, can occur, decreasing the transport or flux through the membrane.
- **Cake formation:** A cake can form on the membrane surface if the concentration of solutes exceeds the maximum solubility concentration, which can occur due to concentration polarization. Also, if the solution contains undissolved particulates, they can deposit on the membrane surface and form a cake.
- **Gel formation:** For certain molecules with gelation properties, their increase in concentration near the membrane surface (concentration polarization) can affect the formation of a gel layer that in turn affects the flux and retention of the solutes.

These various forms of fouling can be studied, for example, by changing the operating conditions and feed solutions and fitting the data to Equations 4.3 and 4.4. However, practically speaking, the terms ‘reversible’ and ‘irreversible fouling’ are simpler when monitoring the process [59]. Equation 4.4 can be rewritten to include the aforementioned resistance values, as seen in Equation 4.10.

$$J = \frac{TMP - \Delta\pi}{\mu(R_m + R_{rev} + R_{irrev})} \tag{4.10}$$

The hydraulic resistance of the membrane (R_m) can be determined prior to using the process solution, wherein other resistances are equal to zero. During operation with the process solution, the sum of the 3 resistances (Equation 4.10) will act on the membrane and influence the flux and retention. Reversible fouling (R_{rev}) is defined as the resistance that acts on the membrane during operation and is equal to zero when switching to pure water. Irreversible fouling (R_{irrev}) is deposition that is removable or difficult to remove using a cleaning sequence. This method was used to monitor membrane fouling in the pilot study in Paper V. However, the method only defines fouling as reversible or irreversible. The type of fouling and its underlying mechanisms cannot be distinguished, based on the results.

Hermia [66] proposed a combined blocking filtration law to describe fouling mechanisms during quasi-steady-state constant pressure filtration. The model is applicable to dead-end filtration using MF and UF membranes but also the initial time of a cross-flow filtration process [67]. The model is defined in Equation 4.11:

$$\frac{d^2t}{dV^2} = \alpha\left(\frac{dt}{dV}\right)^{\beta} \tag{4.11}$$

where α and β are values that depend on the type of fouling that occurs during filtration, as defined in Table 4.1.

Table 4.1: Description of the blocking mechanism variables α and β. K_A, K_B, and K_C describe the reduction in membrane area due to the various mechanisms. u_0 is the mean velocity through the membrane, A_0 is the membrane area, and R_r is the cake resistance.

Blocking mechanism	**α**	**β**
Complete	$K_A u_0$	2
Standard	$(2K_B/A_0^{1/2})u_0^{1/2}$	1.5
Intermediate	K_A/A_0	1
Cake	$(R_r K_C/A_0^2)u_0^{-1}$	0

Hermia [66] divided the blocking mechanisms into 4 types. The first is complete blockage, which occurs when every particle that arrives at the membrane surface blocks a pore ($\beta = 2$) (see Figure 4.6). If the particles adsorb instead to the inner surface of the pores and thus decrease the pore radius, the mechanism is called standard blocking ($\beta = 1.5$). Intermediate blocking occurs when the particles block a pore or deposit themselves onto other particles ($\beta = 1$). Cake filtration ($\beta = 0$) begins when the membrane surface is completely blocked and the particles deposit themselves solely onto other particles. Hermia's combined blocking filtration law

was used in Paper I to describe the main type of fouling that arose during ultrafiltration of SSL with a 100 kDa MWCO membrane.

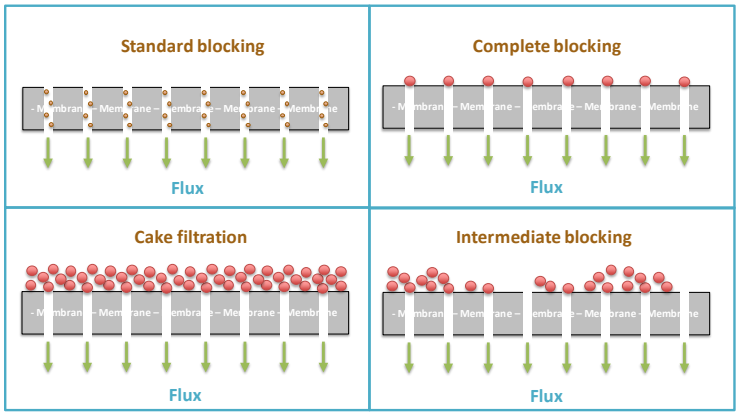


Figure 4.6: Illustration of the various fouling mechanisms.

4.3.2.2 Reduction of fouling

A reduction of fouling or an increase in flux can be achieved using direct or indirect methods [59]. A common direct method is the use of turbulence promotors, such as changing the membrane spacers to increase the shear rate at the membrane surface. This step decreases the thickness of the boundary layer and limits or prevents the build-up of a cake. Back-flushing is another method, in which the permeate flow is reversed to lift the material that has accumulated on the membrane surface for removal by the cross-flow of the feed. Rotating, vibrating, or ultrasonically enhanced membranes can also increase the flux by preventing or decreasing the build-up of a cake on the membrane surface. Changing the membrane module to a stirred cell with rotating blades near the membrane surface can also help enhance the flux. An improvement in flux was observed using a stirred cell module instead of a plate-and-frame module in Paper V.

The cleaning sequence is another important direct method, wherein the choice of cleaning agent, frequency of cleaning, and the operating conditions of the sequence can have a major influence on the resulting permeate flux. This approach was examined in Paper V, in which solely chemical cleaning agents were used.

Indirect methods include prefiltration of the solution, which was tested in Paper I, and the use of more hydrophilic membranes, as implemented in Paper IV. Other important indirect methods are the choice of operating conditions, which can

influence the long-term operation of the plant, which was studied to a limited extent in Paper V.

4.2.4 Separation of hemicellulose

The separation of hemicellulose from acidic SSL has not been published, due to the hydrolysis of the hemicellulose under such conditions. However, membrane filtration has been used successfully to separate hemicellulose from similar waste streams. Al Manasrah*, et al.* [68] used an ultrafiltration membrane with an MWCO of 5 kDa to concentrate and purify hemicellulose from a pressurized hot water extract. They achieved a purity of 63% and a recovery of 70% at a VR of 86%. Diafiltration purified the hemicellulose further by removing the monosaccharides and part of the xylan. However, the separation of hemicelluloses from the lignin was unsuccessful due to the narrow distribution of MWs.

Persson and Jönsson [69] used three ultrafiltration membranes to isolate hemicelluloses from thermomechanical process water. They achieved hemicellulose retentions higher than 90% with the ETNA10 and UFX5 membranes, both of which could be operated at high flux. UFX5 had the benefit of tolerating high temperatures, which is an advantage, given that the temperature of the process water was 75°C to 85°C. The UFX5 had a greater tendency toward fouling compared with the ETNA10, indicating that more frequent cleaning is required if the UFX5 were to be used in a large-scale plant.

Egüés*, et al.* [70] showed that it is possible to separate hemicelluloses from acidic solutions, as well. They used three ultrafiltration membranes to separate hemicellulose from weakly acidic (pH of approximately 4 and 5) corn waste autohydrolysis liquor, reporting that a 10 kDa MWCO membrane yielded the highest concentration of hemicellulose in the retentate and low concentrations of low-MW compounds and inorganics.

Other similar studies with SSL have focused on separating lignosulfonates from the solution, most of the other components in which have been monosaccharides and other inorganics [71-73]. Thuvander and Jönsson [74] used a 2-stage membrane filtration process to recover hemicelluloses from thermomechanical process water. Microfiltration was used in the first stage to remove larger contaminants. An ultrafiltration stage was applied thereafter to concentrate the hemicellulose. The 2-stage process increased the flux from 90 to over 200 L/m^2h. The recovery of hemicellulose during the microfiltration was high, because a pore size that was larger than 0.1 µm was used. Membrane filtration can thus be used as a pretreatment step prior to the main concentration and purification step.

Krawczyk, et al. [56] used microfiltration and dead-end filtration as a pretreatment step before the ultrafiltration to increase the flux and reduce fouling [75,76]. Microfiltration gave the best results with regard to flux. However, 96% of

hemicelluloses were also removed during this pretreatment step. The hemicelluloses were smaller than the microfiltration pores, the removal of which could only be explained by the formation of a gel layer on the membrane surface that increased the retention of solutes. Conventional filtration and dead-end filtration increase flux with virtually no loss of hemicelluloses. These prefiltration methods were used in Paper I to study the influence of prefiltration on the flux, retention, and fouling of ultrafiltration membranes.

4.3 Precipitation

Precipitation is the process by which a dissolved substance comes out of solution as a solid. It is often used to concentrate and purify various types of proteins, nucleic acids, and other cell components [77]. This process also separates biomass components, such as hemicellulose and lignin (Paper II). Precipitation is achieved by the addition of a reagent that alters the solubility of the product and renders it insoluble in solution. The solid (product) is then separated from the solution by centrifugation or conventional filtration, as illustrated in Figure 4.7.

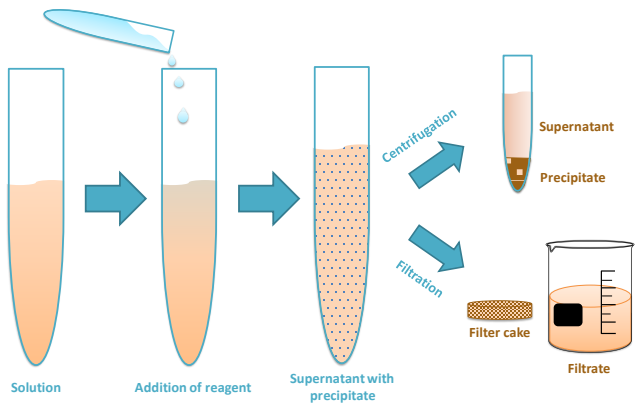


Figure 4.7: Illustration of lab-scale precipitation using centrifugation or conventional filtration for the final separation of the precipitate from the supernatant.

The solubility of a compound depends on many factors, such as pH, temperature, solvent polarity (measured indirectly as the dielectric constant or relative permittivity), ionic strength, and the ability of the solvent to form hydration layers [78]. Macromolecules, such as hemicelluloses, lignin (including lignosulfonates), and proteins are solubilized in solution as a result of having a stable conformation and being surrounded by hydration layers, as seen in Figure 4.8.

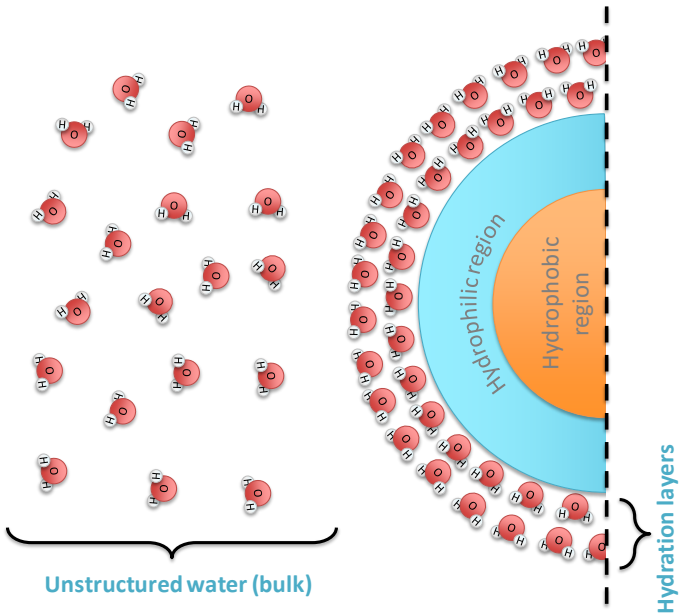


Figure 4.8: Illustration of the hydration layers and the "free" water surrounding a macromolecule. The macromolecule has a stable conformation, wherein the hydrophobic region point inward and the hydrophilic region points in the direction of the water (bulk). This type of conformation is seen in proteins, but lignosulfonates have also been shown to undergo the same conformational changes [79,80].

The hydration layers result from the attraction between the hydrophilic region of the macromolecule and the water molecules in the bulk solution. These highly ordered layers reduce the intramolecular and intermolecular attractions, enhancing the solubility of the solutes [81]. In the case of polysaccharides, the attractions that lead to solvation are primarily between hydroxyl groups and water. However, for solutes with a higher net charge, such as lignosulfonates, the solubility is often higher as a result of the strong association with water molecules and the electrostatic repulsion from other charged molecules [79].

Solutes can be precipitated if the hydration layers are disrupted, the net charge of the solutes changes, or another solute or solvent that promotes precipitation is added. By increasing the solvent's ionic strength, solutes can be precipitated as a consequence of the decreased availability of "free" water for formation of the hydration layer. This phenomenon is commonly called *salting out* and has been used to precipitate hemicellulose, Kraft lignin, and lignosulfonates [4,80]. In another study [82], Kraft lignin was precipitated by decreasing the pH of the solution (black liquor). The decrease in pH increased the protonation of the phenolic groups, which lowered the electrostatic repulsion between lignin molecules, resulting in lower hydrophilicity and solubility. Precipitation can also occur if the overall polarity of the solvent changes. For aqueous solutions, the addition of miscible organic

solvents, such as alcohols, will decrease the dielectric constant of the solution and destabilize the hydration layer around the solutes.

Organic solvents (antisolvents) have been used to precipitate hemicelluloses, lignin, and lignosulfonates (Paper II) [71,83-85]. Song, et al. [83] used ethanol as an antisolvent to precipitate hemicelluloses from spruce hot water extractives. The precipitate contained solely polysaccharides with an MW higher than 4 kDa, a high purity, and a yield of 78%. One disadvantage of using this antisolvent was the high ethanol concentration that was required for precipitation (90%). Zasadowski, et al. [84] used three organic solvents with varying dielectric constants to precipitate hemicelluloses from thermomechanical process water. The highest yield of hemicelluloses was 77% at an antisolvent concentration of approximately 55%. The reason for the lower antisolvent consumption was the use of acetone, which has a lower dielectric constant (~lower polarity). It was also proposed that the precipitation efficiency correlated with the dielectric constant of the bulk solution. However, no detailed results were reported. The GGM that precipitated at low antisolvent concentration (high MW) had an unusually high galactose content. The group, however, did not determine the composition of this fraction.

Duval, et al. [71] used antisolvent precipitation with ethanol to fractionate commercial ammonium lignosulfonates. The precipitated fractions had high polydispersity and a clear trend of decreasing MW with higher ethanol concentrations. The lowest-MW lignosulfonates also had the highest degree of sulfonation, which explains the high solubility and high ethanol concentration that was required for precipitation. Tarasov, et al. [85] used antisolvent precipitation to isolate lignosulfonates from spent liquor from a neutral sulfite semichemical pulping process. They concluded that acetone and isopropyl alcohol were the most efficient antisolvents in terms of consumption. Fractions from the precipitation using ethanol had a higher MW and higher charge density, which are notable properties in certain applications. However, acetone and isopropyl alcohol have low boiling points and are cheaper (energy-wise) to separate and recover from the supernatant compared with ethanol. Based on these findings, methanol, ethanol, and acetone were chosen for the study in Paper II.

4.4 Adsorption

4.4.1 Fundamentals

Adsorption is the collection of components in a liquid or gas onto a solid surface [86]. This process is used to separate or remove components from liquids or gases and is useful for treating waste water or recovering valuable components from various feed streams. In adsorption, the component or solute is called the adsorbate, and the solid onto which the adsorption occurs is termed the adsorbent. The affinity of a solute to a solid surface depends on several factors, such as the size, shape, concentration, and polarity of the solute and the temperature of the system. The adsorption can be physical (physisorption), wherein the forces are weak Van der Waals or hydrophobic interactions, or chemical (chemisorption), in which covalent bonding is imminent. However, the underlying mechanism for adsorption is not always clear, and a mixture of physisorption and chemisorption can occur. The driving force for adsorption is a favorable free energy (ΔG), which must be negative, as seen from Equation 4.12.

$$\Delta G = \Delta H - T\Delta S \tag{4.12}$$

The adsorption of a substance corresponds to the reduction in free movement of the particles, which is thermodynamically equal to the reduction in the system's entropy (ΔS) [87]. Consequently, an adsorption process must be exothermic (negative ΔH) to such an extent that the magnitude of the enthalpy is higher than the negative product of the temperature and entropy. It is important that the bonding energy be sufficiently high for the adsorption to occur but low enough for desorption (removal of adsorbates) and regeneration of the adsorbent [88].

When an adsorbent is placed in a solution that contains adsorbates, the solutes will be transported to the adsorbent until saturation or until an equilibrium is reached between the liquid and solid phases [89]. The adsorption capacity at equilibrium is expressed as the amount of adsorbate that has adsorbed onto the adsorbent per weight of adsorbent (q_e), as seen in Equation 4.13:

$$q_e = \frac{(C_0 - C_e)V}{W} \tag{4.13}$$

where C_0 is the initial adsorbate concentration, C_e is the concentration in the bulk at equilibrium, V is the volume of the liquid, and W is the weight of adsorbent. The

equilibrium at constant temperature is characterized by expressing the adsorption capacity as a function of a varying solute concentration, resulting in an adsorption isotherm. The simplest type of adsorption isotherm is linear, as seen in Equation 4.14.

$$q_e = K_{lin} C_e \tag{4.14}$$

This equation predicts a linear relationship between the adsorption capacity at equilibrium and the solute concentration, with the equilibrium constant (K_{lin}) as the slope. This linear relationship is applicable for systems in which the solutions are diluted and the adsorbent has a homogeneous surface. However, for most systems, the relationship is nonlinear and follows 1 of 6 types of isotherm curves, as seen in Figure 4.9.

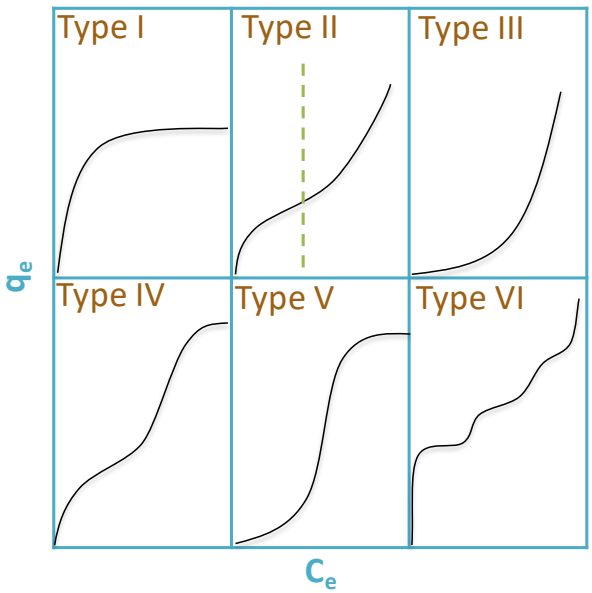


Figure 4.9: The six types of adsorption isotherms, classified per Moises [89]

The *Type I* curve follows a Langmuir-type of adsorption (favorable), in which the solutes adsorb onto a single layer, after which a saturation plateau is reached when all of the adsorption sites are occupied [87]. *Type II* is normally obtained with nonporous or macroporous adsorbents. The curve shows a transition from monolayer (complete coverage) to multilayer adsorption, as highlighted by the

dashed green line in Figure 4.9 [90]. The *Type III* curve is considered to be unfavorable due to the slow rise at low concentrations, which indicates poor adsorbent-adsorbate interactions. The fourth curve (*Type IV*) is common in mesoporous adsorbents. The first part of the curve follows a *Type II* isotherm, which indicates monolayer to multilayer coverage, followed by capillary condensation in the mesopores. The *Type V* curve has a similar trend as *Type III* at low concentrations, which indicates an unfavorable equilibrium, followed by a sharp rise in adsorptive capacity. This trend is indicative of cooperative adsorption, in which the adsorption of solute is inhibited by a competing reaction [90]. The last isotherm (*Type VI*) shows multilayer adsorption with several partial saturation points [91].

4.4.1.1 Adsorption isotherms

The various types of curves can be described by isotherm models, as seen in Table 4.2, which shows several common models. The Langmuir isotherm (Table 4.2), for instance, can be used to describe the *Type I* curve. This model assumes monolayer adsorption and a uniform surface in terms of energy of adsorption and that the adsorbates do not interact with each other or migrate on the adsorbent surface. Although the Langmuir model is applicable to many adsorption systems, other models are required for certain applications.

Table 4.2: Common adsorption isotherms for modeling nonlinear equilibria.

Model	Equation	Ref.
Langmuir	$q_e = \frac{Q_L K_L C_e}{1+K_L C_e}$	[92]
Freundlich	$q_e = K_F C_e^{n_F}$	[93]
Sips (Langmuir-Freundlich)	$q_e = \frac{Q_S K_S C_e^{n_S}}{1+K_S C_e^{n_S}}$	[90]
Modified Brunauer–Emmett–Teller (BET)	$q_e = \frac{Q_B K_B C_e}{(C_S - C_e)(1+(K_B-1)(C_e/C_s))}$	[94]

The Freundlich isotherm is a purely empirical model that was derived to consider the heterogeneity of an adsorbent. This isotherm lacks the linear region at low concentrations and the limiting or maximum adsorption capacity (Q_L, Q_S, Q_B) term that are seen in the other isotherms (Table 4.2). The Langmuir and Freundlich isotherms fail to describe the S-type of curves in Figure 4.9 (*Types II, IV,* and *V*).

The Sips isotherm was derived to compensate for the failures of the aforementioned models. Sips isotherms combine the Langmuir and Freundlich isotherms to yield a

model that has the same assumptions as Langmuir but with the addition of the parameter n_S, which is characteristic of the heterogeneity of the system. The Sips model has been used to describe *Type V* curves but can be used for other types as well [90].

The BET isotherm is used for homogeneous multilayer adsorption with no limitations on the number of layers. This model also allows for the adsorbents to act as an adsorption site for the next adsorbent and generates *Type II* isotherms. These isotherms were used in the analysis of the data in Paper VI.

4.4.1.2 Adsorption kinetics

Equilibrium isotherms are important when designing an adsorption system. Another important parameter is the adsorption kinetics. The kinetics of the adsorption describes the rate of the interaction between adsorbent and adsorbate. Pseudo-first-order (PFO), pseudo-second-order (PSO), Elovich, and intra-particle diffusion (IPD) models (Table 4.3) are common models that can be used to describe the interaction of the solute with an adsorbent [95].

Table 4.3: Common adsorption kinetic models

Model	Equations (linear form)	Ref.
Pseudo-first-order (PFO)	$\ln(q_e - q_t) = \ln(q_e) - k_1 t$	[96]
Pseudo-second-order (PSO)	$\frac{1}{(q_e - q_t)} = \frac{1}{q_e} + k_2 t$	[96]
Elovich	$q_t = \frac{1}{\beta}\ln(\alpha\beta) + \frac{1}{\beta}\ln(t)$	[96]
Intra-particle diffusion (IPD)	$q_t = k_p\sqrt{(t)} + m$	[95]

The PFO model describes adsorption as a first-order mechanism with the first-order rate constant, k_1. The rate constant decreases with increased adsorbent particle size and rises with declines in initial solute concentration [95,97]. This model is often modified to account for various adsorption regimes, such as in the low- and high-concentration regimes. The PSO model can be used to describe a second-order adsorption mechanism. The second-order rate constant (k_2) follows the same trend as the first-order rate constant when changing experimental conditions [98]. However, the calculated adsorption capacity at equilibrium (q_e) more closely approximates the experimental value when using the PSO equation.

The downside of using the PFO and PSO models is that no information on the initial adsorption rate and diffusion mechanisms can be obtained. This information can be acquired using the Elovich and IPD equations in Table 4.3. The Elovich model can give such information as the initial adsorption rate (α) and desorption constant (β). The IPD model can describe the transport phenomenon (film, surface, or pore diffusion) and the rate-limiting step during adsorption. These models were used to describe the adsorption kinetics of SSL lignosulfonates on resins in Paper VI.

4.4.2 Separation of biomass components

Adsorption processes for the separation of biomass components have been applied primarily for the separation of various forms of extractives and lignin. Hemicellulose has been separated and fractionated using anion-exchange, but the hemicellulose was acidic (charged), rendering separation using anion-exchange chromatography possible [99].

The purification of hemicellulose can still be achieved using adsorption to remove the extractives and lignin [100-106]. Nitzsche, et al. [101] used polymeric resins (XAD7HP and SEPABEADS SP700) to remove lignin from beech wood hydrolysate. The removal of lignin was complete, with an approximately 8% loss of hemicellulose. Schwartz and Lawoko [102] and Narron, et al. [105] used hydrophobic polymeric resins to remove acid-soluble lignin from several hydrolysates, eliminating over 90% of the lignin and concluding that the loss of hemicellulose was coupled to the existence of LCCs. Hydrophobic resins can also remove lignosulfonates, as shown by Sumerskii, et al. [103].

Anion-exchange adsorption resins are perhaps more notable, in that they can exploit the sulfonic acid groups on the lignin for selective removal. This method has been presented by Van Blaricom and Russell [107], who removed ammonium lignosulfonates from SSL using weak- and strong-base anion-exchange resins. Weakly basic anion-exchange resins were preferred, because the regeneration of resin was more efficient compared with the strongly basic resins. Liu*, et al.* [108] used weakly basic ion exchangers to separate magnesium lignosulfonates from oligosaccharides. The recovery of lignosulfonates reached 98%, with a yield of oligosaccharides of 93%. Hydrophobic, weakly basic anion, and strongly basic anion-exchangers were used in the screening study in Paper VI.

4.5 Other methods

Another method that can be used to separate biomass components is size-exclusion chromatography (SEC). The method utilizes the difference in size between components and is a promising alternative to such methods as adsorption.

Lundqvist, *et al.* [109] used SEC to fractionate oligo- and polymeric galactoglucomannan from a filtered spruce microwave heat fractionation extract. The collected fractions were reported to be free of UV-absorbing substances, indicating that the extracts were free of lignin. This outcome is not always obtained using other process waters, wherein the presence of other components, such as lignin and LCCs, can create problems with fractionation by SEC (Paper IV).

5. Materials and methods

This chapter contains a brief description of the equipment, chemicals and analytical and experimental methods that are used in this thesis. For a more detailed description, see Papers I to VI.

5.1 Experimental equipment

5.1.1 Membranes

The membranes in Papers I to VI are presented in Table 5.1. Most of the membranes have a polypropylene support material and can withstand pressures of up to 10 bar. The maximum operating temperature is 55–60°C for the hydrophilic membranes, which is why all of the experiments were performed at 50°C.

Table 5.1: List of the membranes used in this thesis. The materials are polysulfone (PS) and regenerated cellulose (RC). MWCOs are in kDa, and pore size (MF) is in µm.

Manufacturer	Designation	Material	Hydrophilicity	Type – MWCO	Max temp. (°C)	pH range	Pressure (bar)
Alfa Laval Nordic A/S	GR60PP	PS	Hydrophobic	UF – 25	75	1-13	1-10
	GR51PP	PS	Hydrophobic	UF – 50	75	1-13	1-10
	GR40PP	PS	Hydrophobic	UF – 100	75	1-13	1-10
	RC70PP	RC	Hydrophilic	UF – 10	60	1-10	1-10
	MFG2	PS	Hydrophobic	MF – 0.2	75	1.5-12	1-3
Microdyn-Nadir GmbH	C30F	RC	Hydrophilic	UF – 30	55[a]	2-11[a]	-
	C20F	RC	Hydrophilic	UF – 20	55[a]	2-11[a]	-
	C5F	RC	Hydrophilic	UF – 5	55[a]	2-11[a]	-
EMD Millipore Co.	Ultracel	RC	Hydrophilic	UF – 1	80	2-10	>5
	PLCAC						

[a] These data are from a similar membrane produced by Microdyn-Nadir GmbH.

5.1.2 Lab-scale membrane filtration

The screening (parameter study) and concentration studies were performed with the membrane filtration equipment in Figure 5.1. The stirred cell module (Figure 5.1a) was used for the concentration and diafiltration studies. The setup consisted of a 400-mL vessel with a 5-cm magnetic rod and was heated on a plate (MR2002, Heidolph Instruments GmbH & Co.KG, Schwabach, Germany), from which the CFV was set, as well. The pressure was set using nitrogen gas and monitored with a pressure gauge (DCS40.0AR, Trafag AG, Bubikon, Switzerland). The permeate flow or flux (3217 mm^2 membrane area) was measured with a scale (PL6001-I, Mettler Toledo Inc., Ohio, USA) that was connected to a PC that ran LabView (National Instruments Co., Austin, Texas, USA).

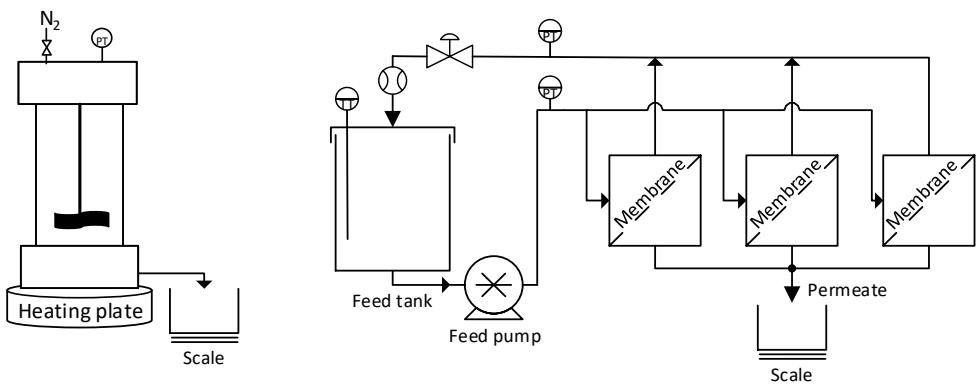


Figure 5.1: Illustration of the lab-scale membrane filtration equipment used in this thesis (adapted from Paper I).

The multimodule equipment (Figure 5.1b) was used to simultaneously screen 3 membranes. A 15-L tank was used as a vessel for the feed/retentate, which was circulated using a feed pump (Hydra-cell D25XL, Wanner, Minneapolis, USA). The pump was thus used to set the pressure in the system (by adjusting the retentate valve) and the CFV. The CFV was monitored with a flow meter (FCH-34-PP-Chemical, B.I.O-TECH e.K., Vilshofen, Germany), and the pressure and flux were tracked using the same method and equipment as with the stirred cell module. The temperature was controlled using an immersion heater (Backer, Elektro-Värme AB, Sösdala, Sweden) that was dipped in the feed tank and regulated with a controller (Model MCM, Shinko Technos Co. Ltd, Osaka, Japan). For a more detailed description of the methods, see Papers I and IV.

5.1.3 Pilot-scale membrane filtration

The setup for the pilot studies in Paper V was based on the Alfa Laval Combi M39 unit (Alfa Laval A/S, Søborg, Denmark), as shown in Figure 5.2. It consisted of a plate-and-frame membrane module with a total membrane area of 1 m^2, a circulation pump, cleaning tank, and inline heat-exchanger. The setup was equipped with a feed pump (DME375 – 10AR, Grundfos Water Treatment GmbH, Pfinztal, Germany), pressure transmitters (DCS40.0AR, Trafag AG, Bubikon, Switzerland), and permeate flow meters (FCH-m-PP, B.I.O-TECH e.K., Vilshofen, Germany). The SSL (150°C) was removed via a heat-exchanger that was connected to cold water (< 10°C), prefiltered through a series of meshes (180, 70, and 40 µm), and ultimately stored in a buffer tank for less than 36 hours before use. For more details on these studies, see Paper V.

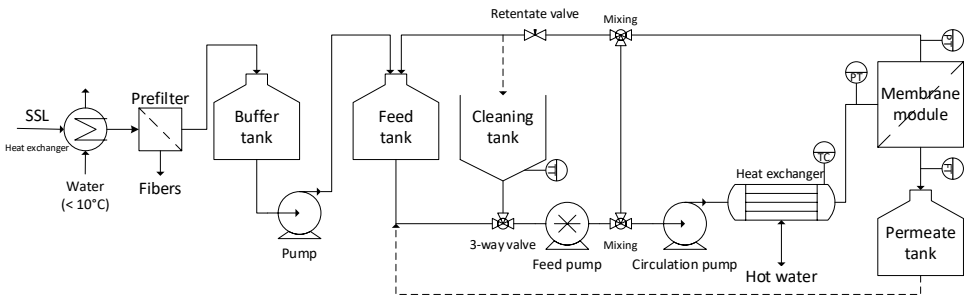


Figure 5.2: Flowsheet of the pilot-scale setup used in Paper V.

5.1.4 Batch antisolvent precipitation

Antisolvent precipitation was performed on a lab scale with 15-mL test tubes. The amount of SSL was 1 mL in all samples. The pH was adjusted using 50% sodium hydroxide solution (Merck KGaA, Darmstadt, Germany) prior to the addition of antisolvent. The concentration of antisolvent was varied by adding several amounts to the samples. The antisolvents were acetone (Merck KGaA, Darmstadt, Germany), ethanol (Altin Corp., Rajamäki, Finland), and methanol (Merck KGaA, Darmstadt, Germany), with concentrations exceeding 99.5%. The procedure was similar to that in Section 4.3, as shown in Figure 4.7. The samples were preheated in a water bath (when required) prior to being mixed with the antisolvent. After the antisolvent was added, the samples were mixed (MS2 Minishaker, IKA®-Werke GmbH & Co. KG, Staufen, Germany) at 2500 rpm for 5 minutes, and the precipitate was allowed to settle for 30 minutes. The samples were centrifuged (Heraeus Labofuge 200,

Thermo Fisher Scientific, Waltham, MA, USA) at 3000 rpm for 15 minutes, after which the liquid was decanted. The precipitate was washed with 5 mL antisolvent and centrifuged in another cycle. The precipitate was dried at 45°C for 48 hours before being dissolved in deionized water for further analysis.

5.1.5 Batch adsorption of lignin

The adsorbents in these studies were a strong-base anion exchanger (Amberlite IRA958, chloride form), weak-base anion exchanger (Amberlite IRA-67, free base), and hydrophobic polyaromatic resin (Amberlite XAD4, 20-60 mesh), all of which were produced by Sigma-Aldrich (Saint Louis, Missouri, USA). All adsorbents were washed 3 times with 6 parts deionized water to 1-part adsorbent and dried at 50°C for 48 hours prior to the experiments.

The screening studies were carried out by mixing an excess of adsorbent (4 g to 20 g SSL) with the SSL in an incubator (combi-H12, FINEPCR, Gyeonggi-do, South Korea) at room temperature for 24 hours. After 24 hours, the solution was separated from the adsorbent by carefully pipetting the solution and analyzed for carbohydrate and lignin content. The equilibrium studies were performed using the same method but with varying additions of adsorbent (see Paper VI).

The kinetics study was performed in a 1-L bottle with 50 g of adsorbent and 500 mL of SSL. The solution was mixed continuously with a magnetic stirrer at 100 RPM, and samples were withdrawn after each predetermined interval (Paper VI). The experiment ended when the difference in lignin concentration was minimal, which took 3 hours.

The desorption studies were conducted by adding 7 g of wet adsorbent (from the kinetics study) to 20 mL of regenerant with a different concentration of sodium chloride in each sample and a constant concentration of sodium hydroxide (Paper VI). This procedure was repeated 3 times in total.

5.2 Analytical methods

5.2.1 Raw material

The raw material in this thesis was a sodium-based SSL that was derived from the first step of a 2-step sulfite pulping process (Domsjö Fabriker, Örnsköldsvik, Sweden). The wood in the pulping process is softwood, with a mixture of spruce and pine (60% *Picea abies* and 40% *Pinus Sylvestris*) (Papers I-VI).

5.2.2 Total dry substance and ash content

Three-milliliter samples were weighed and dried at 105°C for 24 hours in an oven (Heraeus, Heraeus Holding GmbH, Hanau, Germany), after which they were cooled in a desiccator for 30 minutes, and the total dry substance (TDS) was determined from the weights. The dry samples were ashed in a furnace (B150, Nabertherm GmbH, Lilienthal, Germany) at 575°C (4 hours) or 900°C (12 hours), after which the ash content was determined after the samples were weighed (Paper V).

5.2.3 Lignin content

The lignin content was determined with on a UV-spectrophotometer (Shimadzu UV-1800, Kyoto, Japan) at 234 and 280 nm, with extinction coefficients of 31.6 L/(g cm) and 13.01 L/(g cm), respectively (Papers I and V).

5.2.4 Hemicellulose, monosugars, sugar acids, and acid-insoluble solids

Ten-milliliter samples were acid-hydrolyzed by adding 750 µl 72% sulfuric acid and autoclaving them (Systec DX 150, Wettenberg, Germany) at 121°C for 1 h. The samples were filtered to remove acid-insoluble solids and diluted with deionized water before the analysis. The filters were then dried and weighed to determine the acid-insoluble solids content. The liquid was analyzed on a high-performance anion-exchange chromatography (HPAEC) instrument, which consisted of an ICS-5000+ system (Thermo Fisher Scientific Inc., Waltham, Massachusetts, USA) that was equipped with a pulsed amperometric detector. Sugars and acids were separated on a CarboPac PA1 analytical column (Thermo Fisher Scientific Inc., Waltham, Massachusetts, USA) at 30°C. The eluent was deionized water at a flow rate of 1 mL/min with 0.5 mL/min 200 mM sodium hydroxide postcolumn addition; the sample injection volume was 10 µl. The calibration standards were L-arabinose, D-galactose, D-glucose, D-xylose, and D-mannose (Fluka Chemie AG, Buchs, Switzerland), and the hemicellulose content was determined after anhydro corrections of 0.88 for pentoses and 0.90 for hexoses (Paper IV).

5.2.5 Acetic acid and glycerol content

The degree of acetylation and glycerol content were determined by measuring acids and alcohols in the acid-hydrolyzed samples (Section 5.2.4) by high-performance liquid chromatography (HPLC). The column was an Aminex HPX-87H column (Bio-Rad, Hercules, CA, USA), run with 5 mM sulfuric acid eluent at a flow rate of 0.5 ml/min and a column temperature of 50°C (Paper II).

5.2.6 Size-exclusion chromatography

The distribution of MWs was measured by size-exclusion chromatography (SEC) using 2 systems. The Waters system (Waters 600E, Waters, Milford, MA, USA) used deionized water as the eluent at a flow rate of 0.5 mL/min (Waters 600 gradient pump) and had a refractive index detector (Waters 2414 Differential Refractometer) and UV detector (Waters 486 Tunable Absorbance Detector), set at 234 nm. The injection volume was set to 20 µl (Waters 717 plus autosampler), and dextran solutions (2000, 500, 100, 150, 60, 10, and 4 kDa Merck Schuchardt OHG, Germany) were used as calibration standards, with polyethylene glycol as the standard for the lowest MW (400 Da, Merck Schuchardt OHG, Germany). The column was a TSKgel G4000PW_{XL} (TOSOH Bioscience GmbH, Griescheim, Germany), which was used in the second system (Shimadzu Corp., Kyoto, Japan). The Shimadzu system (SIL-10AXL autosampler, LC-10AT pump, CTO-10A column oven, RID-10A refractive index detector, and SPD-10AV UV-detector) was used with the same parameters as the Waters system, except that the eluent was 100 mM NaOH solution (alkali SEC) (Paper IV).

5.2.7 Sulfonate, carboxylic and phenoxyl group content

Samples were prepared by concentrating the SSL by ultrafiltration to a VR of 90% and the diafiltration to a factor of 5 (Papers I and IV). The hemicellulose was removed by antisolvent precipitation, leaving primarily the lignin in solution (Paper II). The solution was dried at 50°C for 48 hours to remove the acetone. The dry powder was dissolved in deionized water (0.6 g powder to 20 mL water), followed by the addition of 2 g Amberlite IR120 H form ion-exchange resin (Thermo Fisher Scientific Inc., Waltham, MA, USA) to convert the sodium lignosulfonates to lignosulfonic acid. After 3 hours of stirring, the solution was separated from the resin by vacuum filtration. The sulfonate and carboxylic acid content was determined by conductometric titration using an autotitrator (665 Dosimat and 728 stirrer, Metrohm AG, Herisau, Switzerland), a conductivity probe (HI 76306, HI 99301, Hanna Instruments Inc., Woonsocket, RI, USA), pH probe (HI 8424, Hanna Instruments Inc., Woonsocket, RI, USA), and 0.1 M NaOH solution. NaOH titrant was added in steps of 0.5 mL until the pH was higher than 13. The method and calculation of the functional groups are described elsewhere [110].

The total phenoxyl group content was measured by ionization difference UV spectrophotometry. The sample was diluted with three 0.1 M buffers at pH 6, 12, and > 12. The measurements were made at 300 and 360 nm, and the hydroxyl content was determined as described elsewhere [111] (Paper V).

5.2.8 Fourier transform infrared spectroscopy

Fourier transform infrared spectroscopy (FTIR) was performed for dried and pulverized samples (at 50°C for 48 hours) on a Bruker ALPHA-p FTIR spectrometer (Billerica, MA, USA). The samples were measured in attenuated total reflectance mode from 4000 to 500 cm^{-1} with 2 cm^{-1} resolution and 72 scans (Paper III).

5.2.9 HSQC 2D-NMR

Samples were prepared by drying 1 mL (feed) or 200 µL (retentate) of sample at 50°C for 48 hours and dissolving it in deuterated solvent. D_2O, D_6-DMSO, or a mixture of both was used as solvent. NMR measurements were made on a Bruker Avance III HD 500 MHz spectrometer (Bruker BioSpin GmbH, Karlsruhe, Germany) with a 5-mm broadband (BBO) probe and Z-gradient coil. The pulse program "hsqcetgpsisp.2" was used for the data collection with the following settings: 136 scans, 1.5 s relaxation delay, 10.3 µs pulse length, 11 ppm spectral width, and 1538 FID size. The results were processed with MestReNova 12 (Mestrelab Research S.L., Santiago de Compostela, Spain) using the "baseline correction" and "phase correction" methods (Papers II and IV).

5.2.10 Thermogravimetric analysis

The thermogravimetric analysis (TGA) was performed on a Q500 TGA (TA Instruments Inc., New Castle, DE, USA) by placing 2 to 5 mg of powdered sample (see Section 5.2.8) in open aluminum trays. The trays were placed in the instrument and heated from 15°C to 600°C at a rate of 10°C/min in a nitrogen atmosphere and a flow rate of 60 mL/min (Paper III).

5.2.11 Swelling capacity

Newly prepared and washed hydrogels were patted dry and weighed. After being dried at 50°C for 24 hours, the hydrogels were weighed again to determine the swelling capacity per Equation 5.1:

$$SC = \frac{m_{wet} - m_{dry}}{m_{dry}} \quad (5.1)$$

where m_{wet} and m_{dry} are the weights of the hydrogel in the wet (swelled) and dry state, respectively (Paper III).

5.2.12 Compression stress and strain

Compression stress and strain were measured using a motorized piston (built in-house) that pressed the hydrogels with a determined geometry against a scale (PL6001-1, Mettler Toledo Inc., Columbus, OH, USA). The rate of axial displacement was constant at 1.0 mm/min. The strain was calculated by multiplying the axial displacement rate with the elapsed time. The stress was measured by dividing the applied force (mass) with the cross-sectional area of the hydrogel (Paper III).

5.2.13 Bromothymol blue diffusion from hydrogels

Diffusion of bromothymol blue (BTB) from the hydrogels was performed by preparing hydrogels with BTB in a reaction mixture (Paper III). The hydrogels were then placed in mesh baskets and submerged in 400 mL 4 g/L NaOH solution. The solution was stirred at 100 RPM with a 2.5-cm magnetic rod. A 2-mL sample was withdrawn at each predetermined time. The BTB concentration was measured by UV-Vis at the isosbestic point (498 nm) with the extinction coefficient 9.31 L/(g cm) (Paper III).

5.2.14 Liquid chromatography–mass spectrometry (LC-MS)

The LC instrument was a 1260 Infinity II line (Agilent Technologies, Waldbronn, Germany), comprising the following modules: a Quaternary Pump VL (G7111A), a Vialsampler (G7129A), and a temperature-controlled column compartment (G7130A). The separation was performed on a Poroshell 120 EC-ECS (4.6 mm × 100 mm) column, which was operated at 50°C. The eluents were 0.1% formic acid solution and 95% acetonitrile in 0.1% formic acid solution at a flow rate of 0.5 mL/min. For the gradient program between these eluents, see Paper III. The injection volume was 1 μL, and the total run time per sample was 12 min. For LC, detection was performed using a UV diode array (G7115A) with a peak width of 0.1 min and a 4-nm slit.

The mass spectrometer (G6545B Q-TOF) was equipped with a dual AJS ESI ion source and was operated in positive mode. The gas temperature was set to 350°C at a flow rate of 12 L/min with a nebulizer pressure of 35 psig. The sheath gas temperature was 400°C, and the flow rate was 12 L/min. The voltage of the nozzle was set to 1000 V, with the collision energy set to 0 eV. Data were acquired between 50 and 3200 m/z.

6. Raw material composition

The aim of this work was to concentrate, separate, and purify hemicelluloses from SSL. The SSL in this work was derived from the first-step cooking of spruce and pine chips in a 2-step sodium-based sulfite pulping process, as detailed in Section 3.3. Several batches of SSL were used throughout this work, with slight variations between studies. Table 6.1 lists the average concentrations of the solutes in the various batches for the study in Paper V. These concentrations are slightly higher than in Papers I and IV, but they represent the most recent concentrations of these solutes at the pulp mill.

The SSL was dilute, with a total dry content (TDS) of approximately 9%. This low TDS rendered the SSL an interesting candidate for the membrane filtration trials. Of the TDS, 39% was ash, which was attributed to the cooking chemicals in the pulping process and possibly the degradation of lignin. The lignin in the SSL was sulfonated, as shown in Paper III and as seen in the FTIR results in Figure 6.1a, in which the 2 low wavenumber signals (highlighted in blue) were attributed to sulfonate groups (Paper III). The degradation of a purified lignin sample from the SSL was also studied using TGA, as seen in Figure 6.1b. Based on these results, the degradation of lignosulfonates yielded nonvolatile products that contributed to the ash content, as indicated by the high residual content at 600°C.

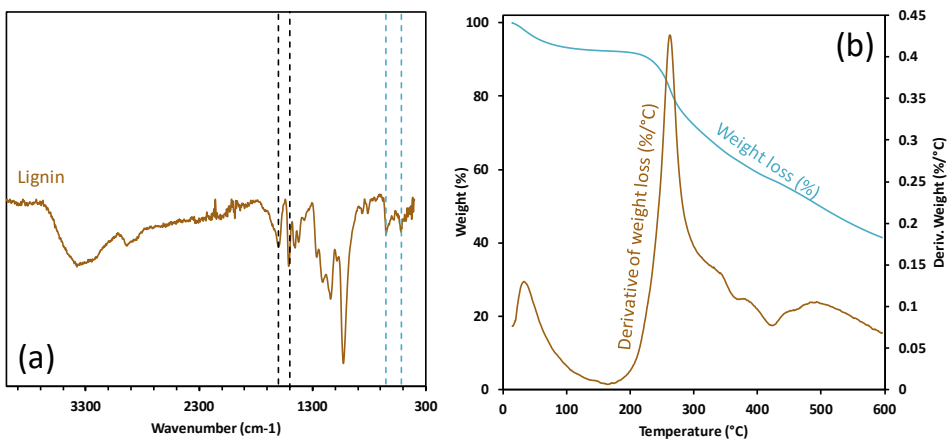


Figure 6.1: (a) FTIR and (b) TGA of a purified lignin sample derived from the SSL used in this work.

Table 6.1: Composition of six SSL feed samples (in g/L) from the pilot study, as presented in Paper V.

Total dry content	90.9±1.5
Ash	35.7±1.6
Total lignin	38.1±0.7
Functional group content	
Sulfonate groups (mmol/g)	1.34[a c]
Carboxyl groups (mmol/g)	1.08[a c]
Total phenoxyl groups (mmol/g)	1.63[a c]
Acid-insoluble lignin	1.2±0.1
GGM	6.7±0.8
Galactan	1.5±0.1
Glucan	1.5±0.1
Mannan	3.8±0.6
Acetyl-groups (as acid)	2.8[c d]
Other hemicellulose	1.9±0.1
Arabinan	0.6±0.0
Xylan	1.2±0.1
Monosaccharides (% of hemicellulose)	
Galactose	7.7
Glucose	8.4
Mannose	3.4
Arabinose	64.8
Xylose	11.3
Sugar alcohols	0.36±0.02[b]
Glycerol	0.31±0.02[b]
Xylitol	0.04±0.01[b]
Sorbitol	0.02±0.00[b]
Sugar acids	0.20[c]
Galacturonic acid	0.11[c]
Glucuronic acid	0.09[c]

[a] Based on precipitated lignin from a diafiltered retentate

[b] Based on 4 samples

[c] Based on 1 sample

[d] Mixture of free and bound acetic acid from Paper II

The total lignin content was the highest in the SSL, at 42% of the TDS, and the functional group content of the lignin in the SSL agreed with the reported values for sodium lignosulfonates [112,113]. The acid-insoluble lignin content was approximately 50% lower in Paper V than in Paper I, perhaps because the SSL solution had aged (condensation reactions over time) or because the acid-insoluble lignin comprised LCCs (Paper VI) that precipitated after the acid hydrolysis, with

the difference being attributed to the lower amount of LCCs in the liquor in Paper V.

The bonding pattern of lignin in the SSL was also determined by HSQC 2D-NMR (Figure 6.2). The lignin was guaiacyl-type, and no *p*-hydroxyphenyl ($\delta_c > 122$ ppm) or syringyl ($\delta_c < 108$ ppm) signals were found in the aromatic region, as expected for softwood-derived liquors (Paper II). Typical bonds, such as β-O-4 (sulfonated and nonsulfonated) (indicated by A) and β-5 (indicated by B), were observed, as were methoxyl and cinnamyl alcohol (X_γ) groups, the semiquantitative values of which were in the same range as reported (Paper IV). Signals in the region for phenyl glycosidic (PhG) bonds were noted, indicating the existence of LCCs in the SSL, likely between the GGM and lignin (Papers IV and VI).

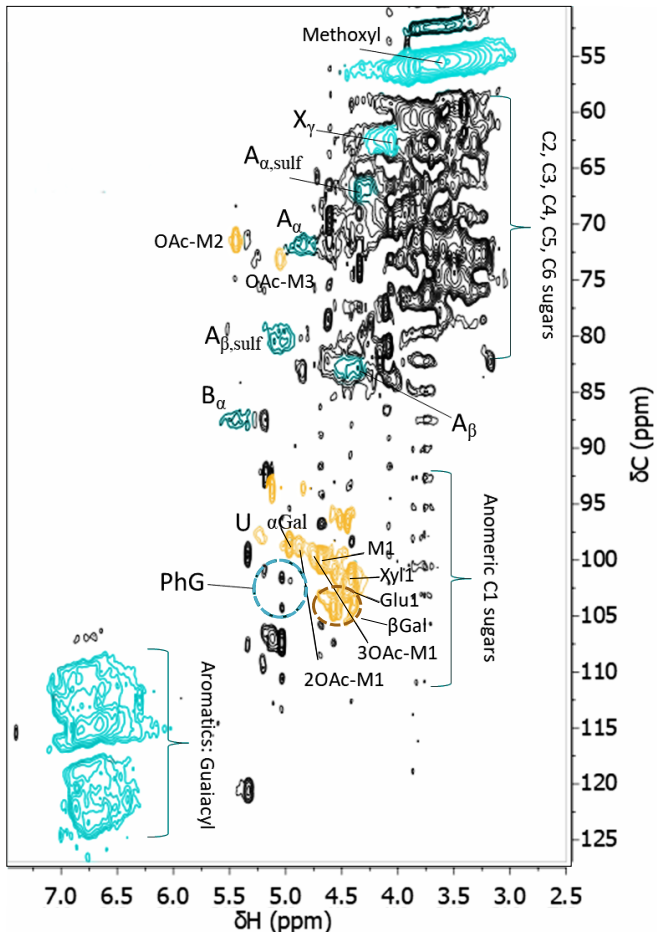


Figure 6.2: HSQC 2D-NMR of SSL retentate from Paper IV.

The third major component in the SSL was hemicellulose, amounting to 9.5% of the TDS. The major hemicellulose was GGM, with a total amount of 7.4% (including monosaccharides) of the TDS, as seen in Table 6.1. The ratio of GGM building blocks was 1.2–1.7:1.2–1.5:3 (Gal:Glu:Man), which was higher compared with what has been reported [29,109] (Paper II). The reason for these high ratios was the existence of other galactan-based polysaccharides in the mixture. This was also seen by 2D-NMR (Figure 6.2), wherein signals for various β-galactopyranose units arose (brown ring, anomeric C1 sugar region). These signals were attributed to the existence of arabinogalactans and β-galactans in the SSL (Paper II), which could not be distinguished in the acid-hydrolyzed HPLC samples in Table 6.1.

The galactose units on the GGM (α-Gal) could be quantified using the 2D-NMR results in Figure 6.2, as performed in Papers II and IV, in which the volume integral of α-Gal to the nonacetylated mannan was between 16% and 22%, yielding a Gal:Man ratio of 0.4 to 0.5:3. Acetylated mannan was also seen, with acetylation of the second and third carbons of the mannopyranose ring (Figure 6.2), constituting 12% and 9% of the total mannan, respectively. These values are slightly lower than in the literature (19% and 17%) [114], perhaps due to overlapping signals in the NMR spectrum or less extensive acetylation of the GGM.

The other major hemicellulose was xylan-based, which, according to the HSQC 2D-NMR data (Figure 6.2), was most likely arabinoglucuronoxylan (AGX) (based on the existing L-arabinofuranose and 4-O-methyl-D-glucuronic acid signals) (Paper II). The total amount of AGX was 2.1% of the TDS (based on arabinan and xylan). However, 65% of the arabinan was in monomeric form, as seen in Table 6.1, and other arabinan-based polysaccharides were indicated (Paper II). Thus, we calculated the retention and separation of the AGX, based on the concentrations of xylan alone. But, the amount of xylan-based polysaccharides should have been higher than 1.3% of the TDS.

Other minor components included monosaccharides (1% of TDS), sugar alcohols (0.4% of TDS), and sugar acids (0.2% of TDS). There was no association between sugar alcohols and other components in the solution. Some correlation between sugar acids and polysaccharides was observed, indicating the existence of pectin substances. The remaining components that were unaccounted for constituted 8.7% of the TDS, including extractives, such as resins and fatty acids, and perhaps due to errors that arose from inefficient drying (leaving some water in the dry content) or the UV measurements for determining the lignin content.

The MW of the components in solution is an important property when using membranes and membrane filtration for separation—to separate the components, there must be a difference in size. The SSL solution was analyzed by SEC, as shown in Figure 6.3. The results for the water-SEC (Figure 6.3a and b) show that the MW distribution was wide, spanning from 2000 to under 0.4 kDa (Paper IV). The UV signals also coincided with the RI signals, which usually indicates the existence of

LCCs [115] (Paper IV). However, other groups have shown that lignosulfonates are ion-excluded when using an electrolyte-free eluent [116]. The same SSL sample was thus analyzed by alkali-SEC, as seen in Figure 6.3 (c and d), which has been reported to be a reliable eluent for analyzing lignin and lignosulfonates [117]. The MW of the solutes was lower, in the range of 60 to 0.4 kDa. However, no separation of the components was seen, indicating that most of the components had similar MWs. The coinciding UV and RI signals in the alkali-SEC also implicated the existence of LCCs, as with water-SEC.

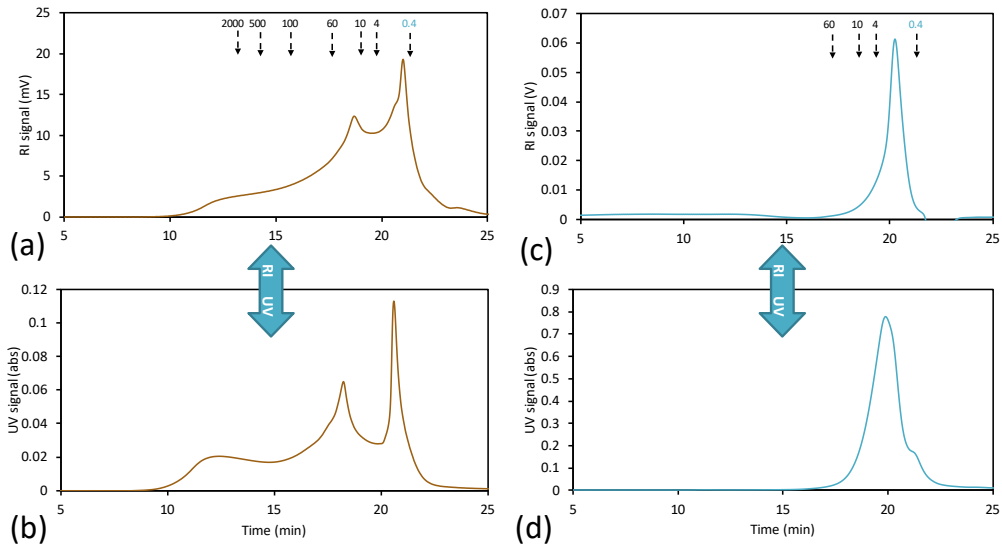


Figure 6.3: SEC of SSL in the water eluent (a and b) and 100 mM NaOH eluent (c and d). (a and c) RI signals. (b and d) UV signals.

7. Membrane filtration of the SSL

This chapter presents the prefiltration and membrane filtration studies that were performed in Papers I, IV, and V. An overview of these studies is shown in Figure 7.1. In Paper I, the SSL was ultrafiltered with three polysulfone membranes (hydrophobic), and the performance was measured and evaluated. Two prefiltration methods were also used to decrease membrane fouling, and diafiltration was performed to improve the purity of the product. In Paper IV, regenerated cellulose membranes (hydrophilic) were used to filter the SSL under the same operating conditions as for the best-performing membrane in Paper I. The results for the hydrophilic and hydrophobic membranes were compared, wherein the flux, retention, and yield of products were several of the important parameters that were studied. In the final membrane filtration paper (Paper V), the best-performing hydrophilic membrane was examined in pilot-scale membrane filtration equipment. The differences between the lab-scale and pilot-scale results are discussed, and the scale-up challenges were addressed through experiments and CFD simulations.

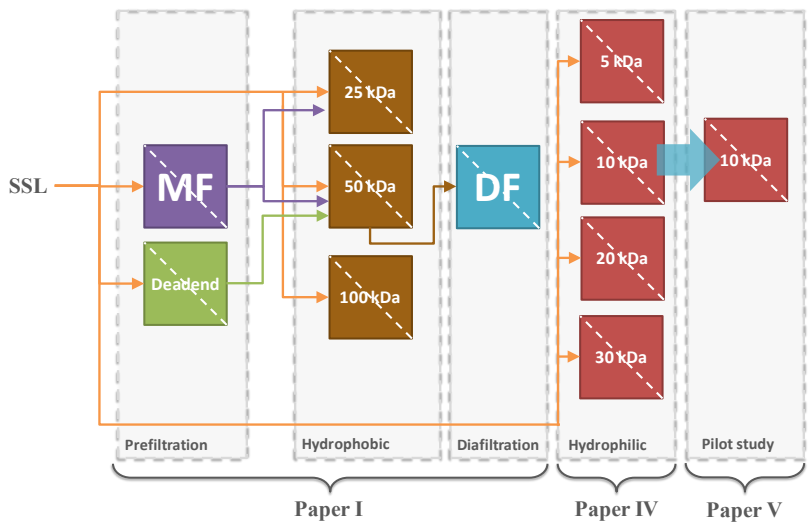


Figure 7.1: Overview of the membrane filtration experiments in this thesis. The orange streams represent the untreated SSL, and the purple and green streams are prefiltered SSL by microfiltration and dead-end filtration, respectively.

7.1 Hydrophobic membranes (Paper I)

In these trials, three polysulfone membranes with MWCOs of 25, 50, and 100 kDa were screened. The choice of MWCO was based on the MW of hemicellulose and lignin, as determined by water-SEC (SEC with deionized water as the eluent) to range from 20 to 200 kDa, based on polyethylene glycol standards (Paper I) and as seen in Figure 7.2. The hemicellulose and lignin were not separable by SEC, with the RI and UV signals coinciding. Enzymatic hydrolysis of untreated SSL hydrolyzed approximately 16% of the xylan and 40% of the arabinan. By SEC of the hydrolysate, low-MW lignin was released (near 2 kDa in Figure 7.2a), indicating that some of the xylan was covalently bound to lignin. The GGM was not hydrolyzed, based on the galactan and mannan concentrations, which were virtually unchanged.

The GGM and other polysaccharides were hydrolyzed by acid hydrolysis and analyzed by SEC. By SEC of the acid-treated hydrolysate (Figure 7.2b), the lignin in the high-MW region (near 200 kDa) was primarily intact (based on the intensity of the peak in the UV spectra), indicating that the lignin in this region was mostly free of carbohydrates. The other peaks with a MW lower than 200 kDa decreased in intensity, suggesting that they were associated with polysaccharides.

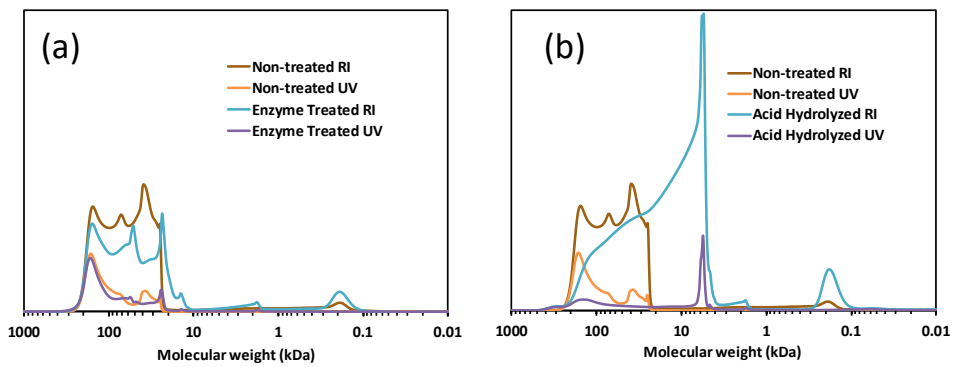


Figure 7.2: Water-SEC curves for enzymatically treated (a), acid-hydrolyzed SSL (b), and non-treated SSL (a) and (b). PEG was used as the standard fitting the MW.

Based on these observations, it was assumed that some lignin existed in "free form" and that the remainder was associated with polysaccharides. Also, the hemicellulose in the SSL was not separable by SEC, and we did not see any indications of free hemicellulose in the solution. Because GGM is the major hemicellulose in the SSL, in this section, the term *lignin-carbohydrate-complex* (LCC) will be used to refer to the sum of the total lignin and GGM in a solution.

7.1.1 Parameter study

A parameter study was performed for the three polysulfone membranes. The 25 kDa MWCO membrane had a flux of 1.8 L/m^{2}h, regardless of the operating parameters, and the fouling degree was high. No further experiments were done with this membrane, because sample collection was difficult (due to low flux and consequently low volume of sample). The 50 kDa and 100 kDa MWCO membranes had higher fluxes than the 25 kDa MWCO membrane, up to 220 L/m^{2}h and 160 L/m^{2}h, respectively (Figures 7.3a and 7.3c). A limiting flux was also achieved for the 50 kDa membrane but difficult to obtain with the 100 kDa membrane in the region of the operating conditions, perhaps due to the more open structure of the latter. However, the flux was lower for the 100 kDa versus 50 kDa membrane, opposite to what was expected, perhaps attributable to the higher fouling in former (85% vs 25%, respectively), resulting in a lower flux but also greater solute retention, as seen in Figure 7.3d. The retention between membranes (Figures 7.3b and 7.3d) did not differ significantly, but that of arabinan was slightly higher for the 100 kDa membrane.

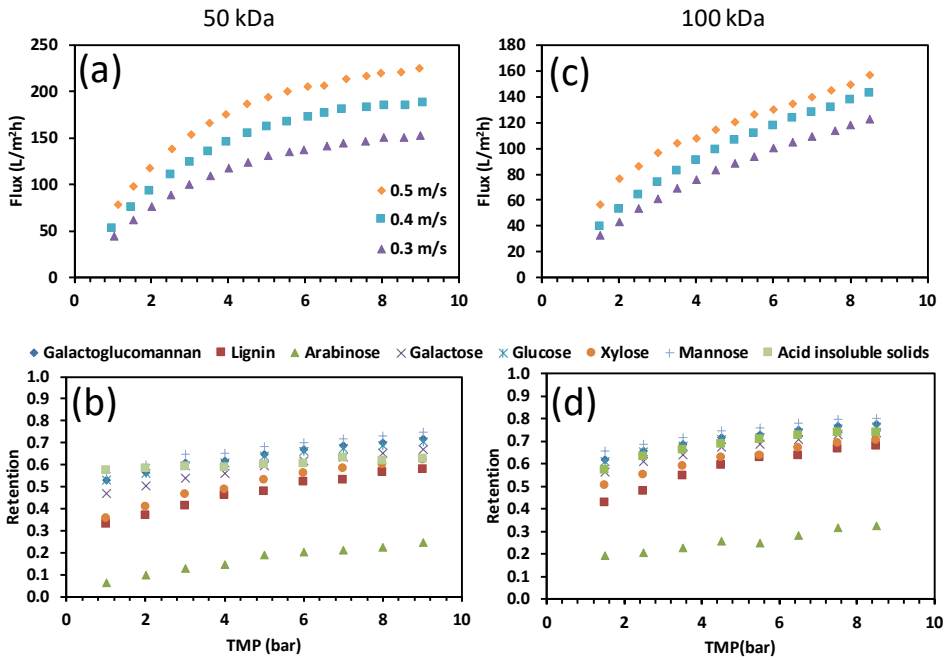


Figure 7.3: TMP vs flux (a and b) and retention (b and d) for the 50 kDa (a and b) and 100 kDa MWCO membranes (c and d). The temperature of the process solution was 50°C.

The retention data indicated that most polysaccharides were associated with lignin. The GGM had a retention that coincided with that of acid-insoluble lignin, as seen

in Figures 7.3b and 7.3d, and the retention of xylan overlapped with that of lignin. The low retention of arabinan was expected, given that 65% existed as monosaccharides, as seen in Table 6.1.

7.1.2 Membrane fouling

The higher retention in the 100 kDa versus 50 kDa membrane could have been caused by pore plugging [118], as shown in Krawczyk and Jönsson [119], in which an increase in MWCO resulted in a decline in flux, increased retention, and irreversible fouling. Also, the group concluded that the fouling was caused by severe pore blockage. The flux change for the 50 kDa membrane during the startup was negligible, and no change was seen for the 25 kDa membrane, indicating immediate fouling of the membrane. The MW of the components in the SSL ranged from 20 to 200 kDa, and thus, pore blockage was also possible for the 25 kDa membrane. Fouling was seen in the startup data in the 100 kDa membrane parameter study, in which the flux decreased from 97 L/m^{2}h to 48 L/m^{2}h at a constant TMP and CFV of 1 bar and 0.5 m/s, respectively. To describe the fouling phenomenon, Hermia's blocking filtration law [120] was used to fit the startup data on the 100 kDa membrane. The data were fitted to a polynomial, numerically differentiated, and fitted to Equation 4.11. The results of the fit are shown in Figure 7.4.

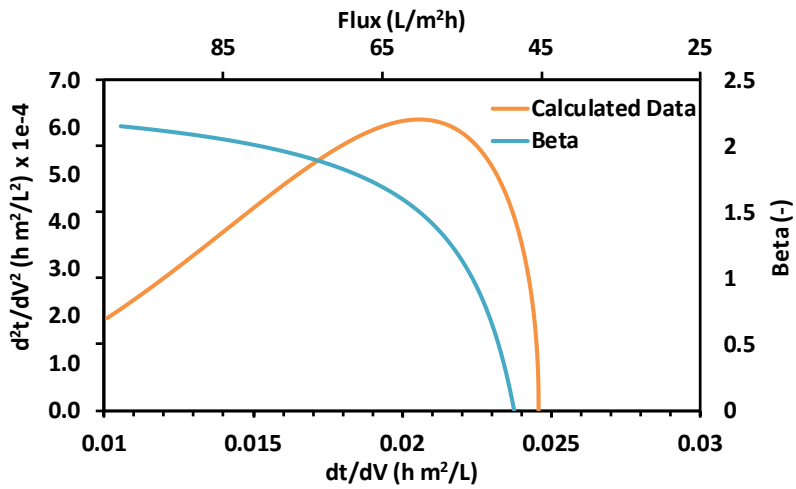


Figure 7.4: Fitting of the 100 kDa MWCO membrane startup data to Equation 4.11 (orange line, calculated data) and the calculated β-coefficient (blue line).

Based on the average value of β, which was close to 2 at the outset, it was apparent that fouling occurred on the membrane by the complete blocking mechanism (Table 4.1). According to Hermia [66], the complete blocking mechanism states that every

particle that arrives to the membrane surface blocks a pore. The results were thus consistent with the earlier assumptions with regard to the membrane pore blockage. The value for β decreased rapidly and reached zero, indicating that the surface was completely blocked and that the particles that arrived at the membrane deposited themselves onto other particles (cake filtration, Figure 4.6). The flux was stable at that point, reaching a final value of 48 L/m^{2}h.

7.1.3 Concentration and diafiltration study

The results in Sections 7.1.1 and 7.1.2 suggested that the 50 kDa membrane was suitable for continued study, considering its high flux, high retention, and low fouling. A concentration and diafiltration study was conducted at the weak critical flux, which was estimated to be approximately 5.5 bar, from Figure 7.3a, at the peak CFV of 0.5 m/s. The results from this study are shown in Figure 7.5.

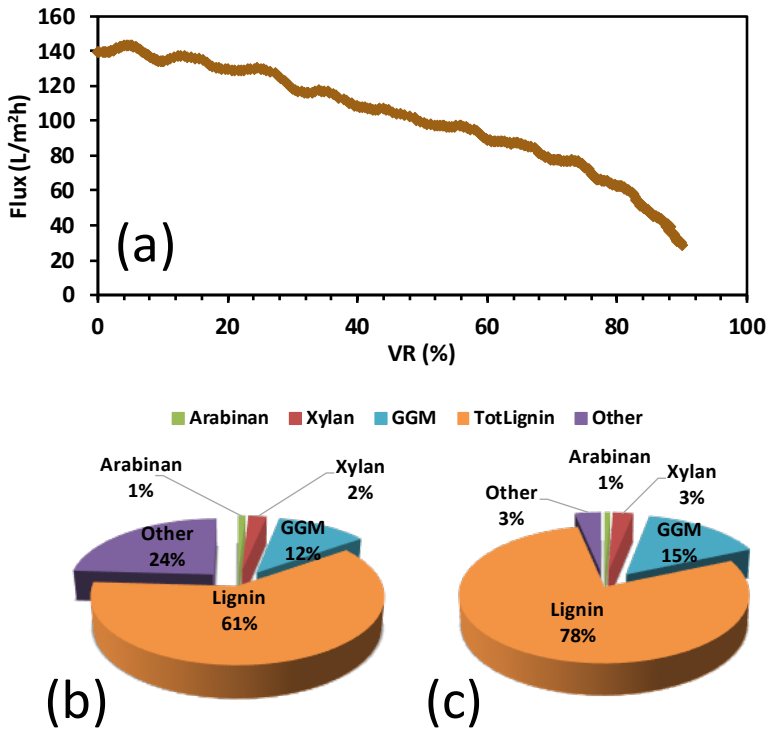


Figure 7.5: Flux-vs-VR curve for the concentration study with the 50 kDa MWCO membrane (a), the SSL content in the VR 90% retentate (TDS of 212 g/L) (b), and the diafiltered retentate (TDS of 132 g/L) (c).

The flux during the concentration study was initially 139 L/m^{2}h (VR 0%) and decreased slowly to 100 L/m^{2}h at a VR of 50%, after which the decline accelerated, ultimately reaching 33 L/m^{2}h at a VR of 90%. The retention of LCCs increased from 63% (VR 0%) to 73% at a VR of 90% and a final GGM concentration of 25 g/L. The ratio between lignin and GGM (L/C ratio) was 5.8 in the feed at VR 0% and decreased to 5.1 in the retentate. Although the change was minimal, it could have been attributed to the loss of some of the total lignin or xylan-lignin complexes, because their retention was on the lower end of the range (Figure 7.3b). The overall purity of the feed rose from 43% to 73%, because a major portion of pulping chemicals was removed during the concentration.

To increase the purity of the LCC mixture, a diafiltration experiment was conducted to wash out the remaining pulping chemicals and monomeric sugars, using a diafiltration factor of 5 under the same operating conditions as for the concentration study. The amount of pulping chemicals and monosugars decreased from 24% to 3%, as seen in Figure 7.5b and 7.5c, resulting in an increase in LCC purity from 73% in the retentate to 93% in the diafiltered retentate. The L/C ratio remained at 5.1. The yield of the components with an MW higher than 50 kDa in the diafiltered retentate was approximately 55%, exceeding the yields that were obtained by the universal solubility method for LCCs in the same range of MWs [121]. However, the yield was lower than for similar ultrafiltration studies on the isolation of GGM [56,68], which was attributed to the low retention of products during the concentration step and the loss of lower-MW LCCs. The yield could be improved by using membrane with a lower MWCO or by adding a membrane filtration step for the recovery of lower-MW components [71].

7.1.4 Prefiltration with MF and DEF

The degree of fouling of the 50 kDa membrane was approximately 25% during the parameter study, rising to 49% during the concentration, which was expected, given that fouling rates depend on the concentration of the solutes [122]. Prefiltration with MF and dead-end filtration (DEF) with kieselguhr were examined with regard to reducing membrane fouling. These methods have the potential to remove foulants from similar waste waters [56]. The results from this study (presented in Figure 7.6) show that the initial flux for the UF increased from 139 L/m^{2}h to 464 L/m^{2}h when MF was used as a prefiltration method, whereas DEF prefiltration increased it to 163 L/m^{2}h—a 3-fold and 1.2-fold increase, respectively (Figure 7.6b). The degree of fouling (Figure 7.6a) in the UF fell from 49% to 7% and 17% for the MF and DEF prefiltration methods, respectively.

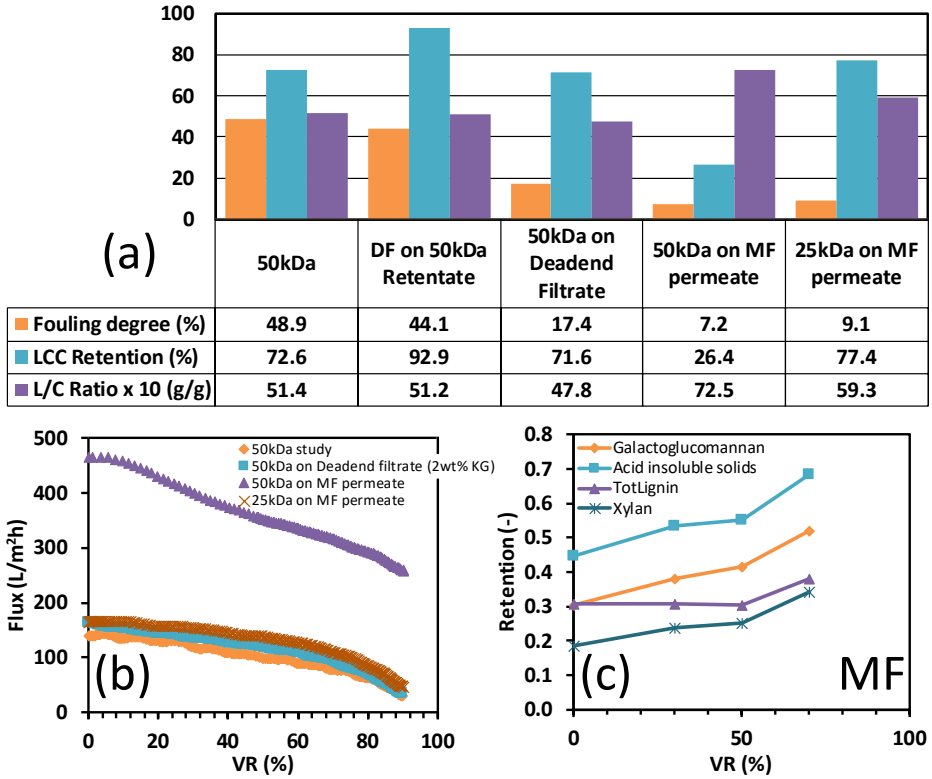


Figure 7.6: Degree of fouling, retention, and L/C ratio for the prefiltration→membrane filtration studies (a). Flux vs VR in these studies (b) and the retention of the solutes in the MF concentration study (c).

These methods clearly removed some of the foulants, given that the flux for the 25 kDa membrane was 166 L/m^{2}h, using the MF permeate as the feed, which was a 92-fold increase in flux compared with the untreated feed. DEF prefiltration removed primarily suspended solids, with a negligible loss of product. The higher flux with UF after DEF suggested that the existence of suspended solids had an effect on the performance of the UF. The MF had high retention of acid-insoluble solids, GGM, and lignin, as seen in Figure 7.6c, and the total loss of these components was approximately 30%. A low flux was observed seen for the MF, roughly 55 L/m^{2}h on average during the concentration study, which was on the same order of magnitude as for the UF. The low MF flux was likely the result of the high degree of fouling during the MF, which was approximately 76%.

The high retention of solutes during the MF, especially GGM and acid-insoluble solids, was unexpected, because these macromolecules were smaller compared with the MF membrane pore size. However, the rejection of these solutes was likely caused by the formation of a gel layer or cake on the membrane surface that in turn increased the retention of these components, as observed by Krawczyk, et al. [56].

Another reason is that hydrophobic components adsorbed to the (hydrophobic) membrane surface and pores, thus decreasing the pore radius and, with it, enhancing the retention of the solutes. This possible mechanism is shown with the blocking filtration law [66], in which pore plugging can occur after adsorption to the membrane. Because the retention of acid-insoluble solids was among the highest, it was likely that this component was responsible for the fouling. The fouling of the MF membrane, however, was reversible when oxidative treatment was applied—complete restoration of the PWF was seen after the addition of hydrogen peroxide to the acidic cleaning step. This observation also indicated that the fouling compounds consisted of components that were sensitive to oxidizing agents, such as for lignin-based agents [123].

7.2 Hydrophilic membranes (Paper IV)

In Section 7.1 and Paper I, conclusions were drawn regarding the use of three hydrophobic UF membranes for treating SSL. The membrane with the lowest MWCO was plugged immediately during filtration, with a flux that was virtually zero and a high degree of fouling. The two best-performing membranes (50 kDa MWCO and 100 kDa MWCO) had similar flux and retention. Thus, I conclude that the rejection of solutes was governed by the properties of the fouling layer that had formed on the membrane surface—not the membrane itself. The best-performing membrane was 50 kDa, with high flux and the least fouling.

To decrease the fouling further, two prefiltration methods were examined, MF and DEF. MF was the best with regard to eliminating fouling in the UF. However, the retention of solutes was high during MF, which resulted in losses of the product. The removal of high-MW product also resulted in a much lower retention during the UF, which in turn created even more losses of the product. The MF membrane also had a high degree of fouling, indicating that a specialized chemical cleaning step is needed for this prefiltration method to be economical. A promising alternative to MF was DEF, which resulted in no loss of product. However, this method required the use of kieselguhr (diatomaceous earth), which can negatively affect pulp mills in the case of failure in the membrane filtration.

Membrane fouling could also be decreased by the use of a hydrophilic instead of a hydrophobic membrane [124]. Lignin and other hydrophobic materials tend to adsorb to hydrophobic surfaces with noncovalent bonds, causing membrane fouling (Paper I) [125]. Li, et al. [125] membrane-filtered a Kraft lignin solution through polysulfone membranes, with fouling (decreasing flux) over time. A yellow coating was also seen on the membrane surface by the group. The fouling was not reversible, based on the inefficient cleaning with water and sodium hydroxide. On switching to a hydrophilic membrane, the flux became unaffected, and no yellow coating formed

on the membrane surface. Similar observations have been made by Puro, *et al.* [126] during the membrane filtration of ground wood mill circulation water, on changing from hydrophobic to hydrophilic membranes. Puro, et al. [126] also determined the foulants to be fatty acids, resins, and lignans, all of which are mainly hydrophobic compounds.

The aim of Paper IV was to compare the 50 kDa polysulfone (PS) membrane in Paper I with regenerated cellulose (RC) membranes in terms of retention, flux, and membrane fouling. The retentates from the PS and RC membranes were also compared with regard to composition and MW.

7.2.1 Concentration study

The hydrophilic membranes were compared with the 50 kDa hydrophilic membrane (GR51PP) from Paper I. The operating conditions were the same as in Paper I: 5.5 bar TMP, 0.5 m/s CFV, and 50°C. The concentration study was conducted up to a VR of 90% for all membranes. The results for the flux profile are shown in Figure 7.7a.

As seen in Section 7.1, the flux for the hydrophobic membrane decreased, with an almost linear curve from a VR of 0% to 60%, after which a rapid decline in flux was observed. The C30F hydrophilic membrane experienced the same linear trend, whereas the tighter hydrophilic membranes (RC70PP and C5F) had a pseudo-steady state up to a VR of 50%. The C20F membrane had an initial sharp decrease in flux, followed by a profile that had the same shape as for the RC7PP and C5F membranes. A similar decline in flux has been reported by Brião, *et al.* [127] and Hwang, *et al.* [118], who attributed it to the build-up of a cake on the membrane surface.

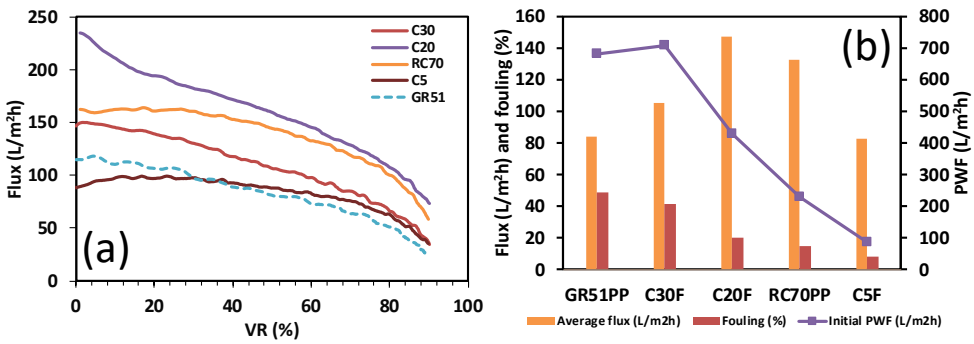


Figure 7.7: (a) Flux vs VR for the hydrophilic membranes (C30, C20, RC70, C5) and the hydrophobic membrane (GR51) at 5.5 bar TMP, 0.5 m/s CFV, and 50°C. (b) Average flux, fouling degree, and PWF for these membranes.

A different trend was seen for the C30F membrane, even though its MWCO was larger versus the C20F membrane. Also, a higher flux was expected for the C30F membrane, given that the PWF was higher compared with the C20F membrane (Figure 7.7b). However, this prediction was not realized, suggesting that pore plugging likely occurred in the C30F membrane [118] and indicating high fouling for the C30F versus C20F membrane (Figure 7.7b). Paper I showed that a 25 kDa membrane was fouled, with fluxes that were virtually zero, which could have happened with the C30F membrane, which had an MWCO that was close to that of the 25 kDa membrane. One explanation for the non-zero flux is the slightly higher MWCO and that the membrane material was hydrophilic, which led to lower lignin adsorption [124].

The retention of the various SSL components is shown in Figure 7.8. The retention of polysaccharides behaved as expected, depending solely on the MWCO of the membrane. The retention was higher for denser membranes and lower for open membranes. The interaction between polysaccharides and the membrane was thus inconclusive. The C30F membrane behaved differently with regard to the retention of polysaccharides, experiencing greater retention than the denser membranes, likely due to the higher fouling with this membrane, as explained above.

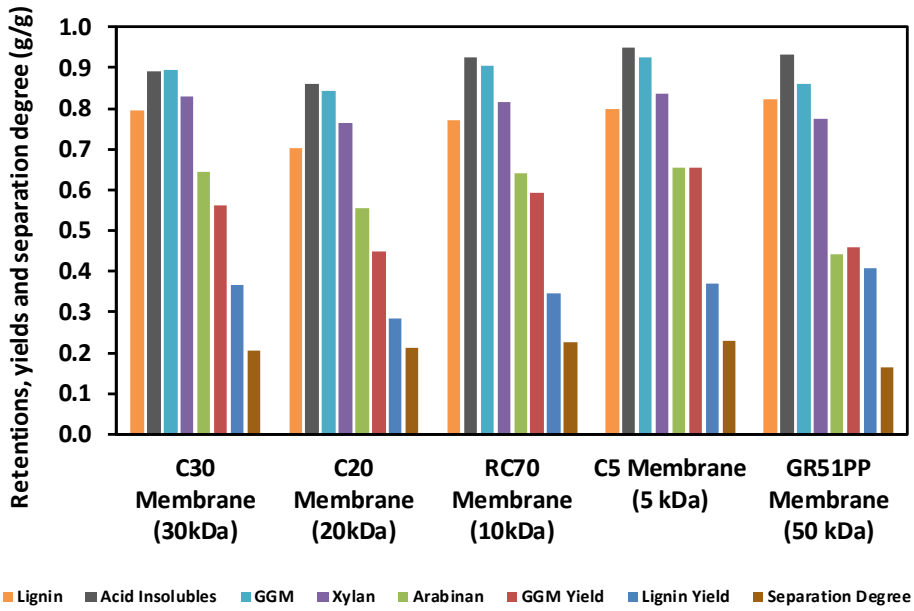


Figure 7.8: Retention of solutes, yields, and separation degree for the hydrophilic and hydrophobic membranes.

The interaction of lignin with the membranes was most evident with the hydrophobic membrane, as reflected by the increase in its retention with decreasing MWCO of the hydrophilic membranes. The separation degree was another indication of this interaction, given that the value was higher overall for the hydrophilic membranes, suggesting greater separation between GGM and lignin.

7.2.2 SEC of retentates

SEC was performed on all retentates, as seen in Figure 7.9. The major change in these SEC curves compared with those for untreated SSL (Figure 6.3) was the shift in peaks from a lower to higher MW range (Figure 7.9a). As described in Chapter 6, this shift was the result of ion-exclusion of the lignosulfonates (lignin) and only visible for the water-SEC (electrolyte-free eluent). Consequently, a lignin-free component appeared between the 10 kDa and 4 kDa standards in Figure 7.9a, which had no corresponding UV signal (Figure 7.9b). This wide peak was shown in Paper II to be lignin-free GGM (discussed in Chapter 8) that did not belong to any LCCs [121]. This peak was not visible in the results of the alkali-SEC (Figure 7.9c), giving the false impression that everything in the solution belonged to LCCs. Although water-SEC overestimates the MW of the components in SSL, the separation of peaks using this method could help identify several components in the system.

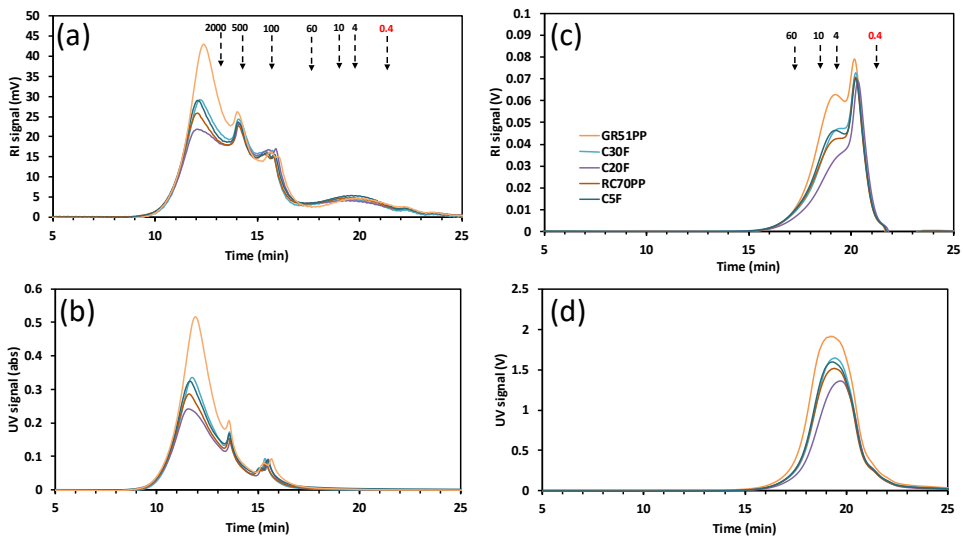


Figure 7.9: SEC curves for the SSL retentates from all UF studies. The water-SEC results are presented in (a) (RI-signal) and (b) (UV-signal). The same samples were analyzed by alkali-SEC, where (c) is the RI signal and (d) is the UV signal.

The retention of components also followed the intensity of the various peaks in the water-SEC results. The highest retention of lignin (Figure 7.8) was seen with the hydrophobic membrane, which corresponded to the highest intensity by water-SEC (Figure 7.9b). The retention of lignin was lower and equal for the C30F and C5F membranes, as shown in the same water-SEC figure. The retention of GGM did not differ tremendously between these studies, but it was the highest for the C5F membrane, appearing as a slightly larger peak in the lignin-free region in Figure 7.9a.

The most open membranes (50 kDa and 30 kDa) had the highest intensities in the alkali-SEC results (Figures 7.9c and 7.9d), even for the low-MW components. These components were expected to pass through the membrane, which likely did not occur, due to the high fouling with these membranes, causing a gel layer or cake to form that held back these compounds [56].

Based on these results, a simplified economic evaluation was performed, which showed that the RC70PP membrane was the most cost-efficient in terms of flux and product yields. The retentate from this membrane was compared with that of the hydrophobic 50 kDa membrane. The water-SEC curve in Figure 7.9a was divided into 6 visible peaks, and their areas were calculated, as seen in Figure 7.10.

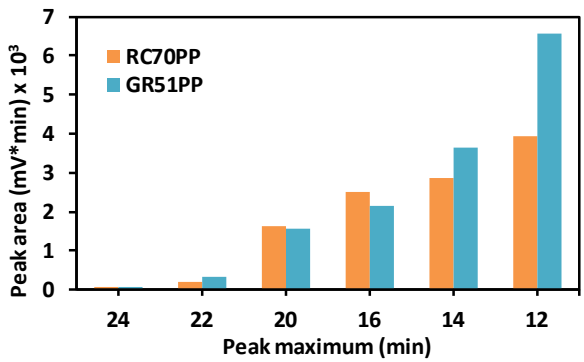


Figure 7.10: Peak area vs peak maxima of the SEC curves in Figure 7.9a.

Three of these peaks had a UV response (at 12, 14, and 16 minutes), and the remainder did not. These results show that the hydrophilic membrane had a larger lignin-free peak (20 minutes), which was the result of its greater retention of GGM. The peak at 16 minutes was also the highest for the hydrophilic membrane. This peak had a UV response, indicating that it likely belonged to lignin or LCCs. The HSQC 2D NMR results in Paper IV also suggested that the amount of LCCs (seen in Figure 6.2) was higher for the hydrophilic membrane. The earlier peaks (12 and 14 minutes) could have also contained LCCs, but the amount of lignin in these peaks was extremely high; thus, the existence of LCCs in these peaks was inconclusive.

7.3 On-site pilot study (Paper V)

In Paper IV, the RC70PP membrane performed best, based on its low fouling, high flux, high retention of the product, and good separation of GGM and lignin. These results, however, were derived in a lab-scale setup and did not consider long-term fouling, declines in flux, or potential problems with scale-up of the process. For instance, Rajniak*, et al.* [128] have shown that flux is not linearly scalable when changing membrane modules, due to the difference in flow resistance that arises from the geometry of the module. Other challenges could be related to the varying feed composition or quality and the hydrodynamics of the system when such studies are performed on site [129].

As of Paper V, there have been no reports with regard to on-site pilot-scale membrane filtration trials for hemicellulose-rich SSL. However, there are several studies on pilot-scale membrane filtration of similar raw materials. Persson*, et al.* [130] membrane-filtered thermomechanical process water through a series of processing steps (MF, UF, and NF). In the prefiltration step (using a drum filter), 90% of suspended solids were removed. The MF step removed extractives, whereas UF was used to concentrate the hemicelluloses. The authors obtained a final hemicellulose concentration of 64 g/L at a VR of 99%. However, the membranes experienced severe fouling, and the PWF was unrecoverable after alkali and acidic cleanses of the membranes, highlighting the importance of conducting pilot trials. Also, the group used a series of membrane-based prefiltration steps that increase the total cost of hemicellulose production [131]. The proposed process in Paper V contains no membrane-based prefiltration steps, rendering a future plant and hemicellulose production cheaper.

The aim of the study in Paper V was to scale up the lab-scale results and present the challenges that were encountered during this process.

7.3.1 Concentration study under lab-scale operating conditions

The pilot study initially rants the equipment under the following lab-scale operating conditions: 5.5 bar TMP, 0.5 m/s CFV, and 50°C feed temperature. The concentration was also done up to a VR of 90%, as in the lab-scale study. The results from these studies are presented in Figure 7.11.

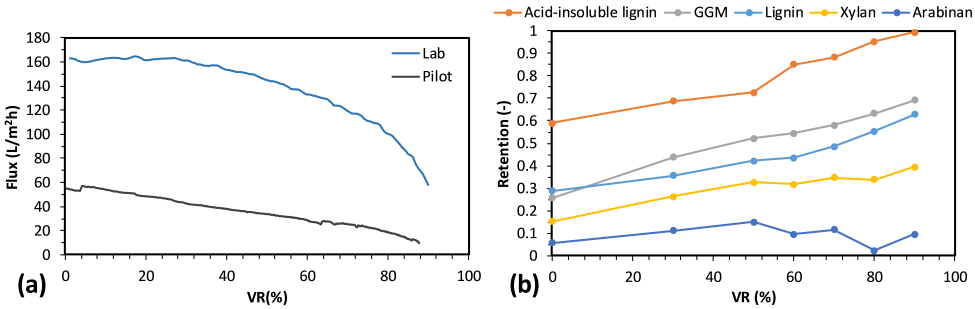


Figure 7.11: (a) Flux vs VR profile for the lab-scale and pilot-scale concentration studies. (b) Retention of the various solutes during the pilot-scale concentration study (Paper V).

The results show that the flux in the pilot started at a value of 55 L/m^{2}h versus 160 L/m^{2}h in the lab-scale equipment under the same operating conditions. The flux was higher overall during the lab-scale trials, even at the end of the concentration range (VR of 90%), at which point the flux was approximately 50 L/m^{2}h and 10 L/m^{2}h for the lab-scale and pilot setups, respectively. This difference is likely due to a disparity in SSL composition between these filtration setups. The lab-scale study was complete 2 years prior to the pilot investigations, validating this assumption. However, as seen in Chapter 6 and Paper V, the difference in composition was minimal, thus rejecting this hypothesis. Also, the membranes in both studies behaved as expected, given the permeabilities of 70 L/m^{2}h bar and 68 L/m^{2}h bar for the lab-scale and pilot systems, respectively.

In the lab-scale filtration, the retention of lignin was 0.77 and 0.91 for GGM. These retention values were lower in the pilot experiments, as seen in Figure 7.11b, possibly resulting from the separation being driven by a gel layer or cake on the membrane surface (Paper I). The formation of a gel or cake is also dependent on the permeate flux, among other factors. The difference in flux in the pilot experiments could explain the disparity in retention. In most of our studies (Papers I, IV), the retention of acid-insoluble lignin always approximated that of GGM during UF of SSL. The difference in Figure 7.11b implicates a structural difference (possibly the MW) in the SSL that was used in Paper V, although the compositions were similar.

7.3.2 Increasing the flux

At the time that the experiments were conducted, our access to analytical equipment was limited, and it was not possible to determine the composition of the feed, retentate, and permeates. However, based on the lower flux in the pilot study, as seen in Figure 7.11a, it was assumed that a difference in the composition of the feed existed, requiring a subsequent parameter study to determine a new operating point. This study was conducted at a CFV of 0.5, 1.0, and 1.5 m/s, at which maximum

flow in the circulation pump was reached. As seen in Figure 7.12a, the higher CFV increased the permeate flux by 3-fold, from 0.5 m/s to 1.5 m/s.

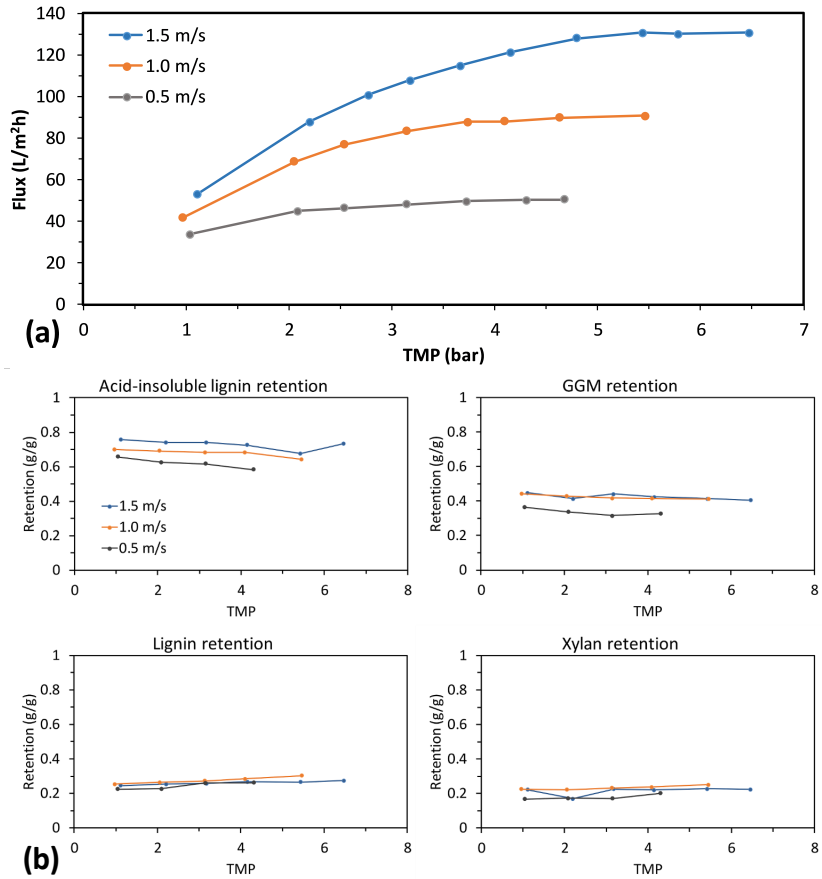


Figure 7.12: (a) Parameter study in the pilot system. (b) Retention of the three major components in the SSL during the parameter study (Paper V).

The limiting flux at these CFVs was 50 L/m^{2}h (0.5 m/s and 3.7 bar TMP), 90 L/m^{2}h (1.0 m/s, 4.6 bar TMP), and 130 L/m^{2}h (1.5 m/s, 5.5 bar TMP), with a minimal change in solute retention, as seen in Figure 7.12b. GGM and acid-insoluble solids were the only components that were affected by the change in TMP and CFV, likely due to their higher MW. The retention of GGM increased by 0.1 units, from a CFV of 0.5 m/s to 1.0 m/s. Acid-insoluble solids were affected over the entire span of CFVs and TMPs, as seen in Figure 7.12b. No other changes were observed. The new operating point was a TMP of 5.5 bar and CFV of 1.5 m/s, based on the filtration capacity, at which point it was the highest.

Using the new operating point, another concentration study was conducted, the results of which are seen in Figure 7.13. The flux improved tremendously, as seen by the change in initial flux—approximately 140 L/m^{2}h compared with 55 L/m^{2}h previously. The improvement in retention was minimal, with that of GGM increasing from 0.52 (CFV of 0.5 m/s) to 0.57, that of lignin falling from 0.45 to 0.41, and that of acid-insoluble solids rising from 0.81 to 0.87. Because the acid-insoluble solids formed a minor portion of the total lignin content, the degree of separation only increased from 18% to 19%.

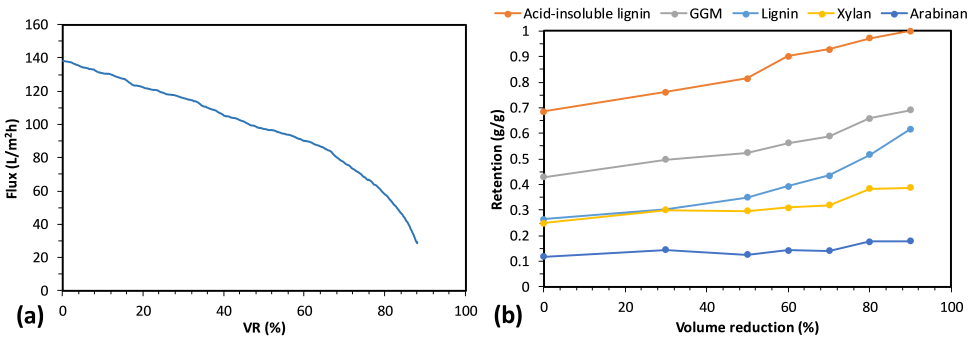


Figure 7.13: Concentration study at a CFV of 1.5 m/s and TMP of 5.5 bar. Flux-vs-VR curve (a) and solute retention (b) (Paper V).

7.3.3 CFD of the membrane modules

The results in Section 7.3.2 show that the flux in the pilot equipment can be improved. However, the capacity remained lower than in the lab-scale experiments, perhaps due to the geometries of the modules, which could have affected the flow profiles and, consequently, the Reynolds number and shear rate. These parameters influence the retention and flux as a result of a changing mass transfer coefficient [132].

These critical parameters were simulated using CFD (in COMSOL Multiphysics) to examine the influence of membrane module geometries on the Reynolds number and shear rate. The results from the simulation are presented in Figure 7.14. According to the simulation, the flow in both modules was turbulent—clearly for the pilot module (Figure 7.14a), wherein the velocity was uniform between the channel walls and middle section. Also, the velocity was nearly constant throughout the module, slightly higher in the middle section of the inlet. The state of the fluid was less clear with regard to turbulence for the stirred-cell module (lab-scale), as seen in Figure 7.14b and 7.14c.

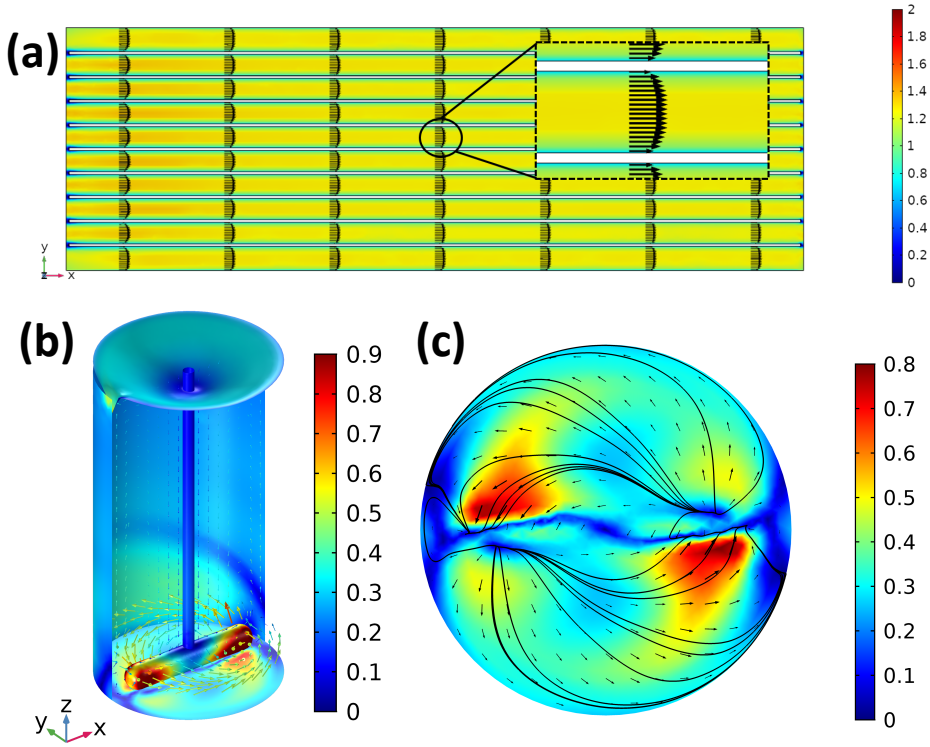


Figure 7.14: CFD results for the pilot (a) and the stirred-cell module (b and c), as presented in Paper V. The results show the velocity profile in the modules; the gradient legends are in m/s.

In these cases, the Reynolds number could be used to determine the state of the fluid. According to the calculated Reynolds number in Table 7.1, both modules were in the turbulent region, which ranged between 3000 and 20,000. The turbulence kinetic energy (Table 7.1) also indicated that the modules were operating in the turbulent region, based on the nonzero value that was obtained in the simulation.

Comparing the pilot and stirred-cell module at the same CFV, the experimental flux was 3 times higher in the latter. The average shear rate of the stirred-cell module was 2-fold higher than for the pilot system, which suggested that the formation of a cake in the stirred-cell module was more difficult, thus explaining the higher flux [133]. However, increasing the CFV beyond 0.5 m/s in the pilot module also increased the average shear rate, as seen in Table 7.1. At a CFV of 1.0 m/s, the average shear rate in the pilot was nearly equal to the lab-scale result, and at 1.5 m/s, it was twice as high as in the lab-scale setup. The higher velocity and shear rate

enhanced the permeate flux in the pilot system, but the flux remained lower than in the lab-scale experiment.

Table 7.1: CFD results of the pilot and stirred-cell modules (lab-scale) as presented in Paper V.

	Experimental inlet CFV (m/s)	Simulation CFV (m/s)	Turbulent kinetic energy 10^4 (m^2/s^2)	Average shear rate (1/s)	Flux (Experimental) (L/m^2h)	Pressure Drop 10^5 (bar)	Reynolds number (-)
Pilot	0.50	0.40	17	148	50	375	3000
	1.00	0.70	42	368	91	968	6100
	1.50	1.05	81	701	138	1940	9100
Lab-scale	0.50	0.35	129	297	162		21000

The reason for this was that the average shear rate was an acceptable measure for the pilot system, in which the velocity was nearly constant throughout the module. The stirred-cell module had different velocities, depending on the position of the stirrer (see Figure 7.14c). The region in which the velocity peaked (red color in Figure 7.14c) had a shear rate of 1074 s^{-1}, explaining the higher experimental flux.

Another explanation is related to the mode of operation of the 2 modules. The stirred-cell module operated at the final VR (Equation 4.8), because no feed or retentate entered or left the module. The pilot setup ran with 2 pumps—a feed pump and circulation pump—giving the process two VRs, as explained in Section 4.2.2.2. The feed pump was set to a flow rate of 280 L/h, yielding a loop VR (LVR) of roughly 40% for a flux of 138 L/m^2h (Equation 4.9). The system thus ran at a VR that was higher than the total VR (Equation 4.8).

This pattern was also seen in Figure 7.15, in which the intercept of the line from the starting flux in the pilot setup to the lab-scale flux was approximately 44%. According to these results, the flux in the pilot system could never match that in the lab-scale module. A high-feed pump flow could reduce the difference between curves, but the cost of running the feed pump at higher flow will also rise. These observations explain the lower retention of solutes. A higher LVR also increases the concentration of solutes near the membrane surface, in turn increasing the concentration in the permeate and thus decreasing their retention [132].

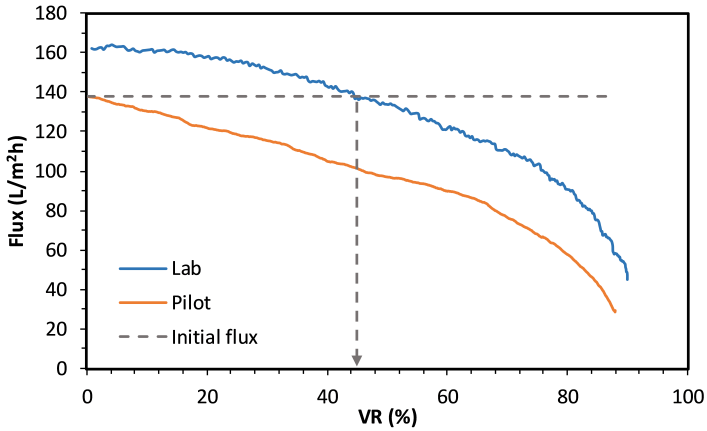


Figure 7.15: VR-vs-flux curves for the pilot and lab-scale modules at a CFV of 1.5 m/s and 0.5 m/s, respectively. The dashed lines highlight the LVR of the pilot study as it intersects the lab-scale curve (Paper V).

The difference in filtration results between membrane modules could also be related to membrane compaction. The operating conditions for both modules were the same. However, the temperature during the filtrations differed by up to 15°C. During the pilot experiments, the temperature was mostly stable, fluctuating slightly between 48°C and 51°C. The stirred-cell module held at 50°C, but at the start of the experiments, the temperature near the permeate outlet and membrane was roughly 60°C, peaking at 65°C. This high temperature, combined with the 5.5-bar TMP, could have compacted the membrane in the stirred-cell module, resulting in the high retention that was observed [134]. Compaction of the membrane also decreases the flux, which was not seen in our results. The increasing flux could have been the result of the declining viscosity with rising temperature (Equation 4.4).

7.3.4 Fouling and cleaning

Membrane fouling and its effect on filtration capacity are important factors in pilot studies [135]. Membrane fouling was monitored by calculating the membrane hydraulic resistance (R_m) after a subsequent concentration experiment and cleaning sequence. Fouling resistance (R_f) was calculated with Equation 4.4, where $\Delta\pi$ was set to zero and R_f was the sum of the resistance values due to concentration polarization, cake formation, and adsorption. The first 5 cycles of cleaning were performed using 0.05 wt% of Ultrasil 10, which yielded a pH of approximately 8 to 9, after which the remaining cycles applied 0.1 wt%, effecting a pH of roughly 11 (the maximum tolerable pH for the membrane). The membrane resistance after each cycle is presented in Figure 7.16a.

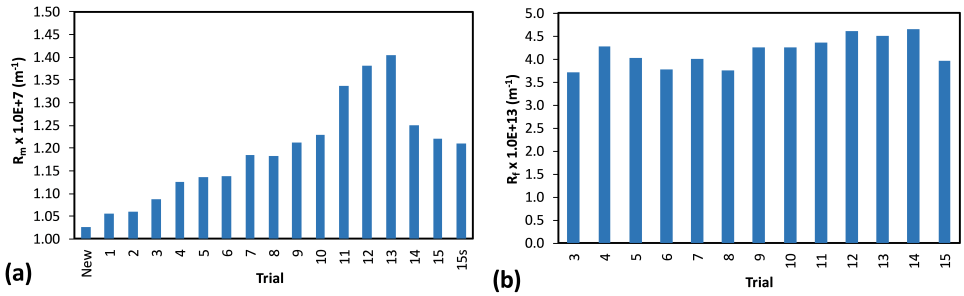


Figure 7.16: (a) Hydraulic membrane resistance after each concentration experiment and (b) fouling resistance during each concentration experiment. Trial is the cycle number, and '15s' is the same cycle with a secondary cleaning step.

As seen from the results, membrane resistance rose steadily after each concentration experiment, with minor changes in fouling after the switch to 0.1 wt% of cleaning agent (after cycle number 5). Based on these trends, we concluded that the increase in membrane resistance was unrelated to fouling but linked to compaction of the membrane. This was also noted for fouling resistance (Figure 7.16b), which did not follow the same trend throughout the study period of 15 cycles. The effect of the cleaning was first noted when it was replaced by rinses with just water (cycles 11 to 13), which increased the membrane resistance by approximately 14% in cycle 13. The fouling was not irreversible, because the membrane resistance returned to the previous value on washing with 0.1 wt% in 2 subsequent cleaning steps.

A 1-hour cleanse with high pH was sufficient to remove any measurable foulants [136], as noted when the high-pH cleaning agent was replaced with an acidic agent (Ultrasil 73) at 0.5 wt% during the cleanse after the 10^{th} trial. The flux during the cleanse was initially stable and constant but began to decrease after 20 minutes. The cleanse was halted when the flux decreased by 10% from the starting value, to avoid any irreversible fouling. The flux was thus restored by performing an alkali cleaning step (0.1 wt%) for 1 hour. One explanation for the decline is membrane fouling by SSL components, but another possibility is a change in the membrane's hydrophilicity with the pH of the cleaning solution [137]. This assumption was based on the isoelectric point for regenerated cellulose (roughly pH 3.4 [138]), which is approximately the same pH of the acidic cleaning agent. This effect, however, was not examined further and is left for future work.

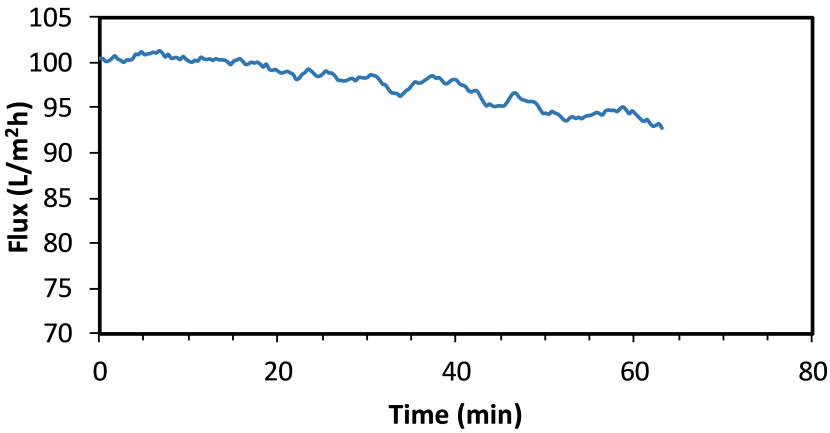


Figure 7.17: Flux vs time during the acidic cleanse using 0.5 wt% of Ultrasil 73 in cycle/trial 10.

The flux during the concentration studies was generally stable, averaging 88 L/m^{2}h. The average flux, however, decline significantly after trial 10, when the cleaning cycles were halted (Figure 7.18a). However, the flux returned after the cleanse in trial 14, resulting in an average flux of 92 L/m^{2}h in trial 15. The retention of GGM was unchanged overall, as seen in Figure 7.18b. The retention of total lignin, however, changed, likely because lignin was responsible for the membrane fouling [125,136].

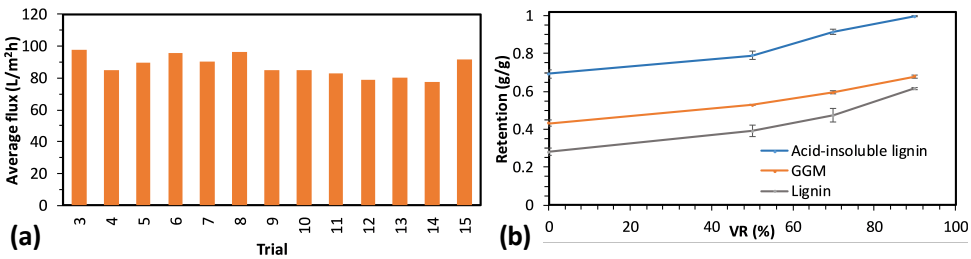


Figure 7.18: (a) Average flux during the concentration experiments and (b) retention of acid-insoluble lignin, GGM, and lignin in trials 3, 8, and 12.

8. Separation of GGM and lignin

In the previous chapter, SSL was processed using various membrane filtration steps. The SSL was concentrated and purified through a series of UF and DF, resulting in the removal of primarily pulping chemicals and other low-MW compounds. The separation of hemicelluloses and lignin was not possible with membrane filtration. The SEC results in Paper I also show that the separation of these components was futile. Based on these observations, the sum of the hemicellulose and lignin was referred to as LCCs in Paper I. The results in Paper IV show that the separation of these components was possible using another SEC column, as detailed in Paper II.

This chapter presents 2 separation techniques: antisolvent precipitation (Paper II) and adsorption (Paper VI). In Paper II, methanol, ethanol, and acetone were used as antisolvents to precipitate hemicellulose from the SSL, with the aim of separating the polysaccharide from lignin. The yield, separation degree, and MW of the precipitates were also determined. HSQC 2D-NMR was performed to determine the structure of the products.

In Paper VI, the aim was to remove the lignin from the untreated SSL using resins by adsorption. The existence of lignosulfonates in the SSL was observed in Paper III. Thus, the removal of lignin was examined using anion-exchangers and hydrophobic resins. The resulting adsorption data were fitted to models, and the underlying mechanisms were discussed. The desorption of lignin was also studied, given the importance of resin regeneration for the future process economy. The resin-treated SSL was filtered by UF and compared against UF of untreated SSL.

8.1 Antisolvent precipitation (Paper II)

Before the antisolvent precipitation, the SSL was concentrated and purified to increase the concentration of polysaccharides and decrease the amount of pulping chemicals (Figure 8.1). The concentration was done using the 50 kDa membrane from Paper I, and the diafiltration was performed using the same membrane, with a diafiltration factor of 5. The diafiltered retentate (‘50 kDa origin.’ in Figure 8.1) was diluted with deionized water (‘50 kDa diluted’) and evaporated (‘50 kDa evapor.’) to increase the concentration of solutes beyond the ability of membrane filtration.

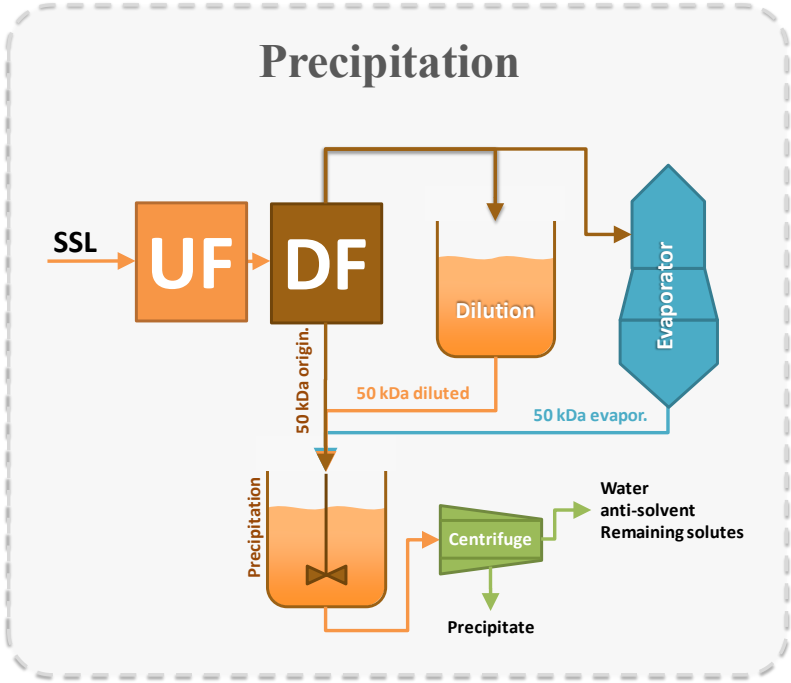


Figure 8.1: Flowchart of the SSL treatment before and after the precipitation step.

These streams were precipitated using the antisolvents above, and the precipitates were separated by centrifugation, as seen in Figure 8.1.

The compositions of the treated streams using UF, DF, dilution, and evaporation are listed in Table 8.1. During the membrane filtration, the lignin had slightly lower retention, resulting in minor separation between the GGM and lignin. Diafiltration increased the purity of the solution, as evidenced by the higher GGM:TDS and lignin:TDS ratios and lower conductivity for the retentates. The ratio between acetic acid and GGM did not change between the retentate (50 kDa origin.) and evaporated retentate (50 kDa evapor.), indicating that the acetic acid in the solution bound to the GGM.

Table 8.1: Compositions of the treated SSL streams. The sample names are highlighted in Figure 8.1. Ara, Gal, Glc, Xyl, Max, and AA are abbreviations for arabinan, galactan, glucan, xylan, mannan, and acetic acid, respectively.

Sample	Concentrations in (g L^{-1})								Conductivity
	TDS	Lignin	L-Ara	D-Gal	D-Glc	D-Xyl	D-Man	AA*	(mS/cm)
Untreated SSL	84	32	1.2	1.5	1.3	1.5	2.7	2.8	48
Membrane filtration retentates									
50 kDa origin.	103	84	1.3	5.6	4.9	3.5	9.9	1.6	14
50 kDa diluted	76	64	1.1	4.5	3.9	2.9	7.8	1.3	11
50 kDa evapor.	228	190	2.0	11	11	7.6	21	3.4	29

* The sum of bound and free acetic acid

8.1.1 Precipitation of the retentate

The precipitation experiments with the 50 kDa diafiltered retentate (50 kDa origin.) using acetone, ethanol, and methanol as antisolvents are shown in Figure 8.2 (a). GGM was the first component to precipitate, followed by lignin. Acetone was the most efficient antisolvent, given that GGM precipitated at its lowest concentration. The highest separation degrees were 76% (acetone), 61% (ethanol), and 59% (methanol) at 48 wt%, 51 wt%, and 61 wt%, respectively. Similar results were obtained by Zasadowski, et al. [84] and Song, et al. [83] using the same antisolvents. However, the amount of antisolvent that was required in our study was lower, perhaps due to the higher solute concentrations in the starting material (50 kDa origin.).

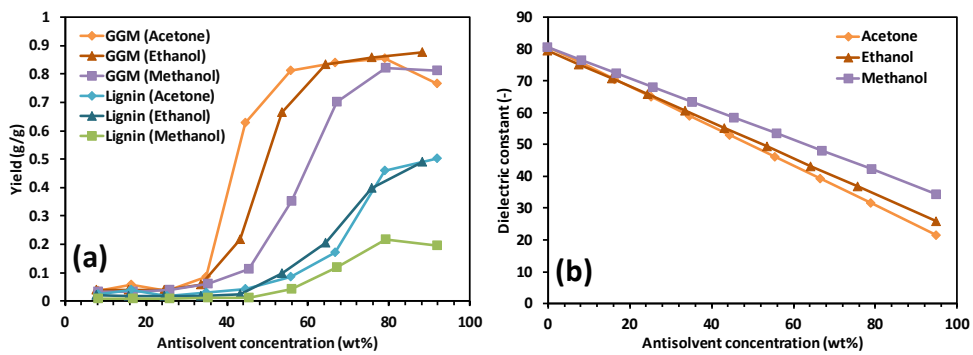


Figure 8.2: (a) Precipitation yields of the various SSL components vs antisolvent concentration. (b) Dielectric constant of the antisolvent and water mixture at various concentrations, as presented by Akerlof [139].

The precipitation yields in Figure 8.2a were related to the polarity of the antisolvents. Acetone had the lowest polarity, whereas methanol had the highest,

which generated the precipitation order in Figure 8.2a. The polarity of the bulk solvent can be approximated by the dielectric constant [140]. Akerlof [139] measured the dielectric constant of solutions that contained mixtures of water and antisolvent at various concentrations. Their results for the 3 systems—water-acetone, water-ethanol, and water-methanol—at room temperature are seen in Figure 8.2b. Assuming that the influence of solutes on the bulk solvent dielectric constant was equal, the data in Figure 8.2a were re-evaluated using the calculated dielectric constant of the solution, as seen in Figure 8.3, which shows strong correlation between yields and dielectric constants.

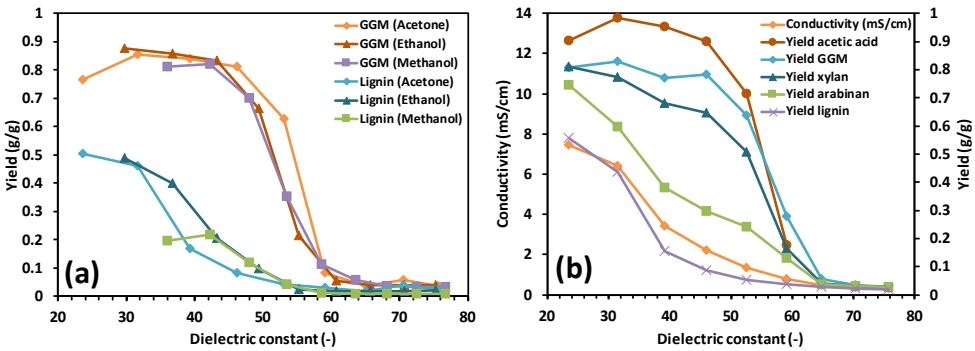


Figure 8.3: (a) The data in Figure 8.2a, substituting antisolvent concentration with dielectric constant. (b) Solute yields and the conductivity of the resulting solution as a function of the dielectric constant using acetone as antisolvent.

A small difference in the correlation was seen between acetone and the alcohols, which was likely related to the interaction of water molecules and the antisolvent. Acetone is an aprotic solvent; thus, it breaks the hydrogen bonds between water and other compounds, such as hemicellulose [141]. Ethanol and methanol are protic solvents, which means that the solubility of other compounds is reduced by the formation of hydrogen bonds with water and that the possibility for other compounds to form hydrogen bonds with water is reduced. The results also show that GGM precipitates at a higher dielectric constant than lignin, indicating that the lignin has a higher polarity than GGM [85,142]. Several studies have shown that lignin has a higher solubility in acetone than in ethanol or methanol [84,143]. The opposite pattern was noted in this study, suggesting that the lignin was sulfonated and thus had a higher polarity [144].

Based on the FTIR measurements in Paper III, the lignin in the SSL was sulfonated, strengthening this assumption. This was also apparent from the conductivity measurements of the various precipitated fractions (Figure 8.3b), wherein a strong correlation existed between lignin yield and the conductivity of the solution. The initial conductivity (14 mS/cm, Table 8.1) failed to be restored at an acetone concentration of 92 wt%, likely due to the low lignin yield (56%) in that cumulative

fraction; thus, we concluded that the lignin was responsible for the high conductivity in the solution [71,145].

The MW of the lignin decreased with increasing amounts of acetone, as seen in Figure 8.4b, which confirmed our earlier observations. However, in Paper IV, the lignin (lignosulfonates) was found to be ion-excluded, resulting in the high MW in Figure 8.4b. The decreasing MW could have resulted from increasing ionic strength (~conductivity), which shifted the MW of lignin to the lower end of the SEC graph (Paper IV). The change in the MW of lignin was thus inconclusive, based on these water-SEC results.

The wide peak in the region around 10 kDa was assigned to lignin-free GGM (Figure 8.4a). This peak lacked a UV response (Figure 8.4b) and underwent a sudden rise between an acetone concentration of 35% to 45%, which was explained by the immediate increase in GGM yield from 0.16 to 0.51, as shown in Figure 8.2a. At higher acetone concentrations, this peak did not increase further, whereas the peak in the region of 200 kDa rose. Based on the UV response for this peak, the lignin likely contributed to the increase in intensity. The peak in the region of 100 kDa generally followed the GGM yield and increased slightly with higher lignin yields beyond an acetone concentration of 56%. This peak likely belonged to LCCs, based on the yields for xylan and arabinan, which had the same trend as for the lignin (Figure 8.3b) [146].

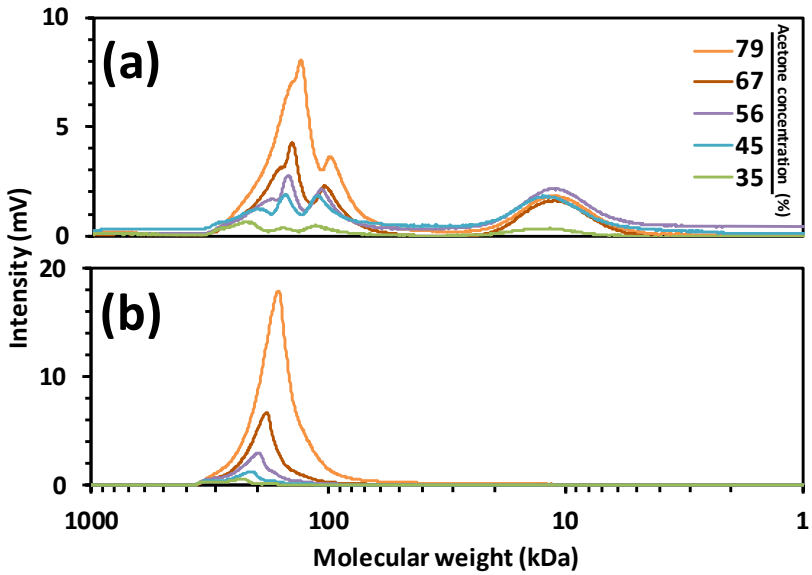


Figure 8.4: Water-SEC results of precipitated fractions at an acetone concentration of 35 wt% to 79 wt%. (a) RI signal and (b) the corresponding UV signal. The time-to-MW conversion on the x-axis was performed using PEG standards.

8.1.2 Characterization of the fractions

To characterize the precipitated fractions, 2 cumulative precipitates were chosen. The first fraction contained the precipitates from 45 wt% acetone. The remaining unprecipitated components were defined as the second fraction. In Paper II, only these 2 fractions were available. A third fraction was added, wherein the first fraction was precipitated a second time using 45 wt% acetone. These 3 fractions were analyzed by HSQC 2D-NMR (Figure 8.5).

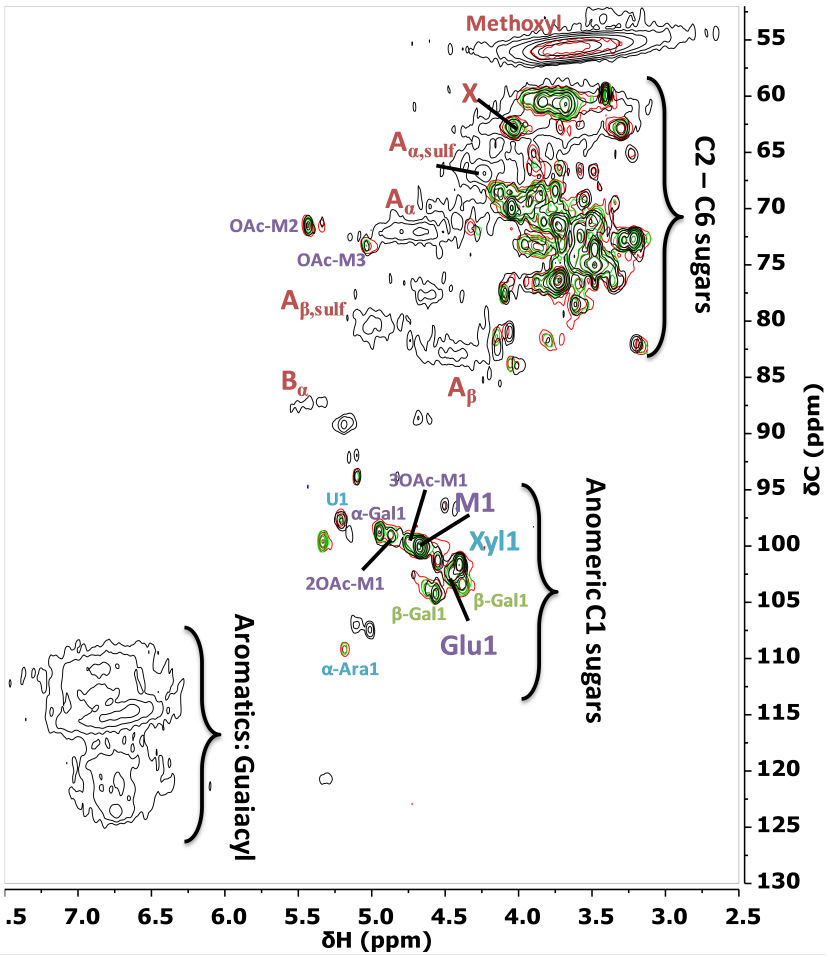


Figure 8.5: HSQC 2D-NMR spectra of 3 acetone-precipitated fractions. The first fraction (red contours), contained mostly polysaccharides (precipitated at 45 wt% acetone). The second fraction (black contours) contained the remaining unprecipitated components. The third fraction (green contours) comprised the second precipitation of the first fraction at 45 wt% acetone. The spectra were assigned per the HSQC 2D-NMR section in Chapter 6 and the literature [114,147-149].

The overall spectrum was similar to the results in Chapter 6, which were representative of the RC70PP retentate. For instance, the lignin was mostly composed of guaiacyl units, with β-aryl-ether (β-O-4) (A) and phenylcoumaran (β-5) (B) as the major intermonolignol bonds. Methoxyl groups were also associated with lignin, as shown in Figure 8.5. GGM (α-Gal1, M1, 2OAc-M1, 3OAc-M1 and Glu1) and arabinoglucuronoxylan (α-Ara1 and Xyl1) were visible in the anomeric C1 sugar region, as explained in Chapter 6.

In Paper II, the existence of sulfonated lignin was not confirmed, and thus, the assignments were missing these signals. In Figure 8.5, these missing assignments were added, denoted as sulfonated β-O-4 signals ($A_{\alpha,sulf}$ and $A_{\beta,sulf}$). These signals were in the same region as for the benzyl-ether linkages in LCCs that were assigned in Paper II. Because the amount of lignin in the sample was high, the existence of LCCs, based on these signals, was uncertain. Also, a signal that was denoted α-glycosyl in Paper II appeared in the region for phenyl-glycosidic LCC linkages. However, the assignments were made, assuming that the data for the d_6-DMSO solvent system were applicable for a D_2O solvent. Paper IV shows the effect of changing the solvent from D_2O to d_6-DMSO, where a shift of the signals in the anomeric C1 sugar region is seen on the proton-axis. The signal was thus believed to result from β-Arabinopyranose-(1 → 6) Mannopyranose bonds or have derived from other sugars with a gluco or xylo configuration [114,150]. The existence of phenyl-glycosidic linkages was indicated by the PhG signals in Figure 6.2 using a different batch of SSL (Paper IV). In Figure 8.5, these signals were missing; thus, based on these NMR data, the existence of LCCs could not be confirmed.

The results clearly show the removal of lignin from the first precipitate (red contours), based on the missing lignin signals [aromatics, β-O-4 (sulfonated and non-sulfonated), and β-5]. However, the methoxyl signal was still visible, with a lower intensity, indicating that traces of lignin remained in the precipitated fraction. The reason for the aromatic region not showing any signals could have been that the lignin had a high MW or was coupled to carbohydrates [151]. In the second precipitation (green contours), the methoxyl signal was not visible, indicating that the remaining lignin was likely removed. However, in the first and second precipitated fractions (green and red contours), a signal for cinnamyl alcohol end-groups (X) remained visible, prompting us to speculate that it was likely a sugar derivative and overlapped with the same region in the spectrum.

8.1.3 Effect of concentration on precipitation

The effects of concentration changes in the SSL retentate were examined by varying the concentration using dilution and evaporation. The results from the precipitation are presented in Figure 8.6.

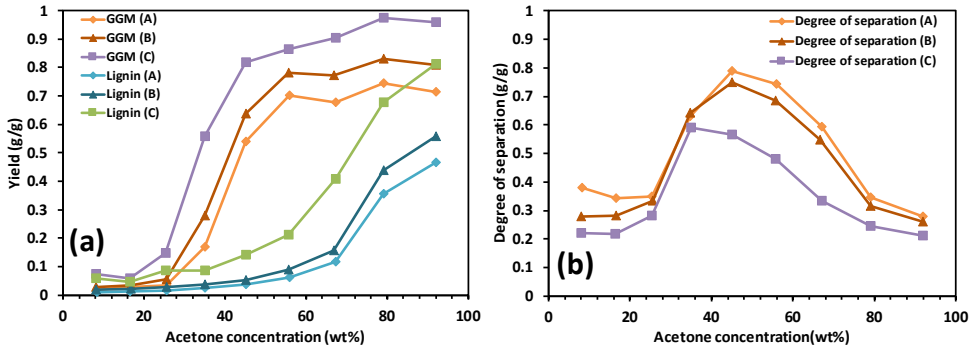


Figure 8.6: GGM and lignin yield (a) and separation degree (b) vs acetone concentration. The 50 kDa retentate is labeled (B), the diluted 50 kDa retentate is labeled (A), and the evaporated 50 kDa retentate is labeled (C).

As seen from the results, the GGM yield increased with solute concentrations, as also observed by Zasadowski, et al. [84], who found that lower antisolvent addition was required to achieve high yields. However, this rise was followed by higher lignin yields, which in turn decreased the degree of separation, as shown in Figure 8.6b. The opposite effect was observed when the 50 kDa retentate was diluted, with lower GGM yields and higher separation degrees. This effect was likely attributed to the availability of free water, which is lower at high solute concentrations and higher at low solute concentrations, as explained in Section 4.3 [80,152,153].

Also, lignosulfonates have a randomly branched structure, with sulfonate groups on the outer layer of the molecule [154,155], stabilized by electrostatic repulsion between molecules. An increase in solute concentration would bring the molecules closer, forcing the lignosulfonates to form larger aggregates (to maintain stability) that can precipitate easily from solution [80,152,153], which is the likely reason for the higher lignin yield with the evaporated 50 kDa retentate.

In Section 8.1.1., the solutes were assumed not to have affected the dielectric constant of the solution during the conversion from acetone concentration to dielectric constant for the results in Figure 8.3. However, changes in the overall solute concentration can create a different situation. Hasted*, et al.* [156] found that by increasing the solute concentration, the dielectric constant of a solution declines as a consequence of newly formed hydration shells around the ions, decreasing the response of the water to the external electrical fields. This observation thus explains the results in Figure 8.6.

8.1.4 Effect of pH and temperature on precipitation

The effects of pH on precipitation were determined with the 50 kDa retentate. The pH was varied between 4 and 12 with sodium hydroxide. The solutions turned from brown to black on the addition of sodium hydroxide, likely due to the dissociation

of phenolic groups on the lignin [157,158]. The high pH was expected to increase the stability of the lignin in solution as an effect of the greater electrostatic repulsion [80]. However, the precipitation yield increased with pH, as seen in Figure 8.7a. The sodium hydroxide likely competed with lignin for the same hydration water, which in turn lowered the stability of the lignin in solution, thus rendering it easier to precipitate. The effect was therefore similar to increasing the concentration of the solutes. The yield for the GGM reached completion at a pH of roughly 12, which was difficult to achieve before the addition of sodium hydroxide or the increase in solute concentrations (Figure 8.6). These results suggest that the unprecipitated GGM (roughly 20% of the total GGM) in Figure 8.2 was low-MW or associated with the lignin.

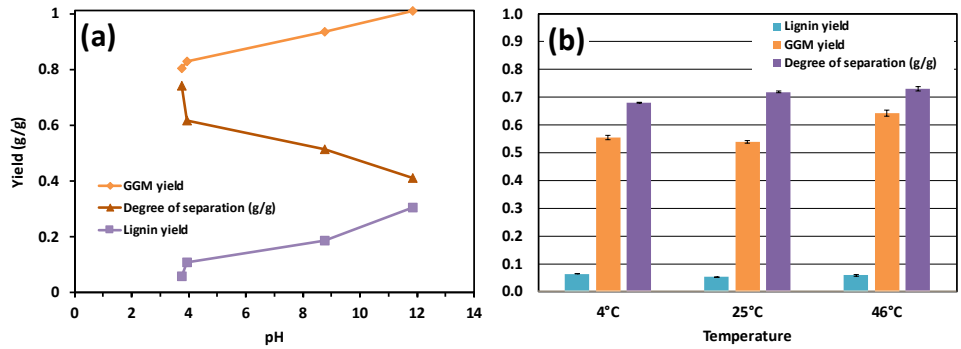


Figure 8.7: Precipitation yields and separation degree vs pH (a) and temperature (b).

The dependence of precipitation on temperature was studied at 3 temperatures; the results are presented in Figure 8.7b. The yields for GGM and lignin improved when the temperature was increased or decreased from 25°C. The reason for this behavior is unknown, but several explanations have been presented in other studies [159-161]. Shinoda and Fujihira [159] interpreted similar results as being the effect of a reduction in the entropy of the system that in turn lowered the Gibbs free energy of solvation, thus decreasing the solubility. However, that study examined the solubility of liquid hydrocarbons in water, perhaps not applicable to the solutes in our study.

Li, et al. [160] studied the effect of temperature on the expansion of lignosulfonate macromolecules, concluding that lignosulfonates become more hydrophobic at elevated temperatures, due to the breakage of hydrogen bonds between the water and solutes, forcing the lignosulfonate to compensate by forming intramolecular hydrophilic bonds and thus turning the surface of the macromolecule more hydrophobic. Perhaps the greater hydrophobicity promoted the higher yields in Figure 8.7b.

Another possible explanation is related to the solvent's dielectric constant, which is temperature-dependent. Luong, et al. [161] studied the influence of temperature on the dielectric constant of water and the ability of the solvent to extract polar and nonpolar organic matter. They observed that the dielectric constant of water decreased with rising temperature, which reduced the ability of the solvent to extract polar compounds. This effect also could have occurred when we increased the temperature of the precipitation from 25°C to 46°C. However, it did not explain the increasing yields at 4°C, the reason for which remains unknown.

8.2 Adsorption (Paper VI)

In this paper, the removal of lignin (including lignosulfonates) from SSL was examined using polymeric resins with varying properties. These properties were based on the functional group composition of the lignin. The lignin was sulfonated (Paper III) in the SSL, and acid-insoluble lignin was also present. The resins chosen were thus the anion-exchange type, with strongly (Amberlite IRA958) and weakly (Amberlite IRA67) basic surface active groups (tertiary and quaternary amines) [107]. Hydrophobic resins have generated promising results with regard to the removal of lignin in other applications [102], which is why we studied Amberlite XAD4 resin for the removal of lignin from SSL.

8.2.1 Adsorbent screening

The 3 selected resins were screened by mixing 4 g of the washed and dried adsorbent with 20 mL of SSL at room temperature for 24 hours. The removal of the major components in the SSL using these resins are shown in Figure 8.8.

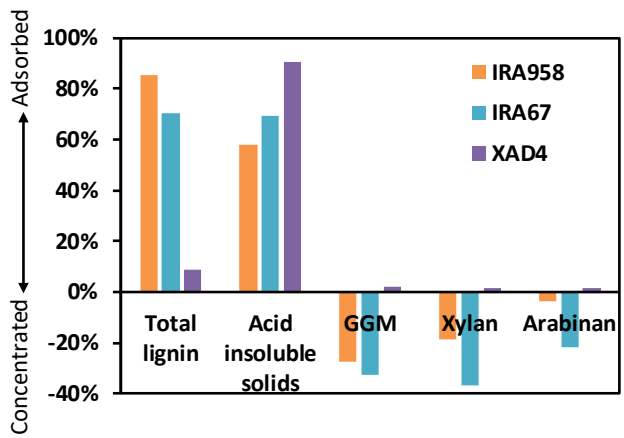


Figure 8.8: Results from the adsorbent screening, showing the removal of various solutes. Negative contributions were the result of the solutes being concentrated.

The best-performing resin was the strongly basic IRA958, with a total lignin removal of 85%. XAD4 had the worst performance with regard to the removal of total lignin (lignosulfonates and acid-insoluble lignin). However, it performed best in the selective removal of acid-insoluble lignin, as shown in Figure 8.8. The anion exchangers in the screening study also removed some acid-insoluble lignin, suggesting that this part of the lignin was sulfonated or coupled to carbohydrates prior to the acid hydrolysis of the samples [113]. The latter was also implied by the non-zero adsorption of polysaccharides with XAD4 (Figure 8.8).

The adsorbates on XAD4 were desorbed using sodium hydroxide and methanol rinses and analyzed for their polysaccharide composition. The desorption recovered 25% of the acid-insoluble lignin, of which 5% was polysaccharides. The arabinan and xylan compositions were similar to the raw material, but the GGM ratios differed: 0.5:0.8:1.0 Gal:Glu:Man in the recovered fraction versus 0.4:0.4:1 in the raw material (Paper VI). This finding strengthened the observations in Paper IV with regard to LCCs and the possibility of phenyl-glycosidic bonds existing between the GGM and lignin.

The polysaccharide removal for the anion exchangers was negative, indicating that the polysaccharides were concentrated during the adsorption study. This phenomenon occurred as a result of using dry adsorbents at the start of the study. The adsorbents have a moisture-holding capacity of 60% to 80%, which was acquired from the water in the SSL. The absorption of water from the SSL and the rejection of polysaccharides was likely the reason for the observed increase in concentration. Based on the high lignin removal, IRA958 was chosen for the remaining studies.

8.2.2 Equilibrium experiments

IRA958 was used for a series of equilibrium experiments, in which the amount of adsorbent was varied while the amount of SSL was kept constant. The results of this study are shown in Figure 8.9.

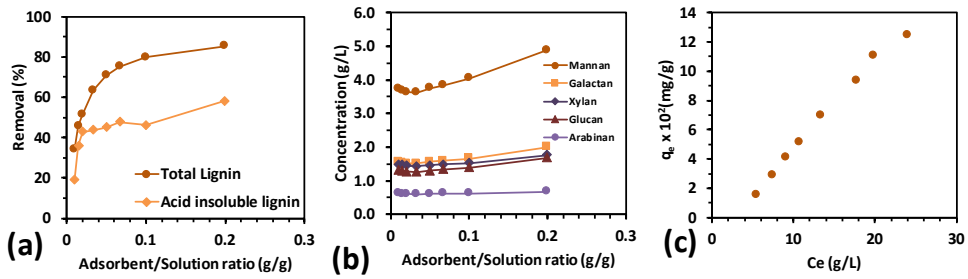


Figure 8.9: Equilibrium experiments with the IRA958 anion exchange resin. Lignin removal (a) and concentration of polysaccharides (b) vs adsorbent/solution ratio. Adsorption capacity vs equilibrium concentration of lignin (c).

The lignin removal was 85% at its peak (0.2 g adsorbent/g solution) (Figure 8.9a), which was the same as in the screening study. However, in practice, a lignin removal of 80% was the most feasible, due to the lower requirement of adsorbent of 0.1 g/g solution versus the amount of lignin that was removed. The adsorption of polysaccharides (Figure 8.9b) was visible at lower adsorbent:solution ratios, wherein the total removal was less than 2%. However, for higher adsorbent:solution ratios, the concentration increased substantially, and the adsorption of polysaccharides could not be measured.

The adsorption of lignin was described by fitting the adsorption capacity-versus-lignin concentration (Figure 8.9c) data to various adsorption isotherms (Table 4.2). The data in 8.9c clearly show that the adsorption was nonlinear, which was evident by the adsorption capacity at high and low lignin concentrations, the extrapolation of which to the x-axis did not reach origin. As a result, the linear isotherm model yielded a poor fit, as seen in Table 8.2.

Table 8.2: Resulting parameters from fitting the equilibrium data in Figure 8.9c to the models in Table 4.2.

Model	Parameters	Unit	R^2
Linear	K_{lin} = 51.67	[mL/g]	0.9679
Langmuir	Q_L = -1621.8	[mg/g]	0.5445
	K_L = -0.0202	[mL/mg]	
Freundlich	K_F = 31.06	$[mL^{nF}mg^{1-nF}/g]$	0.9855
	n_F = 1.1774	[-]	
Sips (Langmuir-Freundlich)	Q_S = 1947.2	[mg/g]	0.9978
	K_S = 0.0035	[mL/mg]	
	n_S = 1.9616	[-]	
Modified Brunauer–Emmett–Teller (BET)	Q_B = 24728	[mg/g]	0.9839
	K_B = 0.3926	[mL/mg]	
	C_S = 216.74	[mg/mL]	

Based on these data, the curve in Figure 8.9c primarily resembled a Type V curve, as described in Section 4.4.1, which is S-shaped. The more common isotherms, such as Langmuir and Freundlich, fail to describes these types of curves. The Sips isotherm, which is the combination of Langmuir and Freundlich, was derived to overcome these limitations and is used to describe such curves. This was also clear, based on the R^2 value in Table 8.2, in which the Sips isotherm gave the best fit to

the data. Further, the results suggest that the adsorption was cooperative, based on the n_S exponent, which was higher than unity. The calculated maximum adsorption capacity (Q_s) exceeded what has been reported for magnesium lignosulfonates [108], perhaps due to a difference in the degree of sulfonation, MW of the lignin, or dryness of the adsorbents.

8.2.3 Adsorption kinetics

Adsorption kinetics can be used to identify key functions of adsorptive mechanisms and is important for scaling up and describing the adsorption process over time [96]. Figure 8.10a shows the lignin concentration in the bulk and the adsorption capacity of the adsorbent over time (0.1 g adsorbent/g solution ratio).

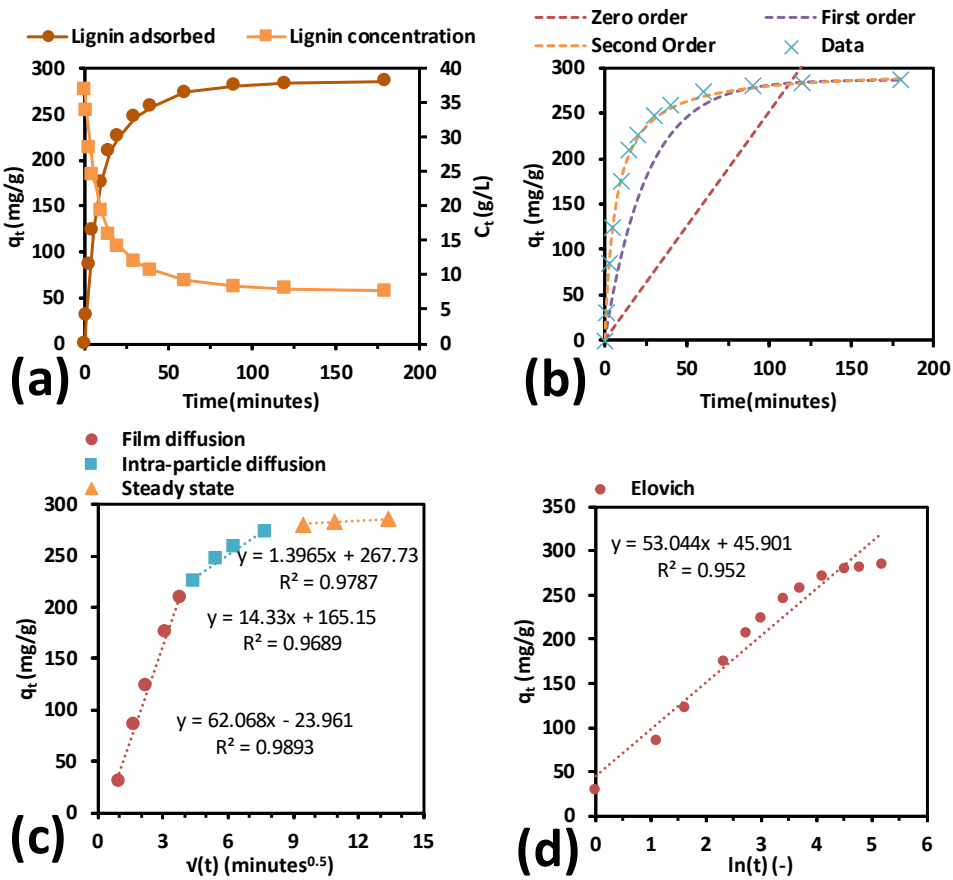


Figure 8.10: Adsorption of lignin vs time for a mixture of 0.1 g adsorbent per g of solution (a). Fit of the time-dependent adsorption capacity to the pseudo-zero-, first-, and second-order models (Table 4.3) (b), intra-particle diffusion model (c), and Elovich model (d).

The adsorption process took roughly 180 minutes, after which the lignin concentration remained constant. The process was approximately 2 to 3 times faster than similar processes in the literature [108], likely due to differences in the solutes (lignosulfonates), operating conditions, and type of adsorbent. Based on fit of the kinetic data to commonly used models (Table 4.3), the PSO model had the best fit, as seen in Figure 8.10b, with an R^2 value of 0.9997, which, according to the literature, indicates that the adsorption type was chemisorption [96]. The PFO model gave an equilibrium adsorption capacity that was closer to the value in our equilibrium studies, but as seen in Figure 8.10b, it could not resolve the kinetics in the region of 0 to 75 minutes. The Elovich model (Figure 8.10d) gave information regarding the initial adsorption rate, which was 126 mg/(g min), and the intra-particle diffusion model attributed this initial adsorption to film or macropore diffusion. The slow adsorption in the subsequent period (t > 10 minutes) was, according to the model, due to intra-particle diffusion.

8.2.4 Adsorbent regeneration

Industrially, adsorbent regeneration is an important factor, because it determines the final cost and viability of the adsorption process. Lignin desorption was studied by washing the resin from the kinetics study in 3 consecutive steps with sodium chloride and sodium hydroxide, as shown in Figure 8.11.

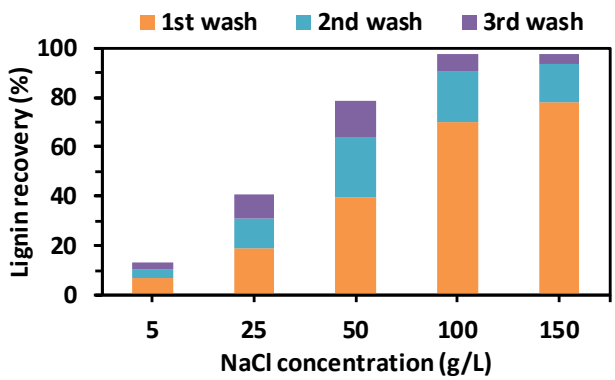


Figure 8.11: Lignin recovery after three consecutive washes using a regenerant with varying NaCl concentrations. The NaOH concentration was constant (10 g/L).

According to the results, a concentration of at least 100 g/L sodium chloride was needed to achieve a maximum lignin recovery of 98%. These observations were similar to those of Liu, et al. [108], who obtained the same lignosulfonate recovery using a sodium chloride concentration of 10%. Higher concentrations of sodium chloride did not yield greater recovery of lignin. However, the recovery still increased during the first wash beyond 100 g/L, as seen by the orange bars in Figure

8.11a. Whereas the recovery of lignin could not be improved further, the results show that it is possible to decrease the number of washes by increasing the concentration of sodium chloride in the first wash step.

8.2.5 Ultrafiltration of adsorption permeate

The effect of lignin removal was examined by UF, using the same hydrophilic membrane (RC70PP) as in our previous studies (Papers IV and V) and other regenerated cellulose membranes, as shown in Figure 8.12.

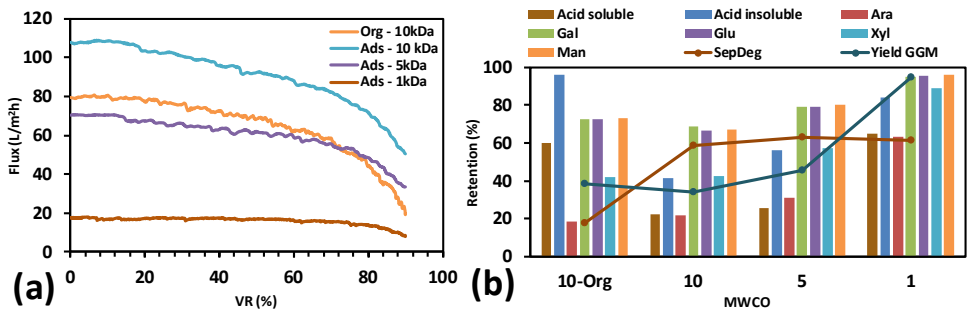


Figure 8.12: Effects of adsorption on UF flux (a) and retention of the solutes (b) at 25°C, 0.5 m/s CFV, and TMP 5.5 bar.

The flux of the untreated SSL (Org – 10 kDa) was half that in our previous study (Paper IV), as seen in Figure 7.7a, which was due to the lower temperature during the filtration—25°C in this study and 50°C in Paper IV. The retention of solutes (Figure 8.12b) was expected to be higher due to the lower flux, but the opposite was observed. The higher retentions in Paper IV were likely due to compaction of the membrane, as explained in Section 7.3.3. The lower flux and retention in Figure 8.12 thus strengthen this assumption.

The removal of lignin improved the flux by a factor of 1.4, with minimal impact on the retention of polysaccharides. The separation degree rose from 17% to 59%, resulting in a higher final purity. The GGM yield decreased slightly from 38% to 34%, due to the decline in mannose retention from 73% to 67%. The yield improved with denser membranes, as shown in Figure 8.12. By using a 5 kDa and 1 kDa MWCO membrane, the yield increased from 34% to 46% and 95%, respectively. The separation degree was constant for all 3 membranes; thus, the purity of the solution was not a determining factor. The flux of the 5 kDa membrane was nearly the same as for the 10 kDa membrane using the original nontreated SSL, rendering a change to this membrane a viable and promising alternative. The flux for the 1 kDa MWCO membrane was much lower, and whether it is economical to use this membrane remains to be examined in future work.

9. Techno-economic analysis

In this chapter, 3 case studies were evaluated economically. In the first case study, UF was used to concentrate the SSL without any further purification. In the second study, an adsorption column was used for the SSL purification. The adsorption column was simulated before and after the UF, and the costs of both subcases were compared. Finally, in the third case study, antisolvent precipitation was considered as the separation process for the UF retentate. The design criteria for the process was an SSL feed flow of 1 m^3/h and a final separation degree of at least 60%. The feed flow was chosen, based on the techno-economic evaluation in Paper IV, and the separation degree limit was selected, based on the results on the hydrogel formation in Paper III.

9.1 Case study I – Ultrafiltration of SSL

In this first case study, the SSL was only concentrated with the RC70PP membrane, without any further purification or refinement. Techno-economic evaluations were already performed for this combination of membrane and SSL in Paper IV. However, the calculations are based on spiral modules and continuous filtration, assuming that the retention of solutes and flux are equal to the lab-scale experimental results. Also, Paper V showed that scaling up from lab-scale data is not trivial, and given the dependence of the retention and flux of the equipment setup and operating conditions, assumptions were made and corrected, based on what was observed during the pilot studies. The lab and pilot studies were conducted in a single-stage batch process, and given the difficulty in predicting the process dynamics in a continuous operation, the scaled-up process was chosen to be run in single-stage batch mode, as well. The assumptions for the cost estimates are presented in Table 9.1. The major differences between these estimates and those in Paper IV are the higher investment cost (plate-and-frame module instead of spiral), the addition of a feed/retentate tank, and separate feed and circulation pump costs.

Table 9.1: Assumptions for the batch ultrafiltration cost estimates. The values are based on the combination of in-house experience and the following references [131,162]. The feed/retentate tank, feed pump, and circulation pumps were calculated based on Ulrich's method using stainless steel as a base material [163].

Investment cost (€/m^2)	2000
Feed/Retentate tank (€/m^3)	4184
Feed pump (€/W)	27
Circulation pump (€/W)	52
Membrane cost (less housing) (€/m^2)	50
Membrane lifetime (years)	1.5
Electricity price (€/MWh)	38
Extra membrane area (safety tolerance) (%)	20
Cleaner dosage (%)	0.1
Cleaner price (€/kg)	2.7
Cleaning time per cycle (h/day)	1
Amount of cleaning solution (L/m^2)	5
Rinsing water volume per cleaning volume	2
Clean water (€/m^3)	0.42
Pump efficiency (-)	0.8
Operating time (h/year)	8000
Maintenance and labor costs (% of capital cost)	5
Annuity factor (/year)	0.1

Further, the pilot studies showed that a 1-hour cleaning cycle with 0.1% Ultrasil 10 was sufficient to keep the membranes clean and minimize fouling. The experimental data for the estimations are presented in Table 9.2. The average flux and concentration of GGM in the feed and retentate were based on the lab-scale study (Paper IV), which were assumed to be valid for a low loop volume reduction (10% in this case) and a processing temperature of 65°C (Paper V). The feed and circulation pump energy demands were calculated per the methods in Paper IV. The remaining operating conditions for the process were derived from the pilot study in Paper V.

Table 9.2: Combination of experimental data and assumptions used in the cost estimates.

Plant feed flow (m^3/h)	1
Volume reduction (%)	90
Loop volume reduction (%)	10
Retentate flow (m^3/h)	0.1
Permeate flow (m^3/h)	0.9
Average flux (L/m^2 h)	132.2
Membrane area required (m^2)	6.8
GGM yield (%)	59.3
GGM concentration in retentate (g/L)	27.5
GGM produced (kg/h)	2.75
Separation degree (%)	22.4
TMP (bar)	5.5
CFV (m/s)	1.5
Circulation flow (m^3/h)	78.5
Maximum pressure drop (bar)	0.16
Feed pump energy demand (kW)	1.72
Circulation pump energy demand (kW)	0.45

The total cost of the process was 1736 €/ton of GGM, as seen in Table 9.3—approximately 30 times higher compared with the calculated value in Paper IV. The reason was the higher investment cost, but the addition of a feed/retentate tank and separate cost calculation for the pumps had a major influence on the total cost. The costs for feed and circulation pumps are often neglected or assumed to be included in the investment cost of 2000 €/m^2, which is likely valid for large processes with hundreds of cubic meters of waste water per hour [162]. However, for the design criteria of 1 m^3/h, the cost of the pumps was calculated separately and added to the capital cost to compensate for the lower feed flow.

The operating cost was also higher overall than in Paper IV, because the cost of electricity increased by a factor of 6 as a result of the low loop volume reduction that was required, in turn raising the volumetric flow that was needed to operate the feed pump and, consequently, the power. Electricity costs can be lowered by running the process at a higher loop VR. However, process variables, such as the flux and retention of solutes, cannot be predicted under such conditions, and thus, the accuracy of the cost estimations will be lower. The total cost of GGM production, however, was reasonable compared with similar cost estimates elsewhere [131].

Table 9.3: Calculated cost of GGM production using ultrafiltration.

Capital cost (€/year)	**18,152**
- Membrane plant (excl. pumps and feed tank) (€/year)	1634
- Pump cost (€/year)	6895
- Feed tank cost (€/year)	9623
Operating cost (€/year)	**1892**
- Electricity cost (€/year)	658
- Membrane replacement cost (€/year)	272
- Cleaning cost (€/year)	54
- Maintenance and labor costs (€/year)	908
Total cost (€/year)	38,196
Total cost / ton GGM	**1736**

9.2 Case study II – Adsorption and ultrafiltration of SSL

9.2.1 Batch adsorption – Calibration of the kinetics

A promising method for lignin removal is the use of resins by adsorption. In the lab-scale experiments (Paper VI), beakers and tubes were used for the batch adsorption trials. Batch adsorption is a convenient operation for estimating adsorbent capacity and sorbate-sorbent interactions and kinetics [164]. However, in an industrial setting, in which large quantities of SSL are continuously generated, the use of adsorption columns is more suitable with regard to economy and process control. In an adsorption column, the adsorbent is introduced continuously to a high concentration of SSL, whereas in batch mode, the concentration decreases, in turn lowering the driving force for the adsorption process. In this thesis, the only operation mode that was used experimentally was batch adsorption.

To design an adsorption column, the data from the batch process can be used to calibrate a model that can in turn be used to simulate the conditions and results in a column design. Paper VI presented several kinetic models, wherein the PSO model was shown to be suitable for describing the adsorption of SSL to IRA958 resin. However, this model lacks the ability to predict the adsorption of SSL with varying initial concentrations, as shown in Table 4.3, which is a crucial property of a model for the simulation of an adsorption column.

Adsorption isotherms are concentration-dependent and are a promising alternative to these kinetic models. However, the isotherms are derived for steady-state conditions, which does not apply to adsorption in a column [164]. Given that the adsorption follows an appropriate adsorption isotherm, the time-dependent version of the isotherm can be used instead. The adsorbent-SSL interaction follows the Sips or Langmuir-Freundlich isotherm. The non-steady-state or time-dependent Langmuir-Freundlich kinetics were derived by modifying the Langmuir kinetics model [165], yielding the expression in Equation 9.1:

$$r = \frac{dq}{dt} = k_{ads} c^n (Q_{max} - q) - k_{des} q \tag{9.1}$$

where r, k_{ads}, and k_{des} are the rate of adsorption, adsorption rate coefficient, and desorption rate coefficient, respectively. The maximum adsorption capacity (Q_{max}), Sips exponent (n), and equilibrium constant (K_s) are known from fitting the equilibrium data to the Sips isotherm (Paper VI). Also, the equilibrium constant is defined as the ratio between the adsorption and desorption coefficients, as seen in Equation 9.2.

$$K_s = \frac{k_{ads}}{k_{des}} \tag{9.2}$$

The only remaining unknown is the adsorption or desorption coefficient, which can be calibrated from the data for the time-dependent batch adsorption experiment. For the calibration, mass balances were defined, based on the setup from which the results in the batch study were derived (see Figure 9.1).

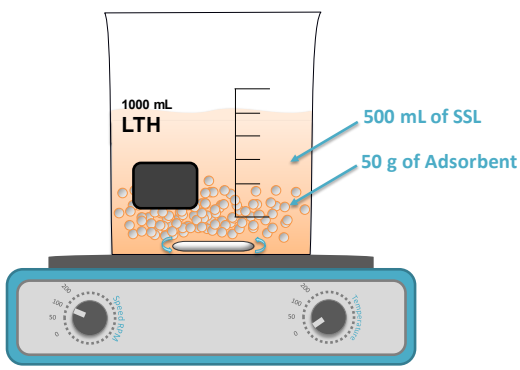


Figure 9.1: Setup for the time-dependent batch adsorption of SSL.

There was no incoming or outgoing stream from the beaker, and the solution was agitated; thus, the change in concentration in the bulk solution depended solely on the adsorption, based on the kinetics, as seen in Equation 9.3:

$$V\frac{dc}{dt} = rW \tag{9.3}$$

where V and W are the volume of the SSL solution and weight of adsorbent, respectively. Equations 9.1 to 9.3 were solved using Matlab with the built-in ordinary differential equations (ODE) solver (ode15s), coupled to the Matlab *fsolve* function, to solve an unknown (the desorption coefficient, k_{des}, was chosen in this case). The problem was only solved for lignin adsorption, given that it was difficult to observe the adsorption of any other component in the solution (Paper VI). At the initial time ($t = 0$), the concentration of lignin in the solution was set to 37 g/L, and the adsorption capacity was set to 0 mg/g. The results from the solver are shown in Figure 9.2, in which the desorption coefficient was calibrated to 0.67e-4 s-1.

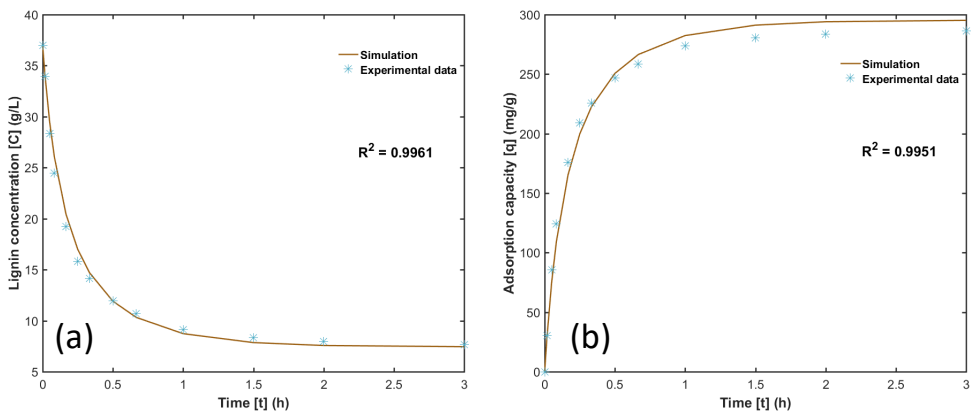


Figure 9.2: Results from the calibration of the adsorption and desorption coefficients. Lignin concentration (a) and adsorption capacity (b) for the simulation against the experimental data.

The calibration yielded a model that was in good agreement with the experimental data, based on the R^2 value, which was close to unity. Visually, minor variations in adsorption capacity were seen below and over 250 mg/g, which could have been caused by other influencing mechanisms, such as intra-particle diffusion, which was not included directly in this homogeneous model (in space) [165]. A heterogeneous model adds at least 2 factors to the system, such as the diffusion of solutes in the particles and the mass transport of solutes to the particle surface [166]. Such a step would likely generate slightly more accurate results. However, it would also require

one more ODE to be solved for the batch case and many more for the adsorption column, which can become computationally expensive. Further, the largest error in the adsorption capacity results was 3.3%, which is equivalent to 10 mg/g, and compared with the maximum adsorption capacity of roughly 2000 mg/g, it was negligible. The model was thus deemed to be suitable for the design of the adsorption column.

9.2.2 Adsorption column

The model that was used to describe the mobile phase in the fixed-bed adsorption column is the dispersion-convection-reaction equation, as defined in Equation 9.4 [166]:

$$\frac{\partial c_j}{\partial t} = D_{ax}\frac{\partial^2 c_j}{\partial z^2} - \frac{F}{\varepsilon A}\frac{\partial c_j}{\partial z} - \frac{1-\varepsilon_c}{\varepsilon}\rho_{sp} r_j \tag{9.4}$$

where c_j is the concentration of component j in the mobile-phase, t is time, z is the axial dimension, F is the flow rate, ε_c is the column void, A is the cross-sectional area for the column, and r_j is the adsorption kinetics in the stationary phase of the column (Equation 9.1). Equation 9.5 shows the definition of the swelled adsorbent density (ρ_{sp}) (kg of dry adsorbent to m^3 of swelled adsorbent), which is related to the amount of water that is absorbed by the particle (x_h). The equation is the result of a mass balance between the dry and swelled adsorbent, assuming that the volume of the dry adsorbent will change proportionally to the volume of water that is absorbed. The density of the dry adsorbent is ρ_{dp}, and the density of the absorbed water is ρ_w.

$$\rho_{sp} = \frac{\rho_{dp}\rho_w(100-x_h)}{(\rho_{dp}x_h+\rho_w(100-x_h))} \tag{9.5}$$

The total volume of fluid in the column (ε) is defined as the sum of the total fluid outside of the packing (ε_c) and the fluid inside of the particles, which is dependent on the particle porosity (ε_p) per Equation 9.6.

$$\varepsilon = \varepsilon_c + (1-\varepsilon_c)\varepsilon_p \tag{9.6}$$

In fixed-bed columns, the existence of particles will affect the mixing in the axial direction of the column. This backmixing can be described by the axial dispersion term (D_{ax}), which is calculated with Equation 9.7 [167]:

$$D_{ax} = \frac{d_p u_{int}}{Pe} \tag{9.7}$$

where d_p is the diameter of the adsorbent particles, Pe is the Peclet number, and u_{int} is the interstitial velocity and is defined as per Equation 9.8.

$$u_{int} = \frac{F}{\varepsilon A} \tag{9.8}$$

The known variables in the simulations are listed in Table 9.4.

Table 9.4: Known variables and design criteria for the simulation of the adsorption column.

Variable	Description	Value	Reference
F	Feed flow (m^3/h)	1.0	Design criteria
ε_c	Column void fraction (m^3/m^3)	0.4	[165]
ε_p	Particle porosity (m^3/m^3)	0.5	[165]
x_h	Amount of water in the adsorbent (%)	66	Adsorbent datasheet
ρ_{dp}	Particle density (g/ml)	1.8	Adsorbent datasheet
ρ_w	Water density (g/ml)	1.0	-
d_p	Particle diameter (µm)	740	Adsorbent datasheet
$(L/D)_{bed}$	Bed length/diameter ratio (m/m)	1.5	Recommended design criteria from
Pe	Peclet number	1.0	[165]
$c_{b,Lig}(t, 0)$	The concentration of lignin in the feed (g/L)	37.0	Paper VI
$c_{b,PS}(t, 0)$	The concentration of polysaccharides in the feed (g/L)	9.0	Paper VI
Min SD	The minimum separation degree (%)	60	Design criteria

The model (Equations 9.1-2 and 9.4-9.8) was solved by discretizing the equations in space using the method of lines (Figure 9.3a and b), which turns the partial differential equations into ODEs. The discretization was based on the finite difference method, in which the second derivative in space was approximated using a 3-point central difference and the first derivative was approximated using a 2-point backward expression (see Equation 9.9) [166]:

$$\frac{\partial^2 c}{\partial z^2} \approx \frac{c_{i+1} - 2c_i + c_{i-1}}{h^2} ; \frac{\partial c}{\partial z} \approx \frac{c_i - c_{i-1}}{h} \tag{9.9}$$

where i is the i^{th} grid point of a maximum of N grid points (Figure 9.3b). The boundary conditions for the system were a Dirichlet for the inlet and a Neumann for the outlet, as seen in Figure 9.3b. The polysaccharides (PSs) were assumed to be inert; thus, the term for the PS kinetics (r_j) was set to zero. The large set of ODEs were solved using Matlab's ODE solver *ode15s*, using a grid of 100 nodes.

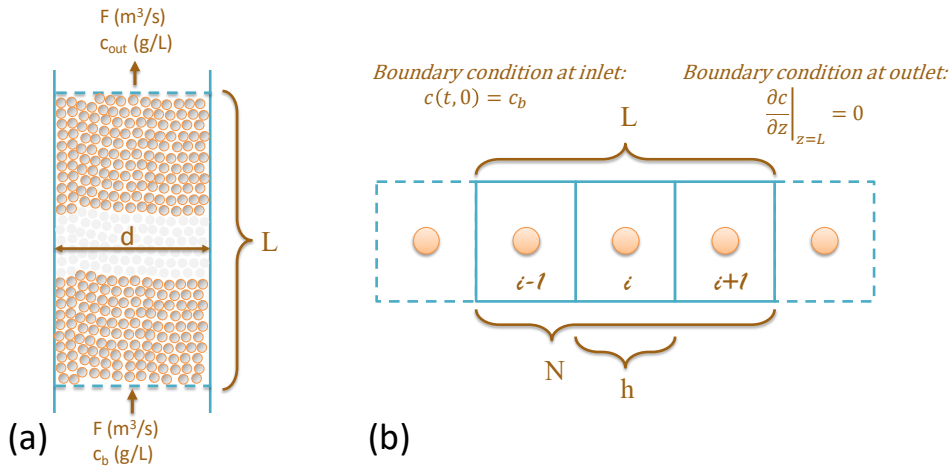


Figure 9.3: (a) The adsorption column with the flow rate (F) and concentration of solute at the inlet (cb) and outlet (cout). (b) Illustration of the discretization of the adsorption column along the length (L) or z-dimension. N is the number of nodes with the length (h) and the Dirichlet boundary condition at the inlet and Neumann at the outlet.

9.2.2.1 Adsorption – Column sizing

For sizing the column, the length and diameter of the column must be obtained. The ratio between the bed length and diameter is known (Table 9.4); thus, optimizing the column based on the length (L) was sufficient. Another important parameter was the operating time or the duration after which the column is saturated and ready for regeneration. The determination of this operating time is illustrated in Figure 9.4, using a breakthrough curve.

The breakthrough curve shows the concentration of the measured component at the outlet of the column as a function of time. As time passes, the stationary phase at the position near the inlet begins to be saturated, causing the component to bleed through to the outlet and the concentration to increase. At time t_s, the column is completely saturated, after which regeneration of the column is necessary. However, in practice, running the column to complete saturation is not always realized or desired, because it is difficult to regenerate a column that is 100% saturated and because specific constraints are placed on the outlet stream. One example is a

concentration constraint, in which a maximum concentration of c_{max} is allowed at the outlet. Using the breakthrough curve in Figure 9.4, the operating time can be determined with the newly set constraint, which in this case is equal to t_b (the breakthrough point).

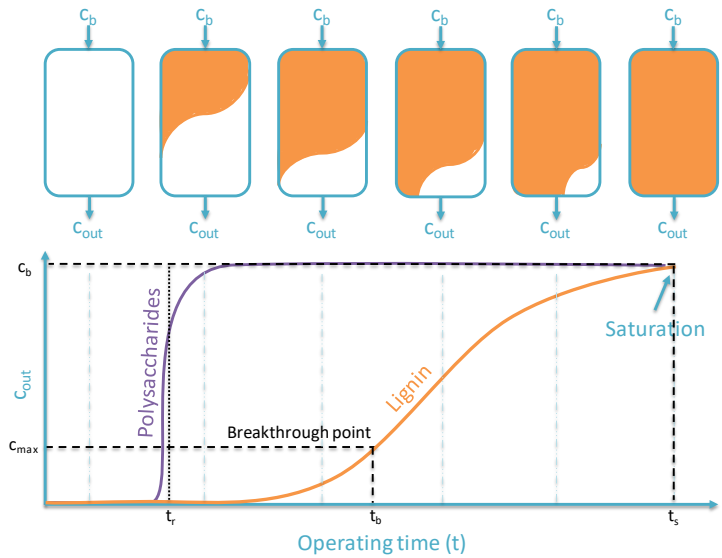


Figure 9.4: Illustration of the breakthrough curve for an adsorption column. c_b is the concentration of adsorbate at the inlet to the column, and c_{out} is the concentration at the outlet. The breakthrough point is defined at the maximum concentration (c_{max}) permissible at the outlet.

The optimization was broken down into 2 parts. In the first stage, the length of the column and the operating time were determined, and in the second step, the operating time was adjusted to meet the design criteria (minimum separation degree of 60%). The length of the column (L) and the operating time (t_b) were determined by simulating the column at lengths between 1–20 m and operating times of 1–30 residence times (volume of the column divided by the flow). The results from the simulation were evaluated using a profit function, $f(L, t_b)$, as defined in Equation 9.10.

$$f(L,t_b) = \underbrace{\left(\frac{m_{PS}(L,t_b)}{m_{adsorbent}(L)}\right)}_{\text{Mass of polysaccharides at the outlet Divided by Mass of adsorbent in the column}} \underbrace{\left(\int_0^{t_b} \frac{c_{PS}(L,y)}{c_{PS}(L,y)+c_{Lig}(L,y)}dy\right)}_{\text{Separation degree of the product}} \underbrace{\left(\int_0^{t_b} \frac{c_{PS}(L,y)}{t_b c_{b,PS}}dy\right)}_{\text{Yield of polysaccharides}} \underbrace{\left(\int_0^{L} \frac{q(x,t_b)}{L\,Q_{max}}dx\right)}_{\text{Adsorbent efficiency}} \quad (9.10)$$

The profit function is built up by the product of important factors per Equation 9.10. The cost for the separation process will depend on the length of the column, the

amount of adsorbent, and the amount of polysaccharides that is produced, among others. These criteria are all weighted into the profit function using various factors. In the first parenthetical term, the cumulative mass of polysaccharides at the outlet, divided by the total mass of adsorbent, is calculated to determine the maximum amount of GGM that is produced and minimum amount of adsorbent in the process. This value is weighted using the separation degree, yield of the polysaccharides, and adsorbent efficiency. The adsorbent efficiency shows how much adsorbent is actually used and is a parameter that also must be maximized.

The column simulation outputs discrete data points; thus, the integrals were evaluated using the MATLAB *trapz* function, which uses trapezoidal numerical integration to approximate the specified integrals. The results that were evaluated using the profit function are presented in Figure 9.5. The resulting 3D curve (9.5c) shows that the length of the column has an effect on the profit function in the range of 1 to 10 m. A longer column had negligible effects, as seen in the figure, because when the length of the column decreases, so, too, does the diameter of the column (constant L:D ratio). The consequence of a decreasing diameter is a rising interstitial velocity (the feed flow is constant), per Equation 9.8. The higher velocity shortens the time that is needed for the lignin to adsorb to the stationary phase, in turn increasing the amount of lignin that passes through the column, which lowers the separation degree and adsorbent efficiency.

The operating time or number of residence times (NOR) (Figure 9.5b) has an effect on profit function in the entire simulated range, with a visible maximum profit at a NOR of approximately 20 units. Below that value, the yield of polysaccharides is the dominating factor in the profit function, whereas at a higher value, the separation degree dominates. This effect can also be explained using the illustration in Figure 9.4, which shows that polysaccharides exit the column at time t_r, which is defined as the column's residence time. If the adsorption process is stopped at the column's residence time, the amount of polysaccharides in the outlet would be approximately zero, whereas the amount of polysaccharides that is fed to the process is not, resulting in a yield that is virtually zero.

The separation degree is equal to 1 at the outset (the lignin concentration is equal to 0; Figure 9.4) and does not affect the profit function. The increase in profit function in Figure 9.5b is thus due primarily to the rising polysaccharide yield. The trend turns when the operating time increases beyond a NOR of 20 units, which highlights the point at which the concentration of lignin at the outlet is sufficiently high to impact the separation degree. Based on these results, the NOR was selected to be 20 units, which is at the point of maximum profit. The length of the column was determined graphically to be 4 m, based on the intersection of the linear section before and after the shoulder (black square in Figure 9.5c).

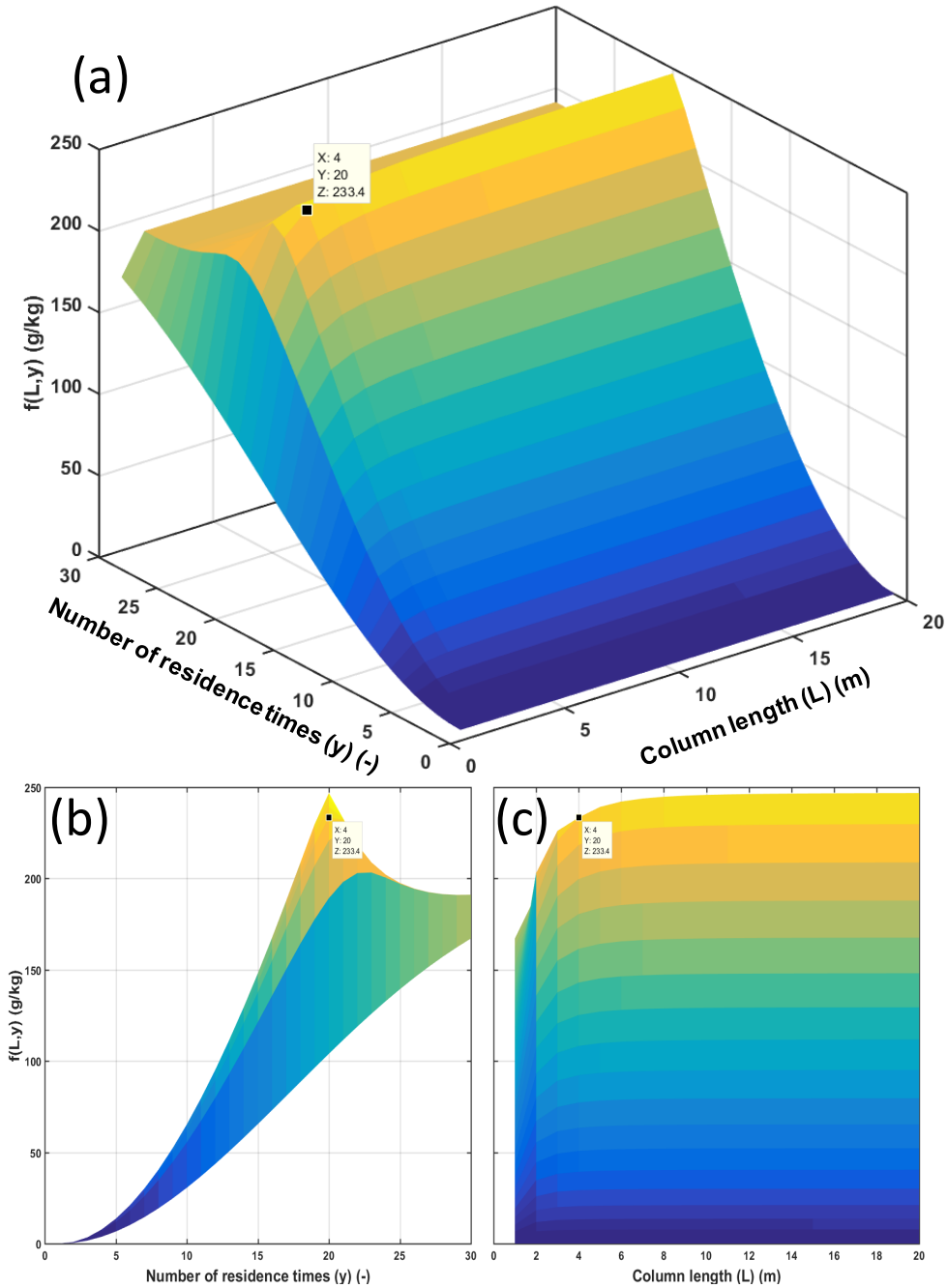


Figure 9.5: Results for profit function as a function of column length (L) and number of residence times (y). (a) Overview of the function in 3D. (b) and (c) The effect of number of residence times and column length on profit function, respectively.

The model was recalculated using a column length of 4 m and a NOR of 20 units to obtain the breakthrough curve of the column. The result of the simulation is shown in Figure 9.6.

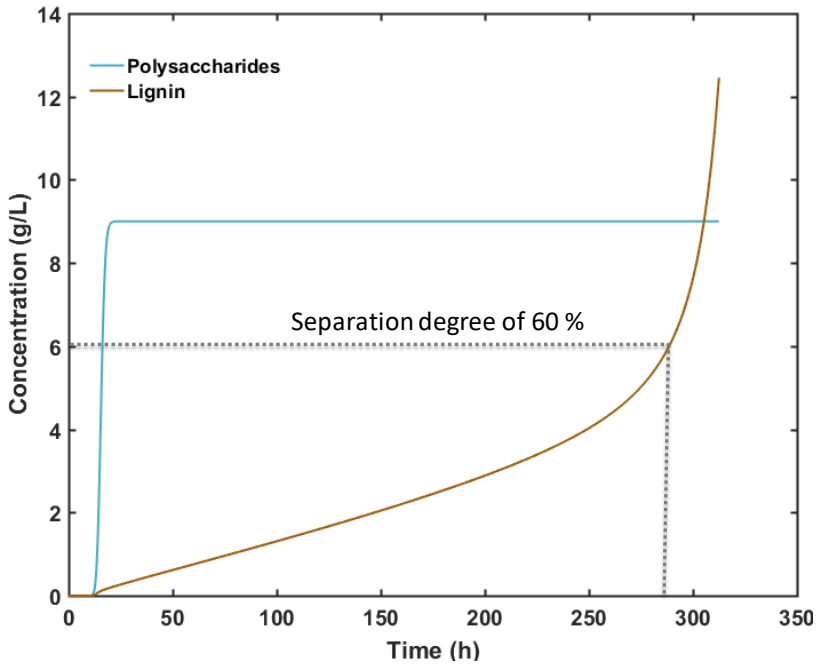


Figure 9.6: Simulation of adsorption column breakthrough curve at a length of 4 m and number of residence times of 20.

The breakthrough curve is similar to that in Figure 9.4, showing an nearly square concentration profile for polysaccharides and a linearly increasing lignin concentration up to approximately 250 hours of operating time, after which an exponential increase is observed. To meet the design criteria of a maximum separation degree of 60%, the concentration of lignin is not allowed to exceed 6 g/L. The adsorption process is thus terminated at an operating time of 289 hours, as highlighted in Figure 9.6, yielding the final adsorption column specifications in Table 9.5.

Table 9.5: Parameters derived from the simulation of the adsorption column.

Parameter	Value
Average separation degree (%)	80
Adsorbent efficiency (%)	74
Yield of polysaccharides (%)	95
Column length (m)	4.0
Column diameter (m)	2.7
Amount of adsorbent (kg)	6521
Total operating time per cycle (h)	289
Interstitial velocity (m/h)	0.26

9.2.2.2 Adsorption column after ultrafiltration

In the previous section, the adsorption column succeeded as a pretreatment step for the ultrafiltration, to decrease the amount of lignin in the feed and increase the permeate flux. However, a drawback of this configuration is that the permeate cannot be sent back to the pulp mill recovery system, because during adsorption, lignin is adsorbed, whereas chloride ions are released from the adsorbent. Hence, the feed and permeate contain sodium chloride, an undesirable chemical in the recovery system [168]. This configuration could also adsorb pulping chemicals, given that the adsorbent has high affinity toward anions, complicating the recovery of pulping chemicals from the adsorbent.

An alternative to pretreating the feed is to treat the retentate after the ultrafiltration using the same adsorbent. Running the ultrafiltration at a VR of 90% (Case I) would effectively recover 90% of the pulping chemicals in the permeate (assuming that the retention is close to 0), thus mitigating disruptions in the pulp mill process and maintaining the chemical balance. By changing the feed for the adsorption column from the nontreated SSL to the ultrafiltration retentate, the volumetric flow and solute concentrations would change, necessitating recalculation of the column size. The volumetric flow was set to 0.1 m^3/h (VR of 90%), and the bulk concentration of lignin and polysaccharides was set to 122 g/L and 30 g/L, respectively. The remaining process variables were the same as for the previous adsorption case. The results of the simulation and profit function are presented in Figure 9.7.

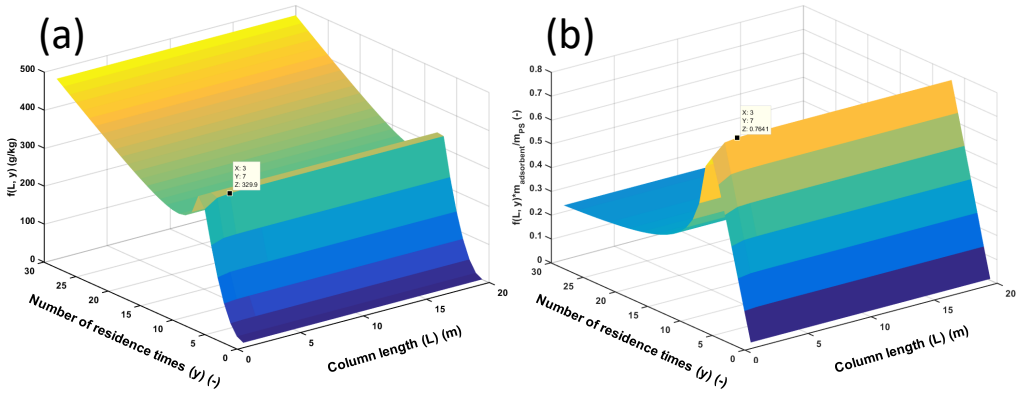


Figure 9.7: Profit function (a) and profit function without the ratio (m_{PS}:$m_{adsorbent}$) (b) for the adsorption of lignin from the ultrafiltered retentate.

Figure 9.7a shows the same trend as in the previous case, in which the profit function was highly dependent on the NOR and less affected by the length of the adsorption column. A maximum was also noted at a NOR of approximately 7 units, which was lower due to the higher lignin concentration. However, this peak was not a global maximum, given that the curve continued to increase with NOR, because the ratio of the mass of polysaccharides to that of adsorbent increased, dominating the profit function. This trend was not visible in the previous adsorption column case, due to the lower polysaccharide concentration in the feed (9 g/L compared with 30 g/L in the retentate). Although the profit function continued to increase, the final column length and NOR were determined to be 3 m and 7 units, respectively, because the separation degree decreases drastically when the NOR is longer, as seen in Figure 9.7b. The breakthrough curve at a column length of 3 m and NOR of 7 units in Figure 9.8 shows that the concentration of lignin at the end of the cycle (462 hours) was roughly 2 g/L, whereas that of polysaccharides was 30 g/L. The criteria for the separation degree were thus fulfilled.

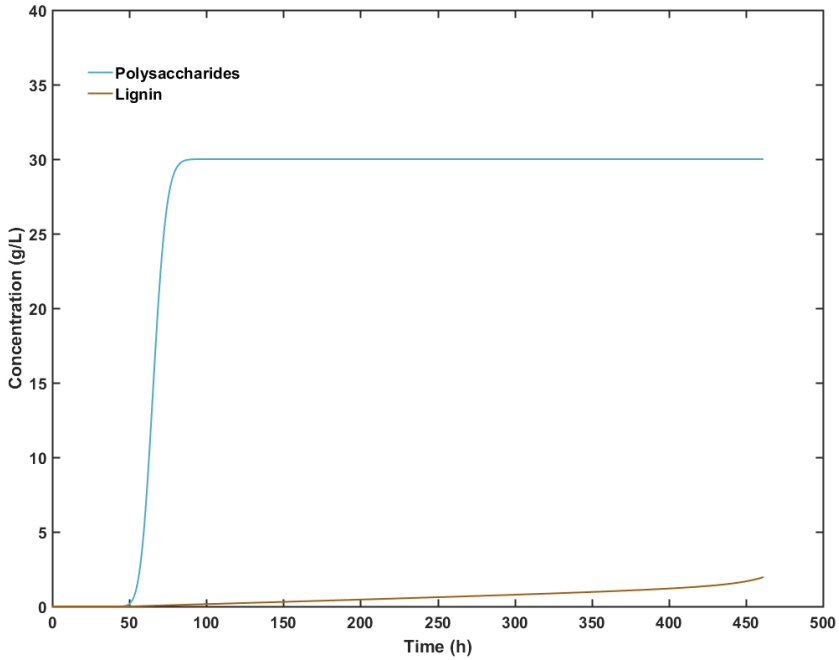


Figure 9.8: Simulation of the adsorption column breakthrough curve at a length of 4 m and number of residence times of 20.

The remaining results that were derived from the simulation are shown in Table 9.6.

Table 9.6: Parameters derived from the simulation of the adsorption column.

Parameter	**Value**
Average separation degree (%)	98
Adsorbent efficiency (%)	91
Yield of polysaccharides (%)	86
Column length (m)	3
Column diameter (m)	2
Amount of adsorbent (kg)	2751
Total operating time per cycle (h)	462
Interstitial velocity (m/h)	0.05

9.2.3 Techno-economic evaluation

The techno-economic evaluation was performed, based on 2 subcases, as seen in Figure 9.9. In the first case (left figure), the ultrafiltration was conducted after the adsorption process, and the second case entailed these steps in the opposite order. The ultrafiltration process was evaluated as a batch process, and the adsorption column was considered to be continuous. Thus, a buffer tank was added to account for the delay in SSL processing and membrane cleaning. Regeneration of the adsorption column was assumed to take the same amount of time as the adsorption process; thus, at least 2 adsorption columns were required to maintain continuity of the process.

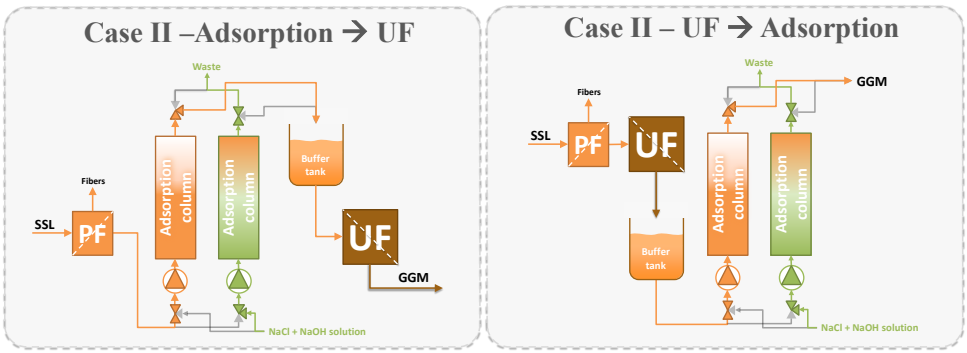


Figure 9.9: The two case studies on which a techno-economic analysis was performed.

The power requirements for the adsorption column pumps was calculated per Equation 9.11:

$$w_s = \frac{F\,(\rho g L + \Delta P + \Delta P_f)}{\eta} \tag{9.11}$$

where ΔP_f is the drop in pressure that was caused by the inlet and outlet filters and ΔP is the drop in pressure in the column, which was calculated using Ergun's equation for fluid flow through a packed column [169], as seen in Equation 9.12:

$$\Delta P = f_p\, L\, \frac{\rho u_s^2}{d_p}\left(\frac{1-\varepsilon}{\varepsilon^3}\right) \tag{9.12}$$

where u_s is the superficial velocity (feed flow divided by the column cross-sectional area) and f_p is the packed bed friction factor and is defined per Equation 9.13.

$$f_p = \frac{150}{Re_p} + 1.75 \tag{9.13}$$

Re_p is the Reynolds number for packed beds, as defined in Equation 9.14.

$$Re_p = \frac{\rho u_s d_p}{(1-\varepsilon)\mu} \quad (9.14)$$

The cost for the ultrafiltration process, when performed prior to the adsorption process, is the same as in Case I (Section 9.1). However, when the adsorption is applied as a pretreatment step to ultrafiltration, the average flux increases by approximately 9% and GGM production declines to 2.4 kg/h, the latter of which is due to the lower retention in the ultrafiltration as a result of the removal of lignin in the adsorption process. The rise in flux decreased the required membrane area from 6.8 m^2 to 5.1 m^2 and the circulation pump energy demand from 0.45 kW to 0.25 kW. The remaining plant data (Table 9.2) for the ultrafiltration remained unchanged. The assumptions for the adsorption column cost estimates are presented in Table 9.7. The price for the columns, pumps, and buffer tank were based on Ulrich's method, with stainless steel as a base material [163]. The *rinse volume,* or volume of regenerant for each adsorption cycle, was based on recommendations from the manufacturer of the adsorption resin, and the *amount of adsorbent to replace* was based on the regeneration results in Paper VI.

Table 9.7: Assumptions for the cost estimates for the two cases in Figure 9.9.

Parameter	**Adsorption → UF**	**UF → Adsorption**
Adsorption column price (€/m^3)	11,735	18,535
Pump price (€/W)	127	799
Pump efficiency (-)	0.6	0.6
Buffer tank price (€/m^3)	4184	4184
Rinse volume (bed volumes)	10	10
Amount of adsorbent to replace (%/cycle)	5	5
Adsorbent price (€/kg)	3.7	3.7
Clean water (€/m^3)	0.42	0.42
NaOH concentration (g/L)	10	10
NaCl concentration (g/L)	100	100
NaOH price (€/kg)	0.28	0.28
NaCl price (€/kg)	0.05	0.05
Electricity price (€/MWh)	38	38
Operating time (h/year)	8000	8000
Maintenance and labor costs (% of capital cost)	5	5
Annuity factor (/year)	0.1	0.1
GGM production (kg/h)	2.4	2.4
Column pressure drop (Pa)	14	1.9
Column packing filter pressure drop (bar)	2	2
Pump power demand (kW)	0.11	0.011

The assumptions in Table 9.7 were used with the adsorption column specifications in Tables 9.5 and 9.6 to estimate the cost of the concentration and purification process, as seen in Table 9.8. The results were divided, based on the capital costs,

operating costs, and ultrafiltration and adsorption processes for both subcases in Figure 9.9. As seen from the results, the total cost for the UF process did not change by a large margin when adsorption was used as a pretreatment step, due to the low average flux increase of 9%. However, the placement of the adsorption process had a major impact on the total cost of the process. The highest cost was recorded for the subcase in which the adsorption process is placed before the UF (Ads→UF).

The capital cost was 48% higher due to the larger adsorption column (4 m versus 3 m for the post-UF treatment). The operating cost depended primarily on the amount of regenerant and the amount of adsorbent that was replaced in the columns. These costs depend on the size of the adsorption column and the number of cycles for which the columns are switched and regenerated. The column in the subcase UF→Ads had an operating time of 462 hours versus the reverse subcase, in which the operating time was 289 hours. The longer operating time resulted in fewer regeneration cycles and a lower cost, as seen in Table 9.8.

Table 9.8: Calculated costs for GGM production using adsorption and ultrafiltration.

Sub-case study	**Adsorption → UF**	**UF → Adsorption**
	Adsorption	
Capital cost (€/year)	**71,023**	**48,294**
- 2x Adsorption column (empty) (€/year)	53,751	34,938
- 2x Adsorbent for columns (€/year)	4826	2036
- 2x Pumps (€/year)	2823	1697
- Buffer tank (€/year)	9623	9623
Operating cost (€/year)	**88,833**	**24,574**
- Column regeneration (€/year)	51,820	13,340
- Adsorbent replacement (€/year)	33,395	8813
- Electricity (€/year)	67	6
- Maintenance and labor cost (€/year)	3551	2415
	Ultrafiltration	
Capital cost (€/year)	**17,747**	**18,152**
- Membrane plant (€/year)	1228	1634
- Pump cost (€/year)	6895	6895
- Feed tank cost (€/year)	9623	9623
Operating cost (€/year)	**1732**	**1892**
- Electricity cost (€/year)	599	658
- Membrane replacement cost (€/year)	205	272
- Cleaning cost (€/year)	41	54
- Maintenance and labor costs (€/year)	887	908
Total cost (€/year)	179,334	92,912
Total cost (€)/ton GGM	**9523**	**4911**

These results assume that the same rinse volume and adsorbent replacement are needed for both subcases. However, the results for the regeneration are most likely underestimated, especially in the subcase UF→Ads. The feed flow to the adsorption process was lower in the subcase UF→Ads, but the concentration of lignin was 3 times higher. The greater concentration of lignin in the column would probably foul the adsorbent more extensively, which would require a higher rinse volume or replacement of the adsorbent. This aspect was not investigated experimentally and is left for future work.

The operating cost could be decreased by adding a regenerant recovery step. Although, this possibility was not studied experimentally in this thesis, other groups have shown that salts can be recovered from highly concentrated streams using nanofiltration [170].

Overall, the results show that the subcase UF→Ads is the most economical setup, with a total cost of 4911 €/ton of GGM. The total cost was higher than using UF alone (Case I) to concentrate the SSL. However, the separation degree for the UF was approximately 22%, versus 98% for the UF→Ads. The higher separation degree results in a purer product that likely has greater value compared with the high lignin content of GGM that is derived from UF.

9.3 Case study III – Ultrafiltration and precipitation of GGM from SSL

In the third and last case study, antisolvent precipitation was used for the separation of GGM and lignin. The results in Paper II show that a membrane filtration step prior to the separation was beneficial, lowering the amount of antisolvent that is used. Also, the best-performing antisolvent was acetone, effecting the highest GGM yield at the lowest addition. Antisolvent precipitation on an industrial scale can be expensive when large volumes of organic solvent are used [83].

Further, the preconcentration step, the recovery of the organic solvent is essential to decrease the cost of the process. For this case study, ultrafiltration was used to preconcentrate 1 m^3/h of SSL to a VR of 90%, which was then transferred to a buffer tank. The retentate was pumped from the buffer tank to the precipitation vessel, where it mixed with acetone to a final antisolvent concentration of 50 wt%. The residence time in the precipitation vessel was set to 15 minutes, and the liquid was agitated continuously using a mixer with a propeller turbine impeller. The liquid and precipitate were separated using a centrifuge (95% recovery), and the acetone

was recovered using a distillation column. The overall process is illustrated in Figure 9.10.

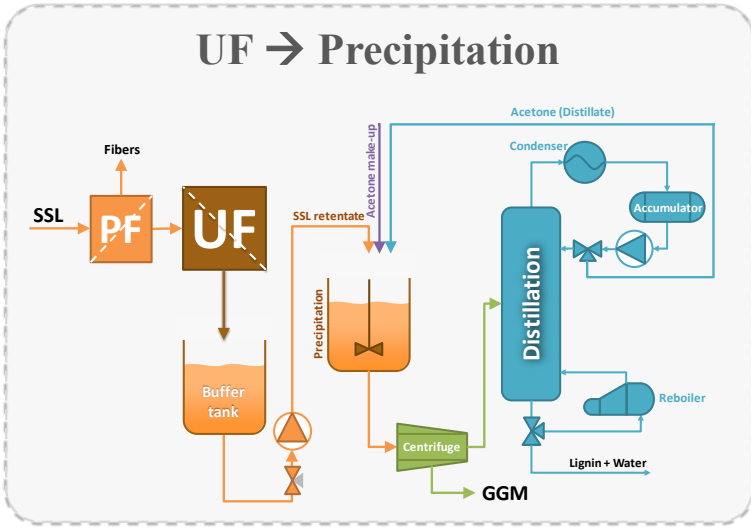


Figure 9.10: Ultrafiltration, followed by the precipitation of GGM from SSL and the recovery of the antisolvent.

The techno-economic evaluation was divided into sections on ultrafiltration, precipitation, centrifugation, and distillation. The cost for the ultrafiltration was the same as the calculations for Case I. The precipitation is performed using a recirculated acetone (distillate) stream from the distillation and an acetone make-up stream that compensated for the loss of acetone in the distillation bottom product (containing lignin and water). To calculate the cost for the precipitation step, the amount of recirculated acetone is needed.

The distillation column was initially set up as a shortcut distillation column using the Winn-Underwood-Gilliland method in Aspen Plus V10 (Aspen Technology Inc., Bedford, Massachusetts, USA). The reflux ratio was set to 1, with acetone and water as the light key and heavy key components, respectively. The recovery in the distillate was set to 98% for acetone and 2% for water. The condenser (total) pressure was set to 1 bar, and the reboiler was set to 1.1 bar; the feed to the column contained 50 wt% acetone at a total mass flow of 200 kg/h (2 times the retentate flow of 100 kg/h). The simulation results indicated that the minimum reflux ratio was 0.48, the minimum number of required stages was 12, and the optimal feed stage was 1 stage above the reboiler. The data were applied in a new simulation using the RadFrac (rigorous 2- or 3-phase fractionation for single columns) distillation column, with complete recirculation of the distillate (TOPS) through a stream mixer (see Figure 9.11).

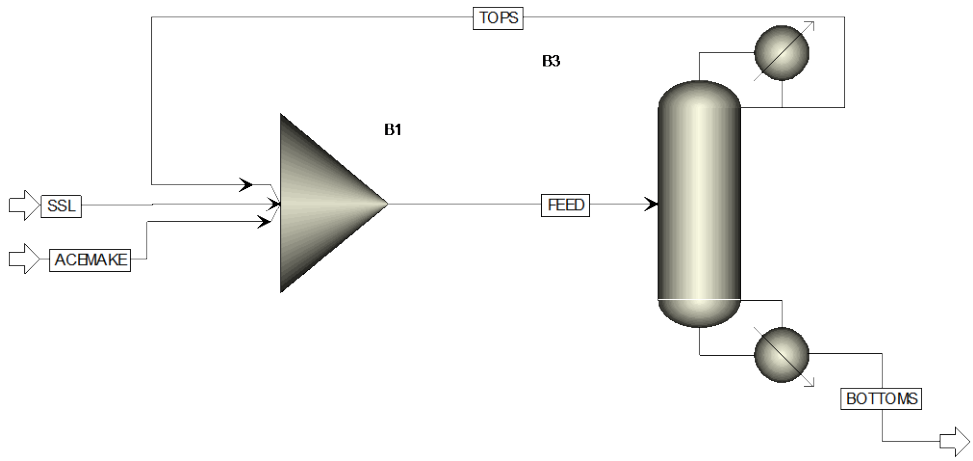


Figure 9.11: Simulation of the distillation column in Aspen Plus V10 using the RadFrac model, with complete recirculation of the distillate through a stream mixer.

The column was set to have 12 stages, with the feeding occurring in the 11th stage. The total condenser was set to have a pressure of 1 bar, and the reboiler was a Kettle type. The reflux ratio and distillate rate (flow of recirculated acetone) were set as variables, and acetone recovery and purity were set as fixed design specifications. Another design specification was set for the FEED stream (the mixture entering the precipitation vessel; Figure 9.10), in which an acetone concentration of 50 wt% was fixed. The distillation process was simulated with various acetone purities (in the distillate) and recoveries, and the total cost was calculated with Aspen Plus. The results of the total cost (including the acetone make-up cost of 0.65 €/kg) are presented in Figure 9.12.

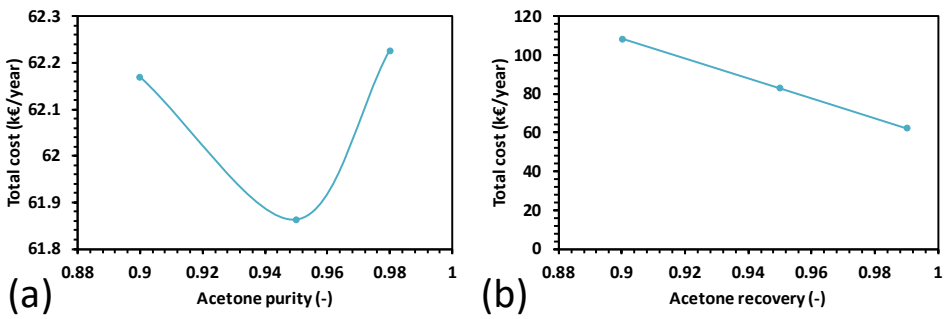


Figure 9.12: Total cost of the distillation process (including the acetone make-up) vs the acetone purity in the distillate at a constant acetone recovery of 0.99 (a) and the acetone recovery at a constant acetone purity of 0.98 (b). The total operating time was set to 8000 h/year, with an annuity factor of 0.1 /year.

Acetone purity did not have a major impact on the total cost, remaining in the region of 62 k€/year. The minimum in Figure 9.12a was due primarily to the change in condenser investment cost, which decreased by 12%. Acetone recovery had a greater influence on the total cost of the process, as seen in Figure 9.12b. Because the number of stages in the distillation column was fixed, the investment cost was generally fixed. The decrease in investment cost with rising acetone recovery was largely due to the decline in the acetone make-up stream. Based on these observations, the final selected acetone purity and recovery were 0.95 and 0.99, respectively. With these parameters, the FEED stream was 211 kg/h, and the acetone make-up was approximately 1.0 kg/h. The precipitation vessel was ultimately calculated to have a volume of 53 L with an agitator power of 822 W (100 RPM) and a feed tank (buffer tank in Figure 9.10) with a volume of 2.4 m^3.

The centrifuge was simulated in Aspen Plus V10, using the solids separator model, with 95% recovery of solids and 99% recovery of liquids using the FEED stream (211 kg/h) from the distillation column simulation. The recovered solids (GGM) contained 22% acetone, which translated into approximately 1 kg/h of additional acetone that was added to the acetone make-up stream. The total GGM that was produced in the process was 2.0 kg/h, which is the product of the GGM that was generated in the ultrafiltration (Table 9.2), the yield in the precipitation (76%, Paper II), and the yield in the centrifugation (95%). The calculated total cost per ton of GGM was 10,553 €, as seen in Table 9.9. The total cost was twice as high as for the adsorption (Case II) and approximately 10 times higher than for the UF (Case I), due to the high cost of the centrifugation and distillation, which constituted approximately 80% of the total cost. The distillation process (47% of the total cost) is dependent on the antisolvent and was optimized to the lowest cost possible for the specified tower stages.

The total cost for the centrifuge was 34% of the total cost, 67% of which was the operating cost (electricity). Centrifuges have a high energy demand [171], and one method of reducing the energy demand is to change the separation process from using centrifugation to conventional filtration. It is important, however, that the filter medium be compatible with organic solvents, which limits the use of filter mediums to strictly hydrophobic or stainless steel types. Filtering the precipitated SSL sludge through a conventional filter has not been done experimentally.

However, to roughly estimate the cost of a conventional filter, it was assumed that the cost is equal to that for the UF. Based on this assumption, the total cost would be roughly 8300 €/ton of GGM, which is still higher than the cost for the process in the second case study. Further cost reductions are difficult without changing the antisolvent or solvent recovery method (distillation). Considering that the precipitation process had the lowest total cost, which was 7% of the process total. The highest cost was for the acetone make-up stream, which was roughly 86% of the cost. The acetone make-up stream can theoretically be lowered by recovering

the lost acetone in the GGM precipitate. However, the cost reduction is not substantial, considering the high cost for the rest of the process.

Table 9.9: Calculated costs for GGM production using UF and antisolvent precipitation.

Ultrafiltration	
Capital cost (€/year)	**18,152**
- Membrane plant (€/year)	1634
- Pump cost (€/year)	6895
- Feed tank cost (€/year)	9623
Operating cost (€/year)	**1,892**
- Electricity cost (€/year)	658
- Membrane replacement cost (€/year)	272
- Cleaning cost (€/year)	54
- Maintenance and labor costs (€/year)	908
Precipitation	
Capital cost (€/year)	**1942**
- Buffer tank cost (€/year)	1004
- Precipitation tank cost (€/year)	61
- Mixer cost (€/year)	872
- Pump (€/year)	5
Operating cost (€/year)	**10,790**
- Acetone make-up	10,442
- Electricity (€/year)	250
- Maintenance and labor costs (€/year)	97
Centrifuge	
Capital cost (€/year)	**17,862**
Operating cost (€/year)	**38,247**
Distillation	
Capital cost (€/year)	**37,743**
- Condenser (€/year)	4587
- Accumulator (€/year)	8945
- Reboiler (€/year)	5615
- Reflux pump (€/year)	2541
- Tower (€/year)	16,055
Operating cost (€/year)	**40,990**
- Electricity (€/year)	29,813
- Cooling Water (€/year)	535
- Steam at 7 bar (€/year)	8756
- Maintenance and labor costs (€/year)	1887
Total cost (€/year)	167,617
Total cost/ton GGM	**10,553**

10. Conclusions and future work

In this work, the separation and purification of GGM from SSL were examined. In Chapter 7, membrane filtration was used for the separation and purification. The first membrane filtration trials with hydrophobic membranes showed that the separation of hemicellulose and lignin was not possible. The SEC results from the same study also indicated that this poor separation was likely due to a narrow difference in MW between components and the presence of LCCs in the solution. The most suitable membrane from that study was the 50 kDa polysulfone membrane, with which a final GGM and lignin purity of 93% was achieved using a combination of concentration and diafiltration. The high purity was obtained by the removal of pulping chemicals and low-MW compounds.

Membrane fouling was an issue with these hydrophobic membranes, with pore blocking being the main fouling mechanism, per the blocking filtration law. A prefiltration study with MF and dead-end filtration was performed to minimize these issues. MF decreased the fouling of the incoming UF from 49% to 7%. However, MF experienced high retention of the products, leading to significant losses. Fouling of the MF membrane was also high, which required special cleaning methods to recover the initial permeate flux—specifically, an oxidative treatment that recovered the initial permeate flux for the UF and MF membranes. Dead-end filtration reduced the fouling to 17%, with negligible loss of products. The results indicated that the foulants were composed of lignin or compounds that were sensitive to oxidative treatments. These foulants were not extracted or characterized in this study, necessitating future examination.

The use of hydrophilic membranes was studied as an alternative to the combination of prefiltration and UF using hydrophobic membranes. In the initial trial, the membranes with the highest MWCO experienced severe fouling, which was likely due to pore blocking, as seen in our previous study and indicated by the SEC results. The overall retention of lignin was lower, and that of GGM was higher compared with the hydrophobic membranes, likely due to the lower affinity of lignin to the hydrophilic membranes and the lower MWCO, which increased the retention of GGM. Consequently, the retentates had higher separation degrees, and the membrane fouling was low.

The SEC and HSQC 2D NMR results indicated that the hydrophilic membrane retained a greater portion of LCCs and that the solutes had a lower MW than in our

previous studies. The high MW that was observed earlier resulted from ion-exclusion effects in the SEC column when water was used as an eluent. By switching to a sodium hydroxide eluent, the MW was determined to be 4 to 5 times lower than those in Paper I. However, the use of water as an eluent effected some separation in the peaks, which was not seen with sodium hydroxide. Future studies should fractionate these peaks and analyze their molecular structure and composition, which could confirm some of the assumptions in our studies. RC70PP was the most cost-efficient membrane, based on its high flux and product yields, another reason for using this membrane in the pilot study.

The aim of the pilot study was to scale up the results from the lab-scale studies and compare the performance of the 2 processes. The pilot setup performed worse than the lab system, as evidenced by its lower flux and retention of products, under the same operating conditions. Analysis of the raw material showed that the changes between the old SSL in the lab-scale studies and the new SSL were minimal, indicating that there were other reasons for the observed differences. A 3-fold increase in CFV in the pilot system increased the flux by a factor of 3 and the retention of GGM by 10%.

However, its performance remained lower than the lab-scale results, for which there are several explanations. A CFD simulation of both modules showed that the shear rate in the pilot study was always lower than in the lab-scale module, even at the highest CFV of 1.5 m/s, explaining the low flux in the experiments. Another reason is related to the feed pump of the pilot study, which operated at a high loop VR, which in turn could have resulted in the low flux and retention. A final likely reason is related to the temperature of the filtration. The temperature of the lab-scale module was as high as 65°C, near the membrane and permeate outlet, increasing the flux (lower permeate viscosity) and retention as a result of membrane compaction. This phenomenon was observed in Paper VI, in which running the lab-scale module at room temperature lowered the flux and retention, the latter of which had the same extent as in the pilot study. Future studies should examine this effect by changing the filtration temperature of the pilot setup from 50°C to 65°C.

The pilot experiments showed that an alkaline cleaning step at pH 11 for 1 hour was sufficient, with several cleaning cycles improving the performance. The pilot module also ran for approximately 1 month, corresponding to 15 experiment/cleaning cycles. The efficiency of the cleaning step was seen when it was switched to a wash with water. However, there was no long-term effect of fouling on the membranes in this study, which required over 15 experiments. The separation of GGM and lignin was not possible in any of the studies in Chapter 7, due to a narrow difference in MW between most of the solutes in the SSL. The separation was instead conducted using 2 other methods—antisolvent precipitation and adsorption—as described in Chapter 8.

Chapter 8 examined antisolvent precipitation of GGM and lignin from an SSL retentate. The antisolvents were acetone, ethanol, and methanol, of which acetone was the most efficient in terms of product yield and amount added. The GGM and lignin were separable with a yield and separation degree of 76% using a 48 wt% acetone. Polysaccharides were the first components to precipitate, followed by lignin. A correlation was noted between the calculated dielectric constant of the solution and precipitation yield, making predictions of the precipitation using other antisolvents possible. Using carbohydrate analysis and HSQC 2D NMR, it was possible to identify the order of the precipitation, which was: arabinogalactan followed by GGM and xylans, and finally arabinans and β-galactans.

Further, most the LCCs were in the lignin fraction. However, a subsequent study (Paper IV) showed that these LCCs were most likely lignosulfonates. Based on these results, the existence of LCCs was therefore inconclusive. The presence of LCCs in this SSL should be studied in greater detail, perhaps using various extraction and pretreatment methods that enrich LCCs, rendering identification with HSQC 2D NMR trivial. Other solvents could be used, as reported in the literature, to move the LCC signals to other known chemical shifts. By increasing the pH or the solute concentration, higher GGM yields were obtained at lower acetone concentrations. However, the yield for lignin also rose, decreasing the separation degree. Thus, we concluded that the final process parameters depend on the requirements in the upstream process.

An alternative to antisolvent precipitation is adsorption with polymeric resins, which was presented in Chapter 8. The resins were anion-exchangers (IRA958 and IRA67) and the hydrophobic XAD4. The best-performing resin was the strongly basic anion-exchanger (IRA958), removing 85% of the lignin. Some acid-insoluble lignin was also removed, indicating that it was sulfonated prior to the acid hydrolysis. XAD4 resin was best at removing acid-insoluble lignin, with a total removal of 90%.

The removal of polysaccharides was minimal with the anion-exchangers, based on the equilibrium studies. An increase in polysaccharide concentrations was observed, indicating that the resins had non-zero rejection of these components, likely because they were in a dry state before use. The XAD4 adsorbed a small amount of polysaccharides, as indicated in the screening study. Desorption of the lignin from XAD4 recovered 25% of the acid-insoluble lignin, of which 5% was polysaccharides. The composition of these polysaccharides also differed compared with the raw material. IRA958 was chosen for the remaining studies, because it had the highest lignin removal and minimal losses in polysaccharide.

The equilibrium studies showed that the adsorption capacity-versus-lignin concentration curve was S-shaped, indicating cooperative adsorption, best described by the Sips isotherm. The adsorption followed pseudo-second-order kinetics, indicative of a chemisorptive process. The first stage of adsorption followed film or

macropore diffusion and then intra-particle diffusion, which was slow. The adsorbent was regenerated using sodium chloride and sodium hydroxide at a concentration (NaCl) of 100 g/L. Approximately 98% of the lignin was recovered after 3 consecutive washes, and the number of washes could be decreased by raising the concentration of NaCl during the first wash.

Finally, the effect of lignin removal was examined in the RC70PP membrane, with other membranes with a lower MWCO. The flux improved by 1.4-fold, with minimal influence on the retention of polysaccharides. Because the lignin was removed in the adsorption pretreatment, the resulting retentate had a higher separation degree of 59%. The yield of GGM fell slightly, but it was possible to use a denser membrane to compensate for the losses. As a result, the GGM yields increased from 34% to 95%, with a constant separation degree for all tested membranes.

In Chapter 9, 3 major case studies were evaluated economically. For the calculations, the design criteria were a feed flow of 1 m^3/h and a separation degree of at least 60%. In the first case study, the cost of running a UF plant was calculated to be 1736 €/ton of GGM—approximately 30 times higher than that in Paper IV. This disparity was attributed to the higher investment cost, due to the inclusion of a feed/retentate tank and the addition of a pump. The criteria for the separation degree was not fulfilled in this case study, due to poor separation between the GGM and lignin.

The second case study was divided into 2 subcases, in which adsorption was used a pretreatment step in the first subcase and as a post-treatment step in the second subcase. The calculated cost for the subcases was 9523 €/ton of GGM (adsorption as pretreatment) and 4911 €/ton of GGM (adsorption as post-treatment), approximately 6 to 12 times higher than the cost for bleached softwood Kraft pulp. The cost was thus lower when using adsorption as a post-treatment step, due to the smaller adsorption column that was required and the lower regeneration frequency and low regenerant demand.

The concentration and amount of regenerant (bed volume basis) were assumed to be the same for both subcases, which might not apply in reality, because the lignin concentration in the adsorption column (post-treatment) was nearly 3 times higher than for the other subcase. A higher lignin concentration would most likely foul the adsorbent to a higher degree, which would require other concentrations of regenerant and probably more washing cycles. This aspect was not tested experimentally and is left for future work. The cost of the UF step in both cases did not change by a large margin due to the low increase in average flux of 9% when adsorption was performed as a pretreatment step.

In the last case study, antisolvent precipitation was implemented as the post-treatment step or separation step after the UF. The total cost for the process (including the antisolvent recovery) was 10,553 €/ton of GGM, which was

approximately 10 times higher than using only UF (first case study). The high cost was attributed primarily to the high cost of the centrifugation and solvent recovery (distillation). The use of conventional filtration instead of centrifugation was suggested, but no experimental data are available for these calculations. The cost for the conventional filtration was instead assumed to be similar to that of UF, which reduced the total cost of the process to 8300 €/ton of GGM. This decrease was not substantial, because the distillation process was responsible for 47% of the total cost. Further cost reductions would therefore be difficult without changing the antisolvent or solvent recovery method. Thus, we conclude that the combination of UF and adsorption as a post-treatment step is the process with the lowest cost that fulfills the design criteria.

References

1. Farrell, A.E.; Plevin, R.J.; Turner, B.T.; Jones, A.D.; O'hare, M.; Kammen, D.M. Ethanol can contribute to energy and environmental goals. *Science* **2006**, *311*, 506-508.
2. Atwood, D.A. *Sustainable inorganic chemistry*; John Wiley & Sons: 2016.
3. Rowell, R.; Pettersen, R.; Han, J.; Rowell, J.; Tshabalala, M. Wood chemistry and wood composites. Chap. 3: Cell wall chemistry. Taylor and Francis Group. Boca Raton, London, New York, Singapore, by CRC Press: 2005.
4. Thuvander, J. *Recovery of Hemicelluloses Extracted from Spruce and Wheat Bran: Membrane Filtration Process Development and Cost Estimates*; Lund University: 2018.
5. Adav, S.S.; Sze, S.K. Trichoderma secretome: an overview. In *Biotechnology and biology of Trichoderma*, Elsevier: 2014; pp. 103-114.
6. Flórez-Pardo, L.M.; González-Córdoba, A.; López-Galán, J.E. Evaluation of different methods for efficient extraction of hemicelluloses leaves and tops of sugarcane. *Dyna* **2018**, *85*, 18-27.
7. Scheller, H.V.; Ulvskov, P. Hemicelluloses. *Annual review of plant biology* **2010**, *61*.
8. Söderqvist Lindblad, M.; Albertsson, A.-C.; Ranucci, E.; Laus, M.; Giani, E. Biodegradable polymers from renewable sources: rheological characterization of hemicellulose-based hydrogels. *Biomacromolecules* **2005**, *6*, 684-690.
9. Maleki, L.; Edlund, U.; Albertsson, A.-C. Synthesis of full interpenetrating hemicellulose hydrogel networks. *Carbohydr. Polym.* **2017**, *170*, 254-263.
10. Hannuksela, T.; Holmbom, B.; Lachenal, D. Effect of sorbed galactoglucomannans and galactomannans on pulp and paper handsheet properties, especially strength properties. *NORD PULP PAP RES J* **2004**, *19*, 237-244.
11. Mikkonen, K.S.; Heikkilä, M.I.; Helén, H.; Hyvönen, L.; Tenkanen, M. Spruce galactoglucomannan films show promising barrier properties. *Carbohydr. Polym.* **2010**, *79*, 1107-1112.

12. Kisonen, V.; Xu, C.; Bollström, R.; Hartman, J.; Rautkoski, H.; Nurmi, M.; Hemming, J.; Eklund, P.; Willför, S. O-acetyl galactoglucomannan esters for barrier coatings. *Cellulose* **2014**, *21*, 4497-4509.
13. Rosengren, A.; Butler, S.J.; Arcos-Hernandez, M.; Bergquist, K.-E.; Jannasch, P.; Stålbrand, H. Enzymatic synthesis and polymerisation of β-mannosyl acrylates produced from renewable hemicellulosic glycans. *Green Chemistry* **2019**, *21*, 2104-2118.
14. Pauly, M.; Gille, S.; Liu, L.; Mansoori, N.; de Souza, A.; Schultink, A.; Xiong, G. Hemicellulose biosynthesis. *Planta* **2013**, *238*, 627-642.
15. Rydholm, S.A. Pulping processes. *Pulping processes.* **1965**.
16. Ragauskas, A.J.; Williams, C.K.; Davison, B.H.; Britovsek, G.; Cairney, J.; Eckert, C.A.; Frederick, W.J.; Hallett, J.P.; Leak, D.J.; Liotta, C.L. The path forward for biofuels and biomaterials. *science* **2006**, *311*, 484-489.
17. Huang, H.J.; Ramaswamy, S. Overview of biomass conversion processes and separation and purification technologies in biorefineries. *Separation and purification technologies in biorefineries* **2013**, 1-36.
18. Liao, B. Membrane Filtration in Biorefinery. In *Encyclopedia of Membranes*, Drioli, E., Giorno, L., Eds. Springer Berlin Heidelberg: Berlin, Heidelberg, 2015; 10.1007/978-3-642-40872-4_2113-1pp. 1-2.
19. McCann, M.; Wells, B.; Roberts, K. Direct visualization of cross-links in the primary plant cell wall. *J. Cell Sci.* **1990**, *96*, 323-334.
20. Abdel-Hamid, A.M.; Solbiati, J.O.; Cann, I.K. Insights into lignin degradation and its potential industrial applications. In *Adv. Appl. Microbiol.*, Elsevier: 2013; Vol. 82, pp. 1-28.
21. Marriott, P.E.; Gómez, L.D.; McQueen-Mason, S.J. Unlocking the potential of lignocellulosic biomass through plant science. *New Phytologist* **2016**, *209*, 1366-1381.
22. Iakovlev, M.; van Heiningen, A. Efficient Fractionation of Spruce by SO2-Ethanol-Water Treatment: Closed Mass Balances for Carbohydrates and Sulfur. *ChemSusChem* **2012**, *5*, 1625-1637.
23. Söderström, J.; Pilcher, L.; Galbe, M.; Zacchi, G. Two-step steam pretreatment of softwood by dilute H2SO4 impregnation for ethanol production. *Biomass Bioenergy* **2003**, *24*, 475-486.
24. Sixta, H.; Iakovlev, M.; Testova, L.; Roselli, A.; Hummel, M.; Borrega, M.; van Heiningen, A.; Froschauer, C.; Schottenberger, H. Novel concepts of dissolving pulp production. *Cellulose* **2013**, *20*, 1547-1561.
25. Bader, T.K.; Hofstetter, K.; Alfredsen, G.; Bollmus, S. Microstructure and stiffness of Scots pine (Pinus sylvestris L) sapwood degraded by Gloeophyllum trabeum and Trametes versicolor–Part I: Changes in chemical composition, density and equilibrium moisture content. *Holzforschung* **2012**, *66*, 191-198.
26. Brown Jr, R.M. Cellulose structure and biosynthesis: what is in store for the 21st century? *J. Polym. Sci., Part A: Polym. Chem.* **2004**, *42*, 487-495.

27. Badiei, M.; Asim, N.; Jahim, J.M.; Sopian, K. Comparison of chemical pretreatment methods for cellulosic biomass. *APCBEE procedia* **2014**, *9*, 170-174.
28. Laine, C. *Structures of hemicelluloses and pectins in wood and pulp*; Helsinki University of Technology: 2005.
29. Lundqvist, J.; Jacobs, A.; Palm, M.; Zacchi, G.; Dahlman, O.; Stålbrand, H. Characterization of galactoglucomannan extracted from spruce (Picea abies) by heat-fractionation at different conditions. *Carbohydr. Polym.* **2003**, *51*, 203-211.
30. Timell, T. Recent progress in the chemistry of wood hemicelluloses. *Wood Sci. Technol.* **1967**, *1*, 45-70.
31. Schaechter, M. *Encyclopedia of microbiology*; Academic Press: 2009.
32. Ek, M.; Gellerstedt, G.; Henriksson, G. *Wood chemistry and biotechnology*; Walter de Gruyter: 2009; Vol. 1.
33. Terashima, N.; Fukushima, K. Heterogeneity in formation of lignin—XI: An autoradiographic study of the heterogeneous formation and structure of pine lignin. *Wood Sci. Technol.* **1988**, *22*, 259-270, doi:10.1007/BF00386021.
34. Watkins, D.; Nuruddin, M.; Hosur, M.; Tcherbi-Narteh, A.; Jeelani, S. Extraction and characterization of lignin from different biomass resources. *J. Mater. Res. Technol.* **2015**, *4*, 26-32.
35. Wen, J.-L.; Sun, S.-L.; Xue, B.-L.; Sun, R.-C. Recent advances in characterization of lignin polymer by solution-state nuclear magnetic resonance (NMR) methodology. *Materials* **2013**, *6*, 359-391.
36. Lawoko, M.; Henriksson, G.; Gellerstedt, G. Characterisation of lignin-carbohydrate complexes (LCCs) of spruce wood (Picea abies L.) isolated with two methods. *Holzforschung* **2006**, *60*, 156-161.
37. Tarasov, D.; Leitch, M.; Fatehi, P. Lignin–carbohydrate complexes: Properties, applications, analyses, and methods of extraction: A review. *Biotechnol Biofuels* **2018**, *11*, 269.
38. Brunow, G.; Lundquist, K. Functional groups and bonding patterns in lignin (including the lignin-carbohydrate complexes). *Lignin and lignans: advances in chemistry* **2010**, 267-299.
39. Košíková, B.; Joniak, D.; Kosakova, L. On the properties of benzyl ether bonds in the lignin-saccharidic complex isolated from spruce. *Holzforschung-International Journal of the Biology, Chemistry, Physics and Technology of Wood* **1979**, *33*, 11-14.
40. Rowell, R.M. *Handbook of wood chemistry and wood composites*; CRC press: 2012.
41. Höglund, H. Mechanical pulping. *Pulp and paper chemistry and technology* **2009**, *2*, 57-90.
42. Bajpai, P. Pulp and paper production processes and energy overview. *Pulp and Paper Industry; Elsevier: Amsterdam, The Netherlands* **2016**.

43. Macfarlane, A.; Mai, M.; Kadla, J. Bio-based chemicals from biorefining: Lignin conversion and utilisation. In *Advances in Biorefineries*, Elsevier: 2014; pp. 659-692.
44. Wenzl, H. *The chemical technology of wood*; Elsevier: 2012.
45. Holtzapple, M.T. LIGNIN. In *Encyclopedia of Food Sciences and Nutrition (Second Edition)*, Caballero, B., Ed. Academic Press: Oxford, 2003; https://doi.org/10.1016/B0-12-227055-X/00699-4pp. 3535-3542.
46. Hocking, M.B. *Modern chemical technology and emission control*; Springer Science & Business Media: 2012.
47. Ek, M.; Gellerstedt, G.; Henriksson, G. *Pulping chemistry and technology*; Walter de Gruyter: 2009; Vol. 2.
48. Guizani, C.; Lachenal, D. Controlling the molecular weight of lignosulfonates by an alkaline oxidative treatment at moderate temperatures and atmospheric pressure: a size-exclusion and reverse-phase chromatography study. *International journal of molecular sciences* **2017**, *18*, 2520.
49. Sjostrom, E. *Wood chemistry: fundamentals and applications*; Gulf professional publishing: 1993.
50. (EPA), E.p.a. *Available and emerging technologies for reducing greenhouse gas emissions from the pulp and paper manufacturing industry*; 2010a.
51. Snyder, S.W.; Petersen, G.; Negri, C.; Ezeji, T.; Qureshi, N.; Magrini, K.; Datta, S.; Peretti, S.; Liang, Y.; Lin, Y. *Commercializing biobased products: Opportunities, challenges, benefits, and risks*; Royal Society of Chemistry: 2015.
52. Wertz, J.-L.; Deleu, M.; Coppée, S.; Richel, A. *Hemicelluloses and lignin in biorefineries*; CRC Press: 2017.
53. Tamime, A.Y. *Cleaning-in-place: dairy, food and beverage operations*; John Wiley & Sons: 2009; Vol. 13.
54. Tamime, A.Y. *Membrane processing: dairy and beverage applications*; John Wiley & Sons: 2012.
55. Uloth, V.; Wearing, J. Kraft lignin recovery: Acid precipitation versus ultrafiltration. Part II: Technology and economics. *Pulp Paper Can* **1989**, *90*, 34-37.
56. Krawczyk, H.; Arkell, A.; Jönsson, A.-S. Impact of prefiltration on membrane performance during isolation of hemicelluloses extracted from wheat bran. *Sep. Purif. Technol.* **2013**, *116*, 192-198.
57. Benjamin, M.M.; Lawler, D.F. *Water quality engineering: Physical/chemical treatment processes*; John Wiley & Sons: 2013.
58. Graff, M. Disposal of metalworking fluids. In *Metalworking Fluids (MWFs) for Cutting and Grinding*, Elsevier: 2012; pp. 389-402.
59. Field, R. Fundamentals of fouling. *Membranes for water treatment* **2010**, *4*, 1-23.
60. Matthiasson, E.; Sivik, B. Concentration polarization and fouling. *Desalination* **1980**, *35*, 59-103.

61. Drioli, E.; Nakagaki, M. *Membranes and membrane processes*; Springer Science & Business Media: 2013.
62. Le-Clech, P.; Chen, V.; Fane, T.A. Fouling in membrane bioreactors used in wastewater treatment. *Journal of membrane science* **2006**, *284*, 17-53.
63. Lee, S.; Boo, C.; Elimelech, M.; Hong, S. Comparison of fouling behavior in forward osmosis (FO) and reverse osmosis (RO). *Journal of Membrane Science* **2010**, *365*, 34-39, doi:https://doi.org/10.1016/j.memsci.2010.08.036.
64. Field, R.W.; Pearce, G.K. Critical, sustainable and threshold fluxes for membrane filtration with water industry applications. *Adv. Colloid Interface Sci.* **2011**, *164*, 38-44.
65. Cheryan, M. *Ultrafiltration and microfiltration handbook*; CRC press: 1998.
66. Hermia, J. Constant pressure blocking filtration laws: application to power-law non-Newtonian fluids. **1982**.
67. Vela, M.C.V.; Blanco, S.Á.; García, J.L.; Rodríguez, E.B. Analysis of membrane pore blocking models applied to the ultrafiltration of PEG. *Sep. Purif. Technol.* **2008**, *62*, 489-498.
68. Al Manasrah, M.; Kallioinen, M.; Ilvesniemi, H.; Mänttäri, M. Recovery of galactoglucomannan from wood hydrolysate using regenerated cellulose ultrafiltration membranes. *Bioresour. Technol.* **2012**, *114*, 375-381.
69. Persson, T.; Jönsson, A.-S. Isolation of hemicelluloses by ultrafiltration of thermomechanical pulp mill process water—Influence of operating conditions. *Chem. Eng. Res. Des.* **2010**, *88*, 1548-1554.
70. Egüés, I.; Sanchez, C.; Mondragon, I.; Labidi, J. Separation and purification of hemicellulose by ultrafiltration. *Industrial & engineering chemistry research* **2012**, *51*, 523-530.
71. Duval, A.; Molina-Boisseau, S.; Chirat, C. Fractionation of lignosulfonates: comparison of ultrafiltration and ethanol solubility to obtain a set of fractions with distinct properties. *Holzforschung* **2015**, *69*, 127-134.
72. Bhattacharya, P.; Todi, R.; Tiwari, M.; Bhattacharjee, C.; Bhattacharjee, S.; Datta, S. Studies on ultrafiltration of spent sulfite liquor using various membranes for the recovery of lignosulphonates. *Desalination* **2005**, *174*, 287-297.
73. Bottino, A.; Capannelli, G.; Kuiper, D.; Salvemini, F. Lignosulfonates from calcium sulfite spent liquor—recovery using anic ultrafiltration membranes. *Journal of Membrane Science* **1983**, *16*, 175-180.
74. Thuvander, J.; Jönsson, A.-S. Extraction of galactoglucomannan from thermomechanical pulp mill process water by microfiltration and ultrafiltration—Influence of microfiltration membrane pore size on ultrafiltration performance. *Chem. Eng. Res. Des.* **2016**, *105*, 171-176.

75. Koivula, E.; Kallioinen, M.; Preis, S.; Testova, L.; Sixta, H.; Mänttäri, M. Evaluation of various pretreatment methods to manage fouling in ultrafiltration of wood hydrolysates. *Sep. Purif. Technol.* **2011**, *83*, 50-56.
76. Persson, T.; Jönsson, A.-S. Fouling of ultrafiltration membranes during isolation of hemicelluloses in the forest industry. *Scholarly Research Exchange* **2009**, *2009*.
77. Tan, S.C.; Yiap, B.C. DNA, RNA, and protein extraction: the past and the present. *BioMed Research International* **2009**, *2009*.
78. DeLucas, L. *Membrane protein crystallization*; Academic Press: 2009.
79. Tang, Q.; Zhou, M.; Yang, D.; Qiu, X. Effects of pH on aggregation behavior of sodium lignosulfonate (NaLS) in concentrated solutions. *Journal of Polymer Research* **2015**, *22*, 50.
80. Myrvold, B.O. Salting-out and salting-in experiments with lignosulfonates (LSs). **2013**, *67*, 549, doi:https://doi.org/10.1515/hf-2012-0163.
81. Guo, M.Q.; Hu, X.; Wang, C.; Ai, L. Polysaccharides: structure and solubility. *Solubility of polysaccharides* **2017**, 7-21.
82. Zhu, W. Equilibrium of lignin precipitation: the effects of ph, temperature, ion strength and wood origins. **2013**.
83. Song, T.; Pranovich, A.; Holmbom, B. Separation of polymeric galactoglucomannans from hot-water extract of spruce wood. *Bioresour. Technol.* **2013**, *130*, 198-203.
84. Zasadowski, D.; Yang, J.; Edlund, H.; Norgren, M. Antisolvent precipitation of water-soluble hemicelluloses from TMP process water. *Carbohydr. Polym.* **2014**, *113*, 411-419.
85. Tarasov, D.; Leitch, M.; Fatehi, P. Production of lignosulfonate in NSSC-based biorefinery. *Biotechnol. Progr.* **2015**, *31*, 1508-1514.
86. Tien, C. *Introduction to adsorption: Basics, analysis, and applications*; Elsevier: 2018.
87. Chiou, C.T. *Partition and adsorption of organic contaminants in environmental systems*; John Wiley & Sons: 2003.
88. Gabelman, A. Adsorption basics: part 1. *American Institute of Chemical Engineers (AIChE)* **2017**, *113*, 48-53.
89. Moises, B.N.D., Cristina Silva de Azevedo; Sebastião, Mardônio Pereira de Lucena. Adsorption. In *Kirk-Othmer Encyclopedia of Chemical Technology*, 10.1002/0471238961.0104191518212008.a01.pub3pp. 1-59.
90. Inglezakis, V.J.; Poulopoulos, S.G.; Kazemian, H. Insights into the S-shaped sorption isotherms and their dimensionless forms. *Microporous Mesoporous Mater.* **2018**, *272*, 166-176.
91. Khalfaoui, M.; Knani, S.; Hachicha, M.; Lamine, A.B. New theoretical expressions for the five adsorption type isotherms classified by BET based on statistical physics treatment. *J. Colloid Interface Sci.* **2003**, *263*, 350-356.
92. Liu, Y. Some consideration on the Langmuir isotherm equation. *Colloids and Surfaces A: Physicochemical and Engineering Aspects* **2006**, *274*, 34-36.

93. Umpleby II, R.J.; Baxter, S.C.; Bode, M.; Berch Jr, J.K.; Shah, R.N.; Shimizu, K.D. Application of the Freundlich adsorption isotherm in the characterization of molecularly imprinted polymers. *Anal. Chim. Acta* **2001**, *435*, 35-42.
94. Saadi, R.; Saadi, Z.; Fazaeli, R.; Fard, N.E. Monolayer and multilayer adsorption isotherm models for sorption from aqueous media. *Korean J. Chem. Eng.* **2015**, *32*, 787-799.
95. Kajjumba, G.W.; Emik, S.; Öngen, A.; Özcan, H.K.; Aydın, S. Modelling of adsorption kinetic processes—errors, theory and application. In *Advanced sorption process applications*, IntechOpen: 2018.
96. Pan, M.; Lin, X.; Xie, J.; Huang, X. Kinetic, equilibrium and thermodynamic studies for phosphate adsorption on aluminum hydroxide modified palygorskite nano-composites. *RSC Adv* **2017**, *7*, 4492-4500.
97. Ho, Y.; McKay, G. Kinetic models for the sorption of dye from aqueous solution by wood. *Trans. IChemE* **1998**, *76*, 183-191.
98. Nethaji, S.; Sivasamy, A.; Mandal, A. Adsorption isotherms, kinetics and mechanism for the adsorption of cationic and anionic dyes onto carbonaceous particles prepared from Juglans regia shell biomass. *International Journal of Environmental Science and Technology* **2013**, *10*, 231-242.
99. Peng, F.; Peng, P.; Xu, F.; Sun, R.-C. Fractional purification and bioconversion of hemicelluloses. *Biotechnol. Adv.* **2012**, *30*, 879-903.
100. Koivula, E.; Kallioinen, M.; Sainio, T.; Antón, E.; Luque, S.; Mänttäri, M. Enhanced membrane filtration of wood hydrolysates for hemicelluloses recovery by pretreatment with polymeric adsorbents. *Bioresour. Technol.* **2013**, *143*, 275-281.
101. Nitzsche, R.; Groengroeft, A.; Kraume, M. Separation of lignin from beech wood hydrolysate using polymeric resins and zeolites–Determination and application of adsorption isotherms. *Sep. Purif. Technol.* **2019**, *209*, 491-502.
102. Schwartz, T.J.; Lawoko, M. Removal of acid-soluble lignin from biomass extracts using Amberlite XAD-4 resin. *BioResources* **2010**, *5*, 2337-2347.
103. Sumerskii, I.; Korntner, P.; Zinovyev, G.; Rosenau, T.; Potthast, A. Fast track for quantitative isolation of lignosulfonates from spent sulfite liquors. *RSC Adv* **2015**, *5*, 92732-92742.
104. Westerberg, N.; Sunner, H.; Gunnar, H.; Mikaela, H.; Martin, L.; Rasmuson, A. Separation of galactoglucomannans, lignin and lignin-carbohydrate complexes from hot-water-extracted Norway spruce by cross-flow filtration and adsorption chromatography. *BioResources* **2012**, *7*, 4501-4516.
105. Narron, R.H.; Chang, H.-m.; Jameel, H.; Park, S. Soluble lignin recovered from biorefinery pretreatment hydrolyzate characterized by lignin–carbohydrate complexes. *ACS Sustainable Chemistry & Engineering* **2017**, *5*, 10763-10771.

106. Heinonen, J.; Sanlaville, Q.; Niskakoski, H.; Tamper, J.; Sainio, T. Separation and recovery of lignin from hydrolysates of lignocellulose with a polymeric adsorbent. *Sep. Purif. Technol.* **2017**, *186*, 125-134.
107. Van Blaricom, L.E.; Russell, G.K. Lignosulfonate recovery from waste sulfite liquor. Google Patents: 1955.
108. Liu, L.; Ren, J.; Zhang, Y.; Liu, X.; Ouyang, J. Simultaneously separation of xylo-oligosaccharide and lignosulfonate from wheat straw magnesium bisulfite pretreatment spent liquor using ion exchange resin. *Bioresour. Technol.* **2018**, *249*, 189-195.
109. Lundqvist, J.; Teleman, A.; Junel, L.; Zacchi, G.; Dahlman, O.; Tjerneld, F.; Stålbrand, H. Isolation and characterization of galactoglucomannan from spruce (Picea abies). *Carbohydr. Polym.* **2002**, *48*, 29-39.
110. Beatson, R. Determination of sulfonate groups and total sulfur. In *Methods in lignin chemistry*, Springer: 1992; pp. 473-484.
111. Goldmann, W.M.; Ahola, J.; Mankinen, O.; Kantola, A.M.; Komulainen, S.; Telkki, V.-V.; Tanskanen, J. Determination of phenolic hydroxyl groups in technical lignins by ionization difference ultraviolet spectrophotometry (Δ ε-IDUS method). *Periodica Polytechnica Chemical Engineering* **2017**, *61*, 93-101.
112. Qin, Y.; Yu, L.; Wu, R.; Yang, D.; Qiu, X.; Zhu, J. Biorefinery lignosulfonates from sulfite-pretreated softwoods as dispersant for graphite. *ACS Sustainable Chemistry & Engineering* **2016**, *4*, 2200-2205.
113. Korntner, P.; Schedl, A.; Sumerskii, I.; Zweckmair, T.; Mahler, A.K.; Rosenau, T.; Potthast, A. Sulfonic acid group determination in lignosulfonates by headspace gas chromatography. *ACS Sustainable Chemistry & Engineering* **2018**, *6*, 6240-6246.
114. Hannuksela, T.; du Penhoat, C.H. NMR structural determination of dissolved O-acetylated galactoglucomannan isolated from spruce thermomechanical pulp. *Carbohydr. Res.* **2004**, *339*, 301-312.
115. Lawoko, M. Unveiling the structure and ultrastructure of lignin carbohydrate complexes in softwoods. *Int. J. Biol. Macromol.* **2013**, *62*, 705-713.
116. Forss, K.; Stenlund, B. The influence of charged groups in gel permeation chromatography of polyelec-trolytes. In Proceedings of Journal of Polymer Science: Polymer Symposia; pp. 951-963.
117. Tolbert, A.; Akinosho, H.; Khunsupat, R.; Naskar, A.K.; Ragauskas, A.J. Characterization and analysis of the molecular weight of lignin for biorefining studies. *Biofuels, Bioproducts and Biorefining* **2014**, *8*, 836-856.
118. Hwang, K.-J.; Liao, C.-Y.; Tung, K.-L. Effect of membrane pore size on the particle fouling in membrane filtration. *Desalination* **2008**, *234*, 16-23.
119. Krawczyk, H.; Jönsson, A.-S. Separation of dispersed substances and galactoglucomannan in thermomechanical pulp process water by microfiltration. *Sep. Purif. Technol.* **2011**, *79*, 43-49.

120. Bowen, W.; Calvo, J.; Hernandez, A. Steps of membrane blocking in flux decline during protein microfiltration. *Journal of Membrane Science* **1995**, *101*, 153-165.
121. Du, X.; Gellerstedt, G.; Li, J. Universal fractionation of lignin–carbohydrate complexes (LCC s) from lignocellulosic biomass: an example using spruce wood. *The Plant Journal* **2013**, *74*, 328-338.
122. Abdelrasoul, A.; Doan, H.; Lohi, A. Fouling in membrane filtration and remediation methods. *Mass transfer-advances in sustainable energy and environment oriented numerical modeling* **2013**, *195*.
123. Alexandri, M.; Papapostolou, H.; Komaitis, M.; Stragier, L.; Verstraete, W.; Danezis, G.P.; Georgiou, C.A.; Papanikolaou, S.; Koutinas, A.A. Evaluation of an integrated biorefinery based on fractionation of spent sulphite liquor for the production of an antioxidant-rich extract, lignosulphonates and succinic acid. *Bioresour. Technol.* **2016**, *214*, 504-513.
124. Ding, Z.; Liu, X.; Liu, Y.; Zhang, L. Enhancing the compatibility, hydrophilicity and mechanical properties of polysulfone ultrafiltration membranes with lignocellulose nanofibrils. *Polymers* **2016**, *8*, 349.
125. Li, J.; O'Hagan, T.; MacLeod, J. Using ultrafiltration to analyze the molar mass distribution of kraft lignin at pH 13. *The Canadian Journal of Chemical Engineering* **1996**, *74*, 110-117.
126. Puro, L.; Tanninen, J.; Nyström, M. Analyses of organic foulants in membranes fouled by pulp and paper mill effluent using solid-liquid extraction. *Desalination* **2002**, *143*, 1-9.
127. Brião, V.B.; Seguenka, B.; Zanon, C.D.; Milani, A. Cake formation and the decreased performance of whey ultrafiltration. *Acta Scientiarum. Technology* **2017**, *39*, 517-524.
128. Rajniak, P.; Tsinontides, S.; Pham, D.; Hunke, W.; Reynolds, S.; Chern, R. Sterilizing filtration—principles and practice for successful scale-up to manufacturing. *Journal of Membrane Science* **2008**, *325*, 223-237.
129. Dolar, D.; Zokić, T.I.; Košutić, K.; Ašperger, D.; Pavlović, D.M. RO/NF membrane treatment of veterinary pharmaceutical wastewater: comparison of results obtained on a laboratory and a pilot scale. *Environmental Science and Pollution Research* **2012**, *19*, 1033-1042.
130. Persson, T.; Krawczyk, H.; Nordin, A.-K.; Jönsson, A.-S. Fractionation of process water in thermomechanical pulp mills. *Bioresour. Technol.* **2010**, *101*, 3884-3892.
131. Thuvander, J.; Lipnizki, F.; Jönsson, A.-S. On-site recovery of hemicelluloses from thermomechanical pulp mill process water by microfiltration and ultrafiltration. *J. Wood Chem. Technol.* **2019**, *39*, 214-223.
132. Prádanos, P.; Arribas, J.; Hernandez, A. Mass transfer coefficient and retention of PEGs in low pressure cross-flow ultrafiltration through asymmetric membranes. *Journal of membrane science* **1995**, *99*, 1-20.

133. Jönsson, A.-S. Influence of shear rate on the flux during ultrafiltration of colloidal substances. *Journal of membrane science* **1993**, *79*, 93-99.
134. Stade, S.; Kallioinen, M.; Tuuva, T.; Mänttäri, M. Compaction and its effect on retention of ultrafiltration membranes at different temperatures. *Sep. Purif. Technol.* **2015**, *151*, 211-217.
135. Sun, W.; Liu, J.; Chu, H.; Dong, B. Pretreatment and membrane hydrophilic modification to reduce membrane fouling. *Membranes* **2013**, *3*, 226-241.
136. Humpert, D.; Ebrahimi, M.; Czermak, P. Membrane technology for the recovery of lignin: A review. *Membranes* **2016**, *6*, 42.
137. Pabby, A.K.; Rizvi, S.S.; Requena, A.M.S. *Handbook of membrane separations: chemical, pharmaceutical, food, and biotechnological applications*; CRC press: 2008.
138. Pontié, M. Effect of aging on UF membranes by a streaming potential (SP) method. *Journal of membrane science* **1999**, *154*, 213-220.
139. Akerlof, G. Dielectric constants of some organic solvent-water mixtures at various temperatures. *J. Am. Chem. Soc.* **1932**, *54*, 4125-4139.
140. Machmudah, S.; Kanda, H.; Goto, M. Hydrolysis of Biopolymers in Near-Critical and Subcritical Water. In *Water Extraction of Bioactive Compounds*, Elsevier: 2017; pp. 69-107.
141. He, N.; Smeds, A.; Friman, R.; Rosenholm, J.B. Solubility parameters of biopolymers. *Phys. Chem. Liq.* **2013**, *51*, 302-316.
142. Quesada-Medina, J.; Lopez-Cremades, F.J.; Olivares-Carrillo, P. Organosolv extraction of lignin from hydrolyzed almond shells and application of the δ-value theory. *Bioresour. Technol.* **2010**, *101*, 8252-8260.
143. Huijgen, W.J.; Reith, J.H.; den Uil, H. Pretreatment and fractionation of wheat straw by an acetone-based organosolv process. *Industrial & engineering chemistry research* **2010**, *49*, 10132-10140.
144. Lo, C.-f. Low-molecular weight lignosulfonates from spent sulfite liquor: isolation, purification and identification. **1970**.
145. Zhou, M.; Qiu, X.; Yang, D.; Lou, H. Properties of Different Molecular Weight Sodium Lignosulfonate Fractions as Dispersant of Coal-Water Slurry. *J. Dispersion Sci. Technol.* **2006**, *27*, 851-856.
146. Willför, S.; Sjöholm, R.; Laine, C.; Roslund, M.; Hemming, J.; Holmbom, B. Characterisation of water-soluble galactoglucomannans from Norway spruce wood and thermomechanical pulp. *Carbohydr. Polym.* **2003**, *52*, 175-187.
147. Steinmetz, V.; Villain-Gambier, M.; Klem, A.; Gambier, F.; Dumarcay, S.p.; Trebouet, D. Unveiling TMP Process Water Potential as an Industrial Sourcing of Valuable Lignin–Carbohydrate Complexes toward Zero-Waste Biorefineries. *ACS Sustainable Chemistry & Engineering* **2019**, *7*, 6390-6400.

148. Lutnaes, B.F.; Myrvold, B.O.; Lauten, R.A.; Endeshaw, M.M. 1H and 13C NMR data of benzylsulfonic acids—model compounds for lignosulfonate. *Magn. Reson. Chem.* **2008**, *46*, 299-305.
149. Marques, A.; Evtuguin, D.; Magina, S.; Amado, F.; Prates, A. Structure of lignosulphonates from acidic magnesium-based sulphite pulping of Eucalyptus globulus. *J. Wood Chem. Technol.* **2009**, *29*, 337-357.
150. Sims, I.M.; Craik, D.J.; Bacic, A. Structural characterisation of galactoglucomannan secreted by suspension-cultured cells of Nicotiana plumbaginifolia. *Carbohydr. Res.* **1997**, *303*, 79-92.
151. Du, X.; Pérez-Boada, M.; Fernández, C.; Rencoret, J.; José, C.; Jiménez-Barbero, J.; Li, J.; Gutiérrez, A.; Martínez, A.T. Analysis of lignin–carbohydrate and lignin–lignin linkages after hydrolase treatment of xylan–lignin, glucomannan–lignin and glucan–lignin complexes from spruce wood. *Planta* **2014**, *239*, 1079-1090.
152. Myrvold, B.O. A new model for the structure of lignosulphonates: Part 1. Behaviour in dilute solutions. *Ind Crops Prod* **2008**, *27*, 214-219.
153. Myrvold, B.O. The polyelectrolyte behavior of randomly branched lignosulfonates. *Tappi J.* **2007**, *6*, 10-14.
154. Salmén, L.; Burgert, I. Cell wall features with regard to mechanical performance. A review COST Action E35 2004–2008: Wood machining–micromechanics and fracture. *Holzforschung* **2009**, *63*, 121-129.
155. Stevanic, J.S.; Salmén, L. Orientation of the wood polymers in the cell wall of spruce wood fibres. *Holzforschung* **2009**, *63*, 497-503.
156. Hasted, J.; Ritson, D.; Collie, C. Dielectric properties of aqueous ionic solutions. Parts I and II. *J Chem Phys* **1948**, *16*, 1-21.
157. Swamy, N.K.; Singh, P.; Sarethy, I.P. Precipitation of phenols from paper industry wastewater using ferric chloride. *Rasayan J. Chem* **2011**, *4*, 452-456.
158. Mussatto, S.I.; Fernandes, M.; Roberto, I.C. Lignin recovery from brewer's spent grain black liquor. *Carbohydr. Polym.* **2007**, *70*, 218-223.
159. Shinoda, K.o.z.o.; Fujihira, M. The analysis of the solubility of hydrocarbons in water. *Bull. Chem. Soc. Jpn.* **1968**, *41*, 2612-2615.
160. Li, H.; Deng, Y.; Ye, H.; Xiao, L.; Qiu, X. Effect of temperature on polyelectrolyte expansion of lignosulfonate. *BioResources* **2015**, *10*, 575-587.
161. Luong, D.; Sephton, M.A.; Watson, J.S. Subcritical water extraction of organic matter from sedimentary rocks. *Anal. Chim. Acta* **2015**, *879*, 48-57.
162. Jönsson, A.-S.; Nordin, A.-K.; Wallberg, O. Concentration and purification of lignin in hardwood kraft pulping liquor by ultrafiltration and nanofiltration. *Chem. Eng. Res. Des.* **2008**, *86*, 1271-1280.
163. Ulrich, G. A guide to chemical engineering process design and economics. John Wiley&Sons. *Inc., New York (USA)* **1984**.
164. Patel, H.; Vashi, R. *Characterization and treatment of textile wastewater*; Elsevier: 2015.

165. Persson, P.; Kempe, H.; Zacchi, G.; Nilsson, B. Estimation of adsorption parameters in a detailed affinity chromatography model based on shallow bed experiments. *Process Biochem.* **2005**, *40*, 1649-1659.
166. Nilsson, B.; Borgqvist, P.; Axelsson, A.; Zacchi, G. Simulation of chromatographic processes using MATLAB. *Computers & Chemical Engineering* **1999**, *23*, S715-S718.
167. Li, S.; Xin, F.; Li, L. *Reaction engineering*; Butterworth-Heinemann: 2017.
168. Ministerråd, N. *Study on Nordic Pulp and Paper Industry and the Environment*; Nordic Council of Ministers: 1993.
169. Ergun, S. Fluid flow through packed columns. *Chem. Eng. Prog.* **1952**, *48*, 89-94.
170. Hilal, N.; Al-Zoubi, H.; Mohammad, A.W.; Darwish, N. Nanofiltration of highly concentrated salt solutions up to seawater salinity. *Desalination* **2005**, *184*, 315-326.
171. Szepessy, S.; Thorwid, P. Low Energy Consumption of High-Speed Centrifuges. *Chemical engineering & technology* **2018**, *41*, 2375-2384.

Paper I

Separation and Purification Technology 187 (2017) 380–388

Contents lists available at ScienceDirect

Separation and Purification Technology

journal homepage: www.elsevier.com/locate/seppur

Influence of prefiltration on membrane performance during isolation of lignin-carbohydrate complexes from spent sulfite liquor

Basel Al-Rudainy, Mats Galbe, Ola Wallberg *

Department of Chemical Engineering, Lund University, Lund, Sweden

ARTICLE INFO

Article history:
Received 22 December 2016
Received in revised form 25 April 2017
Accepted 14 June 2017
Available online 29 June 2017

Keywords:
Galactoglucomannan
LCC
Fouling
Prefiltration
Spent sulfite liquor
Ultrafiltration

ABSTRACT

In this study, we examined the isolation of lignin-carbohydrate complexes (LCCs) from sodium-based spent sulfite liquor, in conjunction with minimization of membrane fouling. We screened 3 polysulfone (PS) membranes with cutoffs of 100, 50, and 25 kDa, respectively. Flux and retention for the 100- and 50-kDa membranes had the same order of magnitude, indicating that these properties were determined by fouling that formed on the membrane—not pore size. The PS membrane with the 50-kDa cutoff performed best in terms of flux and retention of lignin-carbohydrate complexes and experienced the least membrane fouling.

Two prefiltration methods were used to decrease the fouling of the 50-kDa membrane: a 0.2-μm PS microfiltration membrane and dead-end filtration with 10-um filter cloth and a 4 wt% mixture of kieselguhr (diatomite) and spent sulfite liquor prior to filtration.

Prefiltration of the SSL with microfiltration increased the flux 3-fold and decreased the fouling grade from 49% to 7.2%. Dead-end filtration effected a 16% increase in flux and a fouling grade of 17%. The retention of LCC during microfiltration was high, which resulted in a loss of high-molecular-weight products, whereas the loss of LCC during dead-end filtration was negligible.

A 50-kDa PS membrane performed best with regard to the recovery of lignin-carbohydrate complexes from spent sulfite liquor. Also, dead-end filtration is a promising method for eliminating membrane fouling.

© 2017 Elsevier B.V. All rights reserved.

1. Introduction

Spent sulfite liquor (SSL) is a waste stream that is generated in the manufacture of pulp in the sulfite process. The treated SSL is usually concentrated in evaporators before being sent to a recovery boiler where the pulping chemicals are recovered and the organic materials are incinerated to produce power and heat [1]. The solids content in SSL is 8–14% by weight, of which lignosulfonates, hemicelluloses, monosaccharides, and pulping chemicals are the major constituents [1,2]. Studies on the composition of dissolved wood components have established the existence of lignin that is covalently bound to polysaccharides [3–6]. Lawoko et al. [7] discovered that lignin binds to all major polysaccharides in the plant wall, demonstrating that extracted lignin-carbohydrate complexes (LCCs) have a wide array of compositions, depending on the extraction method and plant type. Giummarella et al. [8] discovered that the carbohydrates linked to lignin in spruce were mainly arabinoglucuronoxylan and galactoglucomannan (GGM) The main lignin-carbohydrate linkages detected were benzyl ether (xylan) and phenyl glycosidic (mannan). The LCC structures were not uniform, meaning that significant differences existed in the LCC structures, because of the lignin part of the LCC. The study confirmed the observations made by Lawoko et al. [7]. Similar observations were made by Du et al. [9], where three major LCC fractions were detected in the spruce-based raw material, that is, in mannan, glucan and xylan enriched fractions. All of the mentioned fractions had a high molecular weight and were practically insoluble in dioxane/water mixtures. Possible applications for LCCs have been presented in several studies, which have shown that LCCs can be used in the production of gas-barrier films [10], for polymeric surfactants and as drug carriers [11]. Thus, the isolation and fractionation of LCCs are important for research and development of future products.

The separation and purification of the wood polymers has garnered significant interest, because many applications are being developed for the use of these components. Membrane filtration has become a common method for the fractionation and isolation of wood components from various waste streams. Al Manasrah

* Corresponding author.
E-mail addresses: basel.al-rudainy@chemeng.lth.se (B. Al-Rudainy), mats.galbe@chemeng.lth.se (M. Galbe), ola.wallberg@chemeng.lth.se (O. Wallberg).

http://dx.doi.org/10.1016/j.seppur.2017.06.031
1383-5866/© 2017 Elsevier B.V. All rights reserved.

et al. [12] examined the possibility of using ultrafiltration (UF) membranes for the recovery of GGMfrom pressurized hot water extracts of spruce sawdust. In their study, the GGM retention rate was 88%, the purity was 63%, and the recovery rate was 70%, with an 86% reduction in volume. The purity improved further with diafiltration of the filtrate through the complete removal of monosaccharides and a portion of the xylan. Other studies have shown that UF membranes can be used to recover and purify lignosulfonates from SSL [13–15]. These reports compared various membranes and concluded that polysulfone membranes with a molecular-weight cutoff (MWCO) over 10 kDa were optimal in terms of flux, rejection of lignosulfonates, and high temperature tolerance versus cellulose-acetate and fluoropolymer membranes.

Isolation of LCCs from wood is a relatively new approach, necessitating more research. Lawoko et al. [6] developed a procedure to separate LCCs into several fractions with varying compositions for analytical purposes; however, for industrial separation, a simpler method is needed. Westerberg et al. [16] combined membrane filtration and an adsorption-based process for polymeric resins, isolating LCCs and upgrading GGM. The downsides of this approach were the adsorption process, in which the separation capacity was limited, and the degradation of sorbent material, which was costly. A combination of precipitation with diafiltration has been presented in several research papers showing an effort to develop a method for universal fractionation and purification of LCCs (glucan-lignin, glucomannan-lignin and xylan-lignin) [9,17–19]. Glucan-lignin was precipitated in the first step by dispersing the dimethyl sulfoxide and tetrabutylammonium hydroxide dissolved sample in deionized water. The addition of barium hydroxide to the supernatant precipitated the glucomannan-lignin. The xylan-lignin complex was precipitated by the addition of hydrochloric acid after removal of the glucomannan-lignin precipitate. All of the precipitates were freeze-dried and washed using a diafiltration setup. The method was claimed to yield high purities of the different fractions and was suitable for lab-scale experiments.

Economically, using membranes that result in a high product yield and can withstand the harsh environment of various solvents is critical for membrane filtration as a long-term separation method. Another important economic factor is the decrease in irreversible fouling on the membranes, which can in turn limit the capacity of the process and shorten the lifespan of membranes.

Understanding the fouling phenomenon can help in choosing the proper pretreatment method to minimize fouling without sacrificing product yield. Hermia [20] proposed a combined blocking filtration law that can be used to characterize the blocking mechanism that acts on the membrane during constant pressure filtration (Eq. (1)):

$$\frac{d^2t}{dV^2} = \alpha\left(\frac{dt}{dV}\right)^{\beta} \tag{1}$$

where α and β are assume different values, depending on the type of fouling; see Table 1.

Table 1
α and β values for various blocking mechanisms. K_A is the membrane surface area that is blocked per volume permeating through the membrane. K_B is the decrease in membrane pore cross-sectional area per volume permeate. K_C is the area of the deposited cake. u_0 is the mean initial velocity of the permeate, A_0 is the membrane area, and R_r is the hydraulic cake resistance.

Blocking mechanism	α	β
Complete	$K_A u_0$	2
Standard	$(2\,K_B/A_0^{1/2})u_0^{1/2}$	3/2
Intermediate	K_A/A_0	1
Cake	$(R_rK_C/A_0^2)u_0^{-1}$	0

Complete blockage of the membrane occurs when every particle that arrives to the surface blocks a pore, with no superposition of particles [21,22]. Particles that adsorb to the inner pore walls diminish the pore radius and in turn decrease the flux—referred to as the standard blocking mechanism. Intermediate blocking exists when particles deposit themselves onto the membrane surface or other particles, thus shrinking the available membrane area and, consequently, the flux. When the available membrane surface is completely blocked, particles will deposit solely onto other particles, causing cake formation.

Bowen et al. [21] used the blocking filtration law to analyze fouling mechanisms during the microfiltration of bovine serum albumin. One condition of this law was noise-free data during the numerical differentiation, which was solved by fitting the experimental data to a polynomial and using the fitted data for the numerical differentiation. Vela et al. [23] studied the applicability of the blocking filtration law to the ultrafiltration of PEG, demonstrating that the model was applicable to cases in which the transmembrane pressure was low and the cross-flow velocity was high. In other cases, the results lay outside of the specified range of the model and thus had no physical meaning. Many advanced models have also been studied during the last 20 years; however, these models are not frequently used by engineers or in industrial applications [24].

Pretreatment prior to membrane filtration decreases fouling and increases the flux [25–27]. Krawczyk et al. [26] compared two prefiltration methods: microfiltration and dead-end filtration with kieselguhr (diatomite) as a filtration aid. Using these methods, the flux increased from 70 to 225 and 440 L/m^2 h after dead-end filtration and microfiltration, respectively. The loss of hemicellulose during microfiltration was substantial (only 4% was recovered), whereas that during dead-end filtration was negligible.

The aim of this study was to fractionate and purify high-molecular-weight and GGM-rich LCCs by membrane filtration. Irreversible fouling on the membranes was characterized per Bowen [21]. The impact of two prefiltration methods (microfiltration and dead-end filtration with kieselguhr) was also examined with regard to minimizing membrane fouling.

2. Materials and methods

2.1. Spent sulfite liquor (SSL) solution

The raw material was sodium-based SSL that was provided by Domsjö Fabriker (Örnsköldsvik, Sweden), which was collected after the first step in the pulping of softwood (60% Picea abies and 40% Pinus sylvestris). The composition of the raw material is presented in Section 3.1.

2.2. Equipment and experimental procedure

2.2.1. Membranes

The membranes, obtained from Alfa Laval Nordic A/S (Søborg, Denmark), were made of polysulphone with a polypropylene support. The membranes and their specifications are listed in Table 2.

2.2.2. Membrane filtration set-up

The screening study was performed using the equipment in Fig. 1a. The set-up consisted of a 15-L tank with an immersion heater (Backer, Elektro-Värme AB, Sösdala, Sweden), regulated by a temperature control unit (Model MCM, Shinko Technos Co., Ltd, Osaka, Japan), and two digital pressure gauges (DCS40.0AR, Trafag AG, Bubikon, Switzerland) on the feed and retentate side, respectively. The pressure was adjusted with a needle valve on the retentate side, and the flow was set with a positive displacement pump

Table 2
List of membranes.

Designation	Material	Type – Molecular weight cutoff/Pore size	pH range (measured at 25 °C)	Pressure range (bar)
GR60PP	Polysulfone	UF - 25 kDa	1–13	1–10
GR51PP	Polysulfone	UF - 50 kDa	1–13	1–10
GR40PP	Polysulfone	UF - 100 kDa	1–13	1–10
MFG 2	Polysulfone	MF - 0.2 μm	1.5–12	1–3

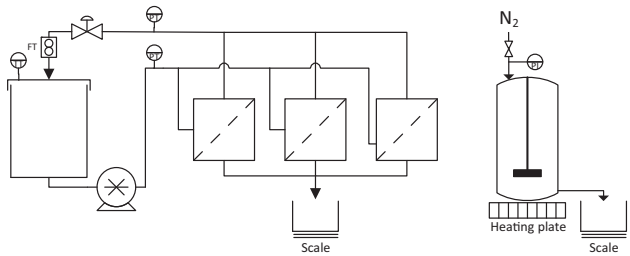


Fig. 1. Equipment set-up used for the screening (a), concentration, and prefiltration (b) studies.

(Hydra-cell D25XL, Wanner, Minneapolis, USA), which was regulated by a frequency converter (ELEX 4000, Bergkvist & Co., AB, Gothenburg, Sweden). Three flat-sheet membrane modules, connected in parallel, were used for the filtration experiments, in which flux was measured with a scale (PL6001-l, Mettler Toledo Inc., Ohio, USA) and cross-flow was measured with a flow-meter (FCH-34-PP-Chemical, B.I.O-TECH e.K., Vilshofen, Germany). The trans-membrane pressure (TMP) was calculated as the average of the difference in pressure between feed and retentate sides.

The concentration and prefiltration studies were performed using the set-up in Fig. 1b. The equipment comprised a sealed 400-mL stirred vessel and a digital pressure gauge (DCS40.0AR, Trafag AG, Bubikon, Switzerland). The pressure was controlled with a valve that was connected to a nitrogen gas line. The temperature and the angular velocity of the stirrer were controlled by a magnetic stirrer with a built-in heating plate (MR2002, Heidolph Instruments GmbH & Co.KG, Schwabach, Germany). The flux was measured using a scale (PL6001-l, Mettler Toledo Inc., Ohio, USA), and the average cross-flow velocity (CFV) was calculated per the following expression:

$$CFV_{av} = \frac{\int_0^{r_s} 2\pi\omega r\, dr}{r_s} = \pi\omega r_s \quad (2)$$

where ω is the stirrer angular velocity (s^{-1}), r is the position along the stirrer radius (m), and r_s is the total stirrer radius (m), which was 2.5 cm.

2.2.3. Membrane cleaning and oxidative treatment

For the screening study, the membranes were initially cleaned for 1 h with 13 L of 0.5 wt% alkaline detergent solution (Ultrasil 10, Ecolab AB, Älvsjö, Sweden) at 50 °C, 1 bar TMP, and a CFV of 0.5 m/s. The detergent was then displaced by deionized water, and the pure water flux (PWF) was measured at 20 °C. After the experiment, the membranes were washed for 2 h with 13 L of 0.04 wt% acid detergent solution (Ultrasil 73, Ecolab AB, Älvsjö, Sweden) and for 1 h with the alkaline detergent solution as above. The PWF was measured again, and fouling grade was calculated per the following expression:

$$Fouling\ grade\ (\%) = 100 * \frac{PWF_{Before} - PWF_{After}}{PWF_{Before}} \quad (3)$$

During the concentration studies, the membranes were cleaned as in the screening studies, except that they were soaked in 350 mL detergent solution during the cleaning period and the detergent was membrane-filtered to a volume reduction (VR) of 50%. The system was washed with two system volumes of deionized water prior to and after each detergent cleaning step to a VR of 50%. The PWF was determined as the average of the flux during membrane filtration of deionized water from VR 0% to 50%.

For the oxiditative treatment, the membranes were soaked in 350 ml of a mixture of 0.04 wt% of the acid detergent solution (Ultrasil 73) and 0.01 wt% hydrogen peroxide at 50 °C, and a CFV of 0.5 m/s for the duration of 1 h. The solution was then permeated to a VR of 50% and washed with two system volumes of deionized water.

2.2.4. Membrane screening

New membranes were placed into the modules and washed. After PWF was measured, the system was drained, and the SSL was poured into the feed tank through a 250-, 180-, and 45-um filter tray (U.S.A. Standard Testing Sieve, WS Tyler Inc., Ohio, USA) to remove large solids, such as fibers. These experiments were performed at 50 °C, a CFV of 0.3–0.5 m/s, and TMP of 1–9 bars. The permeate and retentate were recirculated to the feed tank in all experiments. The experiments began with the recirculation of SSL solution at a CFV of 0.5 m/s and TMP of 1 bar for 1 h to ensure that the flux was stable. The pressure was ramped 0.5 bar every 20 min, and a 30-mL sample was withdrawn from the permeate at each increase.

2.2.5. Concentration study and diafiltration

Concentration studies were performed at the weak critical flux [28] and the highest cross-flow velocity. The TMP, temperature, and CFV were 5.5 bar, 50 °C, and 0.5 m/s, respectively. The membrane was initially washed, and the PWF was measured. The SSL was then added and heated to 50 °C at a stirrer rate that corresponded to 0.5 m/s in CFV. TMP was then applied, and the flux

was logged until a VR of 90% was reached. Samples from the retentate and permeate were then collected, after which diafiltration was performed on the retentate, with a diafiltration factor (DF) of 5. Samples were harvested again before the cleaning and the determination of the PWF.

2.2.6. Prefiltration by microfiltration

The microfiltration membrane was cleaned, and the PWF was measured prior to and after the experiment. An analysis of parameters with microfiltration at 50 °C (data not shown) yielded the highest flux at a TMP and CFV of 0.6 bars and 0.5 m/s, respectively. Several microfiltrations were then performed with these parameters to obtain a sufficient amount of permeate for the ultrafiltration. The final volume reduction after the prefiltration step was 70%.

2.2.7. Prefiltration with dead-end filtration

Prior to dead-end filtration, a mixture of SSL and kieselguhr was prepared. Three liters of SSL was preheated to 50 °C in a baker on a heating plate (MR2002, Heidolph Instruments GmbH & Co.KG, Schwabach, Germany) with a magnetic stirrer (500 RPM). When the final temperature was reached, 120 g of kieselguhr (4 wt%) was added, and the solution was allowed to mix for 1 h. The stirrer was removed from the equipment (Fig. 1b) before the start of the filtration experiment. The filtration was initiated with the build-up of a filter cake by filtering 370 mL of the SSL-kieselguhr mixture at 5 bar. The filtrate was discarded, and a new filtration process was started with the same volume of SSL-kieselguhr on top of the existing filter cake. The filtrate was collected and the filter cake was discarded where after the equipment was washed with deionized water. The same procedure was run three times to obtain enough filtrate for the ultrafiltration trials.

2.3. Analysis

2.3.1. Ash and total dry substance (TDS)

The ash and TDS levels were determined using a heating furnace (Heraeus, Heraeus Holding GmbH, Hanau, Germany), a precision scale (AND Electric balance ER-120, San Jose, CA), and a muffle furnace (B150, Nabertherm GmbH, Lilienthal, Germany) by weighing a ceramic crucible with the sample before and after drying at 105 °C for 24 h. The TDS was then measured from the difference in weight between samples. The residue was ashed in a muffle furnace at 575 °C for 3 h, and the samples were allowed to cool in a desiccator for 30 min before being reweighed and analyzed for ash content.

2.3.2. Soluble lignin

The amount of soluble lignin in the samples was measured with a UV spectrophotometer (Shimadzu UV spectrophotometer UV-1800, Kyoto, Japan) at a wavelength of 234 nm. The extinction coefficient was 31.6 L cm/g, which was derived by calibration with a sodium lignosulfonate powder (Domsjö Fabriker, Örnsköldsvik, Sweden), dissolved in deionized water. All samples and standards were diluted with deionized water prior to analysis.

2.3.3. Hemicellulose and acid-insoluble solids

The hemicellulose composition was determined by acid hydrolysis per a standardized method by the NREL [29]. Acid hydrolysis was performed in a 10-mL sample, containing 750 µl 72% sulfuric acid, in an autoclave (Systec DX 150, Wettenberg, Germany) at 121 °C for 1 h. Acid-insoluble solids were filtered from the sample, dried at 105 °C for 24 h, and weighed. The filtrate was diluted (deionized water) and analyzed for monosaccharide concentrations by high-performance anion-exchange chromatography. The HPLC equipment consisted of an ICS-3000 chromatography system (Dionex Corp., Sunnyvale, CA) with pulsed amperometric detection and a Carbo Pac PA1 analytical column. Deionized water was used as the eluent at a flow rate of 1 ml/min, and the column was washed with a solution of 200 mM NaOH in 170 mM sodium acetate. The sample injection volume was 10 µL, and D-glucose, D-galactose, D-mannose, D-xylose, and L-arabinose (Fluka Chemie AG, Buchs, Switzerland) were used as the calibration standards. The total amount of hemicellulose was determined after anhydro corrections of 0.88 for pentoses and 0.90 for hexoses.

2.3.4. Size-exclusion chromatography (SEC) and LCC detection

SEC was performed on a chromatography system (Waters 600E System Controller, Waters, Milford, MA) that was equipped with an UV detector (Waters 486 Tunable Absorbance Detector) that measured at a wavelength of 234 nm, an RI detector (Waters 410 Differential Refractometer), a pump (Waters 600 Gradient pump), an auto-sampler (Waters 717 plus auto sampler), and a degasser (Waters In-Line Degasser). The column was packed with 30 cm Superdex 30 and 30 cm of Superdex 200 (GE Healthcare, Uppsala, Sweden). Deionized water was used as the eluent at a flow rate of 1 mL/min and a 500-µL sample injection volume. The column was calibrated with polyethylene glycol (PEG) standards of 35 kDa, 10 kDa, 4 kDa, and 400 Da (Merck Schuchardt OHG, Hohenbrunn, Germany). The LCCs were detected by observing the co-elution of the refractive index (carbohydrates and lignin) and ultraviolet (lignin) signals as described by Giummarella et al. [8] and Lawoko [30].

2.3.5. Turbidity

Turbidity was measured with a turbidimeter (2100P ISO, HACH Co., Loveland, CO) that was calibrated with formazin standards (HACH Co., Loveland, CO) of <0, 20, 100, and 800 NTU.

2.3.6. Density

Density was measured by weighing 3 mL of sample on a high-precision scale (AND Electric balance ER-120, San Jose, CA) at room temperature (20 °C). The average of three measurements was recorded as the density of the sample.

2.3.7. Enzymatic hydrolysis

Enzymatic hydrolysis was performed in a 2-L stirred bioreactor (Labfors, Infors AG, Bottmingen/Basel, Switzerland) with a water jacket for temperature control. One liter of SSL was loaded into the fermenter and heated to 45 °C at a stirrer rate of 300 RPM. When the solution reached 45 °C, 10 mL of Cellic HTec enzyme solution (Novozymes A/S, Bagsværd, Denmark) was added. The enzymatic hydrolysis continued for 72 h at the SSL solution's pH of 4.7, before the SSL solution was withdrawn and the monosaccharide content was analyzed.

3. Results and discussion

3.1. SSL content

The total hemicellulose content was defined as the sum of mannan, glucan, galactan, arabinan, and xylan levels. The amount of GGM was approximately 72% (5.5 g/L) of the total hemicellulose in the SSL solution. In a comparison of the monosaccharide content between untreated and acid-hydrolyzed SSL, 43.9% of the arabinan existed in the form of monomers. The retention of arabinan was low versus other polysaccharides (see Section 3.2.1), confirming that most of the arabinan had a low molecular weight. Other than the ash content of 40.2%, the total lignin content had the highest proportion at 36.4% (Fig. 2).

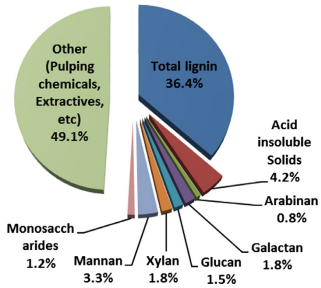


Fig. 2. SSL content in weight percent of TDS (84.6 g/L).

By employing SEC, the molecular weight (MW) of the hemicellulose and lignin was estimated to be 20–200 kDa (Fig. 3). Comparison of the RI (for detection of lignin and carbohydrates) and UV (for detection of lignin) fractions of the chromatograms showed that lignin and hemicellulose eluted at the same time. These results are an indication of the presence of linkages between lignin and carbohydrates, as has been previously described by Giummarella et al. [8] and Lawoko [30].

To measure the amount of hemicellulose that bound to lignin, we performed several analyses and experiments. Enzymatic hydrolysis was conducted to hydrolyze the hemicellulose portion of the LCCs to determine the MW of the bound lignin. By enzymatic hydrolysis, 2.6%, 15.5%, 15.9%, and 39.9% of the total mannan, xylan, glucan, and arabinan, respectively, were hydrolyzed, indicating that in addition to the bonds between lignin and hemicellulose, those between various polysaccharides existed, as discussed by Koshijima et al. and Lawoko et al. [31,32]. An excess of enzyme was used; thus, it was assumed that all of the xylan would be cleaved into monomers. However, this did not occur, possibly because some xylan-bound lignin sterically hindered the enzyme, as has been previously described by Jeffries et al. [33] and Álvarez et al. [34]. The structure of hemicellulose is very complex, thus the degradation of the different linkages and groups requires a wide range of auxiliary enzymes as pointed out by Álvarez et al. [34]. The galactan and mannan concentrations were unchanged, suggesting that no major cleavage of GGM occurred.

Comparison between the SEC curves for enzymatically hydrolyzed and untreated SSL, shows that a part of the lignin was released during the enzymatic hydrolysis, as evidenced by the peak at approximately 1.7 kDa in Fig. 3 (Enzyme Treated UV). This result was another indication of the existence of bonds between lignin and polysaccharides, explaining their inefficient hydrolysis.

SEC of the acid-hydrolyzed SSL resulted in three major lignin peaks, of which the peak at approximately 1.7 kDa was in common with that for enzymatically hydrolyzed SSL (Fig. 4, Acid Hydrolyzed UV). Another major peak lay in the region around 136 kDa, and most of the lignin eluted at 5.5 kDa, according to the UV component of the chromatogram (Fig. 4). The SEC graph also indicated that no major degradation of the lignin occurred, because the peak at roughly 1.7 kDa (Fig. 3) and high-MW lignin (136 kDa in Fig. 4) still existed after the acid hydrolysis (compared with the enzymatically hydrolyzed solution). Some of the lignin was not bound to carbohydrates (136 kDa in Fig. 4), and a proportion of lignin was bound to hemicellulose (5.5 and 1.7 kDa in Fig. 4). In an analysis of the peak areas of the UV curve, at least 18% (78–220 kDa in Fig. 4) of the high-MW lignin was not bound to any hemicellulose. Because GGM is the primary hemicellulose in the SSL, the term lignin-carbohydrate complex (LCC) will be referred to as the sum of the total GGM and lignin throughout this article.

3.2. Parameter study

3.2.1. Membrane screening

In screening experiments, the 25-kDa membrane had the lowest flux and highest degree of fouling. The average flux was approximately 1.8 L/m^{2}h and was unaffected by the CFV or TMP. No further analysis was performed using this membrane, because the flux was too low for sample collection. However, the 50- and 100-kDa membranes had fluxes and retentions of LCCs with the same order of magnitude (Figs. 5–8). Limiting-flux was unachievable with the 100-kDa membrane, most likely due to its more open structure compared with the 50-kDa membrane. With regard to retention, membrane pore size was not the only determining factor of the rejection of solutes (Figs. 7 and 8). However, the retention of solutes for the 100-kDa membrane was slightly higher, which may have been attributed to plugging of the membrane pores [35], which in turn explains the lower permeate flux. Krawczyk and Jönsson [36] observed the same phenomenon where an increase in membrane pore size led to decline of the permeate flux and to irreversible fouling of the membranes with the larger pore size. The authors came to the conclusion that the fouling was attributed to severe pore blocking. This phenomenon was also observed during the initial stage in our 100-kDa membrane study, in which the flux decreased from 97 L/m2 h to 56 L/m2 h at a TMP of 1 bar and CFV of 0.5 m/s (Section 3.2.2). The retention of arabinan was higher for the 100-kDa versus 50-kDa membrane, and no major difference in retention was observed between compounds in the parameter study with the 100-kDa membrane.

The retention data on the 50-kDa membrane verified our assumptions regarding the LCCs. LCCs comprised of a complex between GGM and lignin. The retention of acid-insoluble solids overlapped with that for GGM with the 50-kDa and 100-kDa

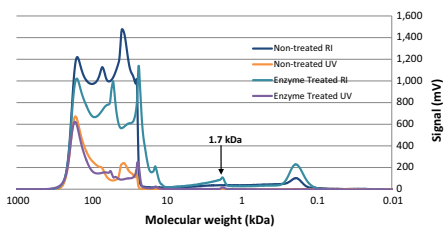


Fig. 3. SEC curves for enzymatically treated and non-treated SSL. RI is the refractive index, and UV is the ultraviolet (234 nm) response.

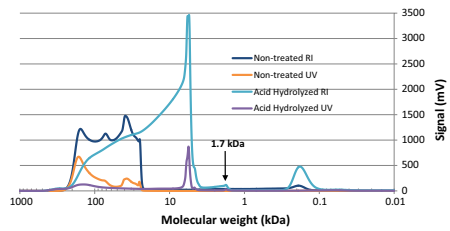


Fig. 4. SEC graph for the non-treated vs. acid-hydrolyzed SSL. RI: refractive index and UV: ultraviolet (234 nm).

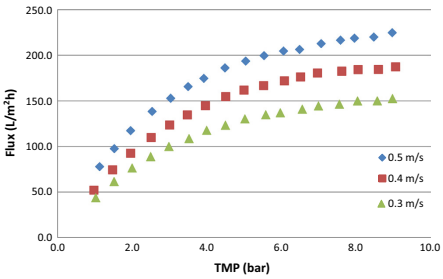


Fig. 5. TMP vs flux and CFV for the 50-kDa parameter study.

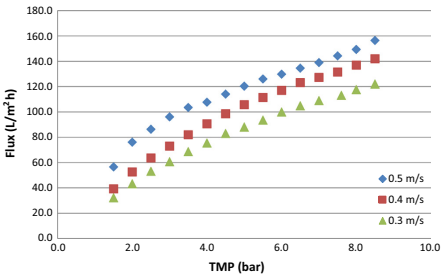


Fig. 6. TMP vs flux and CFV for the 100-kDa parameter study.

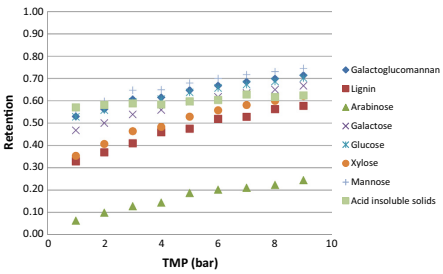


Fig. 7. TMP vs retention for the 50-kDa parameter study.

membranes, indicating that these solids were partly associated with GGM. Also, xylan and lignin were associated, because their retentions were consistent with each other. The retention of GGM was higher than for lignin, and as discussed earlier (Section 3.1), most of the carbohydrates were associated with lignin, suggesting the existence of various LCC fractions with varying amounts of polysaccharides, as observed by Lindgren [37].

3.2.2. Characterization of membrane fouling

In a parameter study of the three membranes, irreversible fouling degrees of 86%, 25%, and 85% were recorded for the 25-, 50-, and 100-kDa membranes, respectively. Pore blocking was expected, because the MWs for the various components ranged

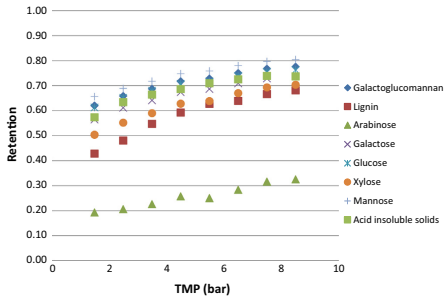


Fig. 8. TMP vs retention for the 100-kDa parameter study.

from 20 to 200 kDa, based on the SEC results (Fig. 4). For the 25-kDa membrane, the pore blocking was immediate, because the flux was virtually zero. Use of the 50-kDa membrane yielded less extensive fouling, and the initial change in flux was negligible (data not shown). However, the flux decreased substantially for the 100-kDa membrane, which can be explained by several models [21]. These models share a characteristic equation that describes the blocking mechanisms during the various stages of filtration (Eq. (1)). Using a fitted polynomial of the start-up data for the 100-kDa membrane at a CFV of 0.5 m/s and TMP of 1 bar, we obtained results (Fig. 9) by numerical differentiation (Eq. (1)).

A complete blocking mechanism was observed on the 100-kDa membrane ($\beta = 2$) prior to the system reaching a stable non-zero flux, as evidenced by the rapid decrease in the second-order derivative after reaching a beta of 0 and a final flux of 48 L/m^2 h. These results are consistent with the assumptions that were made regarding the pore plugging in Section 3.2.1.

3.3. Concentration and diafiltration study

The results of the parameter study implicated the 50-kDa membrane as the optimal membrane in terms of flux, retention, and fouling. Concentration and diafiltration were then examined to separate and purify the high-MW LCC fraction from the SSL solution. In the concentration study, it was possible to separate the high-MW LCCs using a membrane with the 50-kDa cut-off, as indicated by the result from the SEC experiments (Fig. 10). The initial flux was 139 L/m^2 h, stabilizing at approximately 100 L/m^2 h until

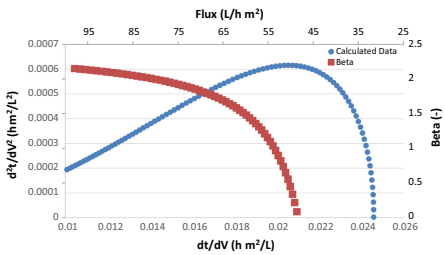


Fig. 9. Numerical differentiation of the 100-kDa start-up data according to Eq. (1) (blue circles). The variable beta in Eq. (1) is also shown (red squares). (For interpretation of the references to colour in this figure legend, the reader is referred to the web version of this article.)

it reached VR 50%, at which point it began to decrease slowly, ultimately obtaining a flux of 33 L/m^2 h at VR 90% (Fig. 13). The average retention of LCCs increased from 62.8% at VR 0% to 72.6% at VR 90%, and the concentration of GGM rose from 5.5 g/L to 25.1 g/L (Fig. 11a). The purity of LCCs improved from 43% in the feed to 73% in the retentate, with the total lignin-to-GGM (L/C) ratio changing from 5.8 in the feed to 5.1 in the retentate. The L/C ratio indicated that the composition of LCCs was not altered significantly during the concentration experiment. This decrease in L/C ratio could be attributed to some of the lignin-bound xylan or non-associated lignin being removed during the concentration study, because the retention of xylan and total lignin was lower than for GGM (Fig. 7).

A diafiltration experiment was performed to wash away the remaining pulping chemicals and thus increase the final purity of the product. The diafiltration (with a diafiltration factor of 5) decreased the amount of pulping salts and monomeric sugars from 24% to 3% of the TDS (Fig. 11b). The final LCC purity improved from 73% to 93%, with a consistent L/C ratio of 5.1. The product (>50 kDa) yield in the retentate was 55.1% as calculated from the SEC chromatogram area in Fig. 10. The yield was an improvement compared with the universal solubility-based fractionation method [9] for glucomannan LCC in the same MW range. The yield was low when compared with ultrafiltration studies on the isolation of GGM [12,26]. The reason for the low yield was the low retention of the LCCs (72.6%) during the concentrating stage. An increase in retention is observed during the diafiltration stage (92.9%), but with the loss of the lower MW fraction, as shown in Fig. 10, and a final product yield of 43.4%. The yield could be improved by increasing the retention of LCC. This can be made possible by decreasing the MW cut-off of the membrane, or by recovering the lost product in the permeate with another membrane filtration step as shown by Duval et al. [38].

3.4. Effect of prefiltration prior to ultrafiltration using a 50-kDa membrane

The fouling grade after the concentration experiment was 48.9% (Fig. 14), as expected, because the fouling rate increases with the concentration of fouling solutes [39]. To minimize the fouling of the 50-kDa membrane, two prefiltration methods were examined—microfiltration (MF) and dead-end filtration (DEF) with kieselguhr have shown potential in removing flux-limiting compounds from hemicellulose-rich solutions [26]. The flux during ultrafiltration (UF) with the 50-kDa membrane could be increased by a factor of 3 and 1.2 after MF and DEF, respectively (Fig. 13). The fouling grade for the UF membrane decreased from 48.9% to 7.2% using the MF permeate and to 17% when the DEF filtrate was used during the concentration study (Fig. 14).

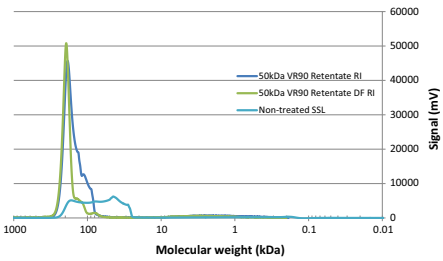


Fig. 10. SEC comparison of the retentate, diafiltrated retentate and the raw material.

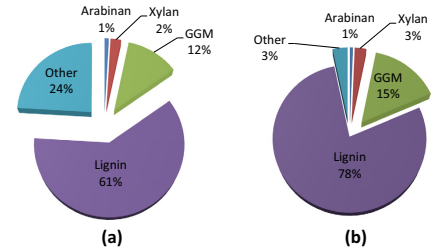


Fig. 11. SSL content in weight percent of TDS in the retentate (211.6 g TDS/L) (a) and diafiltrated retentate (131.7 g TDS/L) (b).

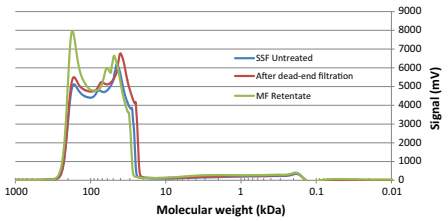


Fig. 12. Comparison of the molecular weight distribution of untreated and prefiltered SSL.

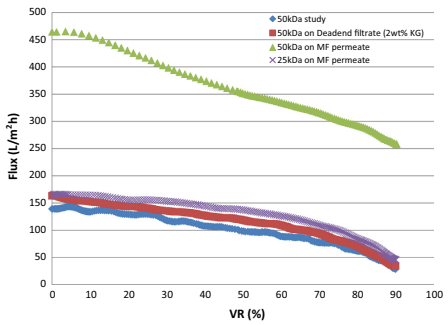
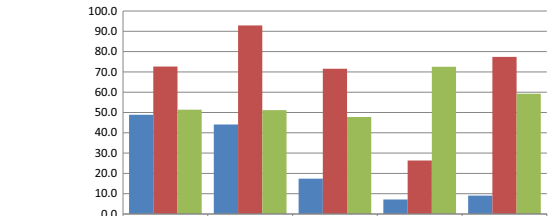


Fig. 13. Comparison of VR vs flux curves for the 50-kDa study before and after prefiltration.

The total loss of LCCs during MF was 29.9%, which comprised primarily the high-MW fraction, as indicated in Fig. 12. This result was also attributed to the low retention of LCCs during the 50-kDa UF studies with MF permeate (Fig. 14). The removal of fouling compounds was confirmed in a 25-kDa UF study on MF permeate, in which a 91.7-fold rise in flux and a low fouling grade of 9.1% were obtained (Figs. 13 and 14). The average flux during MF was approximately 55 L/m^{2}h, which had the same order of magnitude as that for the UF. Krawczyk et al. [26] have reported similar results during MF of a hemicellulose-rich solution from wheat bran. The flux-limiting phenomenon was similar to that observed in the study with the 100-kDa membrane (Section 3.2.1), as evidenced by the



	50kDa	DF on 50kDa Retentate	50kDa on Deadend Filtrate	50kDa on MF permeate	25kDa on MF permeate
Fouling degree (%)	48.9	44.1	17.4	7.2	9.1
LCC Retention (%)	72.6	92.9	71.6	26.4	77.4
L/C Ratio x 10 (g/g)	51.4	51.2	47.8	72.5	59.3

Fig. 14. Data from various concentration studies.

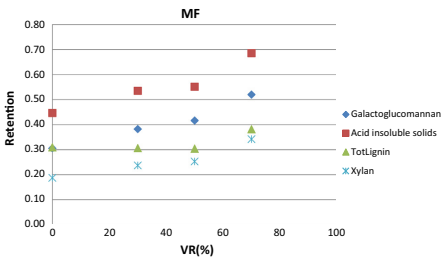


Fig. 15. VR vs retention during the MF concentration study.

high retention of GGM, total lignin, and acid-insoluble solids (Fig. 15). The fouling grade of the MF membrane was 76.4% after concentration of the SSL solution to a VR of 70%, indicating that several cleaning methods are needed for MF to be a sustainable procedure.

This loss in product was not observed after DEF, which removed primarily the suspended solids in the solution, as indicated by the turbidity measurements (Table 3). No absorption of the measured material on the kieselguhr was seen—the losses in polysaccharides and acid-insoluble solids were less than 0.4%. Because the fouling grade decreased after DEF, other compounds that existed as suspended solids were likely to be responsible for some of the membrane fouling. Subsequent comparisons between UF of the MF permeate and DEF filtrate confirmed that a portion of the product caused some of the pore fouling, which was confirmed by the high retention of GGM and acid-insoluble solids during MF (Fig. 15). The reason for the high retention of the considerably smaller macromolecules (compared with the pore size of the MF membrane) was possibly the formation of a gel layer on the surface that increased the retention for the mentioned components, as described by Krawczyk et al. [26]. Another possible reason is that the fouling compounds were adsorbed in the pores of the microfiltration membrane and thereby decreased the amount of fouling compounds and increased the retention of macromolecules. This can be considered a reasonable explanation since the material for the MF and 25 kDa were the same, and pore plugging can begin with an adsorption mechanism as explained by the fundamentals of the blocking filtration law derived by Hermia [20].Thus, the affinity of the different fouling compounds to the membranes were the same in both cases.

Oxidative treatment of the 50-kDa membrane with 0.1 wt% hydrogen peroxide during the acid cleaning step decreased the fouling grade from 48.9% to 13.2%. This treatment was performed for the MF membrane, eliminating the fouling and restoring the original PWF. These results suggest that the fouling compounds contained lignin or other extractives that are sensitive to degradation in the presence of oxidizing agents [40].

4. Conclusions

Analysis and initial membrane trials indicated that most hemicellulose and lignin are associated, and the SEC results implicated the existence of LCCs. Non-associated high-MW lignin was present in the solution, as well. However, various separation methods are needed to separate these components, due to the narrow difference in molecular sizes.

High-MW LCCs were isolated using a 50-kDa polysulfone membrane, and a final purity of 93% (based on the sum of GGM and lignin) and product (>50 kDa) yield of 43.4% was achieved using DF. However, fouling was an issue during the MF, as characterized by the blocking filtration law. Pore blocking was the primary cause of fouling—the molecular sizes of the solutes were in the same range as the membrane cutoff. Fouling was reduced by prefiltration with MF or DEF, of which the former was the least favorable, effecting significant loss of high-MW LCCs. The fouling grade decreased from 48.9% to 7.2% using MF, confirming that part of the product caused the pore blocking. As an alternative

Table 3
Composition of untreated, MF permeate, and dead-end filtrate SSL.

	GGM (g/L)	Lignin (g/L)	Xylan (g/L)	Arabinan (g/L)	Acid-insoluble solids (g/L)	Turbidity (NTU)
Untreated SSL	5.46	31.7	1.48	0.58	2.77	849
MF permeate	3.79	20.9	1.20	0.49	1.37	1
Dead-end filtrate	5.30	31.9	1.43	0.55	2.65	46

prefiltration method, DEF reduced the fouling grade to 17.4% with negligible loss of product, indicating that some of the suspended solids increased the fouling.

Oxidative treatment has tremendous potential in reducing the fouling on the 50-kDa membrane. The combination of DEF and oxidative cleaning could be a promising approach toward removing fouling compounds completely with minimal loss of product.

Acknowledgement

Research on the separation and purification of LCC from spent sulfite liquor was funded by the Swedish Foundation for Strategic Research (SSF), which is gratefully acknowledged.

References

[1] H. Wenzl, The Chemical Technology of Wood, Elsevier, 2012.
[2] M. Weissgram et al., Generation of PHB from spent sulfite liquor using halophilic microorganisms, Microorganisms 3 (2) (2015) 268–289.
[3] A. Björkman, Studies on finely divided wood. Part 1. Extraction of lignin with neutral solvents, Svensk Papperstidning 59(13) (1956) 477–485.
[4] J.-I. Azuma, N. Takahashi, T. Koshijima, Isolation and characterisation of lignin-carbohydrate complexes from the milled-wood lignin fraction of Pinus densiflora sieb. et zucc, Carbohyd. Res. 93 (1) (1981) 91–104.
[5] O. Karlsson, B. Pettersson, U. Westermark, The use of cellulases and hemicellulases to study lignin-cellulose as well as lignin-hemicellulose bonds in kraft pulps, J. Pulp Paper Sci. 27 (6) (2001) 196–201.
[6] M. Lawoko, G. Henriksson, G. Gellerstedt, Characterization of lignin-carbohydrate complexes from spruce sulfite pulp, Holzforschung 60 (2) (2006) 162–165.
[7] M. Lawoko, G. Henriksson, G. Gellerstedt, Structural differences between the lignin-carbohydrate complexes present in wood and in chemical pulps, Biomacromolecules 6 (6) (2005) 3467–3473.
[8] N. Giummarella et al., Structural features of mildly fractionated lignin carbohydrate complexes (LCC) from spruce, RSC Adv. 6 (48) (2016) 42120–42131.
[9] X. Du, G. Gellerstedt, J. Li, Universal fractionation of lignin–carbohydrate complexes (LCCs) from lignocellulosic biomass: an example using spruce wood, Plant J.: Cell Molecul. Biol. 74 (2) (2013) 328–338.
[10] P. Oinonen, D. Areskogh, G. Henriksson, The processing and upgrading of hemicellulose mixtures, in: 16th International Symposium on Wood, Fiber and Pulping Chemistry, Tianjin, China, June 8, 2011.
[11] Y. Uraki et al., Amphiphilicity of a lignin-carbohydrate complex, Holzforschung 60 (6) (2006) 659–664.
[12] M. Al Manasrah et al., Recovery of galactoglucomannan from wood hydrolysate using regenerated cellulose ultrafiltration membranes, Bioresour. Technol. 114 (2012) 375–381.
[13] P. Eriksson, Ultrafiltration for recovery of lignosulfonates from spent sulfite liquor, AIChE Symp. Ser. 76 (197) (1980) 316–320.
[14] P. Bhattacharya et al., Studies on ultrafiltration of spent sulfite liquor using various membranes for the recovery of lignosulphonates, Desalination 174 (3) (2005) 287–297.
[15] Z. Wang, et al., Ultrafiltration treatment and physical properties of ammonia sulfite pulping liquor of wheat straw, in: Advanced Materials Research. Trans Tech Publ, 2012.
[16] N. Westerberg et al., Separation of galactoglucomannans, lignin and lignin-carbohydrate complexes from hot-water-extracted Norway spruce by cross-flow filtration and adsorption chromatography, BioResources 7 (4) (2012) 4501–4516.
[17] F. Zikeli et al., Wheat straw lignin fractionation and characterization as lignin-carbohydrate complexes, Indust. Crops Prod. 85 (2016) 309–317.
[18] J.C. del Río et al., Lignin–carbohydrate complexes from sisal (*Agave sisalana*) and abaca (*Musa textilis*): chemical composition and structural modifications during the isolation process, Planta 243 (5) (2016) 1143–1158.
[19] X. Du et al., Analysis of lignin–carbohydrate and lignin–lignin linkages after hydrolase treatment of xylan–lignin, glucomannan–lignin and glucan–lignin complexes from spruce wood, Planta 239 (5) (2014) 1079–1090.
[20] J. Hermia, Constant pressure blocking filtration law application to powder-law non-Newtonian fluid, Trans. Inst. Chem. Eng. 60 (1982) 183–187.
[21] W. Bowen, J. Calvo, A. Hernandez, Steps of membrane blocking in flux decline during protein microfiltration, J. Membr. Sci. 101 (1) (1995) 153–165.
[22] E. Iritani, N. Katagiri, Developments of blocking filtration model in membrane filtration, KONA Powder Particle J. 2016 (33) (2016) 179–202.
[23] M.C.V. Vela et al., Analysis of membrane pore blocking models applied to the ultrafiltration of PEG, Sep. Purif. Technol. 62 (3) (2008) 489–498.
[24] E. Iritani, A review on modeling of pore-blocking behaviors of membranes during pressurized membrane filtration, Dry. Technol. 31 (2) (2013) 146–162.
[25] E. Koivula et al., Evaluation of various pretreatment methods to manage fouling in ultrafiltration of wood hydrolysates, Sep. Purif. Technol. 83 (2011) 50–56.
[26] H. Krawczyk, A. Arkell, A.-S. Jönsson, Impact of prefiltration on membrane performance during isolation of hemicelluloses extracted from wheat bran, Sep. Purif. Technol. 116 (2013) 192–198.
[27] T. Persson, A.-S. Jonsson, Fouling of ultrafiltration membranes during isolation of hemicelluloses in the forest industry. Scholarly Research Exchange, 2009.
[28] R.W. Field et al., Critical flux concept for microfiltration fouling, J. Membr. Sci. 100 (3) (1995) 259–272.
[29] R. Ruiz, T. Ehrman, HPLC analysis of liquid fractions of process samples for monomeric sugars and cellobiose, Laboratory Analytical Procedure (LAP 013), National Renewable Energy Laboratory, 1996.
[30] M. Lawoko, Unveiling the structure and ultrastructure of lignin carbohydrate complexes in softwoods, Int. J. Biolog. Macromol. 62 (2013) 705–713.
[31] T. Koshijima, T. Watanabe, Association between lignin and carbohydrates in wood and other plant tissues, Springer Science & Business Media, 2013.
[32] M. Lawoko, Lignin polysaccharide networks in softwood and chemical pulps: characterisation, structure and reactivity, 2005.
[33] T.W. Jeffries, Biodegradation of lignin and hemicelluloses, in: Biochemistry of Microbial Degradation, Springer, 1994. pp. 233–277.
[34] C. Álvarez, F.M. Reyes-Sosa, B. Díez, Enzymatic hydrolysis of biomass from wood, Microbial. Biotechnol. 9 (2) (2016) 149–156.
[35] K.-J. Hwang, C.-Y. Liao, K.-L. Tung, Effect of membrane pore size on the particle fouling in membrane filtration, Desalination 234 (1) (2008) 16–23.
[36] H. Krawczyk, A.S. Jönsson, Separation of dispersed substances and galactoglucomannan in thermomechanical pulp process water by microfiltration, Sep. Purif. Technol. 79 (1) (2011) 43–49.
[37] B.O. Lindgren, The lignin-carbohydrate linkage, Acta Chem. Scand 12 (1958) 447–452.
[38] A. Duval, S. Molina-Boisseau, C. Chirat, Fractionation of lignosulfonates: comparison of ultrafiltration and ethanol solubility to obtain a set of fractions with distinct properties, Holzforschung 69 (2) (2015) 127–134.
[39] A. Abdelrasoul, H. Doan, A. Lohi, Fouling in membrane filtration and remediation methods, Mass Transfer-Advances in Sustainable Energy and Environment Oriented Numerical Modeling, 2013. p. 195.
[40] M. Alexandri et al., Evaluation of an integrated biorefinery based on fractionation of spent sulphite liquor for the production of an antioxidant-rich extract, lignosulphonates and succinic acid, Bioresour. Technol. 214 (2016) 504–513.

Paper II

Basel Al-Rudainy, Mats Galbe, Herje Schagerlöf and Ola Wallberg*

Antisolvent precipitation of hemicelluloses, lignosulfonates and their complexes from ultrafiltrated spent sulfite liquor (SSL)

https://doi.org/10.1515/hf-2017-0218
Received December 21, 2017; accepted April 23, 2018; previously published online May 28, 2018

Abstract: The possibility of precipitating high molecular weight (MW) softwood hemicelluloses has been investigated. Solids were precipitated from a sodium-based spent sulfite liquor with the anti-solvents acetone, ethanol and methanol and the effects of solute concentration, pH and temperature on the precipitation were studied. The product yield, degree of separation, MW and structure of the different fractions were determined using gravimetric analysis, high performance liquid chromatography (HPLC), ultraviolet–visible (UV-Vis) spectroscopy, size exclusion chromatography (SEC), and two-dimensional nuclear magnetic resonance (2D NMR). A direct correlation was found between the dielectric constant (also called relative permittivity) of the bulk solution and the yield of precipitants, based on which the separation of the solutes was predictable. The highest yield and degree of separation observed was an intercept around 76% with 47.5% acetone, which was the most efficient anti-solvent.

Keywords: arabinogalactan, dielectric constant, galactoglucomannan, lignin, lignin-carbohydrate-complex, precipitation, softwood, ultrafiltration

Introduction

During the production of pulp and paper, water-soluble components such as hemicelluloses, and complex mixtures of mono-, di- and oligosaccharides, and lignin derivatives are released and accumulated in the process streams, which are usually concentrated and incinerated for the recovery of pulping chemicals in Kraft and sulfite processes and for heat generation (Wenzl 2012). The growing trend toward a more effective and sustainable forest industry is subsumed in the concept "biorefinery", which is aiming at a better utilization of all parts of the wood in process cascades and to minimize the amount of not commercialized byproducts. The utilization of previously less important wood components, such as hemicelluloses and lignin, as raw materials for the development of specialty chemicals and biofuels, are examples for forest biorefinery (Menon and Rao 2012).

Galactoglucomannan (GGM) is one of the major hemicelluloses in softwoods such as Norway spruce and Scots pine, constituting around 20% of the wood dry matter (Lundqvist et al. 2002). GGM is a potential precursor for a range of products, such as surfactants, biofilms and gels (Thuvander and Jönsson 2016). However, valuable waste streams containing GGM often contain water-soluble impurities such as other polysaccharides, lignin-carbohydrate complexes (LCCs) and lignin derivatives (Lundqvist et al. 2002; Ekholm et al. 2012; Du et al. 2014; Al-Rudainy et al. 2017). Lignin has negative effects in applications requiring enzymatic treatment due to its inhibitory effects. These streams are also very diluted, with total dry substance (TDS) concentrations of 5–6 g l^{-1} (Krawczyk and Jönsson 2011), which makes further processing costly. Hence, GGM containing process streams have to be concentrated and purified.

Membrane filtration is effective for this purpose. Al Manasrah et al. (2012) applied ultrafiltration for the recovery of GGM from pressurized hot-water extracts of spruce sawdust. Seventy percent of the GGM was recovered at a purity of 63%, and the feed volume reduction was 86%. Thuvander et al. reported that it was possible to separate lignin and GGM from thermomechanical process water via micro- and ultrafiltration. However, LCCs are difficult to separate, presumably because of the small difference in molecular weight (MW) between GGMs and LCCs. In other cases, the formation of a gel layer on the membrane surface increased the retention of most of the biopolymers in the solution and aggravated the separation and purification (Krawczyk et al. 2013; Thuvander and Jönsson 2016; Al-Rudainy et al. 2017). Al-Rudainy et al. (2017) concluded

***Corresponding author: Ola Wallberg,** Department of Chemical Engineering, Lund University, P.O. Box 124, SE-221 00, Lund, Sweden, e-mail: ola.wallberg@chemeng.lth.se
Basel Al-Rudainy, Mats Galbe and Herje Schagerlöf: Department of Chemical Engineering, Lund University, SE-221 00, Lund, Sweden. http://orcid.org/0000-0002-5692-5542 (B. Al-Rudainy)

that membrane filtration is not efficient enough for the separation.

Song et al. compared membrane filtration to anti-solvent precipitation with ethanol as anti-solvent for the recovery of GGM from hot-water-extractives from spruce. Membrane filtration of the lignin-free solution yielded a poly- and oligosaccharide-rich solution with MWs up to 20 kDa. However, precipitation with ethanol solely yielded polysaccharides (MW > 4 kDa) at high purity with a yield of 78% at an anti-solvent concentration of 90%. A disadvantage is the high amount of ethanol needed to precipitate GGM, thus membrane filtration would be beneficial to concentrate the solution prior to anti-solvent precipitation. Zasadowski et al. (2014) precipitated GGM from thermomechanically treated spruce process water with the anti-solvents methanol, ethanol and acetone. Acetone was found to be the most efficient due its low polarity yielding 77% GGM at an acetone concentration of 54.5%. The amount of bound galactose in the GGM precipitate, obtained at a low anti-solvent concentration, was unexpectedly high. However, the composition of the galactose-rich fraction was not determined. Lignin precipitated at a low anti-solvent concentration can be re-dissolved at higher anti-solvent concentrations, probably because of the lignin's higher solubility in less polar solvents, while the precipitation occurs in the presence of LCCs in the solution. It was also proposed that the precipitation efficiency is correlated to the dielectric constant (relative permittivity, DC) of the anti-solvent; however, no detailed evidences were presented for this assumption. Tarasov et al. (2015) and Duval et al. (2015) fractionated lignosulfonates (LSs) with different anti-solvents. It was observed that an anti-solvent with a lower polarity resulted in the highest product yields. As LSs are negatively charged, they can be precipitated from the solution at a higher anti-solvent concentration, while the hemicelluloses from hardwoods exhibit a maximum separation at an anti-solvent concentration of about 50%. In these studies, the major disadvantage of precipitation was the high polydispersity of the resulting products compared to other fractionation methods (Duval et al. 2015).

The aim of the present study was to investigate the separation of high MW ultrafiltrated hemicelluloses from LSs and LCCs. The anti-solvents acetone, ethanol and methanol will be in focus, and the results should be evaluated in terms of DC of the bulk solutions in the presence of anti-solvents with different concentrations. The parameters pH and temperature during precipitation should also be evaluated in terms of precipitation efficiency and the precipitates will be characterized by two-dimensional nuclear magnetic resonance (2D NMR) to gain structural information.

Materials and methods

Raw material: A sodium-based spent sulfite liquor (SSL) sampled after the first digestion step in a two-step cooking process of a softwood mixture (60% *Picea abies* and 40% *Pinus sylvestris*) was provided by Domsjö Fabriker (Örnsköldsvik, Sweden). The raw material contained 36.4% lignin, 4.2% acid-insoluble solids, 6.6% GGM, 0.8% arabinan, 1.8% xylan and 1.2% monosaccharides, based on the TDS (84.6 g l^{-1}) (Al-Rudainy et al. 2017). The remaining 49.1% consisted mostly of the pulping chemicals (40.2% of TDS) and other components, such as extractives. According to Al-Rudainy et al. (2017), this SSL contains a mixture of GGM, lignin and LCCs with MWs ranging from ~20 to 320 kDa. The exact composition and mass distribution between these components are unknown as the separation via membrane filtration was not successful.

Membrane filtration and evaporation: Membrane filtration was performed according to the methods described by (Al-Rudainy et al. 2017). The membrane equipment consisted of a 400 ml stirred filtration vessel with a 50 kDa membrane (GR51PP, Alfa Laval Corporate AB, Lund, Sweden) and a digital pressure gauge (DCS40.0AR, Trafag AG, Bubikon, Switzerland) connected to a six bar nitrogen gas line. A magnetic stirrer with a built-in heating plate (MR2002, Heidolph Instruments GmbH & Co. KG, Schwabach, Germany) was used for the control of temperature and cross-flow velocity. The membrane was cleaned prior to and after each experiment by soaking in 350 ml of a solution of 0.04% acid detergent solution (Ultrasil 73, Ecolab AB, Älvsjö, Sweden) at 50°C for 1 h. The cleaning solution was then permeated through the membrane at a transmembrane pressure of one bar and a cross-flow velocity of 0.5 m s^{-1} to a volume reduction of 50%. The membrane was then rinsed with two volumes of de-ionized water, after which a 0.5% alkaline cleaning step (Ultrasil 10, Ecolab AB, Älvsjö, Sweden) was performed similar to that of the acid detergent.

The concentration study was carried out with 350 ml of the SSL solution at 50°C, cross-flow velocity of 0.5 m s^{-1} and a transmembrane pressure of 5.5 bar. Once a volume reduction of 90% was reached, diafiltration was performed on the retentate to a final diafiltration factor of 5. The diafiltrated retentate was concentrated at 45°C and 80 mbar in an evaporator (Multivapor P-6, BÜCHI Labortechnik AG, Flawil, Switzerland) to a concentration factor of about 2.3 (based on TDS).

Precipitation and centrifugation: One milliliter of SSL was placed in 15 ml test tubes (Sarstedt AG & Co, Nümbrecht, Germany). The pH of the samples was adjusted with 50% NaOH solution (Merck KGaA, Darmstadt, Germany) before adding the required amount of anti-solvent. The anti-solvents used were 99.8% acetone (Merck kGaA, Darmstadt, Germany), 99.7% ethanol (Altin Corp., Rajamäki, Finland) and 99.9% methanol (Merck KGaA, Darmstadt, Germany). When investigating the effect of temperature on precipitation, the samples and anti-solvent were heated separately in a water bath before mixing. After the addition of the required amount of anti-solvent, the samples were mixed in a mini-shaker (MS2 Minishaker, IKA®-Werke GmbH & Co. KG, Staufen, Germany) at 2500 rpm for 5 min, after which the precipitate was allowed to settle for 30 min. The liquid phase was decanted after centrifugation of the samples at 3000 rpm (850 × *g*) for 15 min (Heraeus Labofuge 200, Thermo Fisher Scientific, Waltham, MA, USA). The precipitate was washed with 5 ml of anti-solvent by mixing the sample in the mini-shaker at 2500 rpm for 5 min and centrifuged at 3000 rpm for 15 min. The samples were dried in an oven

(Memmert GmbH + Co. KG, Schwabach, Germany) at 45°C for 48 h, before weighing and calculation of the TDS of the precipitate. The dry samples were dissolved in 10 ml de-ionized water for further analysis. The procedure described is illustrated in Figure 1.

Ash and TDS analysis: The TDS analysis was carried out by weighing and drying a 3 ml sample at 105°C for 24 h in a furnace (Heraeus, Heraeus Holding GmbH, Hanau, Germany). After cooling in a desiccator for 30 min, the dried sample weight was determined and the TDS determined. The dried sample was then ashed in a muffle furnace (B150, Nabertherm GmbH, Lilienthal, Germany) at 575°C for 3 h, after which the sample was cooled down in a desiccator before weighing.

Lignin analysis: The lignin concentration was measured using UV measurement at 234 nm (Shimadzu UV-Vis spectrophotometer UV-1800, Kyoto, Japan). The lignin concentration was then calculated by the extinction coefficient of 31.6 l g^{-1} cm^{-1} (Al-Rudainy et al. 2017).

Hemicelluloses, monosaccharides and degree of acetylation: The hemicelluloses concentration was determined according to the National Renewable Energy Laboratory (NREL) method (Ruiz and Ehrman 1996). A 10 ml sample was acid hydrolyzed with 750 µl of a 72% sulfuric acid solution (AppliChem GmbH, Darmstadt, Germany) in an autoclave (Systec DX 150, Wettenberg, Germany) at 121°C for 1 h. Acid-insoluble solids were filtrated (Whatman Glass microfiber filters GF/B, GE Healthcare Corp., Chicago, IL, USA), washed with de-ionized water, dried at 105°C for 24 h and then weighed. The monosaccharide content in the liquid fraction was analyzed using HPAEC-PAD (ICS-3000, Dionex Corp., Sunnyvale, CA, USA) coupled with a Carbo Pac PA1 analytical column. The eluent (deionized water) flow rate was of 1 ml min^{-1} with 0.5 ml min^{-1} 200 mM NaOH post-column addition and an injection volume of 10 µl. The column was washed between samples with a solution containing 200 mM NaOH and 170 mM sodium acetate (Merck KGaA, Darmstadt, Germany). The calibration standards used were D-glucose, D-galactose, D-mannose, D-xylose and L-arabinose (Fluka Chemie AG, Buchs, Switzerland). The hemicelluloses concentration were determined as the sum of the monosaccharide concentrations after anhydro corrections of 0.88 for pentoses and 0.90 for hexoses. The degree of acetylation (DAc) was determined by measuring the acetic acid (AA) content in the liquid fraction via liquid chromatography (Aminex HPX-87H column, Bio-Rad, Hercules, CA, USA). The eluent was a 5 mM sulfuric acid solution, at a flow rate of 0.5 ml min^{-1} and a column temperature of 50°C.

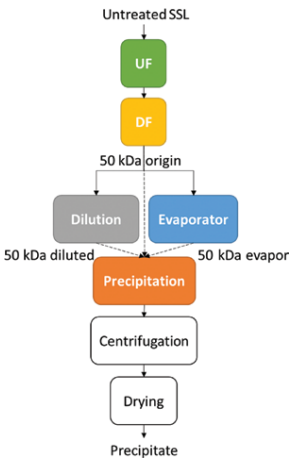


Figure 1: A flow diagram showing the different processes performed on the spent sulfite liquor (SSL) and the resulting product (precipitate).

Size-exclusion chromatography (SEC): MWs were determined via size-exclusion chromatography (SEC) (Waters 600E System Controller, Waters, Milford, MA, USA) combined with an refractive index (RI) detector (Waters 2414 Differential Refractometer), a UV detector (Waters 486 Tunable Absorbance Detector) set at 234 nm, a pump (Waters 600 Gradient pump), an autosampler (Waters 717 plus autosampler), a degasser (Waters In-Line Degasser) and a TSK-gel G4000PWXL column (TOSOH Bioscience GmbH, Griescheim, Germany). De-ionized water served as eluent at a flow rate of 0.5 ml min^{-1}, and the sample injection volume was 20 µl. The column was calibrated by polyethylene glycol standards (100 kDa, 35 kDa, 10 kDa, 4 kDa and 400 Da from Merck Schuchardt OHG, Germany).

Density and pH: The density at room temperature was measured (triplicate experiments) by weighing a 3 ml sample on a scale (AND Electric balance ER-120, San Jose, CA, USA). A pH-meter (HANNA Instruments, Smithfield, RI, USA) was used.

2D NMR spectroscopy at 25°C: Twenty milligram of dried sample was dissolved in 0.6 ml of 99.9% deuterium oxide (Sigma-Aldrich Co., MO, USA), which served also as internal reference ($\delta_C/\delta_H = -4.81$ ppm). Instrument: Bruker Avance III HD 500 MHz spectrometer (Bruker BioSpin GmbH, Karlsruhe, Germany) with a 5 mm broadband observe (BBO) probe and a Z-gradient coil. Data were acquired via the pulse program "hsqcetgpsisp.2". Setting parameters: 136 scans, 1.5 s relaxation delay, 10.3 µs pulse length, spectral width 11 ppm, FID size of 1538 and frequency discrimination in F1 e/a.

Conductivity at 25°C: A Zetasizer nanoseries (Malvern Instruments, Worcestershire, UK) instrument was applied, which was equipped with disposable folded capillary cells (DTS1070) for 0.5 ml sample.

Results and discussion

Membrane filtration and evaporation

Table 1 summarizes the composition of the SSL solutions after membrane filtration, dilution and evaporation. An increase in lignin and GGM concentration is seen after membrane filtration. Lignin (L) had a lower initial retention than GGM, which resulted in minor separation efficiency and a lower L/GGM ratio in the retentate. The overall purity of the SSL was increased by eliminating pulping chemicals during diafiltration, as evidenced by

Table 1: Composition of the SSL solutions.

Sample	All data in (g l^{-1})								Conduct. (mS/cm)
	Total[a]	Lignin	L-Ara	D-Gal	D-Glc	D-Xyl	D-Man	AA[b]	
Untreated SSL	84.0	31.7	1.15	1.49	1.31	1.48	2.65	2.77	48.4
Membrane filtration retentates									
50 kDa Origin	102.5	83.7	1.25	5.57	4.88	3.52	9.93	1.64	14.1
50 kDa Diluted	76.2	64.0	1.09	4.45	3.92	2.91	7.81	1.25	11.3
50 kDa Evapor	227.9	190.4	2.04	11.4	10.7	7.64	20.9	3.40	29.2

[a]Dry substances; [b]mixture of bound and free acetic acid concentration.
AA, Acetic acid.

the increasing L/TDS and GGM/TDS ratios, and the lower conductivity of the retentate. The AA/GGM ratio did not change because of retentate evaporation, which indicates the absence of free AA in the membrane-filtrated SSL, i.e. AA was chemically bound.

Precipitation with different anti-solvents

The experiments were performed with the 50 kDa diafiltrated retentate (Figure 2a). GGM was precipitated first followed by lignin, which precipitated at a higher anti-solvent concentration. Obviously, acetone is the most efficient anti-solvent, in terms of the amount required per unit mass of GGM, followed by ethanol and methanol. Zasadowski et al. (2014) made similar observations (see Introduction). The highest yield and separation degree [SD, the amount GGM/(L + GGM)] was 76, 61, and 59% for acetone, ethanol, and methanol, at concentrations of 47.5, 51.0, and 61.0%, respectively. Low amounts of acetone were required to achieve a high GGM yield and the SD of acetone was also the highest. The differences in phase separation for GGM were considerable but nearly negligible for lignin for the three anti-solvents. The yields were very similar to those presented by Zasadowski et al. (2014) and Song et al. (2013), however, the amount of anti-solvent needed in our study was slightly lower, owing to the higher concentration of solutes.

The difference in precipitation amounts are related to the anti-solvent polarities in the order acetone < ethanol < methanol (Figure 2a). The polarities are reflected by the DC, which was measured according to Akerlof (1932), assuming that the components in the bulk solution have a minimal and equal influence on the DC of the mixture (Figure 2b). The precipitation results presented in Figure 2a were re-evaluated based on the calculated DC data (Figure 3a). There is a strong correlation between the DCs of the medium and the precipitation yield for both GGM and lignin. The results in Figure 3a may serve together with a suitable solubility model to predict the performance of other anti-solvents to optimize precipitation processes.

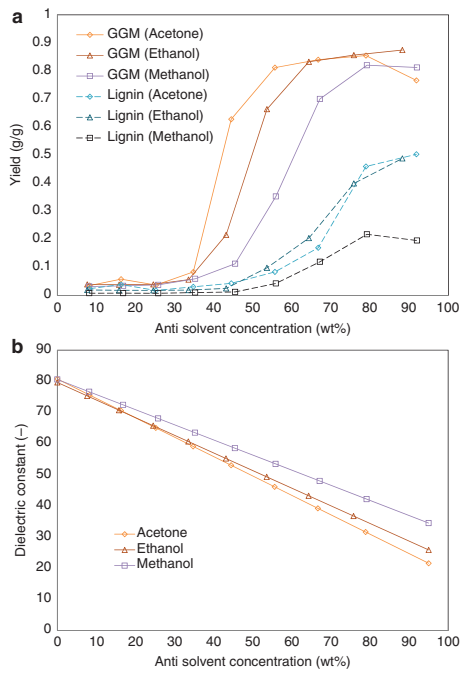


Figure 2: Precipitation yield and dielectric constant curves vs. anti-solvent concentration.
(a) GGM and lignin yields of precipitation with acetone, ethanol, and methanol as anti-solvents from an 50 kDa diafiltrated SSL retentate as the basic solution. (b) The dielectric constant (DC) vs. anti-solvent concentration as presented by Akerlof. Interpolation of the experimental data yielded the following linear regressions: $DC_{acetone} = 80.736 - 0.6225 \times c_{acetone}$, $DC_{ethanol} = 79.635 - 0.5657 \times c_{ethanol}$ and $DC_{methanol} = 80.59 - 0.4852 \times c_{methanol}$, where c is the anti-solvent concentration in %.

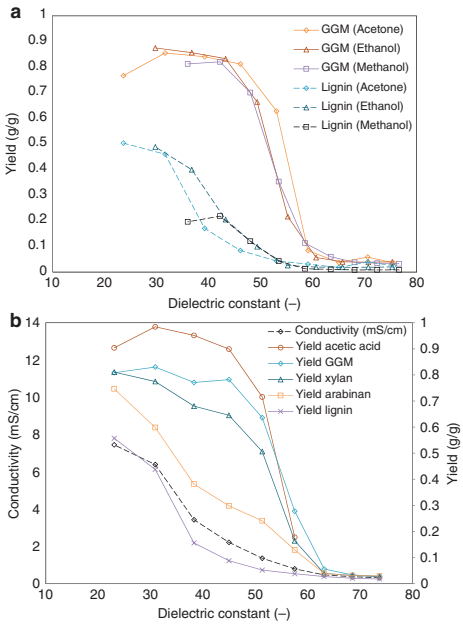


Figure 3: Precipitation yield and solutes yield and conductivity vs. the dielectric constant.
(a) Precipitation yields of GGM and lignin with different anti-solvents. The results are the same as in Figure 1, except the anti-solvent concentration was substituted by the dielectric constant (DC). (b) The precipitation yields of the various solutes and the conductivity of the bulk solution vs. the dielectric constant with acetone as anti-solvent.

Relation of analytical results to solute precipitation

Figure 3a indicates that in the case of acetone, lignin precipitation started at DC 54, while GGM precipitated at DC 61, i.e. sulfonated lignin has a higher polarity than GGM (Quesada-Medina et al. 2010; Tarasov et al. 2015). The trend of increasing conductivity is in accordance with the yield increment for both GGM and lignin at low acetone concentrations. At an acetone concentration of 91.8% and DC 24, the conductivity was not restored to the same magnitude as for the 50 kDa diafiltrated retentate solution before precipitation (Table 1). This was probably due to the low lignin yield (~56% at 91.8% acetone content) during precipitation; thus, the non-precipitated, low MW lignin was responsible for the higher conductivity in the original membrane-filtrated material (Zhou et al. 2006; Duval et al. 2015).

The observed MW of lignin (Figure 4b) confirms this observation, as the MW decreased with increasing acetone concentration, see Table 2 (Peak 2). The MW region ~4–23 kDa (Figure 4a) coincides with the GGM precipitation yield. This was observed by the sudden change in peak area when the acetone concentration was increased from 34.9 to 45.2%, which can be explained by the GGM yield increment from 0.16 to 0.51. The peak area did not change significantly at acetone concentrations higher than 45.2%. Instead, the peak area in the MW region ~65–360 kDa increased. A comparison of the two SEC curves (Figure 4, RI and UV detection) shows that lignin is partly responsible for the increase of that region (~160–226 kDa). The other part (around 100 kDa) is associated with GGM and the co-precipitation of other polysaccharides with lignin (Figure 3b) (Du et al. 2014). This is an indirect hint to the presence of LCCs with xylan and arabinan. It is known that covalent bonds exist between lignin and arabinoxylan in spruce, where lignin is linked through ether bonds to the O-2 or O-3 positions of L-arabinose (Jeffries 1991; Willför et al. 2003). Covalent bounds between arabinans and lignin were also demonstrated (Willför et al. 2003). This could explain the strong

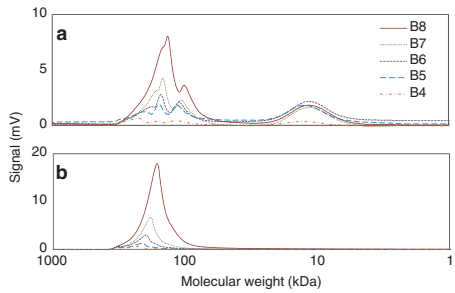


Figure 4: SEC profiles of the MW distribution of the different precipitation fractions.
BX, where X is a number, is the sample abbreviation as defined in Table 2. On the top is the refractive index signal (a), and at the bottom is the UV_{234nm} signal (b).

Table 2: SEC results for the peak maximum in Figure 4 as function of the acetone concentration used for precipitation experiments of the 50 kDa diafiltrated retentate.

	Designation of the fractions				
Sample	**B4**	**B5**	**B6**	**B7**	**B8**
Acetone conc. (%)	34.9	45.2	55.7	66.7	79.0
Peak 1 Mw (kDa)	12.25	12.01	11.53	11.19	11.51
Peak 2 Mw (kDa)	225.9	203.2	191.3	179.2	160.4

correlation between the precipitation yields of arabinan and lignin in the DC interval of ~23–39 (Figure 3b). There are variations in the LCCs, as neither GGM nor xylan and arabinan were completely recovered in the precipitates.

The trend of bound acetyl groups (OAc) coincided with the precipitation of GGM (Figure 3b), proving that the OAc groups are bound to GGM. OAc groups contribute to the solubilization of GGM (Kisonen et al. 2015; Peña et al. 2016). However, no correlation was found between the DAc and the order of precipitation, as the DAc was constant for the major GGM peaks (between 34.9 and 55.7% acetone). Although the MW change of GGM during precipitation was not large (Table 2), this observation indicates that the order of the precipitation follows the MW and not the DAc.

Analytical data of the different fractions

GGM monomers are assumed to be covalently bound to GGM at different degrees (Al-Rudainy et al. 2017) based on the fact that GGM is the major hemicellulose in Norway spruce (Lundqvist et al. 2002). The ratio of the different monomers found in the present study is high (Gal:Glc:Man = 1.68:1.47:3.00) compared with other ratios reported in the literature for spruce GGM (Timell 1967; Lundqvist et al. 2002). Accordingly, the raw material in the present study is a mixture of different polysaccharides, which is also visible on the fractions obtained by precipitation (Figure 5).

Two major polysaccharide fractions are visible in Figure 5. The first one (at an acetone concentration of 34.9%) has the monomeric ratios 0.27 Ara:1.06 Xyl:5.16 Gal:2.66 Glc:3.00 Man:1.61 Ac and the second (at an acetone concentration of 45.2%) has the molar ratios 0.09:0.76:0.70:0.92:3.00:1.66 for the same components. The first fraction is rich in galactose with ratios well above the values in native GGM, while the second fraction is mainly a mannan-based polysaccharide with ratios similar to those reported in the literature. Du et al. (2014) observed a similar trend for three major LCC fractions extracted from spruce.

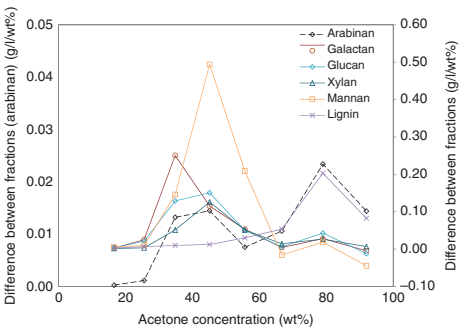


Figure 5: Plots of "Yield differences between precipitation vs. acetone concentration" for precipitation experiments with 50 kDa diafiltrated SSL retentate as the basic solution.

2D-NMR data of two cumulative fractions are presented in Figure 6. One of the fractions contained most of the polysaccharides (at an acetone concentration of 8.1–45.2%), while the other contained most of the lignin and remaining polysaccharides (acetone concentration >55.7%). The major bonds and functional groups were assigned according to chemical shifts reported in the literature (van Hazendonk et al. 1996; Hannuksela and du Penhoat 2004; Zhang and Gellerstedt 2007; Kim et al. 2008; Rencoret et al. 2009; Balakshin et al. 2011; Ekholm et al. 2012; Du et al. 2014; Giummarella et al. 2016).

The NMR signals appearing at δ_C ~ 108–122 ppm in the aromatic region unequivocally demonstrate the guaiacyl-type character of the lignin (G lignin) (Kim et al. 2008). Expectedly, no syringyl signals (δ_C < 108 ppm) or p-hydroxyphenyl signals (δ_C > 122 ppm) are visible (Timell 1967; Giummarella et al. 2016). The bonding pattern of the lignin is also clear (Figure 6a). The major inter-monolignol linkages are β-aryl-ether (β-O-4) indicated by A in Figure 6a, followed by phenylcoumaran (β-5) linkages, indicated by B. Cinnamyl alcohol end-groups (X1) were also detected in the region δ_H/δ_C ~ 4.07/60.93, which coincides with X1 derived from coniferyl alcohol (Kim et al. 2008; Du et al. 2014). Another major peak associated with lignin is the methoxy (OMe) group, which is visible at δ_H/δ_C ~ 3.68/55.75. As expected, the polysaccharide fraction shows these signals with reduced intensities (Figure 6b). However, low intensities of the X1 and OMe groups were still visible in this fraction, with little or no detection in the aromatic region. The same trend was observed by Du et al. (2014), who stated that the lignin was coupled to a high MW polysaccharide, which in turn negatively affected the spin-spin relaxation time (T_2) and led to reduced detection of the aromatic region. Du et al. detected two of the major LCC linkages (benzyl-ether linkages, BE_1 and BE_2) which were not visible in the polysaccharide fraction because of their low abundance. However, they were visible in the lignin-rich fraction, where the overall MW was lower (Figure 4). A signal for α-glycosyl bonds can be seen in the polysaccharide-rich fraction (Figure 6b) but it is absent in the lignin-rich fraction. Balakshin et al. (2011) and Giummarella et al. (2016) assigned this region

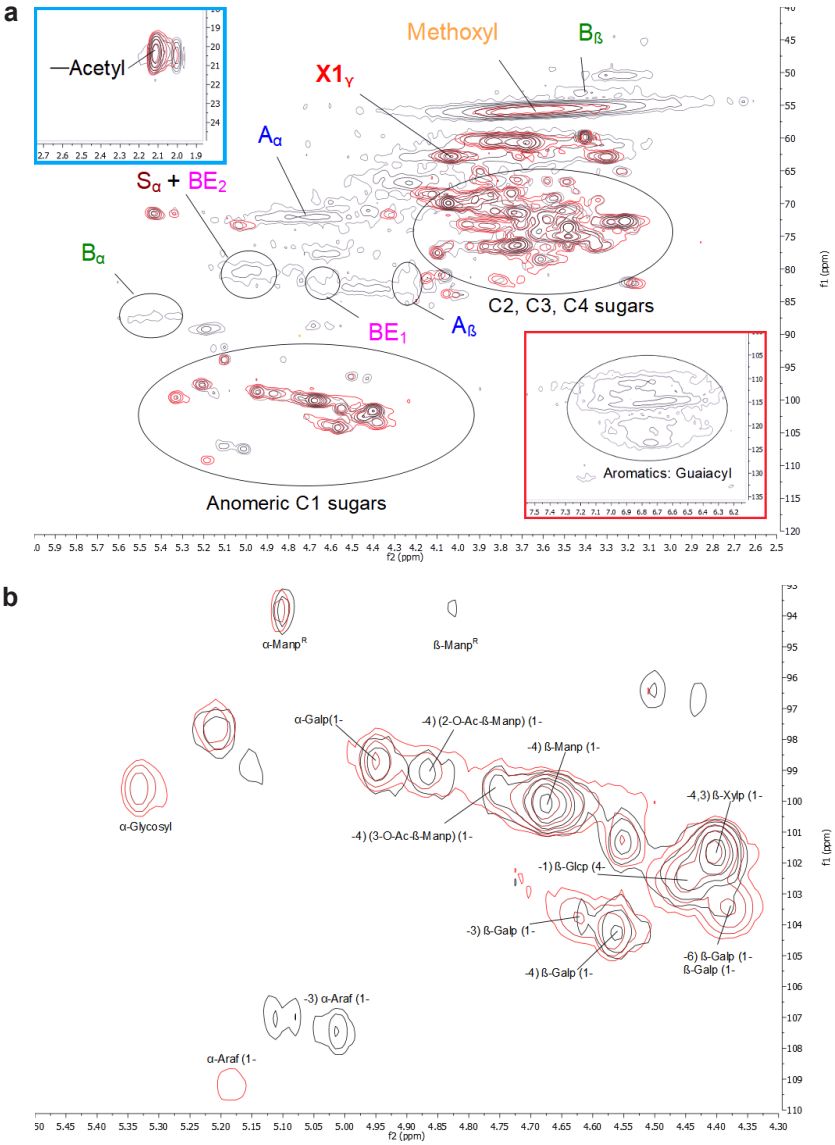


Figure 6: 2D-NMR spectrum of the two major precipitated fractions and magnified presentation that focusses on the carbohydrate part. (a) 2D-NMR spectrum of the two major fractions. The red contours represent the signals for the polysaccharide-rich fraction (at an acetone concentration of 45.2%), while the black contours are for the signals of the lignin-rich fractions (at an acetone concentration higher than 55.7). A_x is β-aryl-ether (β-O-4) bonds, B_x is phenylcoumaran (β-5) linkages, S_x is spiro-dienone functional groups and $X1_x$ is cinnamyl alcohol groups, where the subscripted x is the x-carbon in the linkages. BE_1 and BE_2 are benzyl-ether bonds between lignin and another saccharide (arabinose, xylose, mannose, galactose or glucose). (b) A magnified presentation of the region for the anomeric C1 sugars presented in (a). The results show various signals for different saccharide-saccharide bonds found in the two fractions.

to phenyl-glycosylic bonds, mainly between mannan and lignin. The region for γ-esters (δ_C/δ_H: 65–62/4.0–4.5) gave a signal in the NMR spectrum. However, because of overlapping signals with those of other γ-acetylated lignin structures, a doubtless interpretation of this region is not possible.

GGM was detected in both the polysaccharide and lignin fractions. This is apparent from the signals of β-(1→4)-linked D-mannopyranose (δ_H/δ_C ~ 4.67/100.08) and D-glucopyranose (δ_H/δ_C ~ 4.45/102.54) in the anomeric carbon region (Figure 6b). C2- and C3-acetylated β-(1→4)-linked D-mannopyranose groups are also visible, where the percentage of each in the polysaccharide fraction was 12.3 and 9.3%, respectively (based on the integral of D-mannopyranose signals). The values are lower than those reported in the literature (19 and 17%, respectively) (Hannuksela and du Penhoat 2004). However, the overlapped signals in the presented spectra cannot be quantified. D-galactopyranose units linked by α-(1→6)-bonds to the glucomannan backbone were also detected (δ_H/δ_C ~ 4.95/98.79) at a proportion corresponding to 22.2% of the total non-acetylated mannan in the polysaccharide fraction. This corresponds to a Gal:Man ratio of 0.51:3.00, which is somewhat lower than the values obtained by acid hydrolysis (detected by HPLC), due to the presence of other galactans. Comparing these integrals with those for the lignin fraction (5.9, 6.5, and 12.0%) indicates that the GGM was less acetylated and contains less D-galactopyranose groups in the last mentioned fraction, owing to the higher solubility of the lower MW moiety, but also because of the presence of chemical linkages in the LCCs (Du et al. 2014).

The second major polysaccharide in spruce and pine is arabinoglucuronoxylan (xylan) (Laine 2005), which was also identified by NMR analysis (Figure 6b). The backbone of the polysaccharide (β-(1→4) linked D-xylopyranose) resulted in a peak in the region δ_H/δ_C ~4.41/101.67. The single-unit side chains on the polysaccharide were identified as 4-O-methyl-D-glucuronic acid attached by α-(1→2) bonds (δ_H/δ_C ~ 5.21/97.79), while the L-arabinofuranose units are attached by α-(1→3) bonds (δ_H/δ_C ~ 5.18/109.17). Initially, the structure of the xylan seemed to be identical in both fractions (based on ratios of the peaks). However, the xylan in the lignin fraction did not yield a peak for the L-arabinofuranose groups (visible in the low contours). Probably, arabinan precipitating in the lignin fraction is not associated with xylan (Willför et al. 2003; Laine 2005). Another peak assigned to branched α-(3→1)-L-arabinofuranose units was detected in the lignin fraction in the region δ_H/δ_C ~ 5.01/107.45. Laine discovered that these substituted units could not be associated with any other polysaccharide other than pure arabinan, thereby these findings support the observations regarding the possible linkages between lignin and arabinan (Jeffries 1991; Willför et al. 2003).

The high amount of galactose in the polysaccharide fraction (according to the hydrolysis/HPAEC-PAD results) can be attributed to arabinogalactan and β-galactan, as revealed by the NMR analysis (Figure 6b) (Hannuksela and du Penhoat 2004). The arabinogalactan has a backbone of β-(1→3)-linked D-galactopyranose units and branched with β-(1→6)-linked D-galactopyranose side units, while the β-galactan has a linear backbone of β-(1→4)-linked D-galactopyranose units. According to NMR data, arabinogalactan is dominating among the galactans of polysaccharides, while β-galactan is dominant in the lignin fraction (based on ratios of all integrated D-galactopyranose peaks). This observation indicates that the MW of arabinogalactan is higher than for β-galactan, which is in accordance with observations of Laine.

Effect of solute concentration on the precipitation

The solution concentrations were changed by evaporation or dilution before the precipitation experiments. The results (Figure 7a) showed that the GGM yield increased with increasing solute concentrations as a result of increased GGM/anti-solvent ratios. Similar results were reported by Zasadowski et al. (2014), who observed increasing precipitation yields in the case of less anti-solvent addition. On the other hand, this measurement also increased the lignin yield significantly, leading to a SD decrement from 0.75 (in the membrane filtered solution) to 0.57 (Figure 7b). In diluted solutions the opposite effect was seen, i.e. the GGM yield decrement was accompanied with higher degree of separation (DS) data. This is probably due to the decrease of available "free" water at higher solute concentrations, as theorized by Myrvold. LSs have a randomly branched structure with charged sulfonate groups on the outer ends of the expanded macromolecule (Salmen and Burgert 2009; Stevanic and Salmen 2009). This conformation is favored by the electrostatic repulsion between the charged groups. At higher concentrations, the LSs are more compressed as a result of the suppression of the electrostatic repulsion from the other solutes (Myrvold 2007, 2008, 2013). This can, in turn, form larger LS aggregates, which may easily be precipitated from the solution. A higher ionic strength also affects the overall hydrogen-bonding capacity of the solution via the Hofmeister effect, which may explain the reduced stability

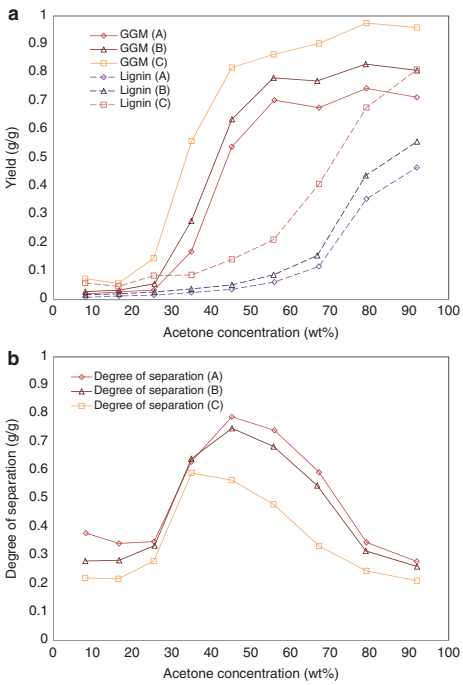


Figure 7: Precipitation yield at different solute concentration and degree of separation vs. anti-solvent concentration.
(a) Plots "Yield of GGM and lignin vs. acetone concentration" for different solute concentrations. (A) diluted solute, (B) original concentration, (C) concentrated solute obtained by evaporation of 50 kDa diafiltrated retentate as presented in Table 1. (b) Plots "The degree of separation vs. acetone concentration" for three different initial solute concentrations. Degree of separation DS is defined as the quotient of the masses GGM/(L+GGM).

of GGM in the solution, and it also explains the higher precipitation yields at lower acetone addition (Baldwin 1996; Mikkonen et al. 2013; Kulasinski et al. 2015).

The higher precipitation yields are also related to the DC data of the bulk solution. As indicated above, DC is probably not affected by the solute concentration, but at varying solute concentrations, this situation may be different. Hasted et al. (1948) found that DC of the solution decreased with increasing ionic strength. This is due to the formation of new hydration shells around the ions, which reduces the response of water molecules to external electric fields and with it the solutions DC (Gavish and Promislow 2016). This may explain the enhanced yield seen with reduced addition of anti-solvent in the present study.

Effect of pH and temperature on precipitation

The pH was varied in four samples in the range of 3.8–11.8. The color of the solution turned from dark brown to black with increasing NaOH concentrations. This is related to the dissociation of the phenolic groups in lignin (Mussatto et al. 2007; Swamy et al. 2011). The dissociation of the phenolic groups increases the electrostatic repulsion of the LS macromolecules, which aggravates agglomeration and contributes to better solubility (Myrvold 2013). This is clearly not the case in the present study, as the yield in lignin precipitation (at 45.2% acetone level) increased with pH (Figure 8a). The kosmotropic NaOH competes with LSs for the same hydration water molecules (Cacace et al. 1997), thus the hydration of the macromolecules is decreased along with their decreased solubility and higher tendency for precipitation (Long et al. 1951). The GGM recovery was

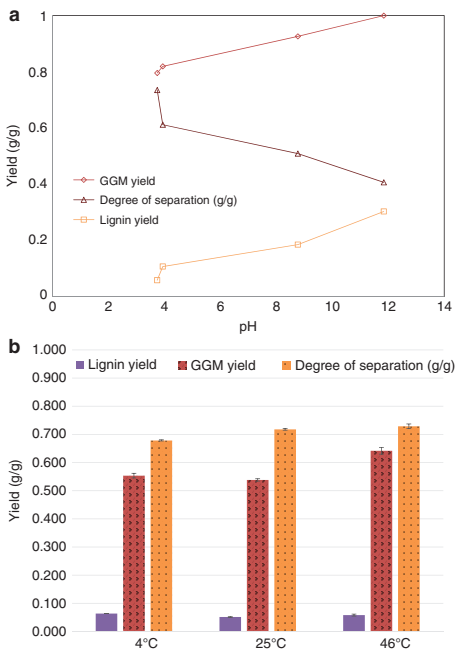


Figure 8: Precipitation yield and degree of separation vs. pH and temperature.
(a) Yield as a function of pH values obtained from the 50 kDa diafiltrated retentate before precipitation with acetone. (b) GGM and lignin yields and degrees of separation as a function of precipitation temperature of the 50 kDa diafiltrated retentate. Acetone was used as anti-solvent and pre-heated to the target temperature before addition.

completed at a pH of 11.8 (yield of ~1.0), which was difficult to achieve at a pH of 3.8 and an acetone concentration of 91.8%. Based on the observations above, the remaining precipitated GGM with a lower DS (Figure 8a) is indicative for associations between GGM and lignin. Accordingly, higher pH favors the GGM yield at the cost of DS. The pH was not decreased below pH 3.8 because of the risk of GGM hydrolysis (Xu et al. 2008; Nebreda et al. 2016).

Figure 8b shows that the yields of GGM and lignin increased at temperatures higher than 25°C. The solubility decrement at higher temperatures has previously been interpreted (Shinoda and Fujihira 1968) as a result of the entropy reduction of the system, which in turn decreases the Gibbs free energy of solvation for different solutes. At elevated temperatures, the hydrogen bonds between water and the solutes break and decrease the stability of lignin by forcing structural changes and compensating the low availability of hydration water on the surface (Li et al. 2014). Hydrophilic groups on the LS surface are forced to form other hydrogen bonds with internal hydrophilic groups (hydroxyl, ether or carboxyl groups), leading to a higher concentration of hydrophobic groups, which lowers the solubility. The DS increased by ~4% when the temperature was increased from 4°C to 25°C, and remained almost constant at temperatures >25°C. This may imply that the change of temperature favors the precipitation of different structures; a low temperature favoring the precipitation of lignin, and a high temperature the co-precipitation of lignin and GGM. However, further studies are needed to clarify this complex situation.

Conclusions

Polysaccharides can be precipitated best from SSL with acetone below 60% concentration and lignin at higher acetone concentrations. Acetone resulted in the best degree of separation (DS) and the highest yields around 76% with an acetone concentration around 47.5% concentration. A direct correlation was found between the DC of the bulk solution and the yields of GGM and lignin. The precipitation with other anti-solvents can be predicted based on the DC data in combination with a suitable model. Arabinogalactan was precipitated first followed by the simultaneous precipitation of GGM and arabinoglucuronoxylan, and finally β-galactan and arabinan were precipitated. LCCs were found mainly in the lignin-rich fraction, according to 2D-NMR analysis showing benzyl-ether bonds between lignin and mannan, xylan, galactan and arabinan. The LCCs found in the polysaccharide fraction, where phenyl-glycosylic bonds were dominating was between mannan and lignin. Judged by the precipitation yields, the polysaccharides were not completely recovered, even at acetone concentrations above 90%. Increasing the pH improves the recovery of the LCC-rich fraction (at acetone concentration of 45.2%) as indicated by the ~100% GGM yield in the precipitation balance. Increasing the solute concentration reduces the amount of acetone required and contributes to higher GGM yields. Under these circumstances the precipitated lignin yields increased significantly, which lowers the overall DS. The parameters of the precipitation process depend on the purity and yield requirements of up-stream processes, where the precipitates are used.

Acknowledgments: This research was funded by the Swedish Foundation for Strategic Research (SSF), which is gratefully acknowledged. Many thanks to Domsjö Fabriker (Sweden) for their support and for providing us with the raw material used in this research. Thanks to Dr. Göran Carlström for the help with the NMR analysis.

Author contributions: All the authors have accepted responsibility for the entire content of this submitted manuscript and approved submission.
Research funding: The research was funded by the Swedish Foundation for Strategic Research (SSF).
Employment or leadership: None declared.
Honorarium: None declared.

References

Akerlof, G. (1932) Dielectric constants of some organic solvent-water mixtures at various temperatures. J. Am. Chem. Soc. 54:4125–4139.

Al Manasrah, M., Kallioinen, M., Ilvesniemi, H., Mänttäri, M. (2012) Recovery of galactoglucomannan from wood hydrolysate using regenerated cellulose ultrafiltration membranes. Bioresour. Technol. 114:375–381.

Al-Rudainy, B., Galbe, M., Wallberg, O. (2017) Influence of prefiltration on membrane performance during isolation of lignin-carbohydrate complexes from spent sulfite liquor. Sep. Purif. Technol. 187:380–388.

Balakshin, M., Capanema, E., Gracz, H., Chang, H.-M., Jameel, H. (2011) Quantification of lignin–carbohydrate linkages with high-resolution NMR spectroscopy. Planta 233:1097–1110.

Baldwin, R.L. (1996) How Hofmeister ion interactions affect protein stability. Biophys. J. 71:2056–2063.

Cacace, M., Landau, E., Ramsden, J. (1997) The Hofmeister series: salt and solvent effects on interfacial phenomena. Q. Rev. Biophys. 30:241–277.

Du, X., Pérez-Boada, M., Fernández, C., Rencoret, J., Del Río, J.C., Jiménez-Barbero, J., Li, J., Gutiérrez, A., Martínez, A.T. (2014) Analysis of lignin-carbohydrate and lignin-lignin linkages after

hydrolase treatment of xylan-lignin, glucomannan-lignin and glucan-lignin complexes from spruce wood. Planta 239:1079.
Duval, A., Molina-Boisseau, S., Chirat, C. (2015) Fractionation of lignosulfonates: comparison of ultrafiltration and ethanol solubility to obtain a set of fractions with distinct properties. Holzforschung 69:127–134.
Ekholm, F.S., Ardá, A., Eklund, P., André, S., Gabius, H.J., Jiménez-Barbero, J., Leino, R. (2012) Studies related to Norway spruce galactoglucomannans: chemical synthesis, conformation analysis, NMR spectroscopic characterization, and molecular recognition of model compounds. Chem. Eur. J. 18:14392–14405.
Gavish, N., Promislow, K. (2016) Dependence of the dielectric constant of electrolyte solutions on ionic concentration: a microfield approach. Phys. Rev. E. 94:012611.
Giummarella, N., Zhang, L., Henriksson, G., Lawoko, M. (2016) Structural features of mildly fractionated lignin carbohydrate complexes (LCC) from spruce. RSC Adv. 6:42120–42131.
Hannuksela, T., du Penhoat, C.H. (2004) NMR structural determination of dissolved O-acetylated galactoglucomannan isolated from spruce thermomechanical pulp. Carbohydr. Res. 339:301–312.
Hasted, J., Ritson, D., Collie, C. (1948) Dielectric properties of aqueous ionic solutions. Parts I and II. J. Chem. Phys. 16:1–21.
Jeffries, T.W. (1991) Biodegradation of lignin-carbohydrate complexes. In: Physiology of Biodegradative Microorganisms. Ed. Ratledge, C. Springer, Dordrecht, Netherlands. pp. 163–176.
Kim, H., Ralph, J., Akiyama, T. (2008) Solution-state 2D NMR of ball-milled plant cell wall gels in DMSO-d 6. Bioenergy Res. 1:56–66.
Kisonen, V., Prakobna, K., Xu, C., Salminen, A., Mikkonen, K.S., Valtakari, D., Eklund, P., Seppälä, J., Tenkanen, M., Willför, S. (2015) Composite films of nanofibrillated cellulose and O-acetyl galactoglucomannan (GGM) coated with succinic esters of GGM showing potential as barrier material in food packaging. J. Mater. Sci. 50:3189–3199.
Krawczyk, H., Jönsson, A.S. (2011) Separation of dispersed substances and galactoglucomannan in thermomechanical pulp process water by microfiltration. Sep. Purif. Technol. 79:43–49.
Krawczyk, H., Arkell, A., Jönsson, A.-S. (2013) Impact of prefiltration on membrane performance during isolation of hemicelluloses extracted from wheat bran. Sep. Purif. Technol. 116:192–198.
Kulasinski, K., Guyer, R., Keten, S., Derome, D., Carmeliet, J. (2015) Impact of moisture adsorption on structure and physical properties of amorphous biopolymers. Macromolecules 48:2793–2800.
Laine, C. Structures of Hemicelluloses and Pectins in Wood and Pulp. Helsinki University of Technology, Espoo, Finland, 2005.
Li, H., Deng, Y., Ye, H., Xiao, L., Qiu, X. (2014) Effect of temperature on polyelectrolyte expansion of lignosulfonate. BioResources 10:575–587.
Long, F., Dunkle, F.B., McDevit, W. (1951) Salt effects on the acid-catalyzed hydrolysis of γ-butyrolactone. II. Kinetics and the reaction mechanism. J. Phys. Chem. 55:829–842.
Lundqvist, J., Teleman, A., Junel, L., Zacchi, G., Dahlman, O., Tjerneld, F., Stålbrand, H. (2002) Isolation and characterization of galactoglucomannan from spruce (Picea abies). Carbohydr. Polym. 48:29–39.
Menon, V., Rao, M. (2012) Trends in bioconversion of lignocellulose: biofuels, platform chemicals & biorefinery concept. Prog. Energy Combust. Sci. 38:522–550.
Mikkonen, K.S., Schmidt, J., Vesterinen, A.-H., Tenkanen, M. (2013) Crosslinking with ammonium zirconium carbonate improves the formation and properties of spruce galactoglucomannan films. J. Mater. Sci. 48:4205–4213.
Mussatto, S.I., Fernandes, M., Roberto, I.C. (2007) Lignin recovery from brewer's spent grain black liquor. Carbohydr. Polym. 70:218–223.
Myrvold, B.O. (2007) The polyelectrolyte behavior of randomly branched lignosulfonates. Tappi J. 6:10–14.
Myrvold, B.O. (2008) A new model for the structure of lignosulphonates: part 1. Behaviour in dilute solutions. Ind. Crops Prod. 27:214–219.
Myrvold, B.O. (2013) Salting-out and salting-in experiments with lignosulfonates (LSs). Holzforschung 67:549–557.
Nebreda, A.P., Grénman, H., Mäki-Arvela, P., Eränen, K., Hemming, J., Willför, S., Murzin, D.Y., Salmi, T. (2016) Acid hydrolysis of O-acetyl-galactoglucomannan in a continuous tube reactor: a new approach to sugar monomer production. Holzforschung 70:187–194.
Peña, M.I.P., Deutschle, A.L., Saake, B., Pizzi, A., Pichelin, F. (2016) Study of the solubility and composition of welded wood material at progressive welding times. Eur. J. Wood Wood Prod. 74:191–201.
Quesada-Medina, J., López-Cremades, F.J., Olivares-Carrillo, P. (2010) Organosolv extraction of lignin from hydrolyzed almond shells and application of the δ-value theory. Bioresour. Technol. 101:8252–8260.
Rencoret, J., Marques, G., Gutiérrez, A., Nieto, L., Santos, J.I., Jiménez-Barbero, J., Martínez, Á.T., del Río, J.C. (2009) HSQC-NMR analysis of lignin in woody (*Eucalyptus globulus and Picea abies*) and non-woody (*Agave sisalana*) ball-milled plant materials at the gel state 10th EWLP, Stockholm, Sweden, August 25–28, 2008. Holzforschung 63:691–698.
Ruiz, R., Ehrman, T. (1996) HPLC analysis of liquid fractions of process samples for monomeric sugars and cellobiose (LAP 013). NREL.
Salmen, L., Burgert, I. (2009) Cell wall features with regard to mechanical performance. A review COST Action E35 2004–2008: wood machining–micromechanics and fracture. Holzforschung 63:121–129.
Shinoda, K., Fujihira, M. (1968) The analysis of the solubility of hydrocarbons in water. Bull. Chem. Soc. Jpn. 41:2612–2615.
Song, T., Pranovich, A., Holmbom, B. (2013) Separation of polymeric galactoglucomannans from hot-water extract of spruce wood. Bioresour. Technol. 130:198–203.
Stevanic, J.S., Salmen, L. (2009) Orientation of the wood polymers in the cell wall of spruce wood fibres. Holzforschung 63: 497–503.
Swamy, N.K., Singh, P., Sarethy, I.P. (2011) Precipitation of phenols from paper industry wastewater using ferric chloride. Rasayan J. Chem. 4:452–456.
Tarasov, D., Leitch, M., Fatehi, P. (2015) Production of lignosulfonate in NSSC-based biorefinery. Biotechnol. Progr. 31:1508–1514.
Thuvander, J., Jönsson, A.-S. (2016) Extraction of galactoglucomannan from thermomechanical pulp mill process water by microfiltration and ultrafiltration – influence of microfiltration

membrane pore size on ultrafiltration performance. Chem. Eng. Res. Des. 105:171–176.
Timell, T.E. (1967) Recent progress in the chemistry of wood hemicelluloses. Wood Sci. Technol. 1:45–70.
van Hazendonk, J.M., Reinerik, E.J., de Waard, P., van Dam, J.E. (1996) Structural analysis of acetylated hemicellulose polysaccharides from fibre flax (Linum usitatissimum L.). Carbohydr. Res. 291:141–154.
Wenzl, H. The Chemical Technology of Wood. Elsevier, Cambridge, MA, USA, 2012.
Willför, S., Sjöholm, R., Laine, C., Roslund, M., Hemming, J., Holmbom, B. (2003) Characterisation of water-soluble galactoglucomannans from Norway spruce wood and thermomechanical pulp. Carbohydr. Polym. 52:175–187.
Xu, C., Pranovich, A., Vähäsalo, L., Hemming, J., Holmbom, B., Schols, H.A., Willför, S. (2008) Kinetics of acid hydrolysis of water-soluble spruce O-acetyl galactoglucomannans. J. Agric. Food. Chem. 56:2429–2435.
Zasadowski, D., Yang, J., Edlund, H., Norgren, M. (2014) Antisolvent precipitation of water-soluble hemicelluloses from TMP process water. Carbohydr. Polym. 113:411–419.
Zhang, L., Gellerstedt, G. (2007) Quantitative 2D HSQC NMR determination of polymer structures by selecting suitable internal standard references. Magn. Reson. Chem. 45:37–45.
Zhou, M., Qiu, X., Yang, D., Lou, H. (2006) Properties of different molecular weight sodium lignosulfonate fractions as dispersant of coal-water slurry. J. Dispersion Sci. Technol. 27:851–856.

Paper III

polymers

MDPI

Article

Impact of Lignin Content on the Properties of Hemicellulose Hydrogels

Basel Al-Rudainy [1], Mats Galbe [1], Monica Arcos Hernandez [2], Patric Jannasch [2] and Ola Wallberg [1,*]

[1] Department of Chemical Engineering, Lund University, P.O. Box 124, SE-221 00 Lund, Sweden; basel.al-rudainy@chemeng.lth.se (B.A.-R.); mats.galbe@chemeng.lth.se (M.G.)

[2] Department of Chemistry, Polymer, and Materials Chemistry, Lund University, P.O. Box 124, SE-221 00 Lund, Sweden; monica.arcos_hernandez@chem.lu.se (M.A.H.); patric.jannasch@chem.lu.se (P.J.)

* Correspondence: ola.wallberg@chemeng.lth.se; Tel.: +46-46-222-46-41

Received: 4 December 2018; Accepted: 23 December 2018; Published: 27 December 2018



Abstract: Hemicellulose is a promising renewable raw material for the production of hydrogels. This polysaccharide exists in large amounts in various waste streams, in which they are usually impure and heavily diluted. Several downstream processing methods can be combined to concentrate and purify the hemicellulose. However, such an approach can be costly; hence, the effect of impurities on the formation and properties of hydrogels must be determined. Lignin usually exists in these waste streams as a major impurity that is also difficult to separate. This compound can darken hydrogels and decrease their swellability and reactivity, as shown in many studies. Other properties and effects of lignin impurities are equally important for the end application of hydrogels and the overall process economy. In this work, we examined the feasibility of producing hydrogels from hemicelluloses that originated from sodium-based spent sulfite liquor. A combination of membrane filtration and anti-solvent precipitation was used to extract and purify various components. The influence of the purity of hemicellulose and the addition of lignosulfonates (emulated impurities in the downstream processing) to the crosslinking reaction mixture on the mechanical, thermal, and chemical properties of hydrogels was determined.

Keywords: galactoglucomannan; lignin; lignin-carbohydrate complex; ultrafiltration; precipitation; hydrogel

1. Introduction

Hydrogels are hydrophilic networks of polymers that are commonly produced by crosslinking various types of synthetic polymers or polysaccharides [1]. The properties of the hydrogels that are produced today are shaped by the type of crosslinker, the inherent nature of the main polymer, and the process with which these hydrogels are produced. Synthetic polymers yield hydrogels with excellent water absorption, strength, and durability. However, the precursors to these synthetic polymers are petroleum-based which makes the products lacking in terms of sustainability.

Polysaccharides and natural polymers are alternatives to synthetic polymers, especially in the development of hydrogels for medical applications, for which biocompatibility and biodegradability are paramount [2]. Many hydrogel products have been synthesized using polysaccharides as raw materials, such as starch, dextran, alginate, cellulose, and chitosan [2–6].

Hemicellulose is a promising polysaccharide for the production of hydrogels. Its high abundance (constituting over 20% of wood cell walls) and current losses in pulp and paper waste streams (incinerated in recovery boilers) make this work important industrially and economically [7]. Hydrogels from hemicellulose with similar properties as synthetic polymer-based hydrogels have

been produced by Söderqvist Lindblad, et al. [8], who showed that it is possible to replace fossil-based polymers with renewable waste material. However, the hemicellulose that was used was derived from steam explosion of spruce chips and did not represent the readily available hemicelluloses that are found in other process water streams.

Maleki, et al. [9] produced hydrogels from hemicellulose (galactoglucomannan) that was derived from thermomechanical pulping process water of spruce chips. The resulting single-network hydrogels were weak, as evidenced by their low shear modulus, which improved after a secondary crosslinking reaction. Consequently, the swelling ratio declined, but the swelling rate increased. Hemicellulose that has been derived from sodium-based spent sulfite liquor is another promising raw material for hydrogel production [10]—the product has swelling equilibria of between 50 and 270 g/g, a desirable property for use as absorbents and in agriculture.

All of the hemicelluloses [in this work, galactoglucomannan (GGM)] in the process waters above have at least one common problem: they exist in impure and highly diluted solutions (total dry substance of 5–6 g/L) and thus can not be used directly without being subjected to a proper concentration and purification method. These challenges have been addressed by other researchers using various types of downstream processing methods, such as membrane filtration, precipitation, and preparative chromatography [11–15].

Membrane filtration is effective in concentrating and, in certain cases, even purifying dilute streams. Al Manasrah, et al. [14] recovered 70% of the GGM in pressurized hot water extracts of spruce sawdust by ultrafiltration and reached a purity of 63%. Thuvander and Jönsson [16] reported that it was possible to separate lignin and GGM from thermomechanical process water using a combination of microfiltration and ultrafiltration. However, in other cases, this separation was difficult, due to membrane fouling [13,16,17]. Thus, membrane filtration was sufficient for concentrating and removing pulping chemicals, but another method was needed to separate lignin and GGM.

In cases in which the separation of GGM and lignin is difficult, anti-solvent precipitation has proven to be an efficient method for separation after membrane filtration [11,15,18]. Zasadowski, et al. [11] precipitated GGM from TMP process water using acetone, obtaining a yield of 77% at an acetone concentration of 54.5%. Song, et al. [15] used ethanol as an anti-solvent to recover GGM from hot water extractives from spruce, achieving a yield of 78% at 90% ethanol and discovering that the precipitate contained solely polysaccharides with molecular weights that exceeded 4 kDa.

Al-Rudainy, et al. [18] combined membrane filtration and anti-solvent precipitation for softwood spent sulfite liquor. Their GGM yield was on the same order of magnitude as those of other groups but with less anti-solvent, as a result of the membrane filtration step. Economically, it is preferable that the separation occurs in one step without the addition of any chemicals, such as anti-solvents. This tactic, however, will decrease the purity of the GGM due to the higher amounts of lignin in the concentrated process water.

The effect of additional lignin on the formation and properties of various products has been studied in other fields, such as in enzymatic treatment, wherein lignin has inhibitory effects on the reactions [19]. With regard to hydrogel production, Maleki, et al. [10] compared 2 hydrogels that were produced using the same methods and the same hemicellulose and but from 2 sources: spent sulfite liquor using ethanol precipitation and centrifugation as the separation and purification step versus a side stream of the steam explosion of spruce wood chips. The solution was concentrated by ultrafiltration and purified through diafiltration. As a result, the second specimen contained more lignin. This led to darker hydrogels with lower reactivity and swellability, which were theorized to have been caused by hydrophobic groups on the lignin, reducing the overall hydrophilicity of the hydrogel. However, the other differences between the 2 hemicelluloses have not been examined since.

In this work, a one-pot reaction was chosen to study the effects of lignin impurities on the properties of GGM hydrogel. Epichlorohydrin (ECH) was used as the crosslinker, and the GGM and lignin were acquired by membrane filtration and anti-solvent precipitation of softwood spent sulfite liquor.

2. Materials and Methods

2.1. Raw Material and Reactants

For the raw material, sodium-based spent sulfite liquor was used, which was extracted from the first step in a 2-step softwood (60% *Picea abies* and 40% *Pinus sylvestris*) pulping process by Domsjö Fabriker (Örnsköldsvik, Sweden). The SSL contained 6.6% galactoglucomannan, 1.8% xylan, 0.8% arabinan, and 36.4% lignin, with a total dry substance of 84.6 g/L [17]. The remaining components were pulping chemicals, monosaccharides, acid-insoluble solids, and extractives.

The reactants that were used for the crosslinking reaction were 99% pure synthesis-grade epichlorohydrin and 50 wt % analytical-grade sodium hydroxide solution (Merck KGaA, Darmstadt, Germany).

2.2. Ultrafiltration and Anti-solvent Precipitation

The product was concentrated and low-molecular-weight components (such as pulping chemicals and monosaccharides) were removed by diafiltration per the membrane filtration methods in a previous study [17]. A 400-mL stirred filtration vessel that was equipped with a 50-kDa membrane (GR51PP, Alfa Laval Corp. AB, Lund, Sweden) and a 10-L feed tank were used for the membrane filtration setup. The pressure was monitored with a digital pressure gauge (DCS40.0AR, Trafag AG, Bubikon, Switzerland) and adjusted using a valve that was connected to a 6-bar nitrogen gas line. The crossflow velocity and temperature were controlled using a magnetic stirrer with a heating plate (MR2002, Heidolph Instruments GmbH & Co. KG, Schwabach, Germany), on top of which the 400-mL vessel was placed. The raw material was concentrated at 50 °C, a cross-flow velocity of 0.5 m/s, and 5.5 bar transmembrane pressure, decreasing in volume by 90% in fed batch mode. Diafiltration was then performed on the retentate to a diafiltration factor of 5 using deionized water in the feed tank. The membrane was washed with 0.04 wt % acid detergent solution (Ultrasil 73, Ecolab AB, Älvsjö, Sweden) at 50 °C for 1 h before and after each experiment. This procedure was repeated until the total weight of diafiltrated retentate exceeded 1 kg.

Precipitation was performed on 1 kg of diafiltrated retentate in a glass beaker with magnetic stirring (500 RPM) at room temperature, with acetone (SupraSolv MS, Merck Schuchardt OHG, Hohenbrunn, Germany) added gradually to a final concentration of 45 wt % [18]. The mixture was agitated for 15 min before being transferred to 750-mL centrifuge bottles (Beckman Coulter, Brea, California, USA) and was then centrifuged at 4000 RPM for 20 min (Jouan S.A., Model C412, Saint-herblain, Nantes, France). The liquid phase was carefully decanted, and the bottles that contained the precipitate (most of the galactoglucomannan) were dried in an oven at 50 °C for 48 h. The liquid phase (most of the lignin) was dried in a vacuum evaporator (BÜCHI Rotavapor R-153, BÜCHI Labortechnik AG, Flawil, Switzerland) at 50 °C and an average absolute pressure of 200 mbar for 60 h. Both powders were re-dissolved in deionized water (2 g powder to 18 g water) to make the stock solutions that were to be used in the hydrogel synthesis steps.

2.3. Preparing Hydrogels

Hydrogels were synthesized per reference [20]. A total of 2 mL stock solution (galactoglucomannan, lignin, or a mixture of both) was pipetted into a 3-mL vial, and 250 µL 50% sodium hydroxide solution was added and mixed for 5 min on a vortex mixer (MS2 Minishaker, IKA®-Werke GmbH & Co. KG, Staufen, Germany). The crosslinking reaction was then started by adding 100–300 µL epichlorohydrin and mixing it until the solution appeared to be homogeneous. Approximately 1 mL of the mixture was then transferred to a mold (flexible plastic bottle caps), covered, and left at room temperature for 48 h. The hydrogel was peeled off carefully from the mold and placed in 50 mL deionized water at room temperature for 24 h; the wash solution was then transferred to a container, and the same procedure was repeated to properly wash away any unbound

reactants. The wash solution that was collected (approximately 100 mL) was later analyzed for lignin, hemicellulose, acetic acid, and glycerol content and epichlorohydrin conversion.

2.4. Analysis

2.4.1. Swelling Capacity

Swelling capacity was measured by carefully patting the newly prepared and washed hydrogel (Section 2.3) dry with tissue paper and weighing it. After the hydrogel was dried at 50 °C for 24 h, it was reweighed, and the swelling capacity (SC) was calculated per the following equation:

$$\mathrm{SC} = \frac{m_{\mathrm{wet}} - m_{\mathrm{dry}}}{m_{\mathrm{dry}}} \quad (1)$$

where m_{wet} and m_{dry} are the mass of the hydrogel in the wet and dry states, respectively.

2.4.2. Lignin Content and Epichlorohydrin Conversion

The concentration of lignin in solution was determined on a UV spectrophotometer (Shimadzu UV-visible spectrophotometer UV-1800, Kyoto, Japan). The wavelength was set to 234 nm, and the extinction coefficient was 31.6 L/g·cm [17].

Epichlorohydrin conversion was measured using chloride titrator strips (Quantab Chloride Low Range titrators, HACH company, Loveland, CO, USA). Chloride concentration was determined for the hydrogel wash solution, which, after the conversion, was calculated as the amount of chloride ions in the wash solution divided by the amount of chloride in the epichlorohydrin that was added.

2.4.3. Hemicellulose, Acetic Acid, and Glycerol Content

The hemicellulose concentration and glycerol content were determined per previous studies [18]. Ten milliliters of a sample were acid-hydrolyzed using 0.75 mL 72% sulfuric acid solution and autoclaved (Systec DX 150, Wettenberg, Germany) at 121 °C for 1 h. The hydrolysate was then vacuum-filtered to remove acid-insoluble solids and analyzed for monosaccharide content on a HPAEC-PAD system (ICS-3000, Dionex Corp., Sunnyvale, CA, USA) with a CarboPac PA1 carbohydrate analytical column. Deionized water was used as the eluent at a flow rate of 1 mL/min and 0.5 mL/min 200 mM sodium hydroxide postcolumn addition. The injection volume was 10 µL, and the hemicellulose concentration was calculated by summing the monosaccharide content and anhydro corrections of 0.88 for pentoses and 0.90 for hexoses.

The acetic acid and glycerol content was determined on an HPLC system (LC-20AT, SIL-20AC, SCL-10A vp, RID-10A, CTO-20AC, Schimadzu Corp., Kyoto, Japan) with an Aminex HPX-87H column (Bio-Rad, Hercules, CA, USA), 5 mM sulfuric acid solution as eluent at a flow rate of 0.5 mL/min, a column temperature of 50 °C, and sample injection volume of 10 µL.

2.4.4. Size-exclusion Chromatography

The molecular weight distribution was examined in liquid samples on a Waters size-exclusion chromatography system (Waters, Milford, MA, USA), with a Waters 600E system controller, coupled with a refractive index detector (Waters 2414 Differential Refractometer), a UV detector (Waters 486 Tunable Absorbance Detector) that was set to 234 nm, and a pump (Waters 600 gradient pump). Samples were injected using an autosampler (Waters 717 plus autosampler) with an injection volume of 20 µL. Fractionation was performed on a TSKgel column (G4000PWXL, TOSOH Bioscience GmbH, Griescheim, Germany), with deionized water as the eluent at a flow rate of 0.5 mL/min. Polyethylene glycol standards (Merck Schuchardt OHG, Germany) were used for the column calibration (100 kDa, 35 kDa, 10 kDa, 4 kDa, 400 Da).

2.4.5. Fourier Transform Infrared Spectroscopy

The samples that were to be measured were dried at 50 °C in a furnace (Heraeus, Heraeus Holding GmbH, Hanau, Germany) and ground to a fine powder using a mortar and pestle. The pulverized samples were then measured with an FTIR (Bruker ALPHA-p FTIR spectrometer, Billerica, MA, USA) in attenuated total reflectance mode, in the wavenumber range of 4000 to 500 cm^{-1} with 2 cm^{-1} resolution and 72 scans per sample.

2.4.6. Compression Stress and Strain

Compression tests were performed on newly prepared and washed cylindrical hydrogels. The hydrogels were prepared per Section 2.3, except that the mold was a 3-mL vial. Compression stress and strain were measured using a scale (PL6001-l, Mettler Toledo Inc., Columbus, OH, USA) and motor-controlled piston, for which the rate of axial displacement was 1.0 mm/min. Given that the axial displacement was constant, the strain was calculated by multiplying the elapsed time with the axial displacement rate. Stress was calculated as the mass that was displayed on the scale divided by the cross-sectional area of the hydrogel.

2.4.7. Thermogravimetric Analysis

Thermogravimetric analysis was conducted on a Q500 TGA (TA Instruments Inc., New Castle, DE, USA). Powdered samples were predried in a furnace at 50 °C for 24 h and cooled to room temperature using a desiccator prior to analysis. The samples were placed in open aluminum trays (2 to 5 mg) and heated from 15 to 600 °C at 10 °C/min under a nitrogen atmosphere (60 mL/min).

2.4.8. Release of BTB from Hydrogels

Hydrogels were prepared as in Section 2.3, except that 4 mg of bromothymol blue powder (Merck Schuchardt OHG, Hohenbrunn, Germany) was added to the reaction mixture and dissolved by mixing prior to the addition of ECH. After 48 h, 2 hydrogel disks were carefully peeled off and placed into a mesh basket, which was then submerged into a beaker with 400 mL 4 g/L NaOH solution. The solution was then stirred magnetically (rod length of 2.5 cm) at 100 RPM, and 2-mL samples were taken at timed intervals to determine BTB concentrations.

The BTB concentration was measured on a UV spectrophotometer (Shimadzu UV-visible spectrophotometer UV-1800, Kyoto, Japan) at the isosbestic point (wavelength 498 nm). The extinction coefficient was 9.31 L/g·cm, which was calibrated using various concentrations of BTB in 4 g/L sodium hydroxide solution.

2.4.9. Liquid Chromatography-mass Spectrometry (LC-MS)

The LC instrument was part of the 1260 Infinity II line (Agilent Technologies, Waldbronn, Germany) and comprised a range of modules: a Quaternary Pump VL (G7111A), a Vialsampler (G7129A), and a temperature-controlled column compartment (G7130A). The column, a 4.6 mm × 100 mm Poroshell 120 EC-ECS, was operated at 50 °C. The eluent flow rate was 0.5 mL/min, with a gradient switch between eluents A (0.1% formic acid solution) and B (95% acetonitrile in 0.1% formic acid solution) according to the program in Table 1. The injection volume was 1 µL, and the total run time per sample was 12 min. LC detection was performed using a UV diode array detector (G7115A) with a peak width of 0.1 min and a 4-nm slit.

The LC system was connected to a mass spectrometer (G6545B Q-TOF) that was equipped with a dual AJS ESI ion source that was operated in ESI positive mode. The nitrogen gas temperature was set to 350 °C at a flow rate of 12 L/min. The nebulizer pressure was 35 psig, with a sheath gas temperature and flow rate of 400 °C and 12 L/min, respectively. The nozzle voltage was 1000 V, the collision energy was set to 0 eV, and the data were acquired in the range of 50 to 3200 m/z.

Table 1. Gradient program for LC of the LC/MS system. Eluent A was 0.1% formic acid solution, and eluent B was 95% acetonitrile in 0.1% formic acid solution. The flow rate was kept constant at 0.5 mL/min.

Time (min)	Eluent A (%)	Eluent B (%)
1	100.0	0.0
8	0.0	100.0
10	0.0	100.0
12	100.0	0.0

3. Results and discussion

3.1. Ultrafiltration and Anti-solvent Precipitation

Table 2 summarizes the results from the re-dissolved fractions after ultrafiltration and anti-solvent precipitation. The separation method clearly fractionated the spent sulfite liquor components into 2 major fractions: a polysaccharide-rich stream and another that contained primarily lignin.

Table 2. Compositions of the re-dissolved products from the ultrafiltered and anti-solvent precipitated fractions. The samples were dried at 50 °C.

Fraction	TS of Prepared Solutions (g/L)	Lignin Content (g/L)	Acetic Acid (g/L)	Arabinan (g/L)	Galactan (g/L)	Glucan (g/L)	Xylan (g/L)	Mannan (g/L)
GGM	100	8.40	3.60	0.60	15.9	13.0	4.60	23.5
Lignin	99.9	94.6	0.75	0.21	1.09	1.64	0.94	4.11

The difference in properties of these fractions was also observed using FTIR spectroscopy (Figure 1). In the region between 3000–3500 cm^{-1}, a broad signal appeared in both fractions and was assigned to the stretching of O–H bonds. The peaks at 2930 and 2852 cm^{-1} were caused by the stretching of C–H bonds in the lignin and polysaccharides [21,22]. The peak at 1736 cm^{-1} was assigned to the acetyl groups on the GGM and was visible in both fractions, albeit at greater intensity in the polysaccharide-rich fraction. Various peaks from aromatic skeletal vibrations appeared in the lignin-rich fraction (1602, 1509, 1451, and 1420 cm^{-1}). These peaks were missing or lower in intensity in the polysaccharide fraction, indicating proper separation between these entities. Other indicators of good separation were the peaks for various guaiacyl moieties (1262–1142 cm^{-1}), which also implicated the lignin as being guaiacyl-type, as shown in our previous study [18].

The signals at 1082 and 1026 cm^{-1} were ascribed to vibrations of asymmetrical C–O–C bonds. The signal at 1082 cm^{-1} was less intense in the lignin-rich fraction, indicating that it originated from internal vibrations of the pyranose structure in the polysaccharides [21]. Two signals were detected in the low wavenumber region and were assigned to the sulfonate groups in the lignin (650 and 517 cm^{-1}).

The properties of various components can also be characterized using TGA, as applied to our 2 fractions; the results are presented in Figure 2. The degradation of lignin occurred in 3 major stages, as indicated by the derivative of the TGA curve (DTG). In the first stage, the DTG peak temperature was approximately 33 °C, due to the release of absorbed water and other solvents, such as acetone, that were used during the precipitation [23,24].

In the second stage, which had a DTG peak temperature of 263 °C, residual hemicelluloses were degraded, perhaps as were lignin-carbohydrate complexes. Certain lignosulfonates begin to degrade at temperatures above 250 °C [24,25]. Because the observed mass of the second-stage peak (~20 wt %) was higher than the total amount of hemicelluloses (Table 2), this result was expected as a possibility, even in our case.

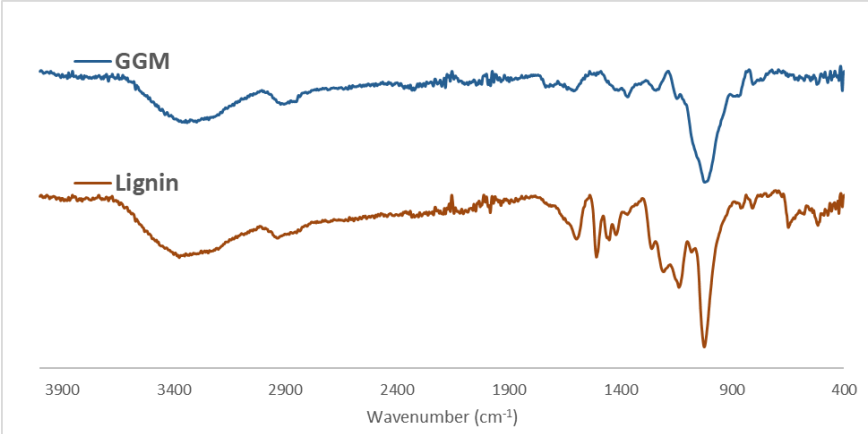


Figure 1. FTIR spectrum comparison of the GGM and lignin fraction.

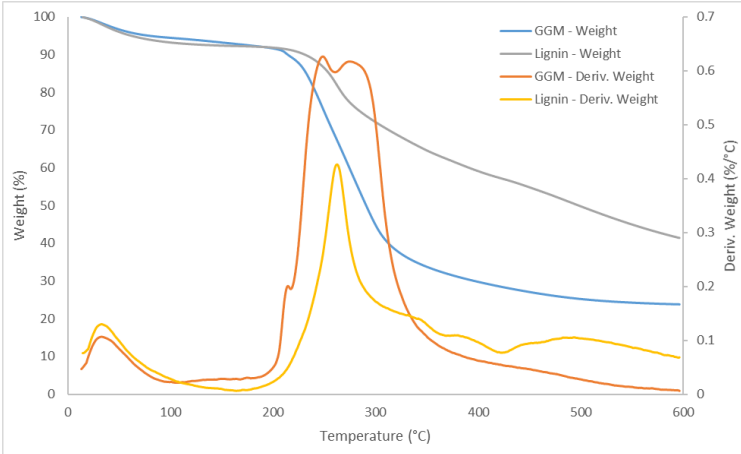


Figure 2. TGA and DTG curves for the GGM and lignin fraction.

In the third stage (temperatures above 300 °C), several DTG peaks were observed. The visible peaks appeared at 344, 390, 441 and 493 °C, corresponding to the pyrolytic degradation of lignin; the release of phenolic derivatives, mercaptans, SO_2, CO, and CO_2; and the decomposition of aromatic rings at temperatures exceeding 500 °C [23]. The residual mass of the lignin-rich fraction at 600 °C was roughly 41 wt %. This high char residue content was anticipated, given that the lignin was sulfonated. According to previous reports [25,26], the remaining chemically bonded sulfonate groups and sodium salts were responsible for the residue and require temperatures above 600 °C for further decomposition.

GGM decomposed in 2 major stages, the first of which was identical to the first stage of lignin decomposition. In the second stage, at least 3 DTG peaks could be observed at 215, 248, and 274 °C, with a residue of 24 wt % at the end of the run. The first DTG peak of the second stage had a mass that corresponded to 3.2 wt % of the total sample, similar to the amount of acetic acid (acetyl groups) in the sample per Table 2, indicating that the acetyl groups were the first components to leave the matrix, as shown by others [27]. The next DTG peak arose at 248 °C, near the reported temperature of the maximum rate of weight loss for softwood xylan [27]. However, the mass of the peak exceeded the amount of xylan that was available in the sample, suggesting that other compounds were decomposing

at approximately the same temperature—likely the highly branched GGM, which has been reported to have a low decomposition temperature compared with low-branched linear GGM.

The last DTG peak (274 °C) most likely contained the remaining GGM but also other galactan-based polysaccharides, as reported by Beall [27]. Overall, these results show that the lignin fraction is thermally more stable than the polysaccharide-rich fraction in terms of the temperature at the maximum rate of weight loss and the slower decomposition rate of the lignin fraction, as seen from the slope of the TGA curve.

3.2. Parameter Study

To determine the amounts of crosslinker and lignin that were required to form a stable gel, we performed a parameter study, based on the results that were presented in another report [20]. The various gels are shown in Figure 3. Vials 1B, 2B, and 3B are the results for the polysaccharide-rich stock solution after crosslinking 2 mL of the solution with 100, 200, and 300 µL epichlorohydrin (ECH), respectively, and a fixed amount of sodium hydroxide. A stable gel was formed with 200 µL ECH and higher. Decreasing the amount of ECH to 100 µL failed to form a coherent gel, due to the low degree of crosslinking, leaving the polysaccharide matrix stable in solution [28].

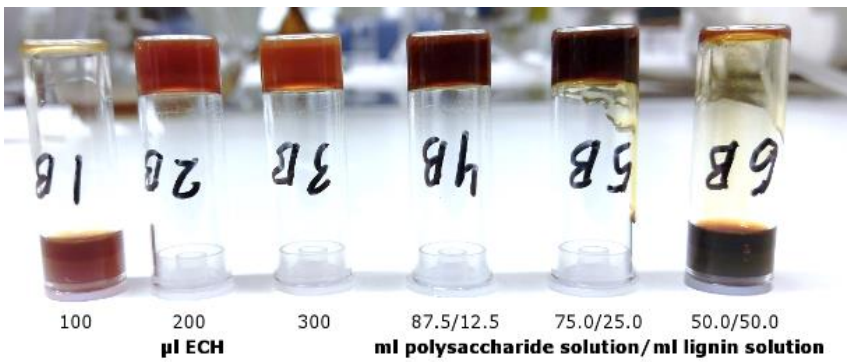


Figure 3. Visual representation of the resulting hydrogels after crosslinking of the polysaccharide solution (1B, 2B and 3B) at different ECH additions. The vials 4B to 6B show the effect of different lignin additions at a constant ECH dosage of 200 µL.

The color of the hydrogels differed, depending on the degree of crosslinking. The color forms from the dissociation of phenolic groups in the residual lignin in the stock polysaccharide solution [29,30] and is an indirect indication of the amount of sodium hydroxide that is consumed in the reaction; thus, the crosslinking reaction progressed further with the higher versus lowest amount of ECH.

Vials 4B to 6B show the effect of increasing amounts of lignin in the reaction mixture. The total dry substance, ECH, and sodium hydroxide levels were kept constant. To emulate the effect of greater lignin impurity in the stock solution, the amount of lignin was changed by decreasing the ratio of polysaccharide to lignin stock solution. Vials 4B to 6B had volumetric ratios of 87.5/12.5, 75.0/25.0, and 50.0/50.0 mL polysaccharide solution/mL lignin solution, respectively. In the latter sample, no coherent hydrogel formed; thus, the lignin concentration below this threshold was chosen for further study.

3.3. Effect of Crosslinking on Hydrogel Content

The parameters that were determined in Section 3.2 were applied to crosslink the polysaccharide-rich fraction with ECH volumes of 200, 250, and 300 µL. The results for the hydrogel content (percentage of component/total amount of component in the reaction mixture) are presented in Figure 4.

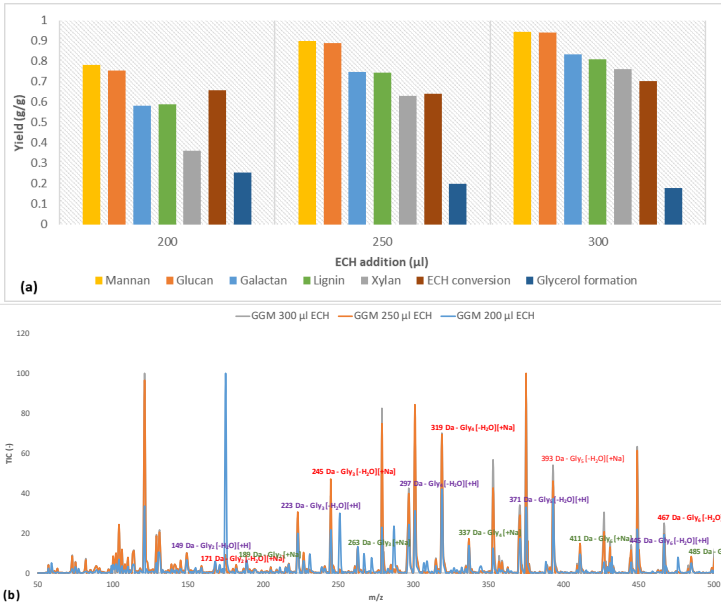


Figure 4. (**a**) The yields at different crosslinker additions for the various hydrogel bound solutes, ECH consumption and glycerol formation after the crosslinking reaction. (**b**) LC-MS of the wash solution (containing non-bound compounds) with highlighted m/z for the formed polyglycerols after the crosslinking reaction. Glyx is a polyglycerol with x number of subunits.

Initially, the mannan and glucan yields were approximately on the same order of magnitude for the 3 amounts of crosslinker. This result was not surprising, because the main polysaccharide in the solution was galactoglucomannan [18]. However, the small difference that existed might have been due to some of the glucans being bound to other components. The yields of galactan followed the increases in mannan and glucan throughout the series but were lower overall, because there were other galactan-based polysaccharides in the solution that were not associated with GGM. The 2 most common such polysaccharides in the raw material are arabinogalactan and B-galactan [18]. Also, certain polysaccharides were bound to lignin and formed lignin-carbohydrate complexes (LCCs). A clear indication of the existence of these complexes is found in the figure, in which the galactan yield approximated that of lignin for all samples (Figure 4). Furthermore, the galactans in the solution have a higher molecular weight than GGM [18,31], demonstrating that the crosslinking reaction did not depend on MW in this case. Overall, the yield was high in terms of the utilization of solutes, reducing the potential waste after the reaction.

The ECH conversion rate was between 64% and 70%; there was no discernable pattern versus the addition of ECH. However, the amount of ECH that was consumed increased as the proportion of ECH became larger, indicating that more glycerol bridges were formed between the polysaccharides (as evidenced by the rising yields in polysaccharides in Figure 4), but the formation of monoglycerol ether units could not be ruled out [32]. A common side reaction of crosslinking is the hydrolysis of ECH to glycerol, which in turn can react with ECH to form polyglycerols, as described by Kartha and Srivastava [32]. As shown in Figure 4, the formation of glycerol after the reaction decreased with higher ECH content.

Earlier studies provide explanations for the phenomenon [32]. One reason is that a higher level of ECH shifted the reaction from homogeneous to heterogeneous due to the low solubility of ECH in water (roughly 7%), wherein the heterogeneous reaction of ECH has been found to result in low

glycerol yields. Also, at an excess of ECH, the reaction may begin to polymerize ECH into dimers and trimers. Therefore, it is also possible that these polyglycerols form and bind to the hydrogels at higher amounts of ECH, thus lowering the observed glycerol yield. This phenomenon was also indicated by the LC-MS measurements, as seen in Figure 4b, in which glycerol polymers were found to contain up to 6 glycerol units. The large number of peaks that were detected was the result of various existing adducts (sodium and proton) and the dehydration of polyglycerols to varying extents [33]. However, the trend was the same, regardless of which adduct or dehydrated peak was compared.

By comparing the signals with the strongest intensity (mono-dehydrated polyglycerols with sodium adduct), we found that the intensity for polyglycerols with over 4 glycerol units rose with increasing ECH levels. Notably, this finding was consistent with decreasing intensity in the region with fewer than 4 glycerol units for the sample with the highest amount of ECH, highlighting the transition from crosslinking monoglycerol units to oligomers. The overall trend in Figure 4b was a shift in the distribution of polyglycerol toward a higher degree of polymerization with increasing ECH levels, strengthening the observations made regarding the decrease in the formation of glycerol.

3.4. Effect of Addition of Lignin on Hydrogel Content

Based on the results of the parameter study (Section 3.2), various amounts of the lignin fraction were added to the reaction mixture. The data on the content of the synthesized hydrogels are presented in Figure 5. Adding lignin to the mixture decreased the yield for most solutes. Mannan and glucan continued to follow the same trend regarding yields, as shown in Section 3.3. The yields at high lignin content (29.9 g/L) were nearly identical to those for GGM hydrogels with low crosslinking (Figure 4), indicating that the crosslinking reaction favored the reaction with GGM, followed by galactans and xylans, independent of the lignin that was added.

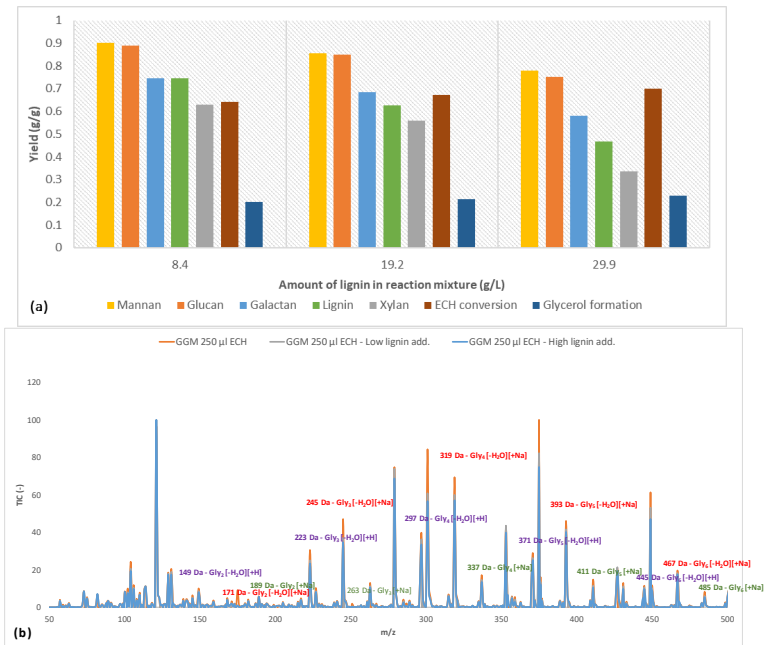


Figure 5. (**a**) The yields at different lignin additions for the various hydrogel bound solutes, ECH consumption and glycerol formation after the crosslinking reaction. (**b**) LC-MS of the wash solution (containing non-bound compounds) with highlighted m/z for the formed polyglycerols after the crosslinking reaction. Glyx is a polyglycerol with x number of subunits.

However, the yields for lignin differed from those in Figure 4. The trend was for more of the lignin to bind to the hydrogel, even with decreasing yield. These results implicate fewer crosslinks between the polysaccharides after the addition of lignin. Nevertheless, the consumption of ECH clearly rose, attributed to the formation of more glycerol (Figure 5a) but also perhaps to the crosslinking of low-MW non-gel-bound lignin. The polymerization of glycerol declined with increases in lignin addition by LC-MS (Figure 5b), supporting the possibility of the polymerization of low-MW non-gel-bound lignin.

3.5. FTIR on Hydrogels

FTIR measurements were performed on the hydrogels (see Figure 6a). The spectra for the hydrogels were nearly identical to that of the polysaccharide fraction, differing only by the disappearance of the peak at 1736 cm^{-1} (acetyl groups) for the hydrogels. Deacetylation usually occurs when the pH is higher than 3 and at high temperatures [34,35]. Further, at high sodium hydroxide concentrations, it could ensue at lower temperatures [20]. Given that the pH after the addition of sodium hydroxide to the reaction mixture was over 13, this latter mechanism was what likely occurred.

No other differences were expected, because the major modification to the hydrogels was the addition of the glycerol bridge and the removal of hydroxyl groups, both of which had signals that coincided with those in the polysaccharide fraction. However, the intensities of these signals will vary, depending on the type of modification that occurred. These changes in intensities were seen by comparing the ratios of the absorbance peak height on various signals (Figure 6b). The gels had a higher ether bond (C-O-C) intensity than the polysaccharide fraction, which was expected, because crosslinking increases the formation of ether bonds and the removal of hydroxyl (OH) groups. However, the ratio decreased with rising ECH, which does not necessarily mean that the proportion of ECH that reacted declined overall. Yet, the proportion of crosslinks was smaller than that of hydroxyl groups, perhaps due to the formation of mono-glycerol ether units instead of a glycerol bridge, instead increasing the hydroxyl groups overall, in turn supporting the previous claim (Figure 4).

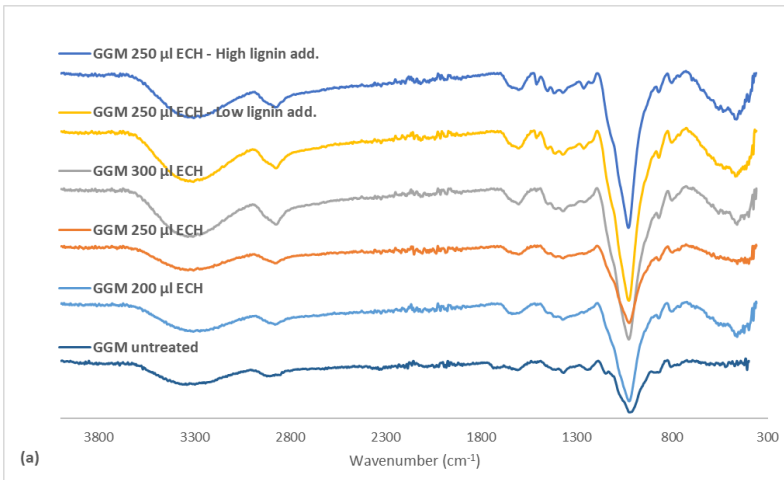


Figure 6. *Cont.*

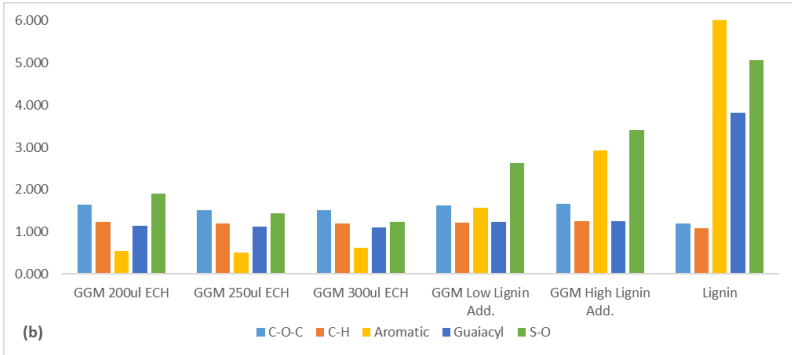


Figure 6. (**a**) FTIR spectrum comparing the produced hydrogels. (**b**) The ratio between the FTIR absorbance of a hydrogel and the non-treated GGM at different wavenumbers. C–O–C is the ratio for the ether bonds (1026 $cm^{-1)}$, the C–H ratio was based on the wavenumber 2930cm^{-1}, aromatic was measured at 1509 cm^{-1}, guaiacyl was calculated as the sum of the three wavenumbers between 1262–1142 cm^{-1} and S–O absorbance was measured at 650 cm^{-1}. The legend includes the ECH and lignin additions for the crosslinking reaction. Low lignin addition represented the 87.5/12.5 mL polysaccharide solution/mL lignin solution and the high lignin addition 75.0/25.0 mL polysaccharide solution/mL lignin solution.

The addition of lignin to the samples increased the C–O–C/OH ratio, likely due to the higher C–O–C/OH ratio in the added lignin. The strong indicators for bound lignin was the peak at 1509 (aromatic skeletal vibrations), the sum of the peaks for guaiacyl structures (1262–1142 cm^{-1}), and the sulfonate groups (650 cm^{-1}). The rise in crosslinking did not have a major impact on the ratios of the aromatic skeletal vibrations or the sum for the guaiacyl signals, indicating that the base structure of the lignin was consistent. However, the ratio for the sulfonate groups decreased. These results thus show that the highly charged (sulfonated) lignin was bound first, followed by the less sulfonated lignin. The increase in lignin before the crosslinking reaction enhanced the intensity of these peaks, wherein the sample that contained the highest amount of lignin had the strongest signals in this region. These results, coupled with the trend in Figure 5, thus show that some of the added lignin bonded to the hydrogel.

3.6. Size-Exclusion Chromatography

The SEC results (Figure 7a) demonstrated that the GGM fraction contained 3 major MW regions. The high-MW region (between 5 and 10 min of retention time) contains the lignin and lignin-carbohydrate complexes [17,18], as evidenced by the UV absorption of that fraction (Figure 7b). The mid-MW region (approximately 20 min, Figure 7a) contained GGM and has little to no UV absorption; thus, it harbored low to negligible amounts of lignin. The third peak (>25 min) contained most of the remaining low-MW compounds, such as monosaccharides and pulping chemicals.

The results in Figure 7a also show the MW of components that were not bound during the hydrogel synthesis (wash solution) at various degrees of crosslinking. The results implicated the mid-MW compounds being consumed first at low ECH concentrations, followed by the high-MW compounds, the consumption of which rose with the addition of ECH. The remaining peak in the mid-MW region was possibly lignin that was released from the high-MW lignin-carbohydrate complexes by hydrolysis, based on the increase in UV absorption in that region, as seen in Figure 7b and confirmed in our previous work [17], in which enzymatic hydrolysis of the carbohydrate segment of the LCCs released lignin in the same MW range. The same trend was seen for the case in which the lignin concentration increased in the reaction mixture (Figure 7c,d).

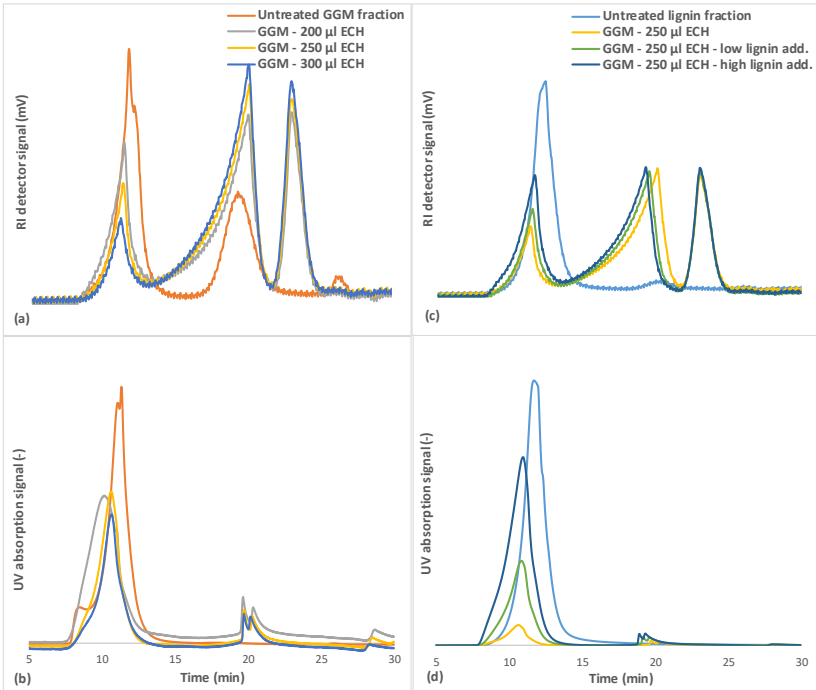


Figure 7. SEC for the untreated GGM and lignin solutions and the wash solutions after the crosslinking reaction. (**a**,**c**) is showing the response from the RI detector, and (**b**,**d**) the UV detector. The legend includes the ECH and lignin additions for the crosslinking reaction. Low lignin addition represented the 87.5/12.5 mL polysaccharide solution/mL lignin solution and the high lignin addition 75.0/25.0 mL polysaccharide solution/mL lignin solution.

Previous observations (Sections 3.4 and 3.5) showed that not all of the lignin was bound to the hydrogel but that more ECH was consumed with increases in lignin, because the crosslinking of the lignin yielded larger water-soluble macromolecules that did not bind to the hydrogel.

The rise in MW can be observed in Figure 7d, in which the MW of the lignin shifted toward the heavier end of the spectrum after the crosslinking reaction. The reason for the lignin failing to bind to the hydrogel could be the difference in solubility between these components. The solubility of GGM likely decreased after the addition of sodium hydroxide to the reaction mixture, due to the deacetylation of the polysaccharide, leading to heterogeneous (slow) crosslinking [36]. The solubilities of lignin and lignosulfonates during alkali conditions do not change (at room temperature), and thus, the crosslinking reaction is more homogeneous (fast). A third peak was observed after the crosslinking reaction in the region at approximately 23 min (Figure 7), likely comprising crosslinked monosaccharides and oligosaccharides or possibly polyglycerols, as identified by LC-MS in Figures 4b and 5b.

3.7. Swelling Degree and Drug Release

The swelling behavior of the hydrogels was determined in deionized water. Swelling degree can be altered by changes in the amount of crosslinker or by the concentration of functional materials [10]. The swelling behavior was therefore expected to change, depending on the amount of ECH that was added but also possibly the lignin levels.

The results on the swelling degree of the hydrogels are presented in Figure 8a. The hydrogel with the lowest degree of crosslinking had an initial swelling degree of 137 g water/g dry hydrogel, which was in the same range as reported by Maleki, et al. [10] using the same raw material. As expected, the swelling degree of the hydrogels decreased with greater amounts of crosslinker, because the higher amount of crosslinks that are formed in turn compacts the hydrogel structure and decreases the number of available sites for water to penetrate [37,38]. At the highest level of ECH, the hydrogel had a swelling degree of approximately 38 g/g—much lower than the low-crosslinked hydrogel but still in the range of usable hydrogels for many applications.

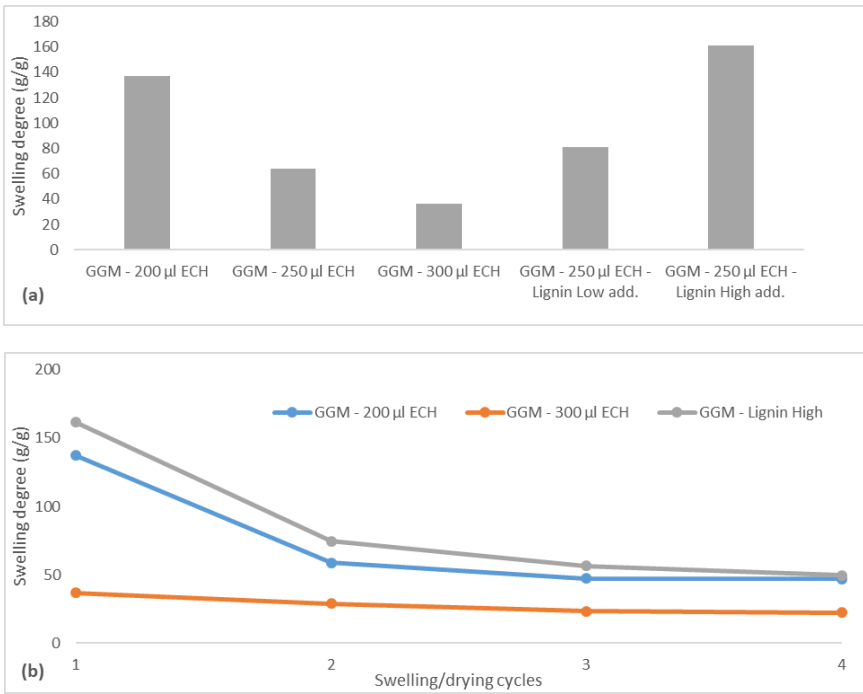


Figure 8. (**a**) The swelling degree for the different hydrogels after synthesis. (**b**) The swelling degree for three selected hydrogels after consecutive swelling and drying cycles. The legend includes the ECH and lignin additions for the crosslinking reaction. Low lignin addition represented the 87.5/12.5 mL polysaccharide solution/mL lignin solution and the high lignin addition 75.0/25.0 mL polysaccharide solution/mL lignin solution.

Increasing the amount of lignin in the hydrogels had the opposite effect, with the swelling degree instead rising, perhaps because the lignin consumed the ECH and remained soluble, yielding a hydrogel that was less crosslinked and had higher swellability, as indicated. Another explanation is that the addition of ionizable components (lignosulfonates) increased the initial osmotic pressure during swelling, thus resulting in a higher driving force for water uptake [39]. This phenomenon was observed when the BTB release was measured (Figure 9). By comparing the hydrogel with low and high ECH content, it was clear that the release of BTB was slower in the latter case, as expected, because the reduced mobility of the polymer impeded the penetration of the solvent [39]. The opposite effect was anticipated for the sample to which a higher amount of lignin was added, given that the swellability was greater (Figure 8a). However, the release was slower, as shown in Figure 9, likely due to the higher osmotic pressure and thus greater water influx at the beginning of the release of BTB.

This effect diminished after approximately 30 min, at which point the high-lignin hydrogel was nearly completely swollen, and thus, the release of BTB increased.

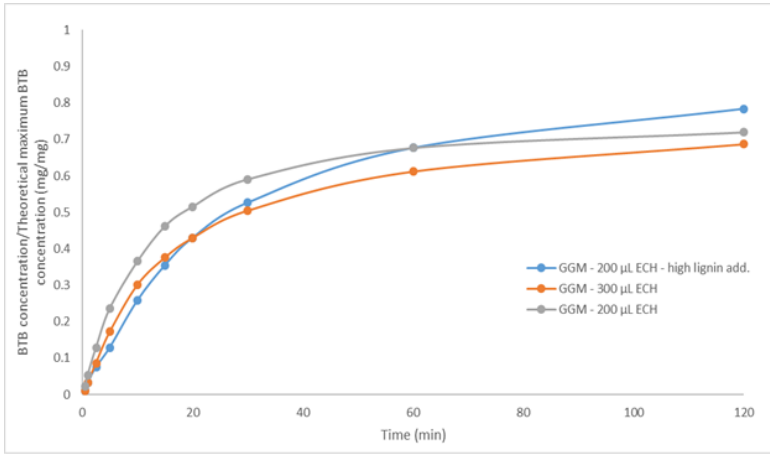


Figure 9. The release of BTB from three different hydrogels as a function of time. The legend includes the ECH and lignin additions for the crosslinking reaction. High lignin addition corresponds to 75.0/25.0 mL polysaccharide solution/mL lignin solution.

The repeated swelling and drying of hydrogels is an important property for certain applications in which the reusability of hydrogels is a key element, such as in agriculture [10]. This step was performed for 3 of the hydrogels, as seen in Figure 8b. All hydrogels experienced the largest change at the beginning of the swelling-drying cycles and reached a constant swelling degree after 2 consecutive cycles. The high-lignin hydrogel and that with the low ECH reached a stable swelling degree of approximately 50 g/g, which was greater than for the highly crosslinked hydrogel (22 g/g). That these hydrogels reached the same equilibrium strengthens the observations in Figure 8a.

3.8. Mechanical Strength

The cylindrical hydrogels were tested mechanically to obtain compression stress-versus-strain curves. All of the hydrogels demonstrated strain tolerances of over 44%, as seen in Figure 10. The curves were not linear but followed an exponential increase, demonstrating the softness of the gels [40]. The maximum ultimate tensile strength (UTS) for these hydrogels was 21 kPa, which is in the same range as for other pure hemicellulose hydrogels [41]. The graphs also show that a yield strength existed wherein further compression of the hydrogels resulted in irreversible deformation, due to internal fractures or breaks, which were visible throughout the transparent hydrogel during compression.

Greater crosslinking enhanced the UTS of the hydrogels, decreasing the strain (Figure 10a), thus yielding hydrogels with greater mechanical strength and less flexibility (higher brittleness). This finding was not apparent from the results because the strain also increased with the addition of ECH. However, the compression modulus—the ratio between compression stress and strain—rose with the addition of ECH; thus, the stiffness of the hydrogels increased [40]. The opposite effect was observed with higher lignin content (Figure 10b). The UTS of the hydrogels decreased with greater amounts of lignin, likely attributed to the fewer crosslinks that formed when lignin was added. The compression modulus also declined, indicating that the hydrogels had greater flexibility, likely caused by the higher swelling degree.

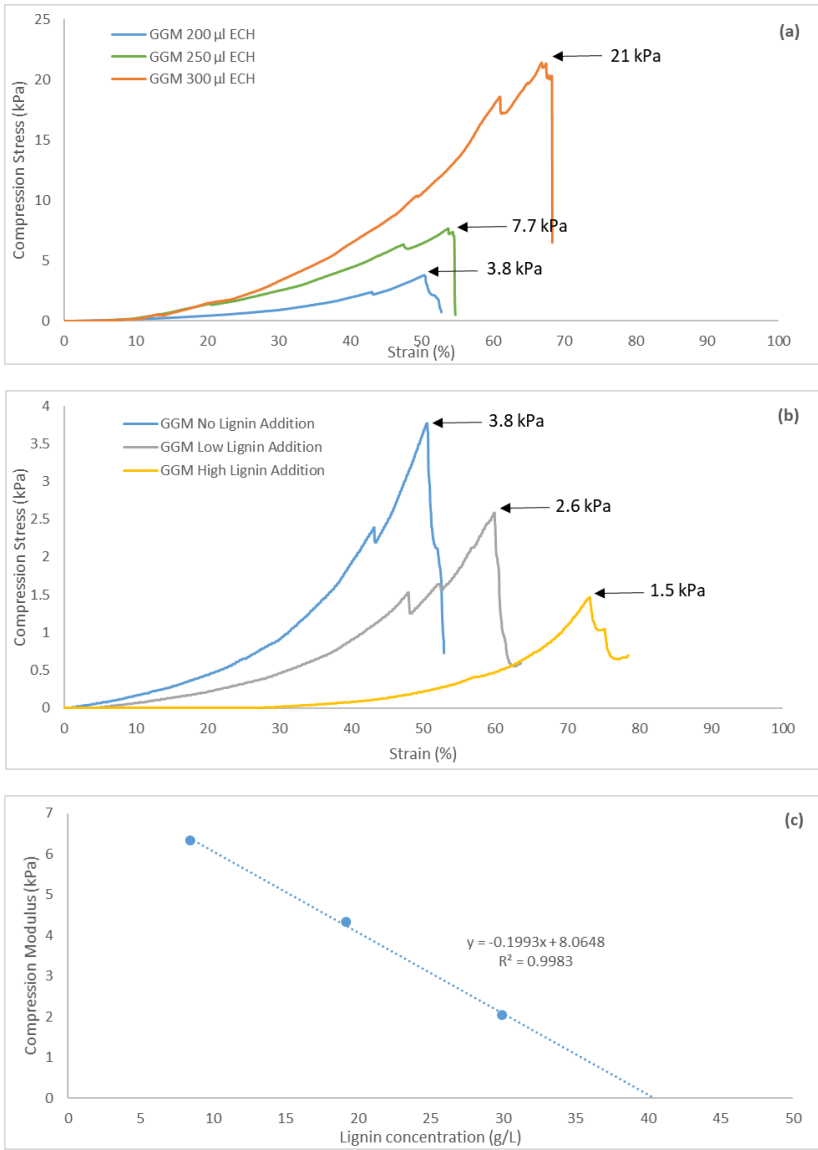


Figure 10. Compression stress and strain for (**a**) three hydrogels at different ECH additions and (**b**) three hydrogels with different lignin additions and a constant (200 µL) ECH addition. Low lignin addition represented the 87.5/12.5 mL polysaccharide solution/mL lignin solution and the high lignin addition 75.0/25.0 mL polysaccharide solution/mL lignin solution. (**c**) A curve of the compression modulus as a function of lignin concentration in the base reaction mixture. The compression modulus was determined at the point of maximum UTS.

During the parameter study, a limit for hydrogel formation was reached when 50/50 mL polysaccharide solution/mL lignin solution was added, corresponding to a near-zero compression modulus, based on the lack of a network structure that resisted the compressible forces [42]. A linear

relationship was observed between compression modulus and lignin concentration in the bulk solution (Figure 10c). Extrapolation of the curve to a compression modulus of 0 gave the lignin a concentration of 40.5 g/L, which was well in the range of the limit that was observed during the parameter study.

3.9. Thermo-gravimetric Analysis

TGA was performed on the synthesized hydrogels (Figure 11). All of the hydrogels had a DTG peak at approximately 33 °C, which corresponded to residual solvents, as seen with the purified GGM and lignin in Section 3.1. In the second degradation stage, 1 DTG peak was observed for the hydrogels with varying amounts of ECH (Figure 11a). For the lowest amount of ECH that was added, the DTG peak occurred at 265 °C, higher than the degradation temperatures of GGM and xylan, as seen in Figure 2. Further, a significant amount of GGM was consumed at the lowest ECH level, as evidenced by SEC and the yields (Figures 4 and 7); thus, the rise in temperature was possibly the result of additional bonds (crosslinks), which was also a factor when the ECH was increased from 200 to 250 µL and the DTG peak temperature climbed to 293 °C. However, the LCCs in the solution were bound at higher ECH levels, which also contributed to the increase in DTG peak temperature (Figure 2). The enhancement in yield between 250 and 300 µL ECH was minimal (Figure 4), which explains the small increase in DTG peak temperature from 293 to 298 °C.

Greater amounts of lignin in the bulk mixture before the reaction had the opposite effect, as apparent from the decrease in DTG peak temperature from 293 to 282 °C in the low-lignin sample and to 271 °C in the high-lignin sample (Figure 11b). This finding is explained by the lower crosslinking, which decreased the amount of bound LCCs, as observed by the change in yields in Figure 5. For the same reason, the results in the previous sections show that the properties of the hydrogel to which the highest amount of lignin was added were similar to that with the lowest ECH content.

In contrast, the thermal properties of the hydrogels developed a disparate pattern. In addition to the higher DTG peak temperature of 271 °C, an increase in the region of 400 to 600 °C could be observed. The peaks in this region were clearly visible on TGA of the lignin but absent in the GGM sample, as seen in Figure 2, confirming previous indications that the added lignin bound to the hydrogel. This bond was also likely the reason for the increase in temperature for the peak in the region of 200 to 300 °C, wherein lignin had a higher degradation temperature compared with GGM (Figure 2). Although the degradation temperature declined with the addition of lignin, the rate of decomposition decreased as well; thus, the thermal properties of the hydrogels approached those of lignin (Figure 2).

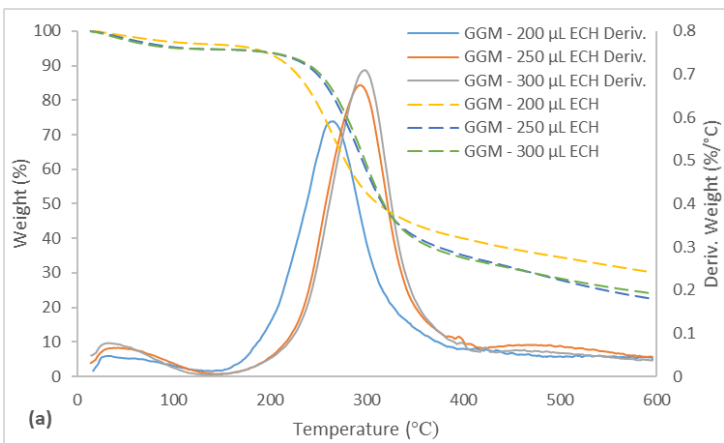


Figure 11. *Cont.*

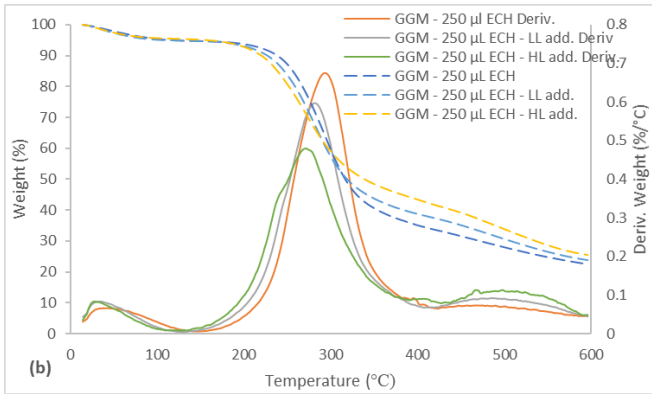


Figure 11. TGA and DTG curves for the synthesized hydrogels between the temperatures of 15 and 600 °C. (**a**) The legend includes the ECH and lignin additions for the crosslinking reaction. (**b**) (LL) Low lignin addition represented the 87.5/12.5 mL polysaccharide solution/mL lignin solution and (HL) the high lignin addition 75.0/25.0 mL polysaccharide solution/mL lignin solution. Deriv. is the acronym for the DTG curve.

4. Conclusions

The combination of ultrafiltration and anti-solvent precipitation was successful in fractionating SSL into 2 streams: polysaccharide-rich and lignin-rich. FTIR measurements of these fractions confirmed the separation of these entities. TGA revealed distinct profiles for GGM and lignin, the latter of which had higher thermal stability. The parameter study showed that the least amount of ECH that was needed for the formation of a hydrogel was 200 µL when 2 mL of stock solution was used. The lignin concentration should also be kept under ~50 g/L to synthesize a coherent gel.

Based on the variation in the degree of crosslinking, the mannan and glucan were linked, given that their yields during the reactions had the same trend and magnitude. Galactans also followed the same pattern, but their overall yield was low compared with the mannans and glucans, because other galactans existed in the mixture. By LC-MS, the increase in crosslinker concentration accelerated the hydrolysis of ECH to glycerol but also the polymerization of glycerol to di-, tri-, tetra-, penta-, and hexamers. The addition of lignin to the reaction mixture decreased the yields for the polysaccharides and the polymerization of glycerol. However, the consumption of ECH rose, due to the lignin consuming the crosslinker and forming larger water-soluble macromolecules, as seen by LC-MS and SEC. Some of the lignin bound to the hydrogel, as confirmed by the FTIR measurements, wherein the peak intensities for aromatic skeletal vibrations (1509 cm^{-1}), guaiacyl structures (1142–1262 cm^{-1}), and sulfonate groups (650 cm^{-1}) increased.

With regard to swelling degree, hydrogels with low crosslinking reached an equilibrium of approximately 137 g water/g dry hydrogel, and for hydrogels that contained lignin, higher water absorption was observed. The hydrogel with the greatest amount of lignin had the slowest initial release of BTB due to the higher osmotic pressure and water uptake. Repeated swelling and drying of the hydrogels yielded an equilibrium after 2 consecutive cycles, peaking at roughly 50 g/g for hydrogels with the lowest amounts of ECH.

The hydrogels were tested mechanically, based on compression (stress vs strain). A maximum UTS of 21 kPa was reached for the pure GGM hydrogels, whereas the UTS fell with increasing amounts of lignin. A linear relationship between lignin concentration and compression modulus was observed, which also yielded a peak lignin concentration of 40.5 g/L for the formation of a coherent hydrogel.

The TGA results showed that the degree of crosslinking had a minor effect on the maximum DTG peak temperature; instead, the DTG temperature depended on the yield of the bound LCCs.

The addition of lignin to the reaction mixture negatively impacted the DTG peak temperature (decreasing). However, the decomposition rate also declined, increasing the thermal stability of the hydrogel.

Author Contributions: Funding acquisition, O.W.; Investigation, B.A.-R. and M.A.H.; Methodology, B.A.-R. and M.G.; Supervision, P.J. and O.W.; Validation, B.A.-R., M.A.H., P.J. and O.W.; Visualization, B.A.-R.; Writing—original draft, B.A.-R.; Writing—review & editing, M.G., P.J. and O.W.

Funding: This research was partially funded by the Swedish Foundation for Strategic Research (SSF) (RBP 14-0046), which is gratefully acknowledged.

Acknowledgments: Thanks to Domsjö Fabriker for providing us with the raw material that was used in this study. Many thanks to Dr. Herje Schagerlöf for the help with the LC-MS analysis.

Conflicts of Interest: The authors declare no conflict of interest. The funders had no role in the design of the study; in the collection, analyses, or interpretation of data; in the writing of the manuscript, or in the decision to publish the results.

References

1. Ahmed, E.M. Hydrogel: Preparation, characterization, and applications: A review. *J. Adv. Res.* **2015**, *6*, 105–121. [CrossRef] [PubMed]
2. Ahmadi, F.; Oveisi, Z.; Samani, S.M.; Amoozgar, Z. Chitosan based hydrogels: Characteristics and pharmaceutical applications. *Res. Pharm. Sci.* **2015**, *10*, 1–16. [PubMed]
3. Lee, K.Y.; Mooney, D.J. Alginate: Properties and biomedical applications. *Prog. Polym. Sci.* **2012**, *37*, 106–126. [CrossRef] [PubMed]
4. Chang, C.; Zhang, L. Cellulose-based hydrogels: Present status and application prospects. *Carbohydr. Polym.* **2011**, *84*, 40–53. [CrossRef]
5. Wang, J.; Sun, H.; Li, J.; Dong, D.; Zhang, Y.; Yao, F. Ionic starch-based hydrogels for the prevention of nonspecific protein adsorption. *Carbohydr. Polym.* **2015**, *117*, 384–391. [CrossRef] [PubMed]
6. Lin, C.; Zhao, P.; Li, F.; Guo, F.; Li, Z.; Wen, X. Thermosensitive in situ-forming dextran–pluronic hydrogels through Michael addition. *Mater. Sci. Eng. C* **2010**, *30*, 1236–1244. [CrossRef]
7. Wenzl, H. *The Chemical Technology of Wood*; Elsevier: Amsterdam, The Netherlands, 2012.
8. Söderqvist Lindblad, M.; Albertsson, A.-C.; Ranucci, E.; Laus, M.; Giani, E. Biodegradable polymers from renewable sources: Rheological characterization of hemicellulose-based hydrogels. *Biomacromolecules* **2005**, *6*, 684–690. [CrossRef]
9. Maleki, L.; Edlund, U.; Albertsson, A.-C. Synthesis of full interpenetrating hemicellulose hydrogel networks. *Carbohydr. Polym.* **2017**, *170*, 254–263. [CrossRef] [PubMed]
10. Maleki, L.; Edlund, U.; Albertsson, A.-C. Unrefined wood hydrolysates are viable reactants for the reproducible synthesis of highly swellable hydrogels. *Carbohydr. Polym.* **2014**, *108*, 281–290. [CrossRef] [PubMed]
11. Zasadowski, D.; Yang, J.; Edlund, H.; Norgren, M. Antisolvent precipitation of water-soluble hemicelluloses from TMP process water. *Carbohydr. Polym.* **2014**, *113*, 411–419. [CrossRef]
12. Jacobs, A.; Lundqvist, J.; Stålbrand, H.; Tjerneld, F.; Dahlman, O. Characterization of water-soluble hemicelluloses from spruce and aspen employing SEC/MALDI mass spectroscopy. *Carbohydr. Res.* **2002**, *337*, 711–717. [CrossRef]
13. Krawczyk, H.; Arkell, A.; Jönsson, A.-S. Impact of prefiltration on membrane performance during isolation of hemicelluloses extracted from wheat bran. *Sep. Purif. Technol.* **2013**, *116*, 192–198. [CrossRef]
14. Al Manasrah, M.; Kallioinen, M.; Ilvesniemi, H.; Mänttäri, M. Recovery of galactoglucomannan from wood hydrolysate using regenerated cellulose ultrafiltration membranes. *Bioresour. Technol.* **2012**, *114*, 375–381. [CrossRef] [PubMed]
15. Song, T.; Pranovich, A.; Holmbom, B. Separation of polymeric galactoglucomannans from hot-water extract of spruce wood. *Bioresour. Technol.* **2013**, *130*, 198–203. [CrossRef] [PubMed]
16. Thuvander, J.; Jönsson, A.-S. Extraction of galactoglucomannan from thermomechanical pulp mill process water by microfiltration and ultrafiltration—Influence of microfiltration membrane pore size on ultrafiltration performance. *Chem. Eng. Res. Des.* **2016**, *105*, 171–176. [CrossRef]

17. Al-Rudainy, B.; Galbe, M.; Wallberg, O. Influence of prefiltration on membrane performance during isolation of lignin-carbohydrate complexes from spent sulfite liquor. *Sep. Purif. Technol.* **2017**, *187*, 380–388. [CrossRef]
18. Al-Rudainy, B.; Galbe, M.; Schagerlöf, H.; Wallberg, O. Antisolvent precipitation of hemicelluloses, lignosulfonates and their complexes from ultrafiltrated spent sulfite liquor (SSL). *Holzforschung* **2018**, *72*, 839–850. [CrossRef]
19. Vermaas, J.V.; Petridis, L.; Qi, X.; Schulz, R.; Lindner, B.; Smith, J.C. Mechanism of lignin inhibition of enzymatic biomass deconstruction. *Biotechnol. Biofuels* **2015**, *8*, 217. [CrossRef]
20. Zhao, W.; Odelius, K.; Edlund, U.; Zhao, C.; Albertsson, A.-C. In situ synthesis of magnetic field-responsive hemicellulose hydrogels for drug delivery. *Biomacromolecules* **2015**, *16*, 2522–2528. [CrossRef] [PubMed]
21. Palamarchuk, I.; Brovko, O.; Bogolitsyn, K.; Boitsova, T.; Ladesov, A.; Ivakhnov, A. Relationship of the structure and ion-exchange properties of polyelectrolyte complexes based on biopolymers. *Russ. J. Appl. Chem.* **2015**, *88*, 103–109. [CrossRef]
22. Rönnols, J.; Schweinebarth, H.; Jacobs, A.; Stevanic, J.S.; Olsson, A.-M.; Reimann, A.; Aldaeus, F. Structural changes in softwood kraft lignin during thermal treatment. *Nord. Pulp Pap. Res. J.* **2015**, *30*, 550–561.
23. Watkins, D.; Nuruddin, M.; Hosur, M.; Tcherbi-Narteh, A.; Jeelani, S. Extraction and characterization of lignin from different biomass resources. *J. Mater. Res. Technol.* **2015**, *4*, 26–32. [CrossRef]
24. Ye, H.; Zhang, Y.; Yu, Z. Effect of desulfonation of lignosulfonate on the properties of poly (lactic acid)/lignin composites. *BioResources* **2017**, *12*, 4810–4829. [CrossRef]
25. Lemes, A.P.; Soto-Oviedo, M.A.; Waldman, W.R.; Innocentini-Mei, L.H.; Durán, N. Effect of Lignosulfonate on the Thermal and Morphological Behavior of Poly(3-hydroxybutyrate-*co*-3-hydroxyvalerate). *J. Polym. Environ.* **2010**, *18*, 250–259. [CrossRef]
26. Leger, C.A.; Chan, F.D.; Schneider, M.H. Fractionation and characterisation of technical ammonium lignosulphonate. *BioResources* **2010**, *5*, 2239–2247.
27. Beall, F. Thermogravimetric analysis of wood lignin and hemicelluloses. *Wood Fiber Sci.* **2007**, *1*, 215–226.
28. Gebelein, C.; Koblitz, F. *Biomedical and Dental Applications of Polymers*; Springer Science & Business Media: Berlin, Germany, 2013; Volume 14.
29. Mussatto, S.I.; Fernandes, M.; Roberto, I.C. Lignin recovery from brewer's spent grain black liquor. *Carbohydr. Polym.* **2007**, *70*, 218–223. [CrossRef]
30. Swamy, N.K.; Singh, P.; Sarethy, I.P. Precipitation of phenols from paper industry wastewater using ferric chloride. *Rasayan J. Chem.* **2011**, *4*, 452–456.
31. Laine, C. *Structures of Hemicelluloses and Pectins in Wood and Pulp*; Helsinki University of Technology: Espoo, Finland, 2005.
32. Kartha, K.; Srivastava, H. Reaction of epichlorhydrin with carbohydrate polymers. Part II. Starch reaction mechanism and physicochemical properties of modified starch. *Starch-Stärke* **1985**, *37*, 297–306. [CrossRef]
33. Medeiros, M.A.; Araujo, M.H.; Augusti, R.; de Oliveira, L.C.; Lago, R.M. Acid-catalyzed oligomerization of glycerol investigated by electrospray ionization mass spectrometry. *J. Braz. Chem. Soc.* **2009**, *20*, 1667–1673. [CrossRef]
34. Xu, C.; Pranovich, A.; Vähäsalo, L.; Hemming, J.; Holmbom, B.; Schols, H.A.; Willför, S. Kinetics of acid hydrolysis of water-soluble spruce O-acetyl galactoglucomannans. *J. Agric. Food Chem.* **2008**, *56*, 2429–2435. [CrossRef] [PubMed]
35. Nebreda, A.P.; Grénman, H.; Mäki-Arvela, P.; Eränen, K.; Hemming, J.; Willför, S.; Murzin, D.Y.; Salmi, T. Acid hydrolysis of *O*-acetyl-galactoglucomannan in a continuous tube reactor: A new approach to sugar monomer production. *Holzforschung* **2016**, *70*, 187–194. [CrossRef]
36. Lundqvist, J.; Teleman, A.; Junel, L.; Zacchi, G.; Dahlman, O.; Tjerneld, F.; Stålbrand, H. Isolation and characterization of galactoglucomannan from spruce (*Picea abies*). *Carbohydr. Polym.* **2002**, *48*, 29–39. [CrossRef]
37. Jyothi, A.N.; Moorthy, S.N.; Rajasekharan, K.N. Effect of cross-linking with epichlorohydrin on the properties of cassava (*Manihot esculenta* crantz) starch. *Starch-Stärke* **2006**, *58*, 292–299. [CrossRef]
38. Hasanah, A.N.; Muhtadi, A.; Elyani, I.; Musfiroh, I. Epichlorohydrin as Crosslinking Agent for Synthesis of Carboxymethyl Cellulose Sodium (Na-CMC) as Pharmaceutical Excipient from Water Hyacinth (*Eichornia Crassipes* L.). *Int. J. Chem. Sci.* **2015**, *13*, 1227–1237.
39. Körner, A. *Dissolution of Polydisperse Polymers in Water*; Physical Chemistry 1, Lund University: Lund, Sweden, 2006.

40. Qi, X.-M.; Chen, G.-G.; Gong, X.-D.; Fu, G.-Q.; Niu, Y.-S.; Bian, J.; Peng, F.; Sun, R.-C. Enhanced mechanical performance of biocompatible hemicelluloses-based hydrogel via chain extension. *Sci. Rep.* **2016**, *6*, 33603. [CrossRef]
41. Peng, X.-W.; Ren, J.-L.; Zhong, L.-X.; Peng, F.; Sun, R.-C. Xylan-rich hemicelluloses-graft-acrylic acid ionic hydrogels with rapid responses to pH, salt, and organic solvents. *J. Agric. Food Chem.* **2011**, *59*, 8208–8215. [CrossRef]
42. Sakai, T.; Matsunaga, T.; Yamamoto, Y.; Ito, C.; Yoshida, R.; Suzuki, S.; Sasaki, N.; Shibayama, M.; Chung, U.-I. Design and fabrication of a high-strength hydrogel with ideally homogeneous network structure from tetrahedron-like macromonomers. *Macromolecules* **2008**, *41*, 5379–5384. [CrossRef]



© 2018 by the authors. Licensee MDPI, Basel, Switzerland. This article is an open access article distributed under the terms and conditions of the Creative Commons Attribution (CC BY) license (http://creativecommons.org/licenses/by/4.0/).

Paper IV

membranes

MDPI

Article

Galactoglucomannan Recovery with Hydrophilic and Hydrophobic Membranes: Process Performance and Cost Estimations

Basel Al-Rudainy, Mats Galbe, Frank Lipnizki and Ola Wallberg *

Department of Chemical Engineering, Lund University, P.O. Box 124, SE-221 00 Lund, Sweden
* Correspondence: ola.wallberg@chemeng.lth.se

Received: 11 July 2019; Accepted: 9 August 2019; Published: 10 August 2019



Abstract: In this study, we compared the GR51PP (hydrophobic/polysulfone) membrane with a series of hydrophilic (regenerated cellulose) membranes with the aim of increasing the retention of products and decreasing membrane fouling. The raw material used was a sodium-based spent sulfite liquor from the sulfite pulping process of spruce and pine. The results show that the hydrophilic membranes were superior to the hydrophobic membranes in terms of higher fluxes (up to twice the magnitude), higher product retentions and less fouling (up to five times lower fouling). The fouling was probably caused by pore blocking as observed in earlier studies. However, the hydrophilic membranes had a lower affinity for lignin, which was indicated by the lower retention and fouling. This also resulted in a separation degree, which was higher compared with the hydrophobic membrane, thus yielding a higher galactoglucomannan (GGM) purity. 2D HSQC NMR results show that no major structural differences were present in the hydrophilic and hydrophobic retentates. A techno-economical evaluation resulted in the RC70PP being chosen as the most cost-efficient membrane in terms of flux and product recovery.

Keywords: galactoglucomannan; lignin; lignin-carbohydrate-complex; lignosulfonates; ultrafiltration; fouling; cost-estimations

1. Introduction

Spent sulfite liquor (SSL) is a waste stream that is generated in the sulfite pulping process, where it is usually incinerated for the production of power and heat [1]. The solids content of SSL is typically 8–14 wt % and the main components are sugars (mono- and polysaccharides), lignosulfonates, extractives, and pulping chemicals [1,2]. Studies concerning the different wood components have also shown that a part of the lignin is covalently bound to polysaccharides, forming the so-called lignin-carbohydrate-complexes (LCC) [3]. This makes the different plant-based waste streams very complex in terms of composition, which depends both on the used biomass raw material and the extraction method.

SSL from spruce contains mainly lignosulfonates (LS), galactoglucomannan (GGM), arabinoglucuronoxylan and LCC [4]. It was further discovered by Giummarella et al. [5] that the main bonds between lignin and a carbohydrates are benzyl ether to xylan and phenyl-glycosidic to mannan. Other possible bonds, which have been established, exist between arabinan or galactan and lignin [4,6]. Du et al. [7] made similar observations, and found that the major LCC formations are found to be between lignin and mannan, xylan or glucan. The LCCs were shown to have a high molecular weight and were insoluble in dioxane/water mixtures.

Potential applications for GGM, lignin, and LCCs have been highlighted in many studies. The mentioned components could be used for the production of gas-barrier films, polymeric surfactants

and as drug carriers [8,9]. This makes the isolation and fractionation of these compounds very important for the future development of innovative products.

Membrane filtration is a technology that has shown promise in this field. Many different studies have been conducted on wood-based process waters to fractionate and isolate these components. Al Manasrah et al. [10] recovered 70% of the GGM in spruce saw dust hot-water extracts with a GGM purity of 63% at a volume reduction (VR) of 86% using ultrafiltration membranes. Duval et al. [11] used regenerated cellulose membranes with a molecular weight cutoff between 1 and 30 kDa to fractionate lignosulfonates with high polydispersity. The authors' results also showed that it was possible to obtain retentates with low polydispersity index and high yields. Bhattacharya et al. [12] used ultrafiltration membranes to recover lignosulfonates from SSL. The authors compared different membrane materials, such as polysulfone, regenerated cellulose, and fluoropolymer. The results showed that a high molecular weight cutoff (MWCO) polysulphone membrane was optimal in terms of flux and rejection. In addition, a tendency for fouling of the polysulphone membranes as part of their flux vs time figures was also noticed; however, the differences between the membranes in terms of fouling were not discussed.

LCCs have been shown to be difficult to isolate using membrane filtration [13]; the reason is the narrow MW difference between the GGM and the LCCs and, in some cases, the formation of a fouling layer on the membrane surface that increases the retention of all solutes and thus prevents fractionation. Membrane filtration has been shown to be successful in concentrating and purifying the SSL from pulping chemicals and other low MW compounds; however, for the separation of the components other methods have to be used.

To solve the fractionation problem, anti-solvent precipitation has been shown to be an effective method. Compared to membrane filtration, anti-solvent precipitation utilizes the difference in solubility of different solutes and thus can separate components with narrow molecular weight differences [4,14,15]. This has been used by Song et al. [14] to separate GGM from a spruce hot-water extract with ethanol as anti-solvent. The efficiency of the precipitation and yield of product was high; however, the amount of ethanol consumed was around 90% of the in-going raw material feed; thus, the conclusion was that the separation process is too costly. Zasadowski et al. [15] separated GGM from lignin using the same process and obtained results showing that acetone was a more efficient anti-solvent. Acetone has a lower dielectric constant (lower polarity), which lowers the polarity of the bulk solvent at a reduced addition compared to ethanol [4]. The process could be further improved by concentrating the raw material before the anti-solvent addition, causing further reduction in solvent requirement and increasing the product yield. In this case, the combination of membrane filtration and anti-solvent precipitation is beneficial. Membrane filtration is used to concentrate the SSL solution and to remove pulping chemicals through diafiltration. The concentrated and purified SSL is then fed to the anti-solvent process to separate the different solutes. This process requires the membrane filtration to be efficient in terms of a high flux, high retention of products, and low fouling.

In a previous study, the isolation of GGM, lignin, and LCCs from spent sulfite liquor, and the minimization of membrane fouling was examined [13]. Three hydrophobic membranes with molecular weight cutoffs (MWCOs) of 100, 50, and 25 kDa, respectively, were screened for this purpose. Flux and retention for the 100 and 50 kDa membranes were identical, which indicated that the separation properties of the membranes were determined by the fouling layer on the membranes and not the pore size. The membrane with the 50 kDa MWCO performed best in terms of flux and retention of product and was less prone to fouling. Prefiltration of the raw material using microfiltration increased the capacity of the 50 kDa MWCO membrane and the effect of membrane fouling was nearly eliminated. The retention of the product was, however, high during the microfiltration. This resulted in high losses of product during the prefiltration stage. Dead-end filtration has been shown to be a promising alternative to microfiltration, because of its potentially lower loss of product. However, dead-end filtration requires the use of filter-aids (e.g., diatomaceous earth) which could affect the pulp mill recovery process in the case of any membrane filtration failures.

Another way of decreasing membrane fouling is by increasing the hydrophilicity of the membrane material. Lignin as a hydrophobic macromolecule usually adsorbs to hydrophobic membrane materials through non-covalent interactions [16]. This adsorption can thus occur on the surface of the membrane, inside the membrane pores and cause blocking and non-reversible fouling [13,17]. Li et al. [17] showed that membrane fouling occurred during ultrafiltration of kraft-lignin using polysulfone membranes. The observed effects were a declining flux over time and the formation of a yellow coating layer on the membrane surface that could not be removed either by water or by a 0.1 M NaOH solution. As a reference, regenerated cellulose membranes were used in the same study. The result was that the permeability was unaffected by exposing the membrane to a kraft-lignin solution and no yellow coating was formed on the membrane surface. This showed that by switching to a hydrophilic membrane, fouling could be decreased or avoided. A similar study was carried out by Puro et al. [18] where a method was developed and evaluated to identify foulants during ultrafiltration of ground wood mill circulation water. In the study, three membranes were used: two hydrophobic (polyethersulfone and polyamide) and one hydrophilic (regenerated cellulose). The major foulants detected were fatty acids, resins, and lignans, all of which are mainly hydrophobic compounds. Consequently, the hydrophobic membranes were heavily fouled while the hydrophilic membrane was mildly fouled. This was also confirmed from a seven day long flux measurement where the hydrophobic membranes experienced a decrease from 200 to 30 L/m^2 h, while the hydrophilic membrane maintained a constant flux of around 360 L/m^2 h.

The aim of this study was to compare the optimal hydrophobic membrane found in a previous study [13] to regenerate cellulose membranes with different MWCOs. The difference between the retentates obtained using the hydrophobic and hydrophilic membranes was examined and a cost estimation was used to determine which membrane was the most cost efficient.

2. Materials and Methods

2.1. Raw Material

The raw material used was a sodium-based spent sulfite liquor, which was extracted from the first step in a two-step softwood (60% *Picea abies* and 40% *Pinus sylvestris*) pulping process (Domsjö Fabriker, Örnsköldsvik, Sweden).

2.2. Equipment and Experimental Procedure

2.2.1. Membranes and Membrane Filtration Set-Up

The hydrophilic membranes used in this study are listed in Table 1. The hydrophobic membrane used in our previous study is also included as reference. All of the membranes withstand 50 °C solutions with pH between 2–10 and operating pressures of 1 to 10 bars.

Table 1. List of membranes used in the study, where MWCO denotes molecular weight cut-off.

Designation	Manufacturer	MWCO (kDa)	Membrane Material	Hydrophilicity
GR51PP	Alfa Laval Nordic A/S	50	Polysulfone	Hydrophobic
C30F	Microdyn-Nadir GmbH	30	Regenerated cellulose	Hydrophilic
C20F	Microdyn-Nadir GmbH	20	Regenerated cellulose	Hydrophilic
RC70PP	Alfa Laval Nordic A/S	10	Regenerated cellulose	Hydrophilic
C5F	Microdyn-Nadir GmbH	5	Regenerated cellulose	Hydrophilic

The studies were done using a 400 mL stirred vessel shown in Figure 1. The vessel was heated using a heating plate (MR2002, Heidolph Instruments GmbH & Co.KG, Schwabach, Germany) and the cross-flow velocity (CFV) was controlled by changing the speed of the internal magnetic stirrer. The conversion between CFV and speed of the internal magnetic stirrer was implemented according to previous work [13]. The pressure was monitored using a digital pressure gauge (DCS40.0AR,

Trafag AG, Bubikon, Switzerland) and changed through a valve connected to a nitrogen gas line. The flux was measured using a balance (PL6001-l, Mettler Toledo Inc., Columbus, OH, USA).

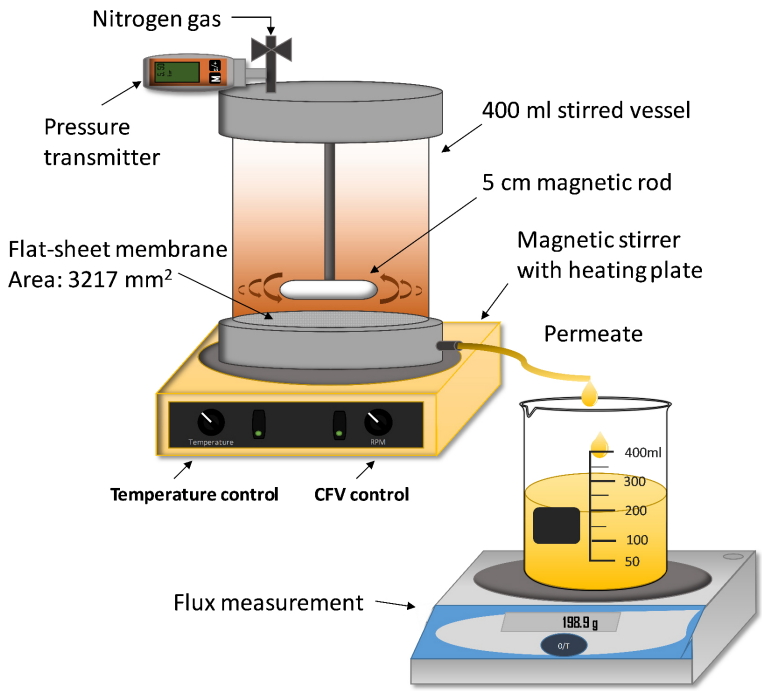


Figure 1. Illustration of the setup used for the membrane filtration. CFV = cross-flow velocity.

2.2.2. Influence of Volume-Reduction on Flux and Retention (Concentration Study)

The concentration studies were performed according to parameters derived in previous work [13]. The temperature, CFV, transmembrane pressure (TMP), and volume reduction were, 50 °C, 0.5 m/s, 5.5 bar and 90%, respectively. The process was started by cleaning a new membrane according to Section 2.2.3 and the pure water flux (PWF) was measured thereafter. The SSL was then filtered through 250, 180, and 45 µm filter trays (U.S.A. Standard Testing Sieve, WS Tyler Inc., Mentor, OH, USA) in series and loaded into the 400 mL vessel (Figure 1). The solution was then heated with the heating plate and pressure was applied when a temperature of 50 °C was reached and the flux recorded. When the specified volume reduction (ratio between the permeate and total initial volume) was achieved, the process was stopped, and samples of both permeate and retentate were taken. The membrane was cleaned again according to Section 2.2.3 and the PWF measured once more.

2.2.3. Membrane Cleaning and Fouling Calculations

The concentration studies began and ended with a cleaning using a 0.04 wt % acid detergent solution (Ultrasil 73, Ecolab AB, Älvsjö, Sweden) followed by measuring the PWF. A detergent volume of 350 mL was loaded into the module and heated to 50 °C under constant stirring (CFV of 0.5 m/s) and was left for around 1 h. The solution was then filtered through the membrane until a volume reduction of 50% was achieved (175 mL of the solution was passed to the permeate). The remaining retentate was discarded and the membrane was washed using 2 module volumes of deionized water at room temperature. The module was then filled with deionized water and the flux was measured at 20 °C,

0.5 m/s in CFV, and a trans-membrane pressure of 5.5 bar. The fouling degree was calculated from the flux of the deionized water (also called PWF) before and after the experiments, as per expression:

$$FoulingDegree(\%) = 100 * \frac{PWF_{\text{Before}} - PWF_{\text{After}}}{PWF_{\text{Before}}} \quad (1)$$

2.3. Analysis

2.3.1. Lignin Content

The concentration of lignin in solution was determined using a spectrophotometer (Shimadzu UV-1800, Kyoto, Japan). The wavelength was set to 234 nm and the extinction coefficient used was 31.6 L/(g cm) [13].

2.3.2. Ash and Total Dry Content

The total dry content was determined by weighing 3 mL of sample in a ceramic crucible and drying it in an oven (Heraeus, Heraeus Holding GmbH, Hanau, Germany) at 105 °C for 24 h after which the sample was weighed again. After determining the total dry content, the samples were placed in a furnace (B150, Nabertherm GmbH, Lilienthal, Germany) where they were ashed at 575 °C for 4 h. The ash content was determined by weighing the samples after they had cooled down to room temperature in a desiccator.

2.3.3. Hemicellulose and Acid-Insoluble Solids

The hemicellulose content was determined according to a standardized National Renewable Energy Laboratory (NREL) method [19]. The samples were acid hydrolyzed by adding 750 µl 72% sulfuric acid to 10 mL sample and autoclaved (Systec DX 150, Wettenberg, Germany) at 121 °C for 1 h. The samples were thereafter filtered to remove the acid-insoluble solids. The filter was then dried and weighed to determine the acid insoluble content. The filtrate was diluted with deionized water and analyzed with high-performance anion-exchange chromatography (HPAEC). The HPAEC system consisted of an ICS-5000+ DC (Dionex, Sunnyvale, CA, USA) equipped with pulsed amperometric detection running at a compartment temperature of 30 °C. The different monosaccharides were separated using a Carbo Pac PA1 analytical column where the eluent was deionized water at a flow of 1 and 0.5 mL/min 200 mM sodium hydroxide solution post-column addition. The injection volume was 10 µl and the standards used were L-arabinose, D-galactose, D-glucose, D-xylose, and D-mannose all manufactured by Fluka Chemie AG (Buchs, Switzerland). The amount of hemicellulose was determined after anhydro corrections of 0.90 for hexoses and 0.88 for pentoses.

2.3.4. Size-Exclusion Chromatography

The molecular weight distribution was determined using size-exclusion chromatography (SEC). The system consisted of a controller (Waters 600E, Waters, Milford, MA, USA) connected to a refractive index detector (Waters 2414 Differential Refractometer) and UV detector (Waters 486 Tunable Absorbance Detector) set to 234 nm. The column used was a TSKgel (G4000PWXL, TOSOH Bioscience GmbH, Griescheim, Germany) and the eluent was deionized water, which was pumped using a Waters 600 gradient pump at a flow rate of 0.5 mL/min and degassed using a Waters in-Line degasser. The injection volume was 20 µL, which was performed using an autosampler (Waters 717 plus autosampler). The standards used were polyethylene glycol (400 Da, Merck Schuchardt OHG, Germany) and dextran (2000, 500, 100, 150, 60, 10 and 4 kDa Merck Schuchardt OHG, Germany). The same standards, instrument parameters and column were used for an alkali SEC (100 mM NaOH eluent) with a Shimadzu (Shimadzu Corp., Kyoto, Japan) system (SIL-10AXL autosampler, LC-10AT pump, CTO-10A column oven, RID-10A refractive index detector and SPD-10AV UV-detector).

2.3.5. Two-Dimensional Nuclear Magnetic Resonance Spectroscopy (2D-NMR)

For the feed sample 1 mL was dried at 50 °C for 48 h and dissolved in 0.6 mL of deuterium oxide (Sigma-Aldrich Co., St. Louis, MO, USA) or 0.6 mL of a mixture of D_2O and D_6-DMSO (ratio of 3:5). The same sample preparation was used for the retentates; however, the amount of sample dried was 200 µL instead of 1 mL. The instrument used for the heteronuclear single quantum coherence spectroscopy 2D-NMR was a Bruker Avance III HD 500 MHz spectrometer (Bruker BioSpin GmbH, Karlsruhe, Germany). A 5 mm broadband (BBO) probe was used together with a Z-gradient coil. The data was acquired with the pulse program "hsqcetgpsisp.2" with the following settings: 136 scans, 1.5 s relaxation delay, 10.3 µs pulse length, 11 ppm spectral width, 1538 FID size and frequency discrimination in F1 e/a. The data was illustrated, processed, and evaluated using MestReNova 12 (Mestrelab Research S.L., Santiago de Compostela, Spain). Processing methods used were base-line correction and phase correction. Semi-quantative calculations and assignments were done according to methods used in the literature [4,20–23].

3. Results and Discussion

3.1. SSL Composition

The results for the raw material composition used in this study are presented in Figure 2. According to these results, approximately 49.1% of the total dry content of the solution (TDS) of 80.1 g/L is composed of pulping chemicals. It is known that sodium-based SSL solutions contain sodium lignosulfonates [8,24]; thus, some of the ash content was a result of the decomposition of the lignosulfonates. Lignin had the second highest proportion of around 38.5% followed by the mono- and polysaccharides of which the total was 7.6%. GGM was the hemicellulose having the highest proportion of around 67% of the total hemicelluloses followed by xylan, and lastly arabinan.

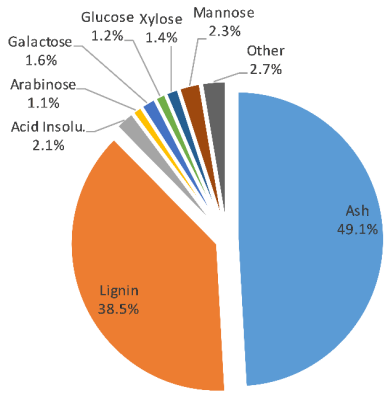


Figure 2. Composition of the untreated spent-sulfite-liquor raw material.

The molecular weight distribution for the untreated SSL solution was determined using SEC as shown in Figure 3. The results show that the major peaks are in the range between 500 and 0.4 kDa (Figure 3A,B), which is in agreement with previous observations using water as an eluent [4]. Although the signal was the strongest in the lower range, the high polydispersity reached molecular weights of up to 2000 kDa. This has not been seen previously, and it appeared only using a high-resolution SEC column. The refractive index (RI) and ultraviolet (UV) signals coincided in the entire measured MW region. This is an indication of the existence of lignin-carbohydrate-complexes [25]. However, previous work has shown that lignin-free polysaccharides exist in the MW region of 20 to 4 kDa. This was not visible in the untreated sample, presumably because of the overlapping signals with lignin or lignin-carbohydrate-complexes.

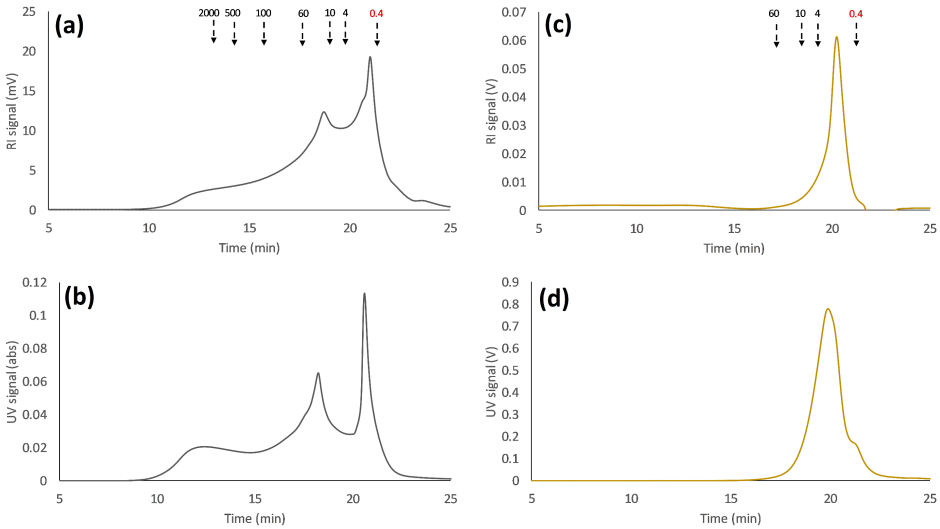


Figure 3. Size-exclusion chromatography (SEC) of the untreated spent-sulfite-liquor raw material; where (**a**,**b**) are the RI and UV detector response respectively using water as eluent. (**c**,**d**) are the RI and UV detector response respectively using 100 mM NaOH as eluent. Arrows point to the peak maximum of the various dextran standards, except for the lowest MW standard (0.4 kDa) which was PEG.

Previous reports have shown that lignosulfonates were ion excluded when water was used as an eluent during SEC measurements [26]. This resulted in the early elution of the solutes and high MW determinations. The ion-exclusion effect was suppressed by using an electrolyte solution as the eluent. The sample was therefore separated with a 100 mM sodium hydroxide solution as SEC eluent (Figure 3C,D), which has been reported to be a reliable electrolyte for the MW determination of both lignin and lignosulfonates [27]. The results in Figure 3C,D show that the MW of the solutes was actually lower than that observed using water as an eluent (Figure 3A,B). This indicates that ion-exclusion effects were suppressed; in addition, it also explains the low lignin retention observed in our previous study [13].

3.2. Influence of Volume Reduction on Flux and Retention

In order to compare the hydrophilic membranes with the optimal hydrophobic membrane from our previous study [13], concentration studies were performed with the hydrophilic membranes using previously chosen parameters of 0.5 m/s CFV, 5.5 bar TMP, and 50 °C and a volume reduction of 90%. The flux vs volume reduction (ratio between the volume of permeate and feed) for the different membrane studies is shown in Figure 4. The hydrophobic membrane (GR51PP) had an almost linear decline of flux with increasing volume reduction. The same trend was observed for the more open hydrophilic membrane (C30F), while for the dense membranes (RC70PP and C5F) the flux was in pseudo steady state up to a volume reduction of 50%–60% thereafter it strongly decreased. The C20F membrane had a sharp decrease in the beginning that transitioned into a pseudo steady state mode and ended with a profile that followed the RC70PP and C5F. The sharp decrease in the beginning was probably caused by the formation of a cake on the surface as seen and explained by Brião et al. [28] and Hwang et al. [29]. The C30F had a larger MWCO than the C20F: thus, it was expected to have an overall higher flux based on this and the higher PWF seen in Figure 5. This did not occur, which implied that pore plugging was the probable main reason for this instantaneous decrease of flux and capacity [29]. This was also indicated by the fouling degree (Figure 5), which was higher for the C30F compared with that of the C20F. It is known that the raw material contains compounds with molecular weights ranging

from approximately 60 to 0.4 kDa (Figure 3C). It has also been shown in our previous work [13] that a hydrophobic 25 kDa MWCO membrane became pore blocked causing a flux of virtually zero using the same raw material. Considering that the C30F membrane was in the same range of MWCO, this can support the concept of pore blockage as the main fouling mechanism. However, the flux was not zero, which probably was because of the slightly higher MWCO, but also because of the hydrophilic nature of the membrane, which can lead to low lignin adsorption [16].

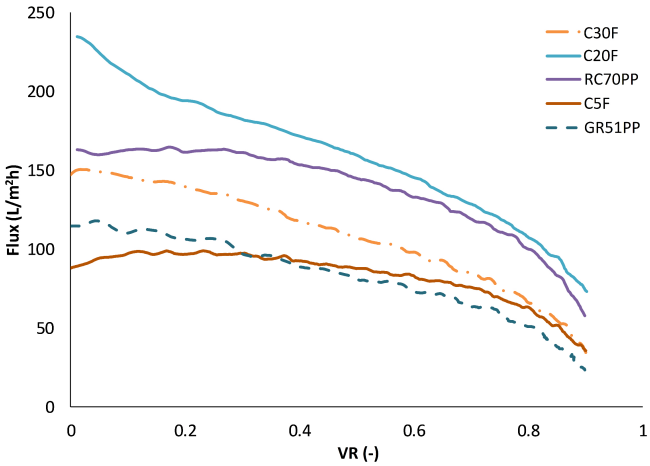


Figure 4. Flux vs volume reduction (VR) curves for the different concentration studies performed using the hydrophobic and hydophilic membranes. The temperature, trans-membrane pressure and cross-flow velocity were 50 °C, 5.5 bar, and 0.5 m/s, respectively.

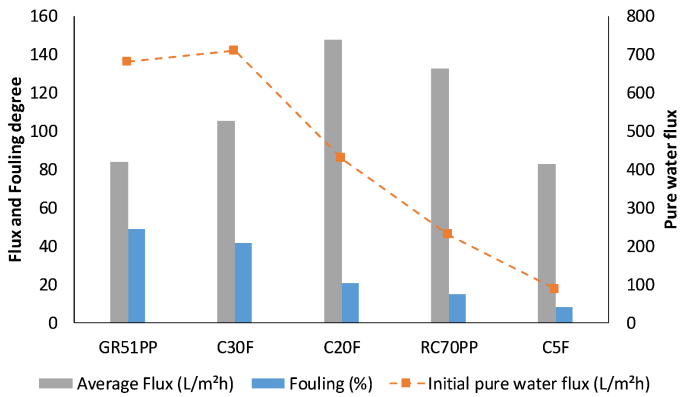


Figure 5. The average flux, fouling degree, and initial pure water flux (new and cleaned membrane) for the studied membranes.

These results were also reflected in the average retention of the different compounds during the concentration study as seen in Figure 6. The average retention for lignin was similar for both the hydrophobic 50 kDa membrane and the hydrophilic 5 kDa membrane even though the MWCO differed by an order of magnitude. The retention for the polysaccharides behaved as expected, while the retention was higher for the denser membranes independently of the hydrophilicity of the membrane. Thus, there was no clear indication of any interaction between the membranes and the polysaccharides. The interaction between lignin and the hydrophobic membrane and the low

retention of polysaccharides (high MWCO) clearly resulted in a separation degree (as defined by the concentration of GGM divided by the sum of the lignin and the GGM concentrations [4]), which was lower compared to the hydrophilic membranes (Figure 6). These observations clearly showed that the hydrophilic membranes in this case are superior when it comes to performance, separation, low fouling, and product yields.

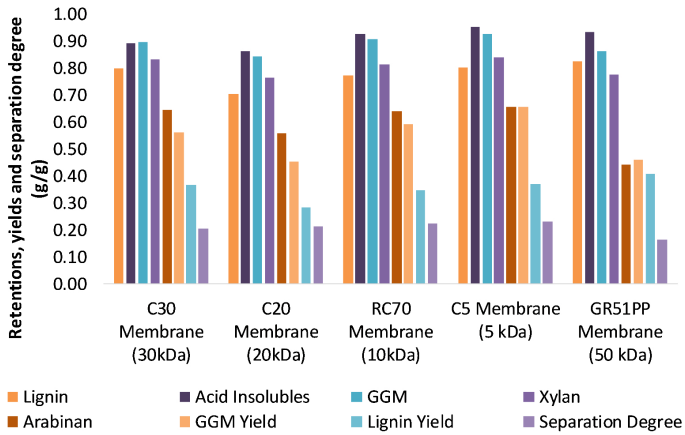


Figure 6. The average membrane retention, yield, and separation degree of the solutes from a volume reduction of 0% to 90%.

The molecular weight distributions for the membrane filtration retentates were determined using SEC and are presented in Figure 7. The peaks showing the lignin-free hemicelluloses were now visible between the standards 10 and 4 kDa using the RI detector (Figure 7A). These peaks did not have a corresponding signal using the UV detector (Figure 7B), which was expected since the polysaccharides were missing the lignin fragments that give rise to these signals [4,30]. The intensity of the peaks appeared to follow the retention of the components as seen in Figure 6. The highest lignin retention was around 0.82 for the 50 kDa hydrophobic membrane, which was in agreement with the highest intensity seen in the UV and RI curves in Figure 7A,B. The lignin retention was slightly lower (0.80) and equal for the 30 and 5 kDa hydrophilic membranes; thus, the SEC curves have approximately the same intensities. The 5kDa hydrophilic membrane had the highest GGM retention, which was complemented with a higher intensity for the peaks that correspond to the lignin-free hemicellulose. The major change observed compared with SEC of the untreated SSL (Figure 3A,B) was the shift of the majority of the peaks from a lower range of MW to a higher range. In Figure 3, lignin signals can be seen in the lower MW range, which do not appear in the results in Figure 7. The lignin retention was greater than zero, and thus, lower MW lignin would be likely to appear in Figure 7 regardless of which membrane was used for filtration. The MW of the lignin was also higher according to Figure 7. This would usually cause lignin to have a higher retention compared with the other components. This, however, did not occur and the retention was lower as seen in Figure 3. As discussed in Section 3.1, this is likely to be caused by ion exclusion effects, which may result in higher MW. The same samples were analyzed using alkali SEC, presented in Figure 7C,D. These results show that the most open membranes (GR51PP and C30F) had the highest intensity of most components, which was probably caused by a higher degree of fouling (Figure 5). This was especially observable for the components with a MW lower than 4 kDa, which had a higher retention for the membranes with a MWCO higher or equal to 30 kDa.

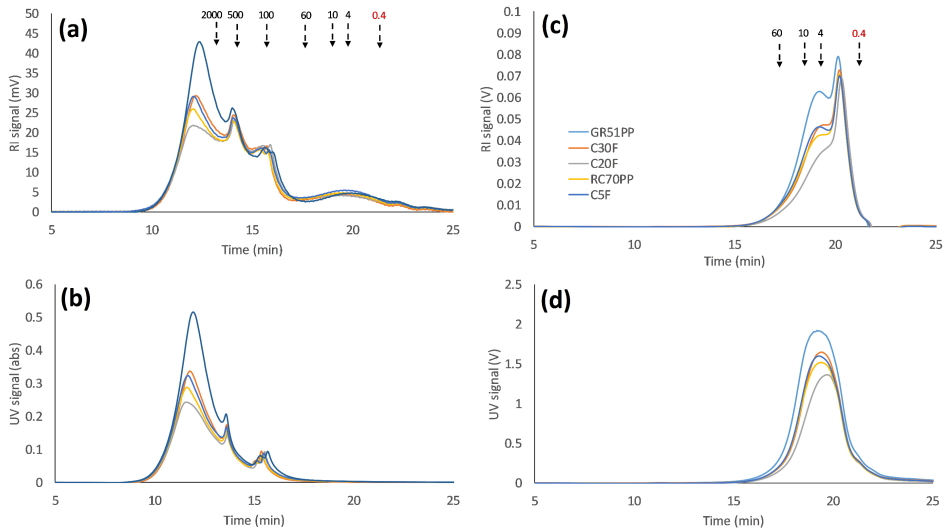


Figure 7. Size-exclusion chromatography of the volume-reduced retentates (90%) for all of the studied membranes; where (**a**,**b**) are the RI and UV detector response respectively using water as eluent. (**c**,**d**) are the RI and UV detector response respectively using 100 mM NaOH as eluent. Arrows point to the peak maximum of the various dextran standards, except for the lowest MW standard (0.4 kDa) which was PEG.

3.3. Differences between the GR51PP and RC70PP Retentates

In order to compare the difference between the hydrophilic and hydrophobic membrane, the retentates from both membrane types were compared. The hydrophilic membrane chosen was the one found optimal in Section 3.4 (RC70PP) and the hydrophobic was the GR51PP. From previous results, it was concluded that the hydrophilic membrane had a higher retention for the polysaccharides compared with the hydrophobic membrane and that the lignin retention was the opposite. This was also indicated by the SEC results shown in Figure 7 and illustrated in Figure 8. The peaks were gathered in six major parts. Three peaks were in the region 12 to 16 min, which also had a UV response (related to lignosulfonates and LCCs). The second three major peaks were in the region 16 to 24 min, which were lignin-free monosaccharides and polysaccharides given the lack of any UV response [30]. The results in Figure 8 show that the lignin-free region was the highest for the hydrophilic membrane (RC70PP). This is caused by the retention for the polysaccharides being higher for this membrane. However, the peak with a maximum intensity around 15 min also yielded a higher intensity using the hydrophilic membrane compared with the hydrophobic since the polysaccharide content is higher in this retentate and the peak has a UV response. This indicates that the hydrophilic retentate contained a higher amount of LCCs. LCCs could also be a part of the peaks in the high MW region (<15 min); however, because of the high amount of lignin in these peaks, this could not be confirmed.

It has previously been shown with 2D HSQC NMR that the major bonds between the polysaccharides and lignin were phenyl glycosyl (PhG) and benzyl ether bonds (BE1 (both hexoses and pentoses) and BE2 (mostly to xylan) [4]. Signals for benzyl ester bonds were also visible; however, because of overlapping signals these could not be confirmed. Our previous study also indicated the existence of sulfonated lignin in the raw material [8]. Thus, the signals for the benzyl ether bonds would overlap as well. The retentates in this study were analyzed employing 2D HSQC NMR using D2O and d6-DMSO as solvents and references (Figure 9). The results showed that a shift of the peaks occurs on the proton axis when changing from D2O to D_6-DMSO. However, the relations between the peaks remain the same for the major interesting peaks. The intensity also becomes lower using D_6-DMSO,

which may be caused by the lower solubility of the polysaccharides in D_6-DMSO (that has a lower dielectric constant than water) [4]. As a result, acetylated mannopyranose (2OAc-M1 and 3OAc-M1), alpha-galactopyranose (α-Gal), and uronic acids (U) were not visible. Possible phenyl glycosidic LCC linkages (PhG) were visible (highlighted with a red circle in the anomeric C1 sugars region) in all of the spectrums. The ratios between the sum of PhG volume integrals and mannopyranose (M1) volume integral (Figure 9c,d) for the RC70PP and GR51PP retentates were 0.20 and 0.15, respectively, indicating that a higher amount of LCCs was in the retentate after filtering, utilizing the hydrophilic membrane. Regarding the GGM composition, the α-galactopyranose groups content linked to the glucomannan backbone was around 16% of the total non-acetylated mannan for both retentates. This corresponds to a Gal:Man ratio of 0.4:3.0 which is in agreement with our previous study [4]. No other major differences in acetylated GGM were observed given that the total acetylated mannan was approximately 14% of the total mannan for both retentates. Semi-quantification of the visible lignin peaks (β-aryl-ether (A), β-5 (B), and methoxyl) was difficult brought about by the highly overlapping regions. However, by comparison between the two retentates the following values were obtained (per 100 aromatic rings): for the total β-O-4 (sulfonated and non-sulfonated) we obtained 37 and 40 for the RC70PP and GR51PP, respectively. Regarding phenylcoumaran (β-5) the values were 10 and 8, and for methoxyl the values were 100 and 86. The values are in the same range as seen in the literature for spruce [5] and the difference between the retentates was negligible.

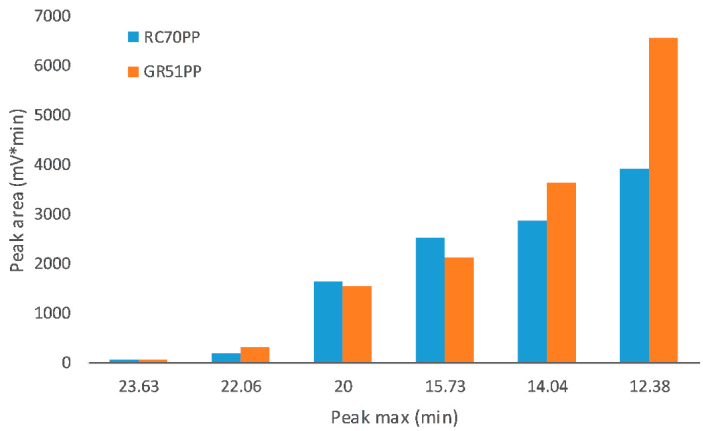


Figure 8. Comparison of the size-exclusion chromatography peak areas (RI) for the results shown in Figure 7 (RC70PP and GR51PP membranes).

3.4. Optimal Membrane and Cost Estimates

In order to decide which membrane is the most optimal, several considerations are required. The decision should rely on a membrane that would deliver the smallest full-scale plant but also has the highest GGM production and separation degree. In terms of separation degree, the differences between the hydrophilic membranes were very small (Figure 6); thus, this does not have to be accounted for. The flux and GGM production were different and thus a method was needed to choose the optimal membrane. This was done by performing plant cost estimations on the different membranes. The assumptions made in these calculations (Table 2) were derived from others [31], based on experience and contact with manufacturers. The cost estimates were accomplished assuming that the plant would be based on a spiral module with 48 mil spacer (Alfa Laval Nordic A/S, Søborg, Denmark). The maximum operating conditions for the module, such as maximum pressure drop, were derived from Alfa Laval's datasheet and are presented in Table 2. Surrounding infrastructure was assumed to be a part of the existing plant where the unit was to be installed. In a typical plant for concentration duties,

two kinds of pump are used. A feed pump is used to feed the untreated solution and increase the inlet pressure to the required operating pressure. A recirculation pump is also used to compensate for pressure drops and maintain a constant operating CFV. The electricity required per cubic meter of permeate to run these pumps was calculated according to Equation (2) (feed pump) and Equation (3) (recirculation pump) [32]:

$$W_{\text{feed}} = \frac{P_{\text{inlet}}}{\eta VR} \left[\text{kWh}/\text{m}^3\text{permeate}\right] \quad (2)$$

$$W_{\text{recirculation}} = \frac{\Delta P_{\text{f}} Q_{\text{housing}}}{\eta\left(J_{\text{avg}} A_{\text{m}}\right)} \left[\text{kWh}/\text{m}^3\text{permeate}\right] \quad (3)$$

where W_{feed} and $W_{\text{recirculation}}$ are the required electrical energy, P_{inlet} is the inlet pressure, η is the pump efficiency, VR is the volume reduction, ΔP_{f} is the pressure drop, Q_{housing} is the feed flow to one module, J_{avg} is the average flux, and A_{m} is the membrane area in one module.

Table 2. Assumptions for the cost estimates (Based on Spiral module (2517) with 48 mil spacer by Alfa Laval).

Investment cost (€/m^2)	500
Annuity factor (/year)	0.1
Membrane cost (less housing) (€/m^2)	50
Membrane life-time (years)	1.5
Electricity price (€/MWh)	38
Cleaning Cost (€/m^2/cycle)	0.13
Cleaning time (h/day)	1
Extra membrane area for cleaning (%)	20
Maintenance and labor costs (% of capital cost)	5
Operation Time (h/year)	8000
Pump efficiency (-)	0.8
Permeate density (kg/m^3)	1100
Maximum pressure drop (at 1.5 m^3/h) (bar)	0.6
Membrane area per module (m^2)	1.2
Plant feed flow (m^3/h)	1
Plant volume reduction (%)	90
Plant transmembrane pressure (bar)	5.5

The results from the cost estimations (Table 3) show that the lowest yearly total cost would be obtained with the C20F membrane; which was expected given that the flux was the highest for that membrane, resulting in the smallest membrane area requirement. However, the C20F did not have the highest GGM retention and thus the cost per ton product was not the lowest. The difference of the total cost between the C20F and RC70PP was small. The RC70PP had the lowest cost per ton product because of the 30% higher GGM production compared with the C20F; in addition, the RC70PP had the second highest average flux and was thus the most cost-efficient membrane. The cost of around 48 €/ton GGM is reasonable compared with similar calculations in other studies [31,32]. Although these cost estimates are appropriate for comparing different membranes and membrane filtration setups, they are not intended for designing a plant. The estimations used assumed that the same cleaning procedure was required and thus they did not include the dynamics of fouling over time. This, however, requires long-term membrane-filtration studies and cleaning optimization on larger pilot scale, which is out of the scope for this paper. The GR51PP had the highest cost per ton product, which was because of the low average flux, given that the GGM production was in the same range compared to the hydrophilic membranes. The GR51PP also had the lowest separation degree of around 16% (highest lignin to GGM content), which made it the least favorable choice in the series.

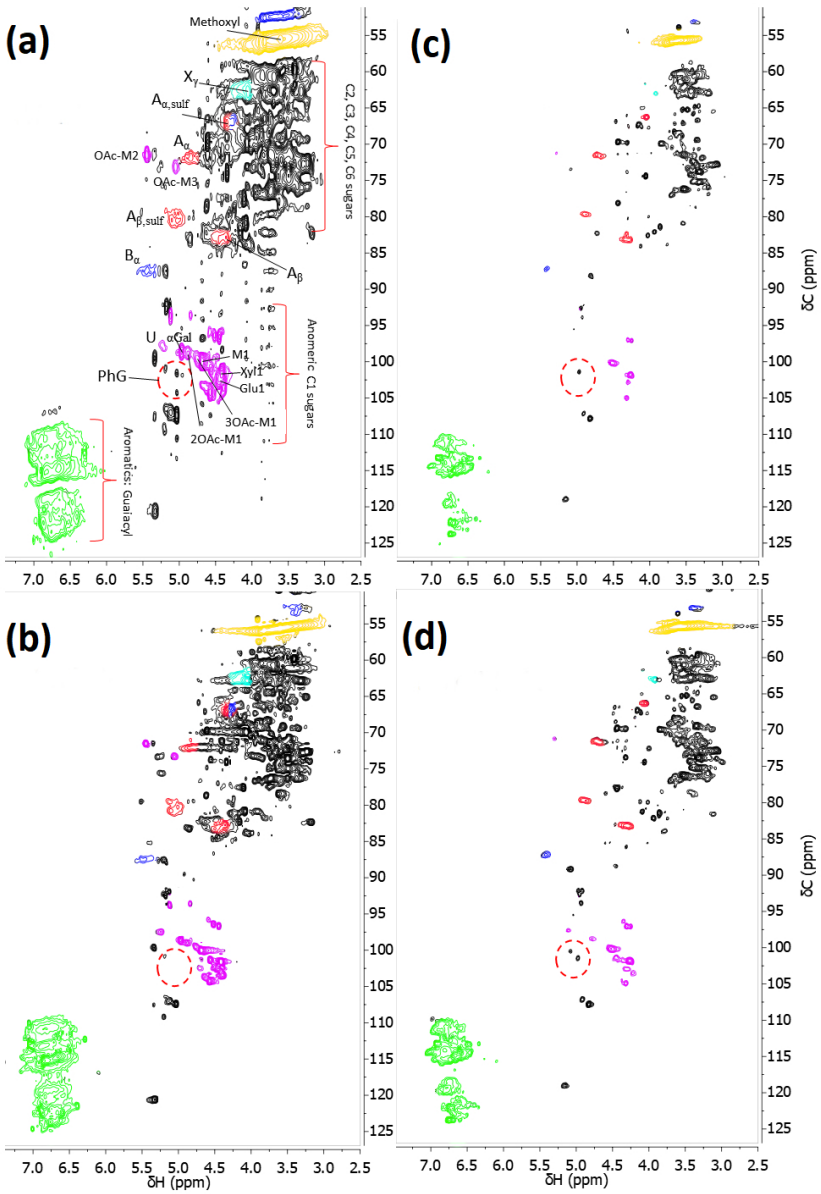


Figure 9. 2D HSQC NMR using D2O (spectrum **a** and **b**) and a mixture of D2O and d6-DMSO (spectrum **c** and **d**) as solvent. Spectrums **a** and **c** represent the RC70PP retentate while spectrums **b** and **d** represent the GR51PP retentate. The identified lignin bonds were: $A_{x,y}$ (B-aryl-ether bonds, red), $B_{x,y}$ (phenylcoumaran, blue), X_γ (cinnamyl alcohol, light blue), PhG (phenyl glycosidic LCC bonds, red circle) and the aromatics in the guaiacyl units (green). The identified polysaccharides and uronic acids (purple) were: MX (mannopyranose), XOAc-MX (O-acetylated mannopyranose), XylX (xylopyranose), GluX (glucopyranose), α-Gal (galactopyranose), and U (glucuronic acid). The notations x and y are the x-carbon and sulfonation respectively.

Table 3. Cost estimations for galactoglucomannan (GGM) recovery using the hydrophobic and hydrophilic membranes.

Parameters	C30F	C20F	RC70PP	C5F	GR51PP
Average flux (L/m^2 h)	105.0	147.4	132.2	82.8	83.9
GGM yield (%)	56.2	45.0	59.3	65.6	45.9
GGM produced (kg/h)	2.61	2.09	2.75	3.04	2.51
Membrane Area (m^2)	7.79	5.55	6.19	9.89	9.75
Feed pump energy demand (kW)	0.17	0.17	0.17	0.17	0.17
Recirculation pump energy demand (kW)	0.20	0.14	0.16	0.26	0.25
Capital cost (€/year)	468	333	371	593	585
Electricity cost (€/year)	114	97	102	131	130
Membrane replacement cost (€/year)	312	222	247	395	390
Cleaning cost (€/year)	405	288	321	514	507
Maintenance and labor costs (€/year)	23	17	19	30	29
Total cost (€/year)	**1322**	**957**	**1060**	**1663**	**1641**
Cost per ton product (€/ton GGM)	**63.36**	**57.26**	**48.23**	**68.31**	**81.86**

4. Conclusions

- Initial membrane filtration trials and comparison of the raw material (SSL) and retentates show that most of the solutes are in the same MW range as the cut-off specifications of the membranes. Therefore, the hydrophilic membranes with highest MWCO, experienced the highest degree of fouling.
- The fouling was due to pore blocking as has been seen previously with the hydrophobic membranes.
- The hydrophilic membranes had an overall lower lignin retention and higher GGM retention compared with the hydrophobic, possibly because of the lower lignin affinity and adsorption.
- The hydrophilic membranes were shown to be superior to the hydrophobic membranes when it comes to separation, fouling, and capacity.
- Analyzing the SSL using SEC with water as an eluent has been shown to be a promising method for the separation of lignosulfonates and LCCs from GGM due to the effect of ion exclusion in the SEC column.
- The optimal membrane (RC70PP) was compared with the GR51PP by analyzing the different retentates using SEC and 2D HSQC NMR.
- The results showed that the hydrophilic membrane retained a higher amount of polysaccharides compared with the hydrophobic membrane. This resulted in a higher portion of LCCs being retained in the hydrophilic membrane; which occurred because of the lower MWCO of the hydrophilic membrane.
- The 2D HSQC NMR indicated that the retentate from the hydrophilic membrane had a higher amount of LCCs. No other major structural differences were observed between the two retentates.
- The most cost-efficient membrane was chosen based on the flux and product yields. The C20F membrane had the lowest total costs per year; however, the RC70PP led to higher GGM production and yields and thus, the cost per ton product was the lowest for the RC70PP.

Author Contributions: Funding acquisition, O.W.; Investigation, B.A.-R.; Methodology, B.A.-R.; Supervision, M.G., F.L., and O.W.; Validation, B.A.-R., M.G., F.L., and O.W.; Visualization, B.A.-R.; Writing—original draft, B.A.-R.; Writing—review & editing, M.G., F.L. and O.W.

Funding: This work was funded by the Swedish Foundation for Strategic Research (SSF) (RBP 14-0046).

Acknowledgments: Many thanks to Domsjö Fabriker (Sweden) for providing us with the raw material used in this work. We would also like to thank Monica Arcos Hernandez for all the help with the NMR analysis.

Conflicts of Interest: The authors declare no conflict of interest. The funders had no role in the design of the study; in the collection, analyses, or interpretation of data; in the writing of the manuscript, or in the decision to publish the results.

References

1. Wenzl, H. *The Chemical Technology of Wood*; Elsevier: New York, NY, USA, 2012.
2. Weissgram, M.; Gstöttner, J.; Lorántfy, B.; Tenhaken, R.; Herwig, C.; Weber, H.K. Generation of PHB from Spent Sulfite Liquor Using Halophilic Microorganisms. *Microorganisms* **2015**, *3*, 268–289. [CrossRef] [PubMed]
3. Lawoko, M. Lignin Polysaccharide Networks in Softwood and Chemical Pulps: Characterisation, Structure and Reactivity. Ph.D. Thesis, Royal Institute of Technology, Stockholm, Sweden, 2005.
4. Al-Rudainy, B.; Galbe, M.; Schagerlöf, H.; Wallberg, O. Antisolvent precipitation of hemicelluloses, lignosulfonates and their complexes from ultrafiltrated spent sulfite liquor (SSL). *Holzforschung* **2018**, *72*, 839–850. [CrossRef]
5. Giummarella, N.; Lawoko, M.; Zhang, L.; Henriksson, G. Structural features of mildly fractionated lignin carbohydrate complexes (LCC) from spruce. *RSC Adv.* **2016**, *6*, 42120–42131. [CrossRef]
6. Willför, S.; Sjöholm, R.; Laine, C.; Roslund, M.; Hemming, J.; Holmbom, B. Characterisation of water-soluble galactoglucomannans from Norway spruce wood and thermomechanical pulp. *Carbohydr. Polym.* **2003**, *52*, 175–187. [CrossRef]
7. Du, X.; Pérez-Boada, M.; Fernández, C.; Rencoret, J.; Del Río, J.C.; Jiménez-Barbero, J.; Li, J.; Gutierrez, A.; Martínez, A.T. Analysis of lignin–carbohydrate and lignin–lignin linkages after hydrolase treatment of xylan–lignin, glucomannan–lignin and glucan–lignin complexes from spruce wood. *Planta* **2014**, *239*, 1079–1090. [CrossRef] [PubMed]
8. Al-Rudainy, B.; Galbe, M.; Hernandez, M.A.; Jannasch, P.; Wallberg, O. Impact of Lignin Content on the Properties of Hemicellulose Hydrogels. *Polymers (Basel)* **2018**, *11*, 35. [CrossRef] [PubMed]
9. Thuvander, J.; Jönsson, A.-S. Extraction of galactoglucomannan from thermomechanical pulp mill process water by microfiltration and ultrafiltration—Influence of microfiltration membrane pore size on ultrafiltration performance. *Chem. Eng. Res. Des.* **2016**, *105*, 171–176. [CrossRef]
10. Al Manasrah, M.; Kallioinen, M.; Ilvesniemi, H.; Mänttäri, M. Recovery of galactoglucomannan from wood hydrolysate using regenerated cellulose ultrafiltration membranes. *Bioresour. Technol.* **2012**, *114*, 375–381. [CrossRef]
11. Duval, A.; Molina-Boisseau, S.; Chirat, C. Fractionation of lignosulfonates: Comparison of ultrafiltration and ethanol solubility to obtain a set of fractions with distinct properties. *Holzforschung* **2015**, *69*, 127–134. [CrossRef]
12. Bhattacharya, P.; Todi, R.; Tiwari, M.; Bhattacharjee, C.; Bhattacharjee, S.; Datta, S. Studies on ultrafiltration of spent sulfite liquor using various membranes for the recovery of lignosulphonates. *Desalination* **2005**, *174*, 287–297. [CrossRef]
13. Al-Rudainy, B.; Galbe, M.; Wallberg, O. Influence of prefiltration on membrane performance during isolation of lignin-carbohydrate complexes from spent sulfite liquor. *Sep. Purif. Technol.* **2017**, *187*, 380–388. [CrossRef]
14. Song, T.; Pranovich, A.; Holmbom, B. Separation of polymeric galactoglucomannans from hot-water extract of spruce wood. *Bioresour. Technol.* **2013**, *130*, 198–203. [CrossRef]
15. Zasadowski, D.; Yang, J.; Edlund, H.; Norgren, M. Antisolvent precipitation of water-soluble hemicelluloses from TMP process water. *Carbohydr. Polym.* **2014**, *113*, 411–419. [CrossRef]
16. Ding, Z.; Liu, X.; Liu, Y.; Zhang, L. Enhancing the Compatibility, Hydrophilicity and Mechanical Properties of Polysulfone Ultrafiltration Membranes with Lignocellulose Nanofibrils. *Polymers (Basel)* **2016**, *8*, 349. [CrossRef] [PubMed]
17. Li, J.; O'Hagan, T.; MacLeod, J. Using ultrafiltration to analyze the molar mass distribution of kraft lignin at pH 13. *Can. J. Chem. Eng.* **1996**, *74*, 110–117. [CrossRef]
18. Puro, L.; Tanninen, J.; Nyström, M. Analyses of organic foulants in membranes fouled by pulp and paper mill effluent using solid-liquid extraction. *Desalination* **2002**, *143*, 1–9. [CrossRef]
19. Sluiter, A.; Hames, B.; Ruiz, R.; Scarlata, C.; Sluiter, J.; Templeton, D. *Determination of Sugars, Byproducts, and Degradation Products in Liquid Fraction Process Samples (NREL/TP-510-42623)*; NREL: Golden, CO, USA, 2008.
20. Steinmetz, V.; Villain-Gambier, M.; Klem, A.; Gambier, F.; Dumarcay, S.; Trebouet, D. Unveiling TMP Process Water Potential as an Industrial Sourcing of Valuable Lignin–Carbohydrate Complexes toward Zero-Waste Biorefineries. *ACS Sustain. Chem. Eng.* **2019**, *7*, 6390–6400. [CrossRef]

21. Hannuksela, T.; Herve, C. NMR structural determination of dissolved O-acetylated galactoglucomanna isolated from spruce thermomechanical pulp. *Carbohydr. Res.* **2004**, *339*, 301–312. [CrossRef]
22. Lutnaes, B.F.; Myrvold, B.O.; Lauten, R.A.; Endeshaw, M.M. 1H and13C NMR data of benzylsulfonic acids—Model compounds for lignosulfonate. *Magn. Reson. Chem.* **2008**, *46*, 299–305. [CrossRef]
23. Marques, A.P.; Evtuguin, D.V.; Magina, S.; Amado, F.M.L.; Prates, A.; Evtuguin, D.; Amado, F. Structure of Lignosulphonates from Acidic Magnesium-Based Sulphite Pulping ofEucalyptus globulus. *J. Wood Chem. Technol.* **2009**, *29*, 337–357. [CrossRef]
24. Myrvold, B.O. Salting-out and salting-in experiments with lignosulfonates (LSs). *Holzforschung* **2013**, *67*, 549–557. [CrossRef]
25. Lawoko, M. Unveiling the structure and ultrastructure of lignin carbohydrate complexes in softwoods. *Int. J. Biol. Macromol.* **2013**, *62*, 705–713. [CrossRef]
26. Forss, K.; Stenlund, B. The Influence of Charged Groups in Gel Permeation Chromatography of Polyelec-Trolytes. *J. Polym. Sci. Polym. Symp.* **1973**, *42*, 951–963. [CrossRef]
27. Tolbert, A.; Akinosho, H.; Khunsupat, R.; Naskar, A.K.; Ragauskas, A.J. Characterization and analysis of the molecular weight of lignin for biorefining studies. *Biofuels Bioprod. Biorefining* **2014**, *8*, 836–856. [CrossRef]
28. Brião, V.B.; Seguenka, B.; Zanon, C.D.; Milani, A. Cake formation and the decreased performance of whey ultrafiltration. *Acta Sci. Technol.* **2017**, *39*, 517–524. [CrossRef]
29. Hwang, K.-J.; Liao, C.-Y.; Tung, K.-L. Effect of membrane pore size on the particle fouling in membrane filtration. *Desalination* **2008**, *234*, 16–23. [CrossRef]
30. Du, X.; Gellerstedt, G.; Li, J. Universal fractionation of lignin–carbohydrate complexes (LCCs) from lignocellulosic biomass: An example using spruce wood. *Plant. J.* **2013**, *74*, 328–338. [CrossRef]
31. Jönsson, A.-S.; Nordin, A.-K.; Wallberg, O. Concentration and purification of lignin in hardwood kraft pulping liquor by ultrafiltration and nanofiltration. *Chem. Eng. Res. Des.* **2008**, *86*, 1271–1280. [CrossRef]
32. Jönsson, A.-S.; Wallberg, O. Cost estimates of kraft lignin recovery by ultrafiltration. *Desalination* **2009**, *237*, 254–267. [CrossRef]



© 2019 by the authors. Licensee MDPI, Basel, Switzerland. This article is an open access article distributed under the terms and conditions of the Creative Commons Attribution (CC BY) license (http://creativecommons.org/licenses/by/4.0/).

Paper V

Separation and Purification Technology 250 (2020) 117187

Contents lists available at ScienceDirect

Separation and Purification Technology

journal homepage: www.elsevier.com/locate/seppur

From lab-scale to on-site pilot trials for the recovery of hemicellulose by ultrafiltration: Experimental and theoretical evaluations

Basel Al-Rudainy, Mats Galbe, Ola Wallberg*

Department of Chemical Engineering, Lund University, P.O. Box 124, SE-221 00 Lund, Sweden

ARTICLE INFO

Keywords:
Lignin
Galactoglucomannan
Ultrafiltration
Pilot-scale
CFD
Fouling

ABSTRACT

Spent sulfite liquor (SSL) is a byproduct of the sulfite pulping process of wood. SSL usually contains monosugars and lignosulfonates, which are fermented to produce ethanol and dried to generate lignosulfonate salts. However, the SSL that was used in this work was derived from the first step of a 2-step sulfite pulping process of softwood under mild pulping conditions in the first stage of cooking. The resulting SSL contained polymeric hemicelluloses, which are not used today but have many potential applications. The up-concentration of this SSL had been performed on a lab scale by ultrafiltration. However, the pilot-scale ultrafiltration of hemicellulose-rich sodium-based SSL has not been reported.

In this study, the operating conditions for the lab-scale concentration of hemicellulose-rich, sodium-based SSL were examined in a pilot-scale membrane filtration unit. The permeate flux and retention of products were lower in the pilot equipment compared with the lab-scale setup, perhaps related to the lower Reynolds number and shear rate in the former, as indicated by simulations of computational fluid dynamics. The pilot equipment also ran at a higher volume reduction compared with the lab-scale system, which could explain the difference in flux and retention. The effects of fouling and cleaning were also determined, wherein an alkaline cleaning step (pH 11) for 1 h was sufficient to remove foulants and maintain a stable average flux of 88 L/m^{2}h and the non-changing retention of products.

1. Introduction

During the production of sulfite pulp, wood components, such as hemicelluloses, lignin, and wood extractives, are dissolved in the cooking liquor, also called spent sulfite liquor (SSL). Sulfite processes usually carry out the extraction under severely acidic conditions, causing all of the hemicellulose to degrade into acids and monosaccharides [1]. The remaining polymeric compounds in the SSL are primarily lignosulfonates. However, in certain processes, the sulfite pulping is performed in 2 stages, of which the first is mildly acidic (pH approximately 4 to 5), leaving the dissolved hemicelluloses mostly intact [2]. First-stage SSL that originates from these processes are valuable, due to the growing trend toward converting pulp and paper plants into biorefineries, with a wide range of sustainable products.

Hemicelluloses, lignin (including lignosulfonates), and lignin-carbohydrate complexes (LCCs) have potential applications, including the possibility of producing gas-barrier films (for food packaging) [3], hydrogels (drug carriers) [4,5], surfactants [6], and emulsion stabilizers (food sector) [7] from hemicellulose and LCCs. Lignin also has promising applications, such as its use as a dispersant in concrete [8] and as an antioxidant [9], the production of carbon fibers [10], the manufacture of foams [11], and as a precursor for specialty chemicals [12]. Yet, few commercial products are made from these wood components (except for lignin), due to the lack of large-scale production facilities and the high cost of the raw materials [13,14]. This disconnect underscores the importance of scaling up the production of biomass components.

SSL that is derived from pulp and paper processes have several drawbacks—it contains many substances and is dilute, with the total dry substance content ranging from 8% to 14% [15]. Thus, these streams must be concentrated and purified before use. Another important factor is the recovery and recycling of the pulping chemicals that are used in the SSL during pulping, with the aim to avoid disruptions in the process.

Abbreviations: CAD, Computer-aided design; CFD, Computational fluid dynamics; CFV, Crossflow velocity; GGM, Galactoglucomannan; LCC, Lignin-carbohydrate complex; LS, Lignosulfonates; LVR, Loop volume reduction; MF, Microfiltration; MW, Molecular weight; NF, Nanofiltration; PWF, Pure-water flux; RANS, Reynolds-averaged Navier–Stokes; SSL, Spent sulfite liquor; TMP, Transmembrane pressure; UF, Ultrafiltration; VR, Volume reduction

* Corresponding author.
E-mail addresses: basel.al-rudainy@chemeng.lth.se (B. Al-Rudainy), mats.galbe@chemeng.lth.se (M. Galbe), ola.wallberg@chemeng.lth.se (O. Wallberg).

https://doi.org/10.1016/j.seppur.2020.117187
Received 20 February 2020; Received in revised form 26 May 2020; Accepted 28 May 2020
Available online 01 June 2020
1383-5866/ © 2020 The Authors. Published by Elsevier B.V. This is an open access article under the CC BY license (http://creativecommons.org/licenses/BY/4.0/).

Nomenclature

A_m	Membrane area (m^2)
C, C2, C3, C4 and C5	RANS model constants (–)
D	Characteristic diameter of a flow channel (m)
$D_{impeller}$	Impeller diameter (m)
h	Channel height (m)
J	Permeate flux (L/m^2h)
k	Turbulent kinetic energy (m^2/s^2)
L	Channel length (m)
LVR	Loop volume reduction (%)
P	The pressure field in RANS equations (bar)
P_{in}	Inlet pressure (bar)
P_{out}	Outlet pressure (bar)
Q_{feed}	Feed flow (m^3/s)
Q_p	Permeate flow (m^3/s)
Re	Reynolds number (–)
R_f	Sum of fouling resistances (1/m)
R_m	Hydraulic membrane resistance (1/m)
TMP	Trans-membrane pressure (bar)
U	Velocity field in RANS (m/s)
u, v and w	Velocity in each third-dimensional direction (m/s)
V_{feed}	Start volume of the feed solution (L)
VR	Volume reduction (%)
Δt	Time difference (s)

Greek letters

μ	Dynamic viscosity (Pa s)
ε	Turbulent dissipation rate (m^2/s^3)
ϑ	Kronecker delta (–)
ν	Kinematic viscosity (m^2/s)
ν_T	Kinematic eddy viscosity (m^2/s)
ρ	Density (kg/m^3)
τ	Reynold's stresses (N/m^2)
ω	Rotational velocity (1/s)

To this end, membrane filtration is a promising selective and energy-efficient technique [16]. The separation of lignin and hemicellulose has been achieved by membrane filtration using other process waste streams [17,18]. However, for the SSL that is used in the current study, only the pulping chemicals have been removed using membrane filtration [15,19], due to the minor difference in molecular weight (MW) between the lignin and hemicellulose [in this work, galactoglucomannan (GGM)] and the existence of LCCs. Membrane filtration remains crucial in lowering the cost of the downstream separation steps, for which a high concentration of GGM and low salt content are required to yield a pure hemicellulose fraction and decrease the use of the precipitating agent [20–22].

According to our previous work [15], the Alfa Laval RC70PP regenerated cellulose membrane (hydrophilic) has been shown to be a promising membrane for the studied SSL in terms of low fouling tendencies, high flux and retention of the products and as a result of this, the lowest cost. However, the results were generated in lab-scale experiments and did not consider long-term fouling or potential declines in flux. The importance of pilot-scale studies has also been noted by Rajniak et al. [23], who showed that pressure-normalized flux is not linearly scalable between modules, due to additional resistance in flow of the various filtration modules.

Another significant issue is the change in raw material composition if the process is run on site. Dolar et al. [24] found that the retention of their product decreased when they switched from lab-scale experiments (flat-sheet module) to pilot-scale operation (spiral-wound module), attributing the differences to varying quality between raw materials and the hydrodynamics of the systems.

On-site pilot-scale separation of hemicellulose-rich SSL has not been reported. However, there are several promising pilot studies on related raw materials. Persson et al. [18] used a series of filtration and membrane filtration steps [drum filter, microfiltration (MF), ultrafiltration (UF) and nanofiltration (NF)] to fractionate thermomechanical process water under industrial conditions, showing that 90% of suspended solids were removed in the first stage (drum filter). Extractives were removed by MF, whereas the UF unit was used to recover hemicellulose, reaching a concentration of 64 g/L at a volume reduction (VR) of 99%. Severe fouling was also observed during the UF process due to the high VR, and cleanses with Ultrasil 10 (alkali) and Ultrasil 70 (acidic) did not recover the pure water flux (PWF).

Thuvander et al. [25] performed on-site pilot trials for the continuous recovery of hemicelluloses using microfiltration and ultrafiltration from thermomechanical process water, achieving an average flux of 112 L/m^2h and 132 L/m^2h, respectively, and obtained a retentate that contained hemicelluloses at a concentration of 47 g/L. Although the final cost for the plant was high (1160 €/ton of hemicellulose), it could be reduced by incorporating the removal of hemicelluloses from the wastewater into the calculations. These results are encouraging for the current study, because the microfiltration component of the process represented 74% of the total cost. In addition, the process that we propose does not include a microfiltration step; thus, a future full-scale plant would be cheaper.

Fernández Rodríguez et al. [26] used a series of 3 membranes (15, 5, and 1 kDa) to fractionate 2 of the main components of SSL: lignosulfonates (LSs) and monomeric sugars. Using this configuration, they removed 73% of the LSs from the permeate and 27% of the monomeric sugars. According to the groups, the removal of monomeric sugars could be improved by optimizing the process, as in their subsequent study [27]. Fractionation and purification of LSs from SSL by membrane filtration has been performed in a full-scale plant by Borregaard (Sarpsborg, Norway), one of the world's most advanced biorefineries, since 1981 [14], demonstrating the importance of performing pilot-scale studies to advance the commercialization of products that are derived from biomass.

Based on our lab-scale studies [15], the operating conditions for the concentrations were as follows: a crossflow velocity (CFV) of 0.5 m/s, a transmembrane pressure (TMP) of 5.5 bar, and a volume reduction of 90% at 50 °C. The aim of the current study was to scale up the results from the lab-scale studies and present the challenges that were encountered in the process. Fouling and cleaning were examined further, and differences in flux and retention were evaluated, based on the analytical and computational fluid dynamics (CFD) results.

2. Materials and methods

2.1. Raw material

The SSL was collected from the first step of a 2-step sodium-based sulfite-pulping process of softwood [60% spruce (*Picea abies)* and 40% pine (*Pinus sylvestris)*]. The SSL was taken directly from the batch digester (approximately 150 °C) and passed through a coiled pipe heat exchanger that was dipped in cold water (< 10 °C). The cooled SSL was prefiltered using a series of 3 steel meshes (180, 70, and 40 μm, respectively) into a buffer tank, where it was stored at room temperature for up to 36 h before use. The composition of the SSL is presented in Table 1.

Table 1
Composition of SSL in g/L, based on 6 feed samples in the pilot study.

Total dry content	90.9 ± 1.5
Ash	35.7 ± 1.6
Total lignin	38.1 ± 0.7
Functional group content	
Sulfonate groups (mmol/g)	1.34[a,c]
Carboxyl groups (mmol/g)	1.08[a,c]
Total phenoxyl groups (mmol/g)	1.63[a,c]
Acid-insoluble lignin	1.2 ± 0.1
GGM	6.7 ± 0.8
Galactan	1.5 ± 0.1
Glucan	1.5 ± 0.1
Mannan	3.8 ± 0.6
Other hemicellulose	1.9 ± 0.1
Arabinan	0.6 ± 0.0
Xylan	1.2 ± 0.1
Monosaccharides (% of hemicellulose)	
Galactose	7.71
Glucose	8.41
Mannose	3.40
Arabinose	64.8
Xylose	11.3
Sugar alcohols	0.36 ± 0.02[b]
Glycerol	0.31 ± 0.02[b]
Xylitol	0.04 ± 0.01[b]
Sorbitol	0.02 ± 0.00[b]
Sugar acids	0.20[c]
Galacturonic acid	0.11[c]
Glucuronic acid	0.09[c]

[a] Based on precipitated lignin from a diafiltrated retentate.
[b] Based on 4 samples.
[c] Based on 1 sample.

2.2. Equipment, experimental procedure, and evaluation

2.2.1. Membrane filtration setup

The lab-scale equipment consisted of a 400-mL stirred cell that was equipped with a 3217-mm^2 membrane area [15]. The vessel was placed on top of a temperature-controlled heating plate with a built-in magnetic stirrer (MR2002, Heidolph Instruments GmbH & Co.KG, Schwabach, Germany). The CFV was controlled by changing the speed of the magnetic stirrer, the TMP was set using a valve that was connected to a nitrogen gas line, the pressure was monitored with a digital pressure transmitter (DCS40.0AR, Trafag AG, Bubikon, Switzerland) that was connected to the vessel, and the flux was measured using a balance (PL6001-l, Mettler Toledo Inc., Ohio, USA).

The following equipment was used for the various membrane filtration studies at the mill: an Alfa Laval Combi M39 pilot unit, which consisted of the plate-and-frame M39 membrane module with 1.0 m^2 of RC70PP membrane (Alfa Laval Nordic A/S, Søborg, Denmark); an in-line heat exchanger; a cleaning tank; and a circulation pump. The setup was equipped with an additional feed pump (DME375 – 10AR, Grundfos Water Treatment GmbH, Pfinztal, Germany), pressure transmitters (DCS40.0AR, Trafag AG, Bubikon, Switzerland), and a flow meter (FCH-m-PP, B.I.O-TECH e.K., Vilshofen, Germany) to run the process semiautonomously and measure the transmembrane pressure (TMP) and flux (Fig. 1).

The TMP and flux (J) were calculated per the following equations (atmospheric pressure on the permeate side):

$$TMP = \frac{P_{in} + P_{out}}{2} \quad (1)$$

$$J = \frac{Q_p}{A_m} \quad (2)$$

where P_{in}, P_{out}, Q_p, and A_m are the membrane module inlet and outlet pressures, permeate flow, and membrane area, respectively.

The volume reduction (VR) during the batch concentration studies was calculated as follows:

$$VR = \frac{\sum_0^n Q_p(t_n - t_{n-1})}{V_{feed}} \quad (3)$$

where t is the time at measurement n, and V_{feed} is the total initial volume of SSL (500 L).

The loop volume reduction (LVR) was defined as the VR of the SSL in the circulation loop (Fig. 1). In contrast to VR, which is based on the total volume reduction of the SSL, LVR was calculated per Eq. (4):

$$LVR = \frac{Q_p}{Q_{feed}} \quad (4)$$

where Q_{feed} is the feed pump flow (Fig. 1).

2.2.2. Pilot-scale parameter study

To determine the operating parameters for the concentration study, the crossflow velocity and TMP were varied for the sampling at each operating point. To reduce the risk of fouling, the measurements began at the higher crossflow velocity and the lowest TMP at which the pressure was increased until the limiting flux or the maximum allowed operating pressure was reached. The experiments were conducted at 50 °C, starting at 1.5 m/s (close to the circulation pump limit) and a TMP of 1 bar. The TMP was increased gradually to a maximum of 10 bar before being lowered to 1 bar, and the crossflow velocity was adjusted to 1.0 m/s. This procedure was repeated for a crossflow velocity of 0.5 m/s. The flux was measured, and the retentate and permeate were recycled back to the feed tank to ensure that the concentration of the SSL was constant throughout the study. The process ended with a membrane-cleaning cycle, as described in Section 2.2.4.

2.2.3. Pilot-scale concentration study

When a suitable operating point was determined for the pilot

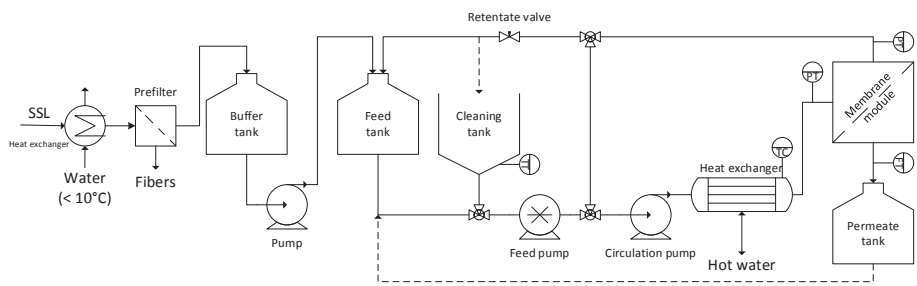


Fig. 1. Illustration of the setup in the pilot study.

equipment (based on the results of the parameter study), a concentration study was performed in batch mode at the determined operating point. The concentration step was performed with a total feed volume of 500 L at 50 °C and by continuous removal of permeate. Samples were collected at a VR of 0% and at 10-percentage-point increases until 90%. The study was terminated by recirculating the permeate in the membrane module overnight (approximately 12 h). The membranes were then cleaned according to the procedure in Section 2.2.4.

For comparison, a concentration study was carried out using the lab-scale equipment at a CFV of 0.5 m/s, a TMP of 5.5 bar, and a temperature of 50 °C to a VR of 90% per previous studies [15].

2.2.4. Membrane cleaning

Before and after each study, the membranes were cleaned by filling the tank with water (steam condensate from the pulp mill) that was heated to approximately 50 °C (Fig. 1). The water was circulated over the membranes, and the retentate and permeate were returned to the tank. When the temperature reached 50 °C, up to 0.5% by weight of an acid detergent solution (Ultrasil 73, Ecolab AB, Älvsjö, Sweden) or up to 0.1% of an alkali detergent solution (Ultrasil 10, Ecolab AB, Älvsjö, Sweden) was added to the water. The solution was circulated over the membranes for 1–2 h at a TMP of 2 bar.

After the specified times had elapsed, the cleaning solution was quenched with water (at least 5 system volumes), and the PWF was measured at 50 °C and a TMP of 2, 2.5, 3, and 3.5 bar.

2.3. Analysis

Polysaccharides, sugar alcohols, and sugar acids were analyzed by high-performance anion-exchange chromatography (Dionex, Sunnyvale, CA, USA) [15] after acid hydrolysis at 121 °C for 1 h using 0.75 mL 72% sulfuric acid per 10-mL sample. The samples were filtered before the analysis, and the filters were dried at 105 °C for 24 h and weighed to determine the acid-insoluble lignin content. The standards were analytical-grade and obtained from Fluka Chemie AG (Buchs, Switzerland) (monosaccharides and sugar acids) and Sigma-Aldrich Co. (St. Louis, MO, USA) (sugar alcohols).

Total dry substance and ash were measured using an oven at 105 °C and 900 °C, respectively, per established methods [15]. The total lignin content was analyzed using a UV spectrometer at 280 nm and an extinction coefficient of 13.01 L/g cm. The extinction coefficient was calibrated with a lignosulfonate solution that was prepared from sodium lignosulfonate powder (Domsjö Fabriker, Örnsköldsvik, Sweden), from which the SSL in this study originated.

To characterize the lignin, the sample preparation entailed diafiltration of a retentate with a VR of 90% to a diafiltration factor of 5 to wash out the pulping chemicals [20]. The hemicellulose was removed by antisolvent precipitation with the addition of acetone to a total concentration of 42 wt%. The remaining supernatant (primarily lignosulfonates, acetone, and water) was dried at 50 °C for 48 h, yielding a brown/black powder.

To determine the sulfonate and carboxylic group content, 0.6 g of the prepared lignin powder was dissolved in 20 mL deionized water. Two grams of Amberlite (IR120, H form ion-exchange resin, Thermo Fisher Scientific Inc., Waltham, MA, USA) was added to the solution, which was stirred for 3 h to convert sodium lignosulfonates to lignosulfonic acid. The solution was vacuum-filtered to remove the Amberlite before the conductometric titration. The titration was performed on an autotitrator (665 Dosimat with a 728 stirrer, Metrohm AG, Herisau, Switzerland) with conductivity (HI 76306, HI 99301, Hanna Instruments Inc., Woonsocket, RI, USA) and pH probes (HI 8424, Hanna Instruments Inc., Woonsocket, RI, USA) and 0.1 M NaOH solution as the titrant. The titrant was added in 0.5-mL increments until the conductivity increased sharply and the pH rose above 13. The sulfonate and carboxylic groups were calculated as described [28].

The total phenoxyl group content was determined by ionization difference ultraviolet spectrophotometry [29] by dissolving the lignin powder in 3 0.1 M buffers (pH 6, 12, and > 12). The measurements were performed at 300 and 360 nm for all samples, and the amount of hydroxyl units was determined per Goldmann et al. [29].

3. Modeling

3.1. Fouling models and calculation

The resistance-in-series fouling model was used to evaluate the results, as shown in Eq. (5) [30]. The breakup of the model is also illustrated in Fig. 2. R_m is the membrane resistance and was calculated when R_f was equal to 0 (the PWF after the membrane was cleaned). R_f is the sum of the resistance values during the membrane filtration of the SSL, as defined in Fig. 2. The flux and TMP were set to the average values that were observed in a concentration study, and the viscosity (μ) was set to the viscosity of water at 50 °C.

$$J = \frac{TMP}{\mu(R_m + R_f)} \tag{5}$$

3.2. Computational fluid dynamics (CFD) in COMSOL

3.2.1. CAD models and boundary conditions

The following membrane modules were modeled: the Alfa Laval M39, which was used in the pilot studies, and a 400-mL stirred cell module that was used in the lab studies, as shown in Fig. 3a and 3b.

For the M39 module, the model was based on the flow region that contained the membrane (Fig. 3a). The spacers were thus omitted, because they would only have affected the flow in the region near the outer corners of the membrane module. The M39 module contained 5 channels with 2 membranes in each channel, as seen in Fig. 3a. To simplify the model, only 1 of the channels was simulated, resulting in the 3D model in Fig. 3c. The highlighted areas (in blue) were set as the inlet and outlet of the flow. The inlet was set to a constant feed mass flow (depending on the velocity), and the outlet was set to a constant

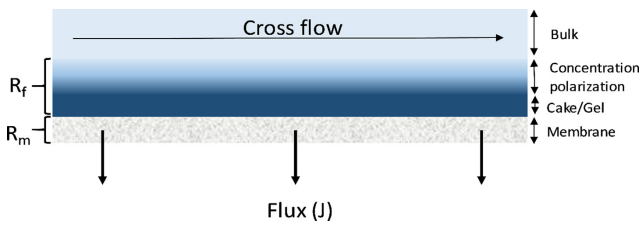


Fig. 2. Illustration of the resistance-in-series model used for the fouling calculations. R_f is the sum of resistance values over the membrane, and R_m is the membrane resistance.

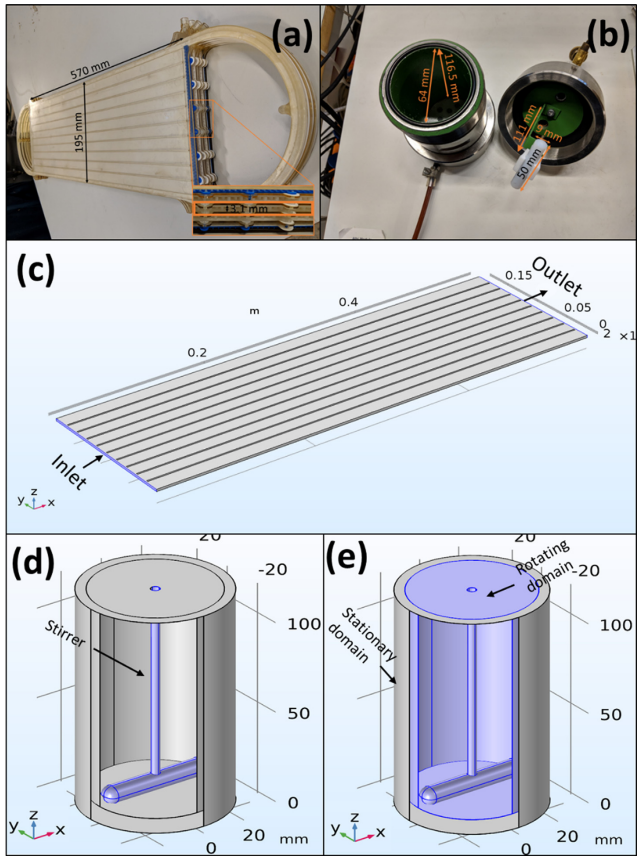


Fig. 3. The pilot (a) and stirred cell (b) modules with geometrical data that were used in designing the 3D models of the pilot flow channel (c) and the stirred cell module vessel and stirrer (d). The rotating and stationary domains of the stirred cell module were defined as shown in (e).

pressure of 0 bar. The remaining boundaries were set to the no-slip wall condition.

For the stirred cell module, COMSOL Multiphysics 5.4 (Comsol AB, Stockholm, Sweden) was used as the rotating machinery interface. The model was initially split into 2 parts: a stationary domain (outside of the stirrer radius) and a rotating domain (inside of the stirrer radius) (see Fig. 3d and 3e). The rotational velocity of the stirrer was set by defining the rotating domain as a moving mesh and was equal to the velocity in the experiments. A pressure-point constraint was set at the top of the vessel as a reference point for the pressure (which was set to 0). Finally, a symmetry boundary condition was set for the top of the vessel, where the velocity was assumed to have a gradient of 0. To estimate the deformation of the top surface (which was in contact with the nitrogen gas), a stationary free surface boundary condition was set as a postprocessing step in the simulation. The surface tension coefficients for water and air were used.

3.2.2. Mathematical model and medium

Reynold's averaged Navier Stokes (RANS) equations were used to solve the problem [31,32]:

$$\frac{\partial U}{\partial t} = -\nabla \cdot UU - \frac{1}{\rho}\nabla P + \nu\nabla^2 U - \nabla < \dot{u}\dot{u} > \tag{6}$$

The equation for the conservation of mass was also included. U (u, v, and w) and P are the velocity and pressure fields. The Reynold's stresses were defined as follows:

$$< \dot{u}\dot{u} > = \begin{bmatrix} <\dot{u}\dot{u}> & <\dot{u}\dot{v}> & <\dot{u}\dot{w}> \\ <\dot{u}\dot{v}> & <\dot{v}\dot{v}> & <\dot{v}\dot{w}> \\ <\dot{u}\dot{w}> & <\dot{v}\dot{w}> & <\dot{w}\dot{w}> \end{bmatrix} \tag{7}$$

Closure for the RANS equations was solved using the k-epsilon model, shown as follows:

$$\frac{\partial k}{\partial t} = \nabla\cdot(\nu + C_2\nu_T)\nabla k - \tau_{ij}\frac{\partial U_i}{\partial x_j} - \varepsilon \quad (8)$$

$$\frac{\partial \varepsilon}{\partial t} = \nabla\cdot(\nu + C_3\nu_T)\nabla \varepsilon + C_4\frac{\varepsilon}{k}\tau_{ij}\frac{\partial U_i}{\partial x_j} - C_5\frac{\varepsilon^2}{k} \quad (9)$$

$$\nu_T = C\frac{k^2}{\varepsilon} \quad (10)$$

$$\tau_{ij} = < u_i' u_j' > = \frac{2}{3}k\vartheta_{ij} - \nu_T\left(\frac{\partial U_i}{\partial x_j} + \frac{\partial U_j}{\partial x_i}\right) \quad (11)$$

where ν is the kinematic viscosity; C, $C2$, $C3$, $C4$, and $C5$ are model coefficients; k is the turbulent kinetic energy; ε is the turbulent dissipation rate; ν_T is the kinematic eddy viscosity; τ is the Reynold's stress; and ϑ is Kronecker delta.

The stationary problem was solved using COMSOL Multiphysics 5.4 (Comsol AB, Stockholm, Sweden), in which a coarse mesh was used for the M39 module and the region above the stirrer was used for the stirred cell module. A fine mesh was set for the region around and under the magnetic stirrer.

The problem was solved with water as the liquid medium, for which such properties as incompressibility and Newtonian fluid were assumed, based on the low total dry content of the SSL (see Section 4.1).

The Reynolds number for the M39 module was calculated as follows:

$$Re = \frac{D\rho u}{\mu} \quad (12)$$

where ρ is the density of water, u is the CFV, μ is the dynamic viscosity of water, and D is the characteristic diameter of the channel, which was calculated as follows:

$$D = \frac{2hL}{h + L} \quad (13)$$

where h and L are the height and depth of the channel, respectively.

The Reynolds number for the stirred cell was calculated as follows:

$$Re_{StirredCell} = \frac{D_{Impeller}^2\omega\rho}{\mu} \quad (14)$$

where D is the impeller diameter and ω is the stirrer speed (1/s).

4. Results and discussion

4.1. SSL composition

The prefiltered SSL had a pH of approximately 4.5 and contained primarily inorganics (ash) and lignin, as shown in Table 1. Its composition was similar to that in earlier studies [15,19]. The largest difference was observed for total dry content, lignin, acid-insoluble lignin, and GGM, all of which were slightly lower in our previous study, except for acid-insoluble lignin, which was lower in the current study. The functional group content of the lignin is consistent with the reported values for softwood lignosulfonates [33,34], rendering our observations notable in a wider perspective.

4.2. Pilot study with lab-scale operational parameters

The first experiment was performed under previously established lab-scale operating conditions [15]. The TMP, CFV, and temperature were constant at 5.5 bar, 0.5 m/s, and 50 °C, respectively, and the concentration was allowed to proceed until a VR of 90%. The flux started at 55 L/m^{2}h (Fig. 4a) and decreased linearly to a VR of approximately 60%, at which point the flux dropped at a faster rate until a VR of 90% and a flux of 10 L/m^{2}h. Compared with the lab-scale concentration in Fig. 4a, the flux was much lower. The flux-vs-VR profile of the lab-scale experiment revealed an initial flux of roughly 160 L/m^{2}h that remained constant until a VR of 40%, at which point the flux decreased slowly until a VR of 70% and the declined rapidly to a VR of 90%.

There are several possible reasons for these differences in the flux-vs-VR profiles. For instance, it is likely that the SSL in the lab-scale and pilot studies differed, because these experiments differed by over 2 years. As discussed in Section 4.1, the difference in composition was minimal. Alternatively, the batch of membranes might have differed compared with those in the lab-scale study. However, this possibility was rejected on measuring the PWF and permeability and comparing the results from the lab-scale study. The permeability of the lab-scale membrane was 70.4 L/m^{2}h bar, versus 68.3 L/m^{2}h bar in the pilot-scale setup (for pristine membranes, measured at 2 bar TMP and 50 °C). The difference in permeability between the equipment was negligible.

Further, a previous study showed that the average retention for lignin, acid-insoluble lignin, GGM, and xylan was 0.77, 0.93, 0.91, and 0.81, respectively [15]. The retention of these components (especially the polysaccharides) in the pilot study was much lower, as seen in Fig. 4b. This result might be attributed to the retention of the various components being determined by the cake/gel layer that formed on the membrane and not by the membrane per se [19]. In addition, because the flux-vs-VR profile (Fig. 4a) differed, the formation of this layer might also have differed. The disparity between the retention of solute contrasted that in previous reports [15,19]. For example, the retention of acid-insoluble lignin and GGM has been similar in most of our earlier reports [15,19,20]. In the current study, the difference was larger, indicating a possible structural difference (eg, lower or higher molecular weight) between the older (lab-scale) and newer SSL (pilot scale), despite the compositions being similar.

4.3. Parameter study

Assuming that a difference between the old and new SSLs existed, a

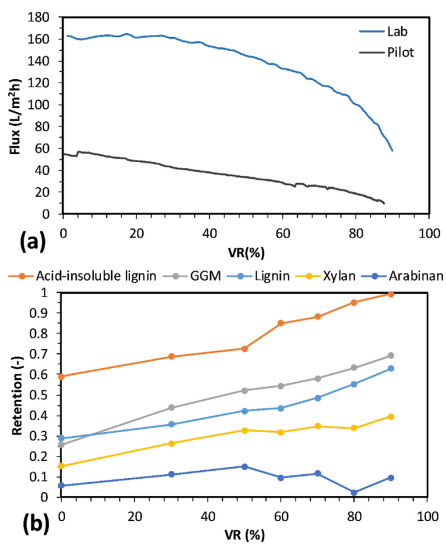


Fig. 4. (a) VR vs flux for the pilot and stirred cell modules at a TMP of 5.5 bar, temperature of 50 °C, CFV of 0.5 m/s, and VR of 90%. (b) The retention during the pilot study at select VRs.

new parameter study was required to determine a new operating point. This parameter study was performed for CFVs of 0.5 to 1.5 m/s, at which near-maximum volumetric flow was attained for the circulation pump. As shown in Fig. 5a, the initial flux was improved significantly by increasing the CFV from 0.5 to a higher velocity. The flux-vs-TMP curves followed a typical process, with the flux increasing as the TMP and CFV rose. The limiting flux was 50 L/m^{2}h at a TMP of 3.7 bar for a CFV of 0.5 m/s. At CFVs of 1.0 and 1.5 m/s, the limiting flux was 90 and 130 L/m^{2}h at a TMP of 4.6 and 5.5 bar, respectively. These results demonstrate that the capacity can be increased by a factor of 3 if the process is run at a CFV of 1.5 m/s.

Another important parameter is the retention of solutes, is related to the yield of products in the final retentate. The retention of GGM (Fig. 5b) increased by over 10 percentage points when the CFV rose from 0.5 m/s to 1.0 m/s. Additional increases in the CFV, however, did not enhance the retention further. Acid-insoluble lignin was the only other solute to improve its retention when the CFV was increased to 1.5 m/s, as seen in Fig. 5b. The retention of other solutes, such as lignin and xylan, did not increase, perhaps due to their low molecular weight compared with other solutes in the solution [15]. Based on these results, the operating point was changed to a 5.5-bar TMP at a CFV of 1.5 m/s for maximum capacity and highest retention of product.

4.4. Concentration study using pilot-scale operating parameters

4.4.1. Pilot experiment

Another concentration study was performed using the new parameters, and the results are shown in Fig. 6. Compared with the first pilot-scale study (Fig. 4), the capacity improved tremendously, with an initial flux of approximately 140 L/m^{2}h and an average flux that was 3 times higher. The retention in the concentration study followed the same trend as in the parameter study (Fig. 5b). The change in the

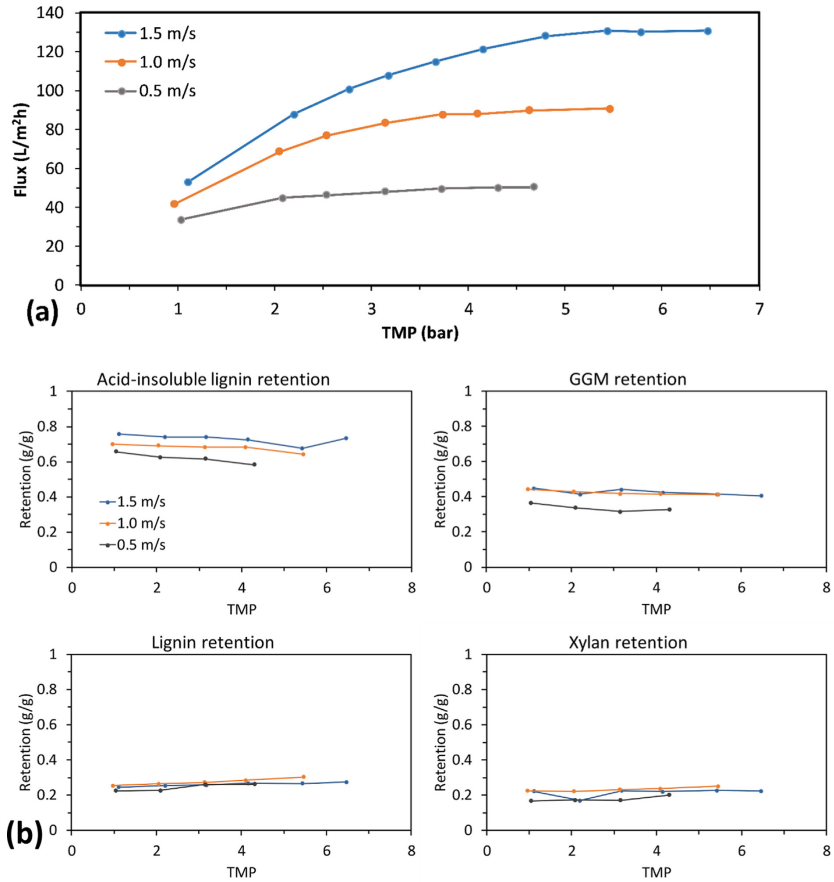


Fig. 5. Parameter study on the spent sulfite liquor (SSL) in the pilot equipment at 50 °C. (a) TMP vs flux at 3 crossflow velocities. (b) Retention of major solutes in the SSL.

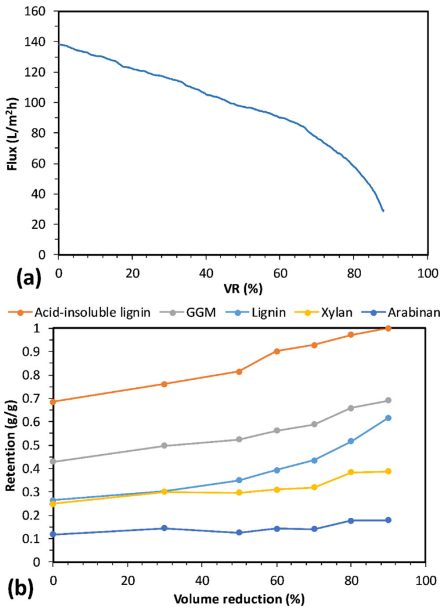


Fig. 6. Concentration study of pilot-scale equipment at 50 °C, 1.5 m/s crossflow velocity, and 5.5 bar transmembrane pressure. (a) VR-vs-flux profile. (b) Retention of solutes during the concentration.

retention of arabinan and xylan was negligible (Fig. 6b). The average retention of GGM increased from 0.52 at a CFV of 0.5 m/s to 0.57 at a CFV of 1.5 m/s, and that of the lignin decreased from 0.45 to 0.41, because of which the separation degree (mass of GGM divided by the sum of the mass of GGM and lignin) rose slightly from 18% to 19%. The average retention of acid-insoluble lignin increased from 0.81 to 0.87. However, because the amount of acid-insoluble lignin relative to the total lignin was much lower, this change had a negligible impact on separation degree.

These results show that the capacity of the membrane filtration unit can be improved but failed to reach the same range as in the lab-scale study (Fig. 4). One explanation is related to the geometries of the modules, which yielded different flow profiles, in turn affecting the Reynolds number and shear rate. These parameters alter the mass transfer of solutes to the membrane surface, which affect retention and flux [35]. The modules from the pilot and lab-scale studies have been simulated and compared in regards to the influence of these critical parameters.

4.4.2. CFD of pilot and lab-scale modules

The simulation results for the M39 module show that the flow was turbulent (see Fig. 7a), as illustrated by the flow profile, in which the velocity distribution was uniform between the middle of the channel and close to the wall, leading to an average velocity that approximated the maximum velocity. The CFV peaked near the inlet but was nearly the same throughout the entire module for the simulated flows. The velocity profile was less clear for the stirred cell module (Fig. 7b), in which the turbulence was less observable.

The state of the fluid can also be determined using the Reynolds number, which ranged from 3000 to 20,000 (Table 2) for both modules, indicating that the velocity profiles were turbulent. The calculated turbulence kinetic energy also showed the tendency to form eddies, or the "strength" of the turbulence. The results in Table 2 indicate that both modules operated in the turbulent region, given that the turbulent kinetic energy was not 0. Compared with the M39 at the same CFV, the experimental membrane fluxes were > 300% higher in the stirred cell module. The average shear rate over the membranes in both modules differed (Table 2). The stirred cell module had a shear rate that was higher by a factor of 2, suggesting that the tendency to form a cake layer on the membrane was lower for the stirred cell module, which explained its higher flux [36]. An increase in the inlet CFV for the M39 from 0.50 to 1.00 m/s resulted in a shear rate that was nearly equal to that for the stirred cell module (Table 2). This change in turn increased the membrane flux, which nevertheless remained lower than that for the stirred cell module. Shifting the M39 CFV to 1.5 m/s enhanced the average shear rate by over 2-fold compared with that for the stirred cell module (Table 2).

One possible reason for the flux remaining lower in the M39 versus the stirred cell module is that the average shear rates are not comparable between modules. The average shear rate is an acceptable approximation when comparing results from the M39 study, because the velocity was nearly constant throughout the entire module (Fig. 7a). In the stirred cell module, the velocity at the membrane surface depended on the position of the stirrer and thus varied to a significant extent (Fig. 7c). At the regions with the highest velocity (highlighted in red, Fig. 7c), shear rates of 1074 s^{-1} were calculated, in turn explaining the higher experimental fluxes that were observed.

Another explanation is the disparate modes of operation for the 2 modules. The stirred cell module was operated at the final VR (Eq. (3)), because neither feed nor retentate entered or exited the module in the concentration study. In contrast, the M39 module was operated with 2 pumps—1 feed and 1 loop (circulation) pump—as shown in Fig. 1, causing the process to run at 2 VRs. The loop functioned at a specific VR, which was set using the feed pump per Eq. (4). The feed pump was set to a flow of approximately 280 L/h (near the maximum flow that the feed pump could handle), and the flux was roughly 138 L/m^2h at the outset of the concentration study (VR of 0%).

From Eq. (4), the loop VR was approximately 40%, implying that the process ran constantly at a VR that exceeded the total VR (Eq. (3)), as seen in Fig. 8, in which the x-intercept of the horizontal line from the start of the M39 flux curve to the stirred cell flux curve indicates that the loop VR at which the M39 module was operating was 44% in this

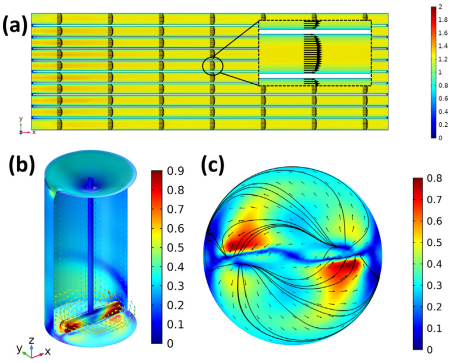


Fig. 7. Velocity profiles for the pilot (a) and stirred cell modules (b) and (c) in the COMSOL simulations. The gradient legends show the velocity in m/s.

Table 2
Comparison of results from experimental (CFV, flux) and COMSOL simulations.

	Experimental inlet CFV (m/s)	Simulation CFV (m/s)	Turbulent kinetic energy 10^4 (m^2/s^2)	Average shear rate (1/s)	Flux (L/m^2h) (Experimental)	Pressure Drop 10^5 (bar)	Reynolds number
M39 module	0.50	0.40	17	148	50	375	3000
	1.00	0.70	42	368	91	968	6100
	1.50	1.05	81	701	138	1940	9100
Stirred cell module	0.50	0.35	129	297	162		21,000

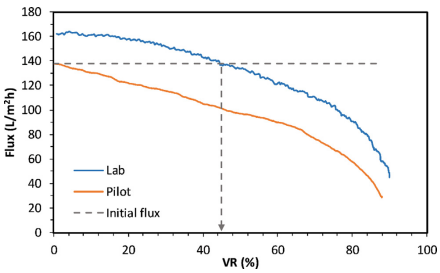


Fig. 8. Comparison of the lab-scale (stirred cell module) and pilot-scale VR-vs-flux profiles. The dashed line represents the initial flux (VR of 0) in the pilot study. The intersection of the dashed line and lab-scale flux curve represents the loop VR (LVR) of the pilot study, per Eq. (4).

case. This observation explains why the M39 flux never matched the capacity in the stirred cell configuration. The same arguments are applicable with regard to the lower retention, wherein a high loop VR would have increased the concentration of solutes near the membrane surface and, consequently, in the permeate, resulting in lower retention [35].

Another explanation for the difference in flux and retention between the lab-scale and pilot-scale experiments is related to the compaction of the membrane and the effect of temperature on the membrane material, which could have induced deformations. Stade et al. [37] measured the effects of compaction on the performance of 3 ultrafiltration membranes at various temperatures, reporting that the molecular weight cutoff (MWCO) could be controlled using pressure and temperature, in turn affecting the flux and retention of solutes. The regenerated cellulose membrane was among the membranes that were mostly affected, wherein the MWCO changed from 30 kDa to 8 kDa.

In our study, the pressure—or rather, the TMP—was the same in the lab-scale and pilot-scale equipment; the only difference was thus the temperature during the membrane filtration or the solute composition. The composition was similar to that in previous studies, and the flux with the new SSL (Fig. 8) was in the same range as published [15]. For the pilot studies, the temperature was mostly stable, fluctuating between 48 °C and 51 °C. For the lab-scale study, the set temperature was reached by heating the stirred cell module from the bottom (near the membrane and permeate outlet) (see Fig. 7). To obtain an average temperature of 50 °C in the solution, the temperature of the heating plate must be higher. We measured the temperature on the bottom of the module (close to the membrane and permeate outlet), which was roughly 60 °C, peaking at 65 °C when the solution and module were heated from room temperature.

The higher retention in the lab-scale study might have resulted from the higher temperature causing compaction of the membrane, thus lowering the MWCO. However, the decrease in MWCO can lower the flux through the membrane, as concluded by Stade et al. [37]. Further, the higher flux could have been an effect of lower permeate viscosity (cf. Eq. (5)). This hypothesis was not tested in the pilot study and remains for future work.

4.5. Fouling and cleaning

Membrane fouling is an important factor that must be accounted for with regard to scaling up, because it affects the capacity of the plant [38]. The membrane fouling was measured over time while examining several cleaning methods. The study was performed through repeated concentration experiments that ended with a specific cleaning method and a measurement of the pure-water flux to calculate the membrane resistance and the resistance from concentration polarization and cake/gel formation; the results are shown in Fig. 9. The selected membrane can withstand a maximum pH of 11, rendering it suitable for the cleaning step at a low concentration of the alkaline cleaning agent, Ultrasil 10 (0.05 wt%), which resulted in a pH of 8 to 9. Cleaning did not have a direct effect, as seen from the gradual rise in membrane resistance (Fig. 9a). After 5 cycles, the Ultrasil concentration increased to 0.1 wt%, and the pH became approximately 11, causing the increase in the rate of membrane resistance to decrease slightly, but a large effect could not be observed. We concluded that the effect was not caused by fouling of the membrane but perhaps due to compaction of the

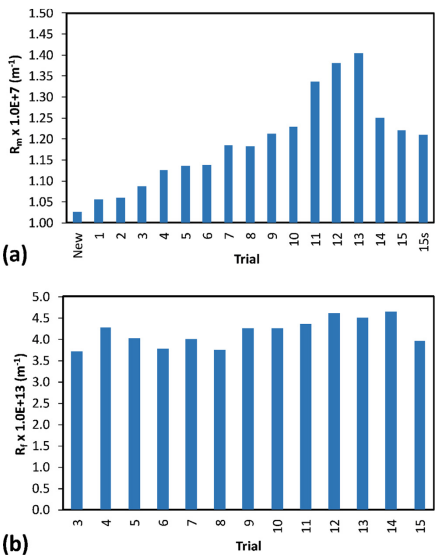


Fig. 9. Membrane resistance (a) after each concentration study (trial), with a 15-s second cleaning cycle at trial 15. Resistance due to fouling (b) was only seen in trials 3 to 15, in which the process parameters (transmembrane pressure, volume reduction, and cross-flow velocity) were the same.

membrane, which in turn increased the membrane resistance over time. The fouling resistance (Fig. 9b), which was approximately constant throughout the study period, also indicated this phenomenon.

The effect of the cleaning agent was more noticeable when the Ultrasil 10 cleaning step was removed, wherein rinses with only water were performed after each concentration experiment. The membrane resistance increased from 1.23e7 to 1.34e7 m^{-1} and peaked at 1.40e7 m^{-1} after 3 concentrations. When cleaning was performed with 0.1 wt % Ultrasil 10, the membrane resistance decreased to 1.25e7 m^{-1}, returning to the original resistance of 1.21e7 m^{-1} after a second wash.

A wash time of approximately 1 h was sufficient—a 2-hour wash did not affect any further improvements. However, 2 consecutive washes improved the cleaning, as demonstrated by the attempts to recover the membrane state in "trial 15" and "trial 15 s cleaning" (Fig. 9a). High pH is also important during the cleaning step, perhaps attributed to the fouling solutes being lignin-related [19,39]. This correlation was most evident when Ultrasil 10 (basic) was switched to Ultrasil 73 (acidic) at 0.5 wt% in trial 10. At the beginning of the procedure, the flux appeared to be stable and constant (Fig. 10a), but after 20 min, the flux began to decrease. When the flux dropped by approximately 10% of the original value (after 60 min), the cleaning was halted, and the detergent was rinsed to prevent irreversible fouling. The flux was restored by washing with 0.1 wt% Ultrasil 10 for 1 h; consequently, no severe irreversible fouling was detected, as seen in Fig. 9a (trial 10).

Maintaining the flux and the retention of the product with time is also important economically. The average flux during the concentration studies was stable at approximately 88 L/m^2h. The variation was not high but notable, especially for the region during which the chemical cleaning was interrupted (Fig. 10b, trial 10 to 14). After the cleanse in trial 14, the average flux increased from 78 to 92 L/m^2h, underscoring the importance of the cleaning step in maintaining a high flux. The retention was unaffected by the minor changes in flux, as shown in Fig. 10c. GGM experienced constant retention, as indicated by the error bars. The acid-insoluble lignin and total lignin had the highest variation in retention, perhaps because lignin was the likely cause of fouling [19,39,40].

5. Conclusions

In this study, the aim was to scale up the results from the lab-scale ultrafiltration of SSL and present the challenges faced in the process. The pilot studies were done on-site in a plate-and-frame based membrane filtration unit to maintain the similarities to the lab-scale equipment. The analysis of the raw material showed that there were no major differences in the composition of the SSL between the pilot-scale and lab-scale studies.. Running the pilot equipment under the same conditions as the lab-scale equipment (TMP, CFV, and temperature) resulted in a much lower permeate flux and retention of the solutes. The flux was improved in the pilot setup by increasing the CFV from 0.5 to 1.0 and 1.5 m/s. The retention of GGM rose by 10% when the CFV was increased to 1.0 m/s, and no further increment was observed for the higher CFV of 1.5 m/s. The flux at the highest CFV (1.5 m/s) was not in the same range as that for the lab-scale experiments. CFD simulations showed that the shear rate in the pilot experiments was lower than in the lab-scale experiments at a CFV of 1.5 m/s and lower, which could explain the lower flux in the former. Another likely reason is the mode of operation of the 2 modules, wherein the low flow of the pilot feed pump resulted in a high loop VR, which in turn effected a low permeate flux and lower retention of the products.

Another important factor in scale-up studies is membrane fouling and cleaning. Our results indicated that an alkaline cleaning agent with a pH of approximately 11 was sufficient. The required cleaning time was 1 h, with longer times yielding the same result. However, increasing the cleaning cycles improved the cleaning of the membrane. The retention of products was unaffected by the cleaning, and a stable average flux of 88 L/m^2h was achieved over the course of the concentration studies.

CRediT authorship contribution statement

Basel Al-Rudainy: Conceptualization, Methodology, Software, Validation, Investigation, Writing - original draft, Visualization. **Mats Galbe:** Writing - review & editing, Supervision. **Ola Wallberg:** Conceptualization, Writing - review & editing, Supervision, Funding acquisition.

Declaration of Competing Interest

The authors declare that they have no known competing financial interests or personal relationships that could have appeared to influence the work reported in this paper.

Acknowledgments

The authors thank Domsjö Fabriker (in particular, Ole Norberg and Magnus Hörnsten) for all their on-site help and support and Alfa Laval (Nakskov) for their provision of the membranes that were used in this study.

This research was funded by the Swedish Foundation for Strategic

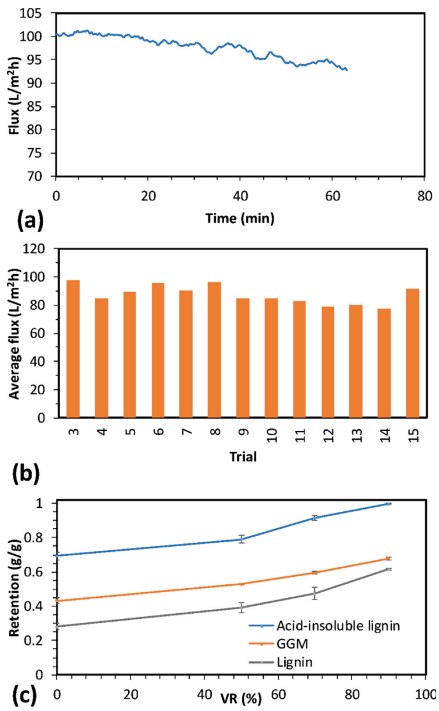


Fig. 10. Results from the acidic cleaning (a) using 0.5 wt% Ultrasil 73 after trial 10, the average flux during each trial (b), and the retention of acid-insoluble lignin, galactoglucomannan (GGM), and lignin (c) based on measurements in trials 3, 8, and 12.

Research (SSF) (RBP 14-0046), which is gratefully acknowledged.

References

[1] H.L. Hintz, Paper: Pulping and Bleaching, in: K.H.J. Buschow, R.W. Cahn, M.C. Flemings, B. Ilschner, E.J. Kramer, S. Mahajan, P. Veyssière (Eds.), Encyclopedia of Materials: Science and Technology, Elsevier, Oxford, 2001, pp. 6707–6711.

[2] L. Stockman, Recent developments and present trends in sulphite pulping, Pure Appl. Chem. 5 (1962) 165–176.

[3] J. Hartman, A.C. Albertsson, M.S. Lindblad, J. Sjöberg, Oxygen barrier materials from renewable sources: Material properties of softwood hemicellulose-based films, J. Appl. Polym. Sci. 100 (2006) 2985–2991.

[4] B. Al-Rudainy, M. Galbe, M. Arcos Hernandez, P. Jannasch, O. Wallberg, Impact of Lignin Content on the Properties of Hemicellulose Hydrogels, Polymers 11 (2018) 35.

[5] M. Söderqvist Lindblad, A.-C. Albertsson, E. Ranucci, M. Laus, E. Giani, Biodegradable polymers from renewable sources: rheological characterization of hemicellulose-based hydrogels, Biomacromolecules 6 (2005) 684–690.

[6] A. Rosengren, S.J. Butler, M. Arcos-Hernandez, K.-E. Bergquist, P. Jannasch, H. Stålbrand, Enzymatic synthesis and polymerisation of β-mannosyl acrylates produced from renewable hemicellulosic glycans, Green Chem. 21 (2019) 2104–2118.

[7] K.S. Mikkonen, M. Tenkanen, P. Cooke, C. Xu, H. Rita, S. Willför, B. Holmbom, K.B. Hicks, M.P. Yadav, Mannans as stabilizers of oil-in-water beverage emulsions, LWT-Food Sci. Technol. 42 (2009) 849–855.

[8] C. Huang, J. Ma, W. Zhang, G. Huang, Q. Yong, Preparation of lignosulfonates from biorefinery lignins by sulfomethylation and their application as a water reducer for concrete, Polymers 10 (2018) 841.

[9] C. Pouteau, P. Dole, B. Cathala, L. Averous, N. Boquillon, Antioxidant properties of lignin in polypropylene, Polym. Degrad. Stab. 81 (2003) 9–18.

[10] J.F. Kadla, S. Kubo, R.A. Venditti, R.D. Gilbert, A.L. Compere, W. Griffith, Lignin-based carbon fibers for composite fiber applications, Carbon 40 (2002) 2913–2920.

[11] V. Mimini, V. Kabrelian, K. Fackler, H. Hettegger, A. Potthast, T. Rosenau, Lignin-based foams as insulation materials: a review, Holzforschung 73 (2018) 117–130.

[12] W. Wu, T. Dutta, A.M. Varman, A. Eudes, B. Manalansan, D. Loqué, S. Singh, Lignin Valorization: Two Hybrid Biochemical Routes for the Conversion of Polymeric Lignin into Value-added Chemicals, Sci. Rep. 7 (2017) 8420.

[13] V. Kisonen, C. Xu, R. Bollström, J. Hartman, H. Rautkoski, M. Nurmi, J. Hemming, P. Eklund, S. Willför, O-acetyl galactoglucomannan esters for barrier coatings, Cellulose 21 (2014) 4497–4509.

[14] A.-S. Jönsson, Membranes for lignin and hemicellulose recovery in pulp mills, Membrane Technologies for Biorefining, Elsevier, 2016, pp. 105–133.

[15] B. Al-Rudainy, M. Galbe, F. Lipnizki, O. Wallberg, Galactoglucomannan Recovery with Hydrophilic and Hydrophobic Membranes: Process Performance and Cost Estimations, Membranes 9 (2019) 99.

[16] H. Krawczyk, P. Oinonen, A.-S. Jönsson, Combined membrane filtration and enzymatic treatment for recovery of high molecular mass hemicelluloses from chemithermomechanical pulp process water, Chem. Eng. J. 225 (2013) 292–299.

[17] J. Thuvander, A.-S. Jönsson, Extraction of galactoglucomannan from thermomechanical pulp mill process water by microfiltration and ultrafiltration—Influence of microfiltration membrane pore size on ultrafiltration performance, Chem. Eng. Res. Des. 105 (2016) 171–176.

[18] T. Persson, H. Krawczyk, A.K. Nordin, A.S. Jönsson, Fractionation of process water in thermomechanical pulp mills, Bioresour. Technol. 101 (2010) 3884–3892.

[19] B. Al-Rudainy, M. Galbe, O. Wallberg, Influence of prefiltration on membrane performance during isolation of lignin-carbohydrate complexes from spent sulfite liquor, Sep. Purif. Technol. 187 (2017) 380–388.

[20] B. Al-Rudainy, M. Galbe, H. Schagerlöf, O. Wallberg, Antisolvent precipitation of hemicelluloses, lignosulfonates and their complexes from ultrafiltrated spent sulfite liquor (SSL), in: Holzforschung, 2018, pp. 839.

[21] T. Song, A. Pranovich, B. Holmbom, Separation of polymeric galactoglucomannans from hot-water extract of spruce wood, Bioresour. Technol. 130 (2013) 198–203.

[22] D. Zasadowski, J. Yang, H. Edlund, M. Norgren, Antisolvent precipitation of water-soluble hemicelluloses from TMP process water, Carbohydr. Polym. 113 (2014) 411–419.

[23] P. Rajniak, S. Tsinontides, D. Pham, W. Hunke, S. Reynolds, R. Chern, Sterilizing filtration—principles and practice for successful scale-up to manufacturing, J. Membr. Sci. 325 (2008) 223–237.

[24] D. Dolar, T.I. Zokić, K. Košutić, D. Ašperger, D.M. Pavlović, RO/NF membrane treatment of veterinary pharmaceutical wastewater: comparison of results obtained on a laboratory and a pilot scale, Environ. Sci. Pollut. Res. 19 (2012) 1033–1042.

[25] J. Thuvander, F. Lipnizki, A.-S. Jönsson, On-Site Recovery of Hemicelluloses from Thermomechanical Pulp Mill Process Water by Microfiltration and Ultrafiltration, J. Wood Chem. Technol. 39 (2019) 214–223.

[26] J. Fernández Rodríguez, A. García Núñez, A. Coz Fernández, J. Labidi, Fractionation of spent sulphite liquor into monomeric sugars and lignosulphonates by an ultrafiltration series system, (2015).

[27] J. Fernández-Rodríguez, A. García, A. Coz, J. Labidi, Spent sulphite liquor fractionation into lignosulphonates and fermentable sugars by ultrafiltration, Sep. Purif. Technol. 152 (2015) 172–179.

[28] R. Beatson, Determination of sulfonate groups and total sulfur, Methods in lignin chemistry, Springer, 1992, pp. 473–484.

[29] W.M. Goldmann, J. Ahola, O. Mankinen, A.M. Kantola, S. Komulainen, V.-V. Telkki, J. Tanskanen, Determination of phenolic hydroxyl groups in technical lignins by ionization difference ultraviolet spectrophotometry (Δ ε-IDUS method), Periodica Polytech., Chem. Eng. 61 (2017) 93–101.

[30] G.D. Bella, D.D. Trapani, A Brief Review on the Resistance-in-Series Model in Membrane Bioreactors (MBRs), Membranes 9 (2019) 24.

[31] S.B. Pope, Turbulent flows, IOP Publishing, 2001.

[32] J.H. Ferziger, M. Perić, Computational methods for fluid dynamics, Springer, 2002.

[33] Y. Qin, L. Yu, R. Wu, D. Yang, X. Qiu, J. Zhu, Biorefinery lignosulfonates from sulfite-pretreated softwoods as dispersant for graphite, ACS Sustain. Chem. Eng. 4 (2016) 2200–2205.

[34] P. Korntner, A. Schedl, I. Sumerskii, T. Zweckmair, A.K. Mahler, T. Rosenau, A. Potthast, Sulfonic acid group determination in lignosulfonates by headspace gas chromatography, ACS Sustain. Chem. Eng. 6 (2018) 6240–6246.

[35] P. Prádanos, J.I. Arribas, A. Hernández, Mass transfer coefficient and retention of PEGs in low pressure cross-flow ultrafiltration through asymmetric membranes, J. Membr. Sci. 99 (1995) 1–20.

[36] A.-S. Jönsson, Influence of shear rate on the flux during ultrafiltration of colloidal substances, J. Membr. Sci. 79 (1993) 93–99.

[37] S. Stade, M. Kallioinen, T. Tuuva, M. Mänttäri, Compaction and its effect on retention of ultrafiltration membranes at different temperatures, Sep. Purif. Technol. 151 (2015) 211–217.

[38] W. Sun, J. Liu, H. Chu, B. Dong, Pretreatment and membrane hydrophilic modification to reduce membrane fouling, Membranes 3 (2013) 226–241.

[39] D. Humpert, M. Ebrahimi, P. Czermak, Membrane Technology for the Recovery of Lignin: A Review, Membranes 6 (2016) 42.

[40] J. Li, T. O'Hagan, J. MacLeod, Using ultrafiltration to analyze the molar mass distribution of kraft lignin at pH 13, Canadian J. Chem. Eng. 74 (1996) 110–117.

Paper VI

molecules

MDPI

Article

Hemicellulose Recovery from Spent-Sulfite-Liquor: Lignin Removal by Adsorption to Resins for Improvement of the Ultrafiltration Process

Basel Al-Rudainy *, Mats Galbe and Ola Wallberg

Department of Chemical Engineering, Lund University, SE-221 00 Lund, Sweden; mats.galbe@chemeng.lth.se (M.G.); ola.wallberg@chemeng.lth.se (O.W.)

* Correspondence: basel.al-rudainy@chemeng.lth.se

Received: 30 June 2020; Accepted: 27 July 2020; Published: 28 July 2020



Abstract: In this work, three polymeric resins were examined as alternatives for the separation of hemicellulose and lignin. The aim was to remove the lignin from spent-sulfite-liquor (SSL) prior to ultrafiltration, producing a hemicellulose-rich retentate with high purity, and increase the capacity of the membrane filtration. The lignin in the SSL was sulfonated; thus, two of the resins were anion exchangers and 1 was hydrophobic. The data from the equilibrium studies and adsorption kinetics were fitted to established models, and the results were interpreted based on these observations. The strongly basic anion exchanger performed best with regard to lignin removal. The adsorption followed the Sips isotherm, indicating that the process was cooperative with chemisorption as the main reaction between the adsorbate and adsorbent based on the kinetics. Regeneration of the adsorbent was also possible, wherein 100 g/L NaCl was sufficient to recover 98% of the lignin. The lignin removal had a positive effect on the ultrafiltration process, in which the flux increased by 38% and the extent of separation between the hemicellulose and lignin rose from 17% to 59%.

Keywords: galactoglucomannan; lignin; lignin–carbohydrate-complex; lignosulfonates; adsorption; ultrafiltration; spent-sulfite-liquor

1. Introduction

There is growing interest in replacing fossil-based carbon sources with renewable bio-based alternatives. To this end, forest-based lignocellulosic biomass is a promising renewable alternative. It contains primarily cellulose, hemicellulose, and lignin of which cellulose is the most widely known and utilized component. Because lignin and hemicellulose account for over 50% of the available biomass, greater utilization of this material is important with regard to sustainability [1]. In the past several decades, lignin has been the focus regarding the development of various extraction methods and applications [2,3]. This strategy has led to the development of products such as adhesives, plasticizers, and biofuels [4–6].

Conversely, hemicellulose is a promising raw material for the production of barrier films, hydrogels, surfactants, and biofuels [7–10]. However, unlike lignin, large-scale production of hemicellulose does not exist, impeding the development of applications and the commercialization of hemicellulose-based products [11]. This deficiency has rendered research on the production of hemicellulose important for the advancement of sustainability goals.

Hemicellulose can be extracted from wood using such techniques as pressurized hot-water extraction, microwave heat fractionation, and steam explosion [12–14]. However, regardless of technique, all of them require the design of an entire process, which also entails separation and recovery steps. An alternative source from which hemicellulose can be recovered is waste streams in the pulp

and paper industries, which remain largely untapped [15]. By utilizing the waste streams in pulp mills, their product portfolio will expand, and the load on the wastewater treatment plant will decrease.

Spent-sulfite-liquor (SSL) is a waste stream that is generated during the production of sulfite pulp. SSL is usually concentrated using evaporators and incinerated to recover pulping chemicals and generate power and heat [16]. SSL from conventional pulp and paper industries usually contains monosaccharides, lignosulfonates, extractives, and pulping chemicals [17]. When the pulping is performed in two stages, one of which has a pH of 4 to 5, the SSL also contains polysaccharides, such as hemicelluloses, but also lignin–carbohydrate complexes (LCCs) [11,17]. In this work, SSL was taken from the first step of the 2-step sodium-based sulfite pulping of spruce and pine, in which polymeric hemicellulose exists and is intact. SSL from spruce and pine contains primarily the hemicellulose galactoglucomannan, as expected in softwoods. Other minor hemicelluloses in SSL are xylan-based, but arabinogalactans are also present [18,19]. Given this complex mixture of polysaccharides, monosaccharides, lignosulfonates, and their complexes, its separation is challenging.

Membrane filtration technology has been used to separate similar waste streams, generating promising results [20–22]. Persson and Jönsson [20] concentrated a solution (softwood masonite wastewater) that contained 1–2 g/L to 60 g/L hemicellulose, reducing the volume by 99%. Hydrophobic compounds, such as lignin, were separated prior to the membrane filtration using activated carbon. The authors concluded that this method was an effective solution, but the cost of the activated carbon was high, and the regeneration was difficult. Krawczyk, et al. [22] combined membrane filtration and enzymatic treatment to separate high-molecular-weight hemicelluloses from chemi-thermomechanical process water. The group separated impurities such as colloids and fibers by microfiltration and concentrated the microfiltration permeate using ultrafiltration. The retentate was enzymatically treated to polymerize the hemicellulose–lignin complexes and further ultrafiltered to remove smaller, unreacted polysaccharides. The process yielded a high-quality hemicellulose solution with a concentration of 54 g/L.

Membrane filtration alone can be used in certain cases to separate and purify hemicellulose solutions [23,24]. However, in many cases, the combination of membrane filtration with another separation technique or pretreatment of the raw material is needed [18,23], perhaps because the hemicellulose and lignin have a slight difference in molecular weight, there are other impurities that hinder the separation, fouling increases the retention of all solutes, or they exist as LCCs [18,23].

As discussed above, Persson and Jönsson [20] and Krawczyk, et al. [22] presented several solutions for these problems. The use of activated carbon to remove hydrophobic compounds, such as lignin, increases the membrane filtration capacity (i.e., decreases fouling) and separates compounds. However, given the difficult task of regenerating activated carbon and recovering the adsorbed lignin and due to the high price of the adsorbent, this was not feasible [20,25]. Krawczyk, et al. [22] solved the separation issue by changing the molecular weight of the hemicellulose enzymatically prior to the final ultrafiltration step. Although this method worked, it required the product to be altered and a membrane filtration step to be added. Anti-solvent precipitation has also been shown to be an effective solution for separation of hemicellulose and lignin using either alcohols or acetone [18,26,27].

In our previous study, membrane filtration prior to the precipitation step was beneficial for cases in which the solutions were diluted [18]. Using this method, a degree of separation (mass of galactoglucomannan (GGM) divided by the sum of the lignin and galactoglucomannan mass) and yields above 76% were achieved. Although this method is efficient with regard to separation, it requires additional high-energy-demanding processing steps to recover the anti-solvent to become a viable solution. In addition, ideally, the method should be used after membrane filtration, given that anti-solvent precipitation of dilute solutions requires large amounts of anti-solvent, and thus does not increase the membrane filtration capacity [18].

Polymeric resins have been used to separate lignin, lignosulfonates, and other phenolic compounds from many sources [28–34]. Nitzsche, et al. [29] implemented the hydrophobic resins XAD7HP and SEPABEADS SP700 to remove 100% of the lignin from beech-wood hydrolysate, with a hemicellulose

recovery of over 92%. The adsorption of phenol followed the Freundlich equation in single-component experiments and the extended Freundlich isotherm in multicomponent experiments. Schwartz and Lawoko [30] used XAD-4 hydrophobic resin to remove acid-soluble lignin from acid-hydrolyzed hemicelluloses (hardwood). The resin removed 100% of the furan derivatives and 90% of the acid-soluble lignin.

Narron, et al. [33] applied XAD16N, removing approximately 90% of the soluble lignin hardwood autohydrolysate and determined by NMR that the sugar loss was due primarily to the existence of LCCs. Heinonen, et al. [34] used the same type of resin on monosaccharide-rich hardwood hydrolysates and removed 80% of the lignin, with minimal loss of sugar (95% recovery). The primary goal of most of these studies was to produce high-quality lignin or improve the downstream fermentation process. Koivula, et al. [28] aimed to recover hemicellulose from birch and pine/eucalyptus hydrolysates and simultaneously enhance the membrane filtration by adsorbing the membrane foulants onto XAD-7 and XAD-16, decreasing membrane fouling and improving the flux. They also found that the decline in fouling was due to the removal of lignin-like material from the hydrolysates and that with large amounts of adsorbent, the loss of hemicellulose was significant. The type of lignin in these studies was not reported to contain sulfonic acid groups and was thus not comparable with the SSL in our work.

However, a similar resin (XAD-7) was used by Sumerskii, et al. [31] to isolate lignosulfonates from SSL, with which a lignosulfonate with high purity was generated, and the method was reported to be faster than ultrafiltration. The lignosulfonates that were produced using this method contained lower levels of sulfonic acid groups, which the group attributed to the high hydrophilicity of the lignosulfonates and the desorption that occurs during the washing of the resin.

Charged polymeric resins, or ion exchangers, constitute a potentially significant separation method. Lignosulfonates are negatively charged; thus, anion exchangers could be used to selectively adsorb the lignosulfonates. A patent by Van Blaricom and Russell [35] describes a method for separating lignosulfonates from ammonium-based SSL using anion exchange resins. According to these authors, a resin that contains primary or secondary amino groups is unsuitable for lignosulfonate-containing solutions, because such groups react with the lignosulfonates or other groups in the SSL and thus decrease the adsorption capacity. They suggested using resins with tertiary amino groups, which yield weakly basic resins, instead of quaternary amino groups, which generate strongly basic resins. The authors found that strongly basic resins were less efficient in the regeneration using sodium hydroxide. The authors used weakly basic resins to adsorb lignosulfonates from SSL (pH of approximately 4) and observed no adsorption of monosugars. The effluent after the adsorption had a pH of 9 to 11 when the free base form of the resin was used, which did not pose a problem, because the effluent contained ammonium hydroxide, which could be recovered and used in the pulping process.

Takahashi, et al. [36] removed acetic acid from SSL prior to fermentation to mitigate the inhibition of ethanol production using a strong-base anion-exchange resin to adsorb acetic acid. However, lignosulfonates were also adsorbed and thus decreased the amount of acetic acid that could be adsorbed. The (OH^-) form of the resin also created problems, because the pH of the solution changed, in turn decomposing the monosugars in the solution. These problems were addressed by performing the adsorption in two stages with a neutralization treatment using CaO and CO_2, resulting in 90% removal of acetic acid and greater ethanol production.

Liu, et al. [37] used a fixed-bed column with weakly basic anion exchangers to separate magnesium lignosulfonates from xylo-oligosaccharides, obtaining adsorption capacities as high as 390 mg/g resin and recovery yields of 98% for lignosulfonates and 93% for xylo-oligosaccharides. Other studies have performed lignosulfonate adsorption as a pretreatment method prior to further processing; thus, this method was not their focus [38,39].

The goal of this work was to remove lignin (here also lignosulfonates) from SSL using anion exchangers and hydrophobic resins. The adsorption data were fitted to commonly used adsorption models, and the results were interpreted based on the models and the underlying mechanisms. Another important factor of the industrial use of these resins is their regenerative ability. Thus, lignin desorption

by the best-performing resin was also studied, and the SSL with the lower lignin content was filtered and compared with the original SSL solution.

2. Results and Discussion

2.1. Screening of Adsorbents

The raw material in this study was sodium-based SSL with a pH of approximately 4.5, containing primarily lignin (including lignosulfonates), pulping chemicals, and polysaccharides, as seen in Table 1. GGM was the main hemicellulose that was detected, with a monomeric composition of 0.41:0.36:1 (galactose/glucose/mannose). These values are higher than what was expected for pure GGM [40], based on our previous report [18], due to the presence of other galactan-based polysaccharides, such as arabinogalactan and β-galactan. Other minor hemicelluloses in the solution were xylan-type, as evidenced by the amounts of xylan and arabinan. Overall, this batch of SSL did not differ in composition from what has been reported [11,18,23,41].

Table 1. Composition of the spent-sulfite-liquor (SSL) raw material.

	Concentration (g/L)
Total dry substance	84.7
Ash	31.3
Acid soluble lignin	34.1
Acid insoluble lignin	2.0
Arabinan	0.6
Galactan	1.6
Glucan	1.4
Xylan	1.5
Mannan	3.9

Three resins were used to screen adsorbents: strong basic (IRA958), weak basic (IRA67), and hydrophobic (XAD4). The anion exchangers were chosen based on the functional group composition, for which a tertiary or quaternary amine was a requirement [35]. The hydrophobic resin was selected based on previous successful utilization of the resin in lignin removal applications [30].

The results of the adsorption screen for the raw SSL solution are presented in Figure 1. At first glance, the two adsorbents that performed best in selectively removing the lignin were IRA958 and XAD4. IRA958 outperformed all of the other adsorbents in adsorbing the highest amount of lignin per gram of adsorbent, resulting in a total removal of 85%. XAD4 poorly adsorbed the acid-soluble lignin (which included lignosulfonates) but removed acid-insoluble lignin well, with rates reaching as high as 90%. IRA958 and IRA67 removed a substantial amount of acid-insoluble lignin, suggesting that the acid-insoluble lignin was sulfonated before the acid hydrolysis, explaining the desulfonation and consequent precipitation of the lignin [42].

Coupling of the acid-insoluble lignin to the carbohydrates was also suggested by the adsorption of polysaccharides to XAD4, as seen in Figure 1. The amounts of polysaccharides adsorbed on the XAD4 was low, the polysaccharides together with the lignin were desorbed to confirm that the polysaccharides did indeed adsorb on the resin and that the results presented in Figure 1 were not due to errors. The XAD4 was rinsed with a total of 60 mL deionized water (20 mL for each rinse), and the adsorbates were desorbed sequentially using 60 mL 4 g/L sodium hydroxide solution and 60 mL methanol (20 mL for each rinse).

Through this procedure, 25% of the total adsorbed acid-insoluble lignin was recovered, of which 4.7% comprised polysaccharides. The composition of the desorbed polysaccharides with regard to xylan and arabinan was the same as in Table 1 but differed for GGM, which had a monomeric composition of 0.50:0.80:1 (Gal/Glu/Man). The comparison of desorbed GGM with the GGM in the raw material suggested that a major portion of the LCCs in this fraction comprised a bond between

the glucose or mannose component of the GGM and lignin, possibly phenyl glycosidic bonds [23]. No adsorption of polysaccharide was observed in this initial screen for IRA958 and IRA67; instead, the concentration of polysaccharides increased. The adsorbents were dry before use, and according to the manufacturer, the moisture-retaining capacity of the resins ranges from 60% to 80%.

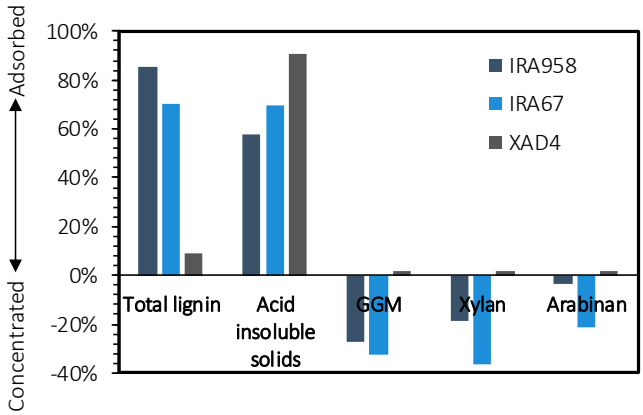


Figure 1. Removal of solutes from the SSL using the resins under examination. Negative removal indicates that the solute was concentrated in the solution.

If the resins had swelled using the SSL as a wetting agent, the concentration of polysaccharides would have been the same in the bulk solution as in the resins themselves (assuming no adsorption of the solutes). However, the increase in polysaccharide concentrations suggests that not only did the resins swell, they also held back polysaccharides. The reason for these observations is unknown, but we hypothesize that the polysaccharides were larger than the pores on the resin, which led to the absorption of water molecules and the retention of large polysaccharides.

Based on these results, IRA958 was chosen for subsequent study, because it had the highest lignin removal per weight of adsorbent and no observable loss of polysaccharides. Another reason for this choice is that IRA958 (chloride form) did not raise the pH to a basic value, as IRA67 (free base) had done, increasing the pH to as high as 9 in certain samples, potentially deacetylating the GGM and degrading the polysaccharides [36].

2.2. Equilibrium Adsorption for IRA958

In the screening study, a fixed adsorbent/solution ratio was used to identify the adsorbent that had the highest adsorption of lignin per weight of resin. To better understand the type of adsorption that occurred and determine the maximum adsorption capacity, an equilibrium adsorption study was performed in which the adsorbent/solution ratio was varied. With IRA958, lignin adsorption rose with increasing amounts of adsorbent (the amount of SSL solution was constant) (Figure 2a). The highest and most substantial removal of lignin occurred between 0 and 0.1 g adsorbent/g solution, wherein the removal reached as high as 80%. The remaining increase of approximately 5% required the addition of 0.1 g adsorbent/g solution, twice the amount that was needed to remove 80% of the lignin. The removal of acid-insoluble lignin was substantial with little adsorbent (approximately 42% removal) but nearly constant for the entire interval, increasing to 58% only at the end.

The adsorption of polysaccharides was not detected during the screening (Figure 1) but clearly showed a decrease of the concentration at low adsorption/solution ratios (up to 0.02 g/g), as seen in Figure 2b. At higher adsorbent/solution ratios (up to 0.1 g/g), the concentration of polysaccharides increased by approximately 8%, rising by another 21% with the last 0.1 g/g increment.

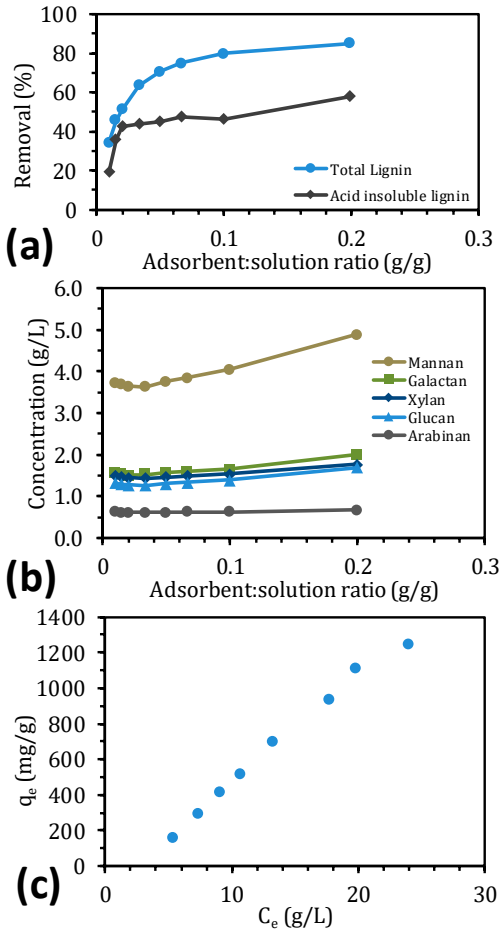


Figure 2. Lignin removal from solution (**a**) and the concentration of polysaccharides (**b**) at various adsorbent/solution ratios. (**c**) Amount of adsorbed lignin per gram of adsorbent (q_e) vs. the concentration at equilibrium (C_e).

To describe the adsorption of lignin to IRA958, common adsorption isotherm models were used (Table 2). Data on the adsorptive capacity versus the lignin concentration were used to fit the models at equilibrium, as seen in Figure 2c. The data were not linear, especially near the higher concentration ranges, which explains the poor fit of the linear model (Table 2). Although the saturation did not plateau, the data at the high concentration indicate that the adsorption capacity leveled. The linear region at low concentrations does not intercept the y-axis (when extrapolated), indicating that the curve is S-shaped. The Langmuir model fails to describe these curves [43], which was also evident from the R^2 value of 0.5445 and the negative coefficients, which have no tangible meaning (Table 2). The Freundlich isotherm fit these data better, and although the model is empirical, it has been used to describe multilayer adsorption systems on heterogeneous surfaces [37].The intensity of the adsorption (n_F) was higher than unity, which indicates cooperative adsorption and that the curve has an S-shape [44,45]. Although R^2 was close to unity, the model still failed to fit the data at high concentrations, which is a known limitation of this model [46]. The Sips and Brunauer–Emmett–Teller (BET) models have been used to overcome these issues. The BET equation is a multilayer adsorption model that has

no limits in the number of adsorption layers that are available on the homogeneous surface of the adsorbent [43]. In addition, the BET model resolves a limited amount of S-shaped experimental data, which explains the low R^2 value. Conversely, the Sips isotherm was derived to account for the limitations of the Freundlich and Langmuir models. When the concentration is low, the isotherm resembles the Freundlich model, versus the Langmuir model when the concentration is high [46]. The results in Table 2 show that the Sips model fit our data the best and that the exponent (n_S) was larger than unity, indicating that the type of adsorption was cooperative, as seen with the Freundlich model. Further, the maximum adsorption capacity (Q_s) was unable to be predicted using the Freundlich model and was calculated to be 1947 mg adsorbate/g adsorbent. The calculated maximum adsorption capacity was higher than in the study by Liu, et al. [37], perhaps due to differing lignosulfonate types, the molecular weight of the adsorbates, the type of adsorbent, and the fact that the resins were dry before adsorption.

Table 2. Adsorption models for fitting the lignin adsorption data. The equilibration concentration (C_e) was expressed in mg/mL, the adsorption capacity (q_e and q_t) was expressed in mg/g, and time (t) was expressed in minutes.

Model	Fitted Parameters	Unit	R^2	Equation	Ref
Adsorption isotherms					
Linear	K_{lin} = 51.67	(mL/g)	0.9679	$q_e = K_{lin}C_e$	[47]
Langmuir	Q_L = −1621.8 K_L = −0.0202	(mg/g) (mL/mg)	0.5445	$q_e = \frac{Q_L K_L C_e}{1+K_L C_e}$	[48]
Freundlich	K_F = 31.06 n_F = 1.1774	($mL^{nF}mg^{1-nF}$/g) (-)	0.9855	$q_e = K_F C_e^{n_F}$	[48]
Sips (Langmuir–Freundlich)	Q_S = 1947.2 K_S = 0.0035 n_S = 1.9616	(mg/g) (mL/mg) (-)	0.9978	$q_e = \frac{Q_S K_S C_e^{n_S}}{1+K_S C_e^{n_S}}$	[43]
Modified Brunauer–Emmett–Teller (BET)	Q_B = 24,728 K_B = 0.3926 C_S = 216.74	(mg/g) (mL/mg) (mg/mL)	0.9839	$q_e = \frac{Q_B K_B C_e}{(C_S - C_e)(1+(K_B-1)(C_e/C_s))}$	[49]
Adsorption kinetics					
Pseudo-zero-order	k_0 = 2.5145	(mg/(g min))	−0.6910	$q_t = k_0 t$	[50]
Pseudo-first-order	k_1 = 0.0389 q_e = 286.44	(1/min) (mg/g)	0.9781	$\ln(q_e - q_t) = \ln(q_e) - k_1 t$	[50]
Pseudo-second-order	k_2 = 4.869e−4 q_e = 299.22	(g/(mg·min)) (mg/g)	0.9997	$\frac{1}{(q_e - q_t)} = \frac{1}{q_e} + k_2 t$	[48]
Elovich	α = 126.02 β = 0.0189	(mg/(g·min)) (g/mg)	0.9520	$q_t = \frac{1}{\beta}\ln(\alpha\beta) + \frac{1}{\beta}\ln(t)$	[48]
Intra-particle diffusion	k_p = 14.33 m = 165.15	(mg/(g·$min^{0.5}$)) (mg/g)	0.9689	$q_t = k_p\sqrt{(t)} + m$	[48]

2.3. Adsorption Kinetics

Adsorption kinetics are important when identifying the mechanisms of adsorption and can also be used for simulations and scale-up of the process [51]. The kinetic models that were chosen for the modeling were the commonly used pseudo zero-, first-, and second-order expressions but also the Elovich and intra-particle diffusion, as presented in Table 2. The data that were used for the models are shown in Figure 3a, in which the lignin that has adsorbed and the lignin concentration in the bulk are plotted versus time.

The trend was similar to what has been reported [37], the major difference being the time scale. In Figure 3a, the entire adsorption process took 2 to 3 h to reach equilibrium compared with the 6 to 8 h in the literature; as discussed in the previous section, the difference in solutes, adsorbents, and operating conditions could have resulted in this deviation. Between pseudo-kinetic models, the second-order equation gave the best fit (R^2 = 0.9997), indicating that the adsorption type was chemisorption [51]. The calculated adsorption capacity at equilibrium (q_e) was closer to what was observed experimentally (286.3 mg/g) for the pseudo-first-order equation (Table 2); however, this model did not properly resolve the kinetics in the region between t = 0 and 75 min (Figure 3b).

The intra-particle diffusion and Elovich models (Figure 3c,d) gave more information regarding the adsorption process. According to the Elovich model, the initial adsorption rate for the lignosulfonates was approximately 126 mg/(g min), which is 30 times higher than in the literature [37]. Moreover, according to the intra-particle diffusion model, the rapid adsorption of lignin at the outset was due primarily to film, boundary layer, or macropore diffusion, which occurred in the first 10 min of adsorption (Figure 3c). The subsequent slow adsorption (t > 10 min) was attributed to intra-particle diffusion, followed by a steady-state interval in which the intra-particle diffusion rate constant (k_p) began to approach 0.

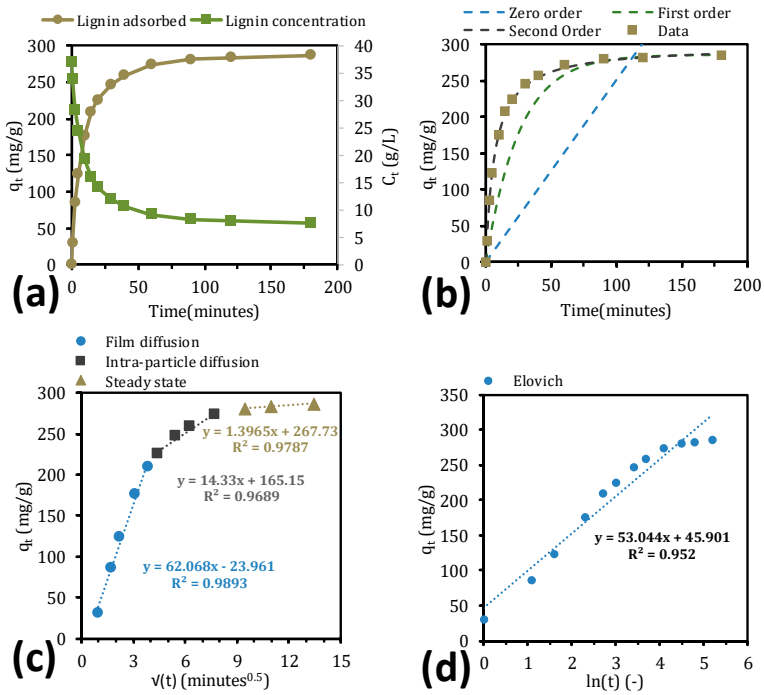


Figure 3. Lignin adsorption and concentration vs. time (**a**) and the resulting fit of the kinetic models to the data (**b**–**d**).

2.4. Lignin Desorption

For the implementation of the adsorption-type recovery process on an industrial scale, the recovery of lignosulfonates and the regeneration of the resin are important. These aspects were examined by washing the resin with various concentrations of the regenerant in a sequence of three washes (Figure 4). According to the results, 100 g/L sodium chloride was a suitable concentration of regenerant, effecting a total lignosulfonate recovery of 97.6% after three consecutive washes. Increasing the concentration further did not improve the desorption of lignosulfonates, as seen in Figure 4a. These results are similar to those of Liu, et al. [37], who obtained a lignosulfonate recovery of 98% using a regenerant concentration of 10% NaCl and 2% NaOH, with a total volume that was comparable with the one that we used. In addition, the purity of lignosulfonates was approximately 92%, which could be attributed to the salt that was used during the regeneration.

It is unknown whether the recovery of salts from the recovered lignosulfonates is beneficial for the process economy. Hilal, et al. [52] have shown that it is feasible to recover NaCl using nanofiltration

membranes from highly concentrated salt solutions (up to 25,000 ppm), rendering the use of resins for the separation of lignosulfonates from GGM a promising industrial method.

According to the results in Figure 4, there remains the possibility to simplify the process by decreasing the number of washes that is required, as evidenced by the first wash, with which the lignin recovery clearly increased. The data in Figure 4b also indicate this pattern, because the saturation of chloride adsorption did not plateau. Using the Sips isotherm to fit the data in Figure 4b (R^2 = 0.9972), a theoretical maximum adsorption capacity is reached at 364 mg chloride/g resin. However, to reach such a high level, the concentration of sodium chloride must approach the solubility limit, which is not desired, especially if the recovery of salts using nanofiltration is important [52,53].

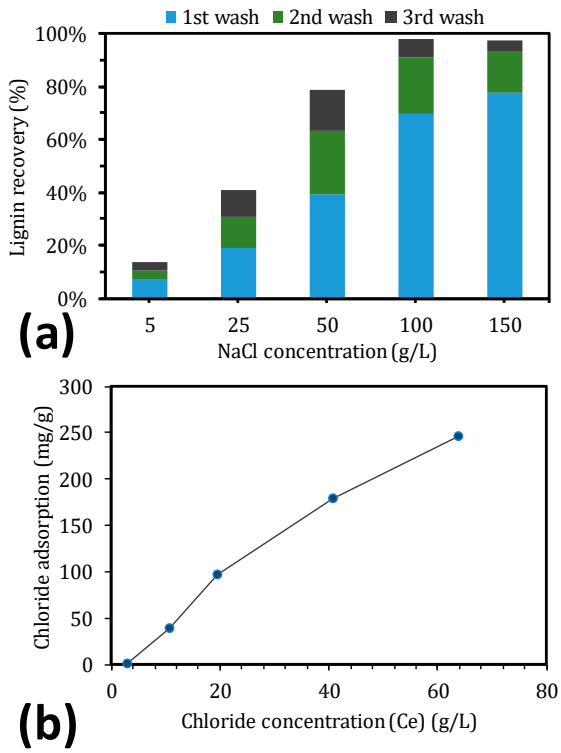


Figure 4. Lignin recovery vs. initial sodium chloride concentration at various wash steps (**a**). Chloride concentration at equilibrium during the first wash step (**b**).

2.5. Ultrafiltration before and after Adsorption

To determine the effects of adsorption on ultrafiltration, the delignified SSL was ultrafiltered and compared with the ultrafiltered raw SSL solution. The flux for the ultrafiltered raw SSL solution (Org – 10 kDa, Figure 5a) was 50% lower than that for the same solution and membrane in our previous study [23]. The retention of all solutes was also lower, likely due to the filtration temperature, room temperature in this study versus 50 °C in our earlier report. An increase in flux is usually followed by a decline in solute retention, and vice versa, as posited by the film theory [54]. However, in this case, we believe that the rise in temperature also softened the membrane, causing it to compress and thus lead to a decrease in pore size, in contrast to the higher retentions in our previous study [23,55].

The results in Figure 5a clearly show the effect of the adsorption prior to ultrafiltration (Ads – 10 kDa). The removal of lignin increased the flux by 38% (Org – 10 kDa vs. Ads – 10 kDa) as

the degree of separation (Figure 5b) improved from 17% to 59%, which increased the capacity of the membrane filtration and the purity. The flux at the end of the membrane filtration (Ads − 10 kDa) was also higher than that for the untreated SSL solution, allowing the membrane filtration to proceed to a greater reduction in volume, resulting in higher concentrations and possibly higher purities (i.e., greater retention of polysaccharides compared with lignin) (Figure 5b). The retention of polysaccharides was not affected considerably by the lignin removal, given the minor change in mannose retention from 73% to 67%. This decline caused the GGM yield to decrease from 38% to 34%.

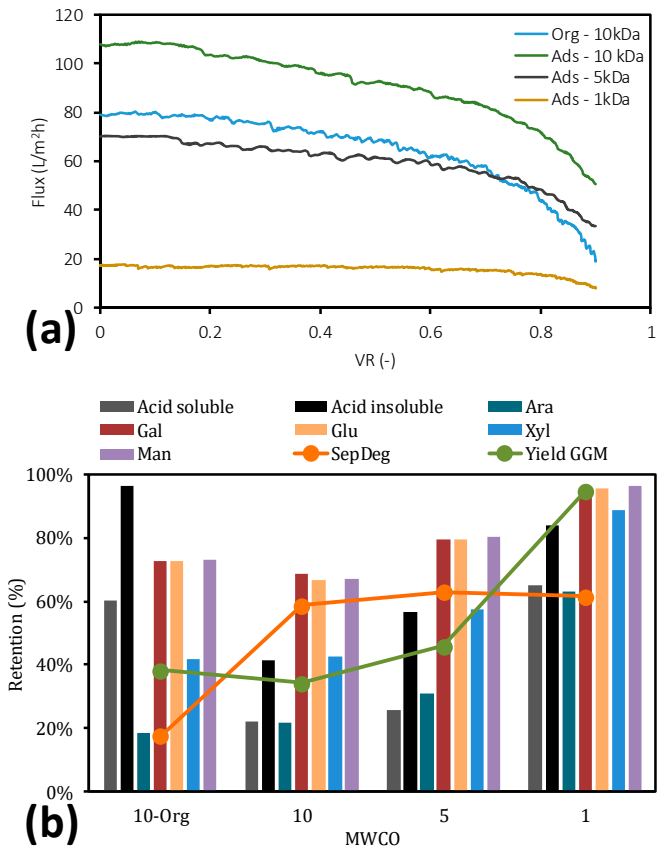


Figure 5. Flux vs. volume reduction (VR) during the ultrafiltration of treated and non-treated SSL (**a**). Retention of solutes during the ultrafiltration studies (**b**).

The reduction in yield can be compensated for by operating with a denser membrane. The results are presented in Figure 5 (Ads − 5kDa and Ads − 1 kDa). By switching to a 5-kDa cutoff membrane, the flux decreased compared with Ads − 10 kDa, as expected. However, the average flux was roughly the same as for the original solution (Org − 10 kDa), rendering this a promising alternative. The switch to a denser membrane also increased the retention of polysaccharides from 67% to 80%, which in turn improved the yield to 46%. The degree of separation rose from 59% to 63%, indicating that the treated SSL was purer than before. Incorporation of the densest membrane (1 − kDa cutoff) significantly increased the GGM yield (up to 95%). The degree of separation was approximately constant, indicating that the treated SSL did not increase in purity and that the lignin was concentrated, like the GGM, as noted for the retentions (Figure 5b). Although the densest membrane is promising, based on its high

yield of GGM, the flux was four times lower than that of the original solution. Nevertheless, the flux was not 0, and whether the use of the densest membrane is economical requires a technoeconomic analysis.

3. Materials and Methods

3.1. Raw Material

The sodium-based SSL originated from the first step in a 2-step softwood (60% *Picea abies* and 40% *Pinus sylvestris*) sulfite pulping process (Domsjö Fabriker, Örnsköldsvik, Sweden).

3.2. Preparation of the Adsorbents

The adsorbents were produced by Sigma-Aldrich (Saint Louis, MO, USA) and consisted of a strong-base anion exchanger (Amberlite IRA958, chloride form), weak-base anion exchanger (Amberlite IRA-67, free base), and hydrophobic polyaromatic resin (Amberlite XAD4, 20–60 mesh). The resins were first soaked in deionized water (6 parts water to 1 part resin) for 3 h. The wash was repeated until the conductivity of the solution was less than 1 µS/cm, which required three washes for each resin. The washed resins were then dried in an oven at 50 °C for 48 h before the experiments.

3.3. Adsorbent Screen and Equilibrium Adsorption Studies

The screen was performed by adding excess dried adsorbent (4 g) to 50 mL vials that were filled with 20 mL of SSL solution, yielding a solution/adsorbent ratio of 5. The vials were mixed (continuous rotation on setting 2) in an incubator (combi-H12, FINEPCR, Gyeonggi-do, South Korea) at room temperature for 24 h. The adsorbent and remaining solution were carefully separated using a pipette before the solution was analyzed for lignin and carbohydrate composition.

The equilibrium studies were conducted by varying the amount of adsorbent that was added to the 50 mL vials: 0.20, 0.30, 0.40, 0.67, 1.0, 1.33, 2.00, and 4.00 g. The same amount of SSL and method were used as described for the screen. The adsorption capacity (amount of adsorbed material per weight dry adsorbent (q_e)) was calculated per Equation (1):

$$q_e\left(\frac{mg}{g}\right) = \frac{(C_0 - C_e)V}{W} \quad (1)$$

where C_0 and C_e are the initial and equilibrium concentrations of the measured substance, respectively; V is the volume of the solution; and W is the weight of the dry adsorbent.

The removal of solutes (percentage) was calculated per Equation (2):

$$Removal\ (\%) = 100\frac{(C_0 - C_e)}{C_0} \quad (2)$$

3.4. Adsorption Kinetics

The adsorption kinetics were analyzed at room temperature in a 1 L bottle with 50 g of dry adsorbent and 500 mL of SSL. The solution and adsorbent were mixed continuously using a magnetic stirrer at 100 rpm. Samples were initially withdrawn (1 mL) once every minute, increasing to once every 5, 10, 20, and 30 min, for a total of 3 h, after which the change in lignin concentration was minimal. The adsorption capacity and lignin removal were calculated per Equations (1) and (2), where the equilibrium concentration (C_e) was replaced with the concentration at time (t).

3.5. Lignin Desorption

Five samples were prepared, containing 7 g of wet adsorbent (approximately 2 g of dry adsorbent) from the kinetics study. Twenty milliliters of regenerant was added to each sample with varying concentrations of sodium chloride (5, 25, 50, 100, and 150 g/L) and a constant concentration of sodium hydroxide (10 g/L) per the recommendations in the Amberlite specifications datasheet. Both chemicals

were analytical-grade and obtained from Merck Millipore (Burlington, MA, USA). This procedure was repeated three times to desorb as much lignin as possible for the given concentrations.

3.6. Membrane Filtration

The membrane filtration studies were performed using three flat-sheet regenerated cellulose membranes. The membranes had a molecular weight cutoff of 10 kDa (RC70PP, Alfa Laval Nordic A/S, Søborg, Danmark), 5 kDa (C5F, Microdyn-Nadir GmbH, Wiesbaden, Germany), and 1 kDa (Ultracel PLAC, EMD Millipore Co., Billerica, MA, USA). The equipment consisted of a 400 mL stirred module, as illustrated in Figure 6. The crossflow velocity was set by changing the rotational velocity of the magnetic rod [41], and the temperature was controlled using a heating plate (MR2002, Heidolph Instruments GmbH & Co.KG, Schwabach, Germany). The pressure was controlled using a valve that was connected to a nitrogen gas supply and monitored with a digital gauge (DCS40.0AR, Trafag AG, Bubikon, Switzerland). The flux was monitored using a digital balance (PL6001-l, Mettler Toledo Inc., Columbus, OH, USA) that was connected to a computer.

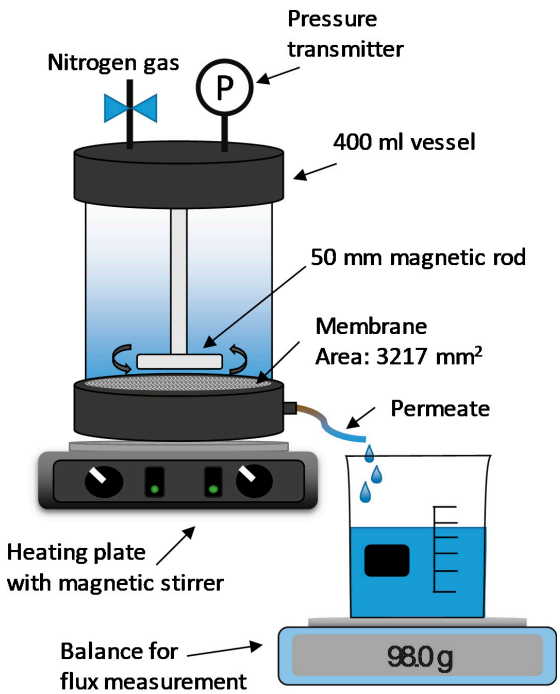


Figure 6. Illustration of the membrane filtration equipment.

3.7. Analytical Measurements

3.7.1. Total Dry and Ash Content

Three milliliters of various samples were weighed in ceramic crucibles and dried in an oven (Heraeus, Heraeus Holding GmbH, Hanau, Germany) at 105 °C for 24 h. The dry samples were weighed again, and the total dry content was calculated. The dry samples were placed in a furnace (B150, Nabertherm GmbH, Lilienthal, Germany) and heated slowly from room temperature to 900 °C over 1 h, after which they were left at 900 °C for 12 h. The samples were then weighed to determine the ash content.

3.7.2. Hemicellulose and Acid-Insoluble Solids

The hemicellulose content and amount of acid-insoluble solids were measured according to previous studies [23]. Ten milliliters of the liquid samples was mixed with 750 μL 72% sulfuric acid and autoclaved (Systec DX 150, Wettenberg, Germany) at 121 °C for 1 h to hydrolyze the polymeric sugars. The samples were then filtered to remove insoluble solids, and the filters were dried overnight in an oven at 105 °C. The acid-insoluble solids content was determined by measuring the dried filters before and after filtration of the samples.

The hemicellulose content was determined by analyzing the liquid fraction after the filtration by high-performance anion-exchange chromatography (HPAEC). The HPAEC system (ICS-5000+ DC, Dionex, Sunnyvale, CA, USA) was a pulsed amperometric detector with a compartment temperature of 30 °C, and the separation was performed on a Carbo Pac PA1 analytical column. Deionized water at 1 mL/min was used as the main eluent, and 200 mM sodium hydroxide solution was used as the postcolumn addition at 0.5 mL/min. The samples were diluted with deionized water, and the injection volume for the HPAEC was 10 μL for all samples. The standards were D-mannose, D-xylose, D-glucose, D-galactose, and L-arabinose (Fluka Chemie AG, Buchs, Switzerland), and the hemicellulose content was determined after anhydro corrections of 0.90 for hexoses and 0.88 for pentoses.

3.7.3. Lignin and Chloride Content

The lignin content in the samples was determined on a spectrophotometer (Shimadzu UV-1800, Kyoto, Japan) at a wavelength of 280 nm using an extinction coefficient of 13.01 L/(g cm). The chloride content was measured using titrator strips (Quantab Chloride Low Range titrators, HACH, Loveland, CO, USA).

4. Conclusions

The aim of this work was to remove lignin from SSL using two anion exchangers and one hydrophobic resin. The strong-base anion exchange resin (IRA958) performed best during the screen, obtaining the highest removal of total lignin. XAD4 (hydrophobic resin) removed the most acid-insoluble lignin, approximately 5% of which constituted polysaccharides. This finding suggests that the acid-insoluble lignin was bound to carbohydrates. Polysaccharides were not removed with the anion exchangers because the concentration of polysaccharides increased in the treated SSL. The equilibrium study with the best-performing resin (IRA958) showed that the S-shaped adsorption capacity–concentration curve followed the Sips isotherm, indicating that the adsorption was cooperative. The kinetics study with the same resin demonstrated that the adsorption was chemisorptive, reflected by film diffusion in the first stage of the adsorption and intra-particle diffusion for the remainder before reaching the steady state. The regeneration of adsorbent was possible using sodium chloride and sodium hydroxide, for which a concentration of 100 g/L was sufficient. Higher regenerant concentrations did not increase the total recovery of lignosulfonates, but they decreased the number of washes for regeneration that was required.

The removal of lignin from the SSL resulted in a 38% increase in ultrafiltration flux and a rise in separation degree from 17% to 59%. The GGM yield fell slightly during the ultrafiltration of the treated SSL as a result of the low retention compared with the nontreated SSL. It was possible, however, to increase the yield by using a membrane with a lower molecular-weight cutoff.

Author Contributions: Funding acquisition, O.W.; Investigation, B.A.-R.; Methodology, B.A.-R.; Supervision, M.G. and O.W.; Validation, B.A.-R., M.G. and O.W.; Visualization, B.A.-R.; Writing—original draft, B.A.-R.; Writing—review and editing, M.G. and O.W. All authors have read and agreed to the published version of the manuscript.

Funding: This study was funded by the Swedish Foundation for Strategic Research (SSF) (RBP 14-0046), which is gratefully acknowledged.

Acknowledgments: We would like to thank Domsjö fabriker for providing us with the raw material (SSL).

Conflicts of Interest: The authors declare no conflict of interest. The funders had no role in the design, execution, interpretation, or writing of the study.

References

1. Wang, S.; Dai, G.; Yang, H.; Luo, Z. Lignocellulosic biomass pyrolysis mechanism: A state-of-the-art review. *Prog. Energy Combust. Sci.* **2017**, *62*, 33–86. [CrossRef]
2. Norgren, M.; Edlund, H. Lignin: Recent advances and emerging applications. *Curr. Opin. Colloid Interface Sci.* **2014**, *19*, 409–416. [CrossRef]
3. Duval, A.; Lawoko, M. A review on lignin-based polymeric, micro-and nano-structured materials. *React. Funct. Polym.* **2014**, *85*, 78–96. [CrossRef]
4. Schneider, M.H.; Phillips, J.G. Furfuryl Alcohol and Lignin Adhesive Composition. U.S. Patent 6,747,076 B2, 8 June 2004.
5. Kamoun, A.; Jelidi, A.; Chaabouni, M. Evaluation of the performance of sulfonated esparto grass lignin as a plasticizer–water reducer for cement. *Cem. Concr. Res.* **2003**, *33*, 995–1003. [CrossRef]
6. Ragauskas, A.J.; Beckham, G.T.; Biddy, M.J.; Chandra, R.; Chen, F.; Davis, M.F.; Davison, B.H.; Dixon, R.A.; Gilna, P.; Keller, M.; et al. Lignin Valorization: Improving Lignin Processing in the Biorefinery. *Science* **2014**, *344*, 1246843. [CrossRef] [PubMed]
7. Al-Rudainy, B.; Galbe, M.; Arcos Hernandez, M.; Jannasch, P.; Wallberg, O. Impact of Lignin Content on the Properties of Hemicellulose Hydrogels. *Polymers* **2018**, *11*, 35. [CrossRef]
8. Rosengren, A.; Butler, S.J.; Arcos-Hernandez, M.; Bergquist, K.-E.; Jannasch, P.; Stålbrand, H. Enzymatic synthesis and polymerisation of β-mannosyl acrylates produced from renewable hemicellulosic glycans. *Green Chem.* **2019**, *21*, 2104–2118. [CrossRef]
9. Saha, B.C. Hemicellulose bioconversion. *J. Ind. Microbiol. Biotechnol.* **2003**, *30*, 279–291. [CrossRef]
10. Hartman, J.; Albertsson, A.-C.; Sjöberg, J. Surface-and bulk-modified galactoglucomannan hemicellulose films and film laminates for versatile oxygen barriers. *Biomacromolecules* **2006**, *7*, 1983–1989. [CrossRef]
11. Al-Rudainy, B.; Galbe, M.; Wallberg, O. From lab-scale to on-site pilot trials for the recovery of hemicellulose by ultrafiltration: Experimental and theoretical evaluations. *Sep. Purif. Technol.* **2020**, 117187. [CrossRef]
12. Liu, S. Woody biomass: Niche position as a source of sustainable renewable chemicals and energy and kinetics of hot-water extraction/hydrolysis. *Biotechnol. Adv.* **2010**, *28*, 563–582. [CrossRef] [PubMed]
13. Lundqvist, J.; Jacobs, A.; Palm, M.; Zacchi, G.; Dahlman, O.; Stålbrand, H. Characterization of galactoglucomannan extracted from spruce (*Picea abies*) by heat-fractionation at different conditions. *Carbohydr. Polym.* **2003**, *51*, 203–211. [CrossRef]
14. Li, J.; Henriksson, G.; Gellerstedt, G. Carbohydrate reactions during high-temperature steam treatment of aspen wood. *Appl. Biochem. Biotechnol.* **2005**, *125*, 175–188. [CrossRef]
15. Polari, L.; Ojansivu, P.; Mäkelä, S.; Eckerman, C.; Holmbom, B.; Salminen, S. Galactoglucomannan Extracted from Spruce (*Picea abies*) as a Carbohydrate Source for Probiotic Bacteria. *J. Agric. Food. Chem.* **2012**, *60*, 11037–11043. [CrossRef]
16. Wenzl, H. *The Chemical Technology of Wood*; Elsevier: Amsterdam, The Netherlands, 2012.
17. Macleod, J.M.; Benko, J.V. Sugars and Sugar Acids in Lignosulphonate Products. *J. Wood Chem. Technol.* **1982**, *2*, 207–219. [CrossRef]
18. Al-Rudainy, B.; Galbe, M.; Schagerlöf, H.; Wallberg, O. Antisolvent precipitation of hemicelluloses, lignosulfonates and their complexes from ultrafiltrated spent sulfite liquor (SSL). *Holzforschung* **2018**, *72*, 839. [CrossRef]
19. Berglund, J.; Azhar, S.; Lawoko, M.; Lindström, M.; Vilaplana, F.; Wohlert, J.; Henriksson, G. The structure of galactoglucomannan impacts the degradation under alkaline conditions. *Cellulose* **2019**, *26*, 2155–2175. [CrossRef]
20. Persson, T.; Jönsson, A.-S. Fouling of ultrafiltration membranes during isolation of hemicelluloses in the forest industry. *Sch. Res. Exch.* **2009**, *2009*, 624012. [CrossRef]
21. Steinmetz, V.; Villain-Gambier, M.; Klem, A.; Gambier, F.O.; Dumarcay, S.P.; Trebouet, D. Unveiling TMP Process Water Potential as an Industrial Sourcing of Valuable Lignin–Carbohydrate Complexes toward Zero-Waste Biorefineries. *ACS Sustain. Chem. Eng.* **2019**, *7*, 6390–6400. [CrossRef]

22. Krawczyk, H.; Oinonen, P.; Jönsson, A.-S. Combined membrane filtration and enzymatic treatment for recovery of high molecular mass hemicelluloses from chemithermomechanical pulp process water. *Chem. Eng. J.* **2013**, *225*, 292–299. [CrossRef]
23. Al-Rudainy, B.; Galbe, M.; Lipnizki, F.; Wallberg, O. Galactoglucomannan Recovery with Hydrophilic and Hydrophobic Membranes: Process Performance and Cost Estimations. *Membranes* **2019**, *9*, 99. [CrossRef] [PubMed]
24. Thuvander, J.; Lipnizki, F.; Jönsson, A.-S. On-Site Recovery of Hemicelluloses from Thermomechanical Pulp Mill Process Water by Microfiltration and Ultrafiltration. *J. Wood Chem. Technol.* **2019**, *39*, 214–223. [CrossRef]
25. Mohan, S.V.; Karthikeyan, J. Removal of lignin and tannin colour from aqueous solution by adsorption onto activated charcoal. *Environ. Pollut.* **1997**, *97*, 183–187. [CrossRef]
26. Song, T.; Pranovich, A.; Holmbom, B. Separation of polymeric galactoglucomannans from hot-water extract of spruce wood. *Bioresour. Technol.* **2013**, *130*, 198–203. [CrossRef] [PubMed]
27. Zasadowski, D.; Yang, J.; Edlund, H.; Norgren, M. Antisolvent precipitation of water-soluble hemicelluloses from TMP process water. *Carbohydr. Polym.* **2014**, *113*, 411–419. [CrossRef]
28. Koivula, E.; Kallioinen, M.; Sainio, T.; Antón, E.; Luque, S.; Mänttäri, M. Enhanced membrane filtration of wood hydrolysates for hemicelluloses recovery by pretreatment with polymeric adsorbents. *Bioresour. Technol.* **2013**, *143*, 275–281. [CrossRef]
29. Nitzsche, R.; Groengroeft, A.; Kraume, M. Separation of lignin from beech wood hydrolysate using polymeric resins and zeolites–Determination and application of adsorption isotherms. *Sep. Purif. Technol.* **2019**, *209*, 491–502. [CrossRef]
30. Schwartz, T.J.; Lawoko, M. Removal of acid-soluble lignin from biomass extracts using Amberlite XAD-4 resin. *BioResources* **2010**, *5*, 2337–2347.
31. Sumerskii, I.; Korntner, P.; Zinovyev, G.; Rosenau, T.; Potthast, A. Fast track for quantitative isolation of lignosulfonates from spent sulfite liquors. *RSC Adv.* **2015**, *5*, 92732–92742. [CrossRef]
32. Westerberg, N.; Sunner, H.; Gunnar, H.; Mikaela, H.; Martin, L.; Rasmuson, A. Separation of galactoglucomannans, lignin and lignin-carbohydrate complexes from hot-water-extracted Norway spruce by cross-flow filtration and adsorption chromatography. *BioResources* **2012**, *7*, 4501–4516. [CrossRef]
33. Narron, R.H.; Chang, H.-M.; Jameel, H.; Park, S. Soluble lignin recovered from biorefinery pretreatment hydrolyzate characterized by lignin–carbohydrate complexes. *ACS Sustain. Chem. Eng.* **2017**, *5*, 10763–10771. [CrossRef]
34. Heinonen, J.; Sanlaville, Q.; Niskakoski, H.; Tamper, J.; Sainio, T. Separation and recovery of lignin from hydrolysates of lignocellulose with a polymeric adsorbent. *Sep. Purif. Technol.* **2017**, *186*, 125–134. [CrossRef]
35. Van Blaricom, L.E.; Russell, G.K. Lignosulfonate Recovery from Waste Sulfite Liquor. International Patent Application No U.S. 29230652A, 6 July 1955.
36. Takahashi, S.; Tanifuji, K.; Shiell, K.; Fatehi, P.; Jahan, M.S.; Ohi, H.; Ni, Y. Removal of acetic acid from spent sulfite liquor using anion exchange resin for effective xylose fermentation with Pichia stipitis. *BioResources* **2013**, *8*, 2417–2428. [CrossRef]
37. Liu, L.; Ren, J.; Zhang, Y.; Liu, X.; Ouyang, J. Simultaneously separation of xylo-oligosaccharide and lignosulfonate from wheat straw magnesium bisulfite pretreatment spent liquor using ion exchange resin. *Bioresour. Technol.* **2018**, *249*, 189–195. [CrossRef] [PubMed]
38. Yu, G.; Li, B.; Wang, H.; Liu, C.; Mu, X. Preparation of concrete superplasticizer by oxidation-sulfomethylation of sodium lignosulfonate. *BioResources* **2013**, *8*, 1055–1063. [CrossRef]
39. Qiu, X.; Kong, Q.; Zhou, M.; Yang, D. Aggregation behavior of sodium lignosulfonate in water solution. *J. Phys. Chem. B* **2010**, *114*, 15857–15861. [CrossRef] [PubMed]
40. Lundqvist, J.; Teleman, A.; Junel, L.; Zacchi, G.; Dahlman, O.; Tjerneld, F.; Stålbrand, H. Isolation and characterization of galactoglucomannan from spruce (*Picea abies*). *Carbohydr. Polym.* **2002**, *48*, 29–39. [CrossRef]
41. Al-Rudainy, B.; Galbe, M.; Wallberg, O. Influence of prefiltration on membrane performance during isolation of lignin-carbohydrate complexes from spent sulfite liquor. *Sep. Purif. Technol.* **2017**, *187*, 380–388. [CrossRef]
42. Korntner, P.; Schedl, A.; Sumerskii, I.; Zweckmair, T.; Mahler, A.K.; Rosenau, T.; Potthast, A. Sulfonic acid group determination in lignosulfonates by headspace gas chromatography. *ACS Sustain. Chem. Eng.* **2018**, *6*, 6240–6246. [CrossRef]

43. Inglezakis, V.J.; Poulopoulos, S.G.; Kazemian, H. Insights into the S-shaped sorption isotherms and their dimensionless forms. *Microporous Mesoporous Mater.* **2018**, *272*, 166–176. [CrossRef]
44. Hinz, C. Description of sorption data with isotherm equations. *Geoderma* **2001**, *99*, 225–243. [CrossRef]
45. Foo, K.Y.; Hameed, B.H. Insights into the modeling of adsorption isotherm systems. *Chem. Eng. J.* **2010**, *156*, 2–10. [CrossRef]
46. Kumara, N.; Hamdan, N.; Petra, M.I.; Tennakoon, K.U.; Ekanayake, P. Equilibrium isotherm studies of adsorption of pigments extracted from kuduk-kuduk (*Melastoma malabathricum* L.) pulp onto TiO_2 nanoparticles. *J. Chem.* **2014**, *2014*, 468975. [CrossRef]
47. Ayawei, N.; Ebelegi, A.N.; Wankasi, D. Modelling and interpretation of adsorption isotherms. *J. Chem.* **2017**, *2017*, 11. [CrossRef]
48. Mezenner, N.Y.; Bensmaili, A. Kinetics and thermodynamic study of phosphate adsorption on iron hydroxide-eggshell waste. *Chem. Eng. J.* **2009**, *147*, 87–96. [CrossRef]
49. Saadi, R.; Saadi, Z.; Fazaeli, R.; Fard, N.E. Monolayer and multilayer adsorption isotherm models for sorption from aqueous media. *Korean J. Chem. Eng.* **2015**, *32*, 787–799. [CrossRef]
50. Villarante, N.R.; Bautista, A.P.R.; Sumalapao, D.E.P. Batch adsorption study and kinetic profile of Cr (VI) using lumbang (Aleurites moluccana)-derived activated carbon-chitosan composite crosslinked with epichlorohydrin. *Orient. J. Chem.* **2017**, *33*, 1111–1119. [CrossRef]
51. Pan, M.; Lin, X.; Xie, J.; Huang, X. Kinetic, equilibrium and thermodynamic studies for phosphate adsorption on aluminum hydroxide modified palygorskite nano-composites. *RSC Adv.* **2017**, *7*, 4492–4500. [CrossRef]
52. Hilal, N.; Al-Zoubi, H.; Mohammad, A.; Darwish, N. Nanofiltration of highly concentrated salt solutions up to seawater salinity. *Desalination* **2005**, *184*, 315–326. [CrossRef]
53. Haynes, W.M. *CRC Handbook of Chemistry and Physics*; CRC press: Boka Raton, FL, USA, 2014.
54. Luis, P. *Fundamental Modeling of Membrane Systems: Membrane and Process Performance*; Elsevier: Amsterdam, The Netherlands, 2018.
55. Stade, S.; Kallioinen, M.; Tuuva, T.; Mänttäri, M. Compaction and its effect on retention of ultrafiltration membranes at different temperatures. *Sep. Purif. Technol.* **2015**, *151*, 211–217. [CrossRef]

Sample Availability: Samples of the compounds SSL and purified GGM are available from the authors.



© 2020 by the authors. Licensee MDPI, Basel, Switzerland. This article is an open access article distributed under the terms and conditions of the Creative Commons Attribution (CC BY) license (http://creativecommons.org/licenses/by/4.0/).

In the production of pulp and paper, water-soluble components, such as hemicellulose (in this work: galactoglucomannan), monosaccharides, and lignin, are released and accumulate in the process water. The process water is usually concentrated and incinerated for heat generation and the recovery of pulping chemicals, such as in the Kraft and sulfite processes. The growing trend toward a more sustainable forest industry has increased the interest in the biorefinery concept. The utilization of wasted wood components, such as hemicelluloses and lignin, as raw materials for the development of specialty chemicals and biofuels is essential for continued growth of the forest industry.

The aim of the work that is described in this thesis was to separate and purify hemicellulose from softwood-based spent sulfite liquor. To this end, various separation techniques were investigated, of which membrane filtration, antisolvent precipitation, and adsorption were primarily used. The separation of hemicellulose and lignin using membrane filtration was not possible, likely due to the narrow difference in molecular weight between them and the formation of a gel layer or cake on the membrane surface that made the separation difficult. The separation was however, possible using the two other methods, with antisolvent precipitation giving a separation degree of 76% using acetone as the antisolvent, versus 60% for adsorption, corresponding to an 85% removal rate of lignin.

Finally, a techno-economic evaluation was performed on various predetermined process configurations, showing that the combination of UF and adsorption (as the post-treatment step) was the most cost-efficient process that also fulfilled the design criteria.



Basel Al-Rudainy with background in computer science and electronics, started his studies at the Department of Chemical Engineering in 2007. He received his master's degree in chemical engineering – process design in 2012 following his thesis titled: *Development of a simulator for the simulation of membrane performance in tubular membranes.* The following three years, Basel has been working together with KIRAM AB and Lund University as a R&D engineer on a project involving the fractionation, separation and conversion of Kraft lignin to bio-oil. In 2015, Basel started his PhD studies at Lund University with the aim of separating and purifying hemicelluloses from an industrial waste stream, from which this thesis became the final product.

Printed by Media-Tryck, Lund 2020 NORDIC SWAN ECOLABEL 3041 0903

ISBN: 978-91-7422-748-2

Department of Chemical Engineering
Faculty of Engineering, LTH
Lund University